University of Granada

Doctoral Program in Information and Communication Technologies

Mobile Brain-Computer Interface for the Cloud-Computing of Neurophysiological Responses

Presented by

Jesús Minguillón Campos

Supervised by

Prof. Francisco J. Pelayo Valle

Prof. Miguel A. López Gordo

October 2018

Abstract

Thanks to the development of mobile technology and real-time capable algorithms, traditional BCIs coexist with new mobile-BCI-based applications nowadays. The aim of this thesis was to research and develop mobile-BCI-based applications and to apply them to field-research studies.

First, hardware and software requirements for mobile-BCI-based applications have been analyzed. In particular, the limitations of current wireless and low-cost EEG acquisition systems have been reviewed. In addition, the use of signal processing algorithms (artifact removal, feature extraction and classification) in mobile BCIs has been investigated. These requirements have been used to develop a portable, wireless, low-cost hardware/software system for real-time acquisition and processing of biosignals (i.e., RABio w8). The developed system improves the existing commercial systems in terms of cost, configurability, portability and usability, being a reliable and useful instrument for the research community and, in the future, for the general public.

The next stage has been to develop several functional and ubiquitous out-of-lab applications based on mobile BCI and on cloud-computing. In particular, for the detection and training of attention, for the assessment and detection of stress level, for the generation of secure passwords through EEG signals and for the diagnosis of visual-system-related pathologies through visual evoked potentials. In most cases the RABio w8 system was used. These applications have demonstrated a considerable potential, with the option of having a relevant impact on society.

Finally, all the above has been applied to field-research studies related to physiological, cognitive and affective computing. Specifically, in studies related to attention, stress, EEG-based password generation and visual evoked potentials, among others.

Valuable scientific results have been obtained from the field-research studies, thus proving the usefulness of the developed technology, and giving rise to a considerable number of publications in international journals with impact factor and congresses. In conclusion, the results of this thesis could generate a relevant impact on the research community and, potentially, on various areas of society including work and military defense, education, mental health, sports and e-sports, art and communications.

Acknowledgments

Acronyms

ADHD: Attention-Deficit Hyperactivity Disorder

API: Application Programming Interface

BCI: Brain-Computer Interface

DRL: Driven Right Leg

ECG: Electrocardiography

EEG: Electroencephalography

EMG: Electromyography

EP: Evoked Potential

ERD: Event-Related Desynchronization

ERS: Event-Related Synchronization

GSR: Galvanic Skin Response

GUI: Graphical User Interface

HR: Heart Rate

IoT: Internet of Things

JCR: Journal Citation Reports

MIST: Montreal Imaging Stress Task

NIRS: Near-Infrared Spectroscopy

NIST: National Institute of Standards and Technology

PCB: Printed Circuit Board

PSD: Power Spectral Density

PSK: Phase Shift Keying

RG: Relative Gamma

SC: Skin Conductance

SNR: Signal-to-Noise Ratio

SSR: Steady-State Response

SSVEP: Steady-State Visual Evoked Potential

TA: Trapezius Activity

USB: Universal Serial Port

VEP: Visual Evoked Potential

WBAN: Wireless Body Area Network

Contents

x

List of Figures

Chapter 1

Introduction

This chapter provides an overview of the motivation, objectives, field of study and publications related to this thesis.

1.1 Motivation

The brain naturally communicates using muscles and nerves. A brain-computer interface (BCI) is an artificial system that provides an alternative and direct communication channel between the brain and the outer world. A BCI records and processes brain activity to generate useful information and commands to communicate and control electronic devices. The polarization and depolarization of large populations of neurons (i.e., brain activity) causes voltage differences on the scalp (i.e., brain signals) that can be recorded through superficial electrodes. This technique is called electroencephalography (EEG). In the context of this thesis, the term BCI refers to EEG-based BCI.

EEG was used in humans, for the first time, by Hans Berger in 1929 [1]. From an electronic point of view, the main disadvantages of this technique are the attenuation produced by the skull and the skin-electrode interface. Both of them cause a decrease in the signal amplitude, giving rise to amplitude ranges of microvolts. Conductive gel is usually applied to the electrodes in order to improve the skin-electrode interface. Another disadvantage is that EEG signals are highly susceptible to electrical artifacts. All this translates into low signal-to-noise ratios

(SNR). Signal processing plays an important role to cope with them. Despite the cited disadvantages, the EEG is one of the most used techniques for brain recording as it offers numerous benefits, for example: it provides a great temporal resolution (i.e., milliseconds), it is non-invasive and it is low-cost in comparison with other techniques such as the functional magnetic resonance.

Traditionally, BCIs have been intended to help people with motor impairment. Some examples of traditional BCIs are the speller of Birbaumer [2] and the BCI for cursor control of Wolpaw [3] and Pfurtscheller [4]. However, nowadays traditional BCIs coexist with new mobile-BCI-based applications intended for the general public and out-of-lab situations. This has been possible thanks to the advances in electronics, the development of mobile technology and the evolution of algorithms for signal processing.

1.2   Objectives

As cited in the previous section, technological advances have opened the door to mobile-BCI-based applications. The aim of this thesis was to research and develop mobile-BCI-based applications and to apply them to field-research studies. The particular objectives of this thesis were the following:

- To design and develop a full (hardware/software) and functional biosignal acquisition system that can be used in mobile-BCI-based applications. The hardware and software requirements of these applications must be analyzed prior to the development of the system. Real-time operation and compatibility with cloud-computing-based applications are mandatory. Despite wireless and supposedly low-cost EEG acquisition systems are commercially available, they have a number of limitations. In addition, current signal processing algorithms including artifact removal must be analyzed. Numerous approaches have been proposed. Nevertheless, it is necessary to investigate which methods are more suitable for mobile-BCI-based applications.

- To develop specific ubiquitous out-of-lab mobile-BCI-based applications and to conduct field-research in this context in order to prove the usefulness of this technology. This includes the use of the whole development in research studies related to physiological, cognitive and affective computing.

1.3   Field of Study

The research period of this thesis has comprised multiple areas such as:

- Information and communication technologies: hardware and software development, communication systems and signal processing.

- Physiology: physiological processes and electrophysiological signals.

- Psychology: attention and stress.

Therefore, this thesis has a multidisciplinary character.

1.4   Publications

Eight journal articles indexed by Journal Citation Reports (JCR) have been published during the research period of this thesis.

Six of them are the "group of publications" that form this thesis. In five of them, the PhD candidate is the first author:

- J. Minguillon, M. A. Lopez-Gordo, and F. Pelayo (2016). **Detection of Attention in Multi-Talker Scenarios: a Fuzzy Approach**. Expert Systems With Applications, 64, 261-268. JCR ranked this journal 18 out of 133 (Q1) in category COMPUTER SCIENCE, ARTIFICIAL INTELLIGENCE and 37 out of 262 (Q1) in category ENGINEERING, ELECTRICAL AND ELECTRONIC in 2016. Preprint annexed in Appendix A.

- J. Minguillon, M. A. Lopez-Gordo, and F. Pelayo (2016). **Stress Assessment by Prefrontal Relative Gamma**. Frontiers in Computational Neuroscience, 10(September), 101. JCR ranked this journal 20 out of 57 (Q2) in category MATHEMATICAL AND COMPUTATIONAL BIOLOGY in 2016. Original article annexed in Appendix B.

- J. Minguillon, M. A. Lopez-Gordo, and F. Pelayo (2017). **Trends in EEG-BCI for daily-life: Requirements for artifact removal**. Biomedical Signal Processing and Control, 31, 407-418. JCR ranked this journal 25 out of 78 (Q2) in category ENGINEERING, BIOMEDICAL in 2017. Preprint annexed in Appendix C.

- J. Minguillon, M. A. Lopez-Gordo, D. A. Renedo-Criado, M. J. Sanchez-Carrion, and F. Pelayo (2017). **Blue lighting accelerates post-stress relaxation: Results of a preliminary study**. PLoS One, 12(10), e0186399. JCR ranked this journal 15 out of 64 (Q1) in category MULTIDISCIPLINARY SCIENCES in 2017. Original article annexed in Appendix D.

- J. F. Valenzuela-Valdés, M. A. López, P. Padilla, J. L. Padilla, and J. Minguillon (2017). **Human Neuro-Activity for Securing Body Area Networks: Application of Brain-Computer Interfaces to People-Centric Internet of Things**. IEEE Communications Magazine, 55(2), 62-67. JCR ranked this journal 2 out of 87 (D1, Q1) in category TELECOMMUNICATIONS and 4 out of 260 (D1, Q1) in category ENGINEERING, ELECTRICAL AND ELECTRONIC in 2017. Preprint annexed in Appendix E.

- J. Minguillon, E. Perez, M. A. Lopez-Gordo, F. Pelayo, and M. Sanchez-Carrion (2018). **Portable System for Real-Time Detection of Stress Level**. Sensors, 18(8), 2504. JCR ranked this journal 16 out of 61 (Q2) in category INSTRUMENTS AND INSTRUMENTATION in 2017. Original article annexed in Appendix F.

Two more JCR journal articles have been published during that period, as a result of research stays and collaborations with external research groups:

- E. Pirondini, M. Coscia, J. Minguillon, J. del R. Millán, D. Van De Ville, and S. Micera (2017). **EEG topographies provide subject-specific correlates of motor control**. Scientific Reports, 7(1), 13229. JCR ranked this journal 12 out of 64 (Q1) in category MULTIDISCIPLINARY SCIENCES in 2017.

- L. J. Barrios, J. Minguillón, F. J. Perales, R. Ron-Angevin, J. Solé-Casals, and M. A. Mañanas (2017). **Estado del Arte en Neurotecnologías para la Asistencia y la Rehabilitación en España: Tecnologías Auxiliares, Trasferencia Tecnológica y Aplicación Clínica**. Revista Iberoamericana de Automática e Informática Industrial RIAI, 14(4), 355-361. JCR ranked this journal 60 out of 61 (Q4) in category AUTOMATION AND CONTROL SYSTEMS in 2017.

In addition, seven conference papers have been published in that period:

- J. Minguillón, C. Morillas, F. Pelayo, S. Medina, and M. A. López-Gordo (June 2016). **Módulos Plat-EEG para medidas laplacianas con elec-**

trodo seco. In 8th Simposio CEA de Bioingeniería, Cognitive Area Networks, 3(1), 69-73.

- J. Minguillón, C. Morillas, F. Pelayo, and M. A. López-Gordo (July 2017). **Sistema BCI multiusuario**. In 9th Simposio CEA de Bioingeniería, Cognitive Area Networks, 4(1), 49-53.

- J. Minguillon, M. A. Lopez-Gordo, C. Morillas, and F. Pelayo (June 2017). **A Mobile Brain-Computer Interface for Clinical Applications: From the Lab to the Ubiquity**. In 7th International Work-Conference on the Interplay Between Natural and Artificial Computation, LNCS 10338, 68-76, Springer International Publishing.

- M. A. Lopez-Gordo, J. Minguillon, J. F. Valenzuela-Valdes, P. Padilla, J. L. Padilla, and F. Pelayo (June 2017). **Securing Passwords Beyond Human Capabilities with a Wearable Neuro-Device**. In 7th International Work-Conference on the Interplay Between Natural and Artificial Computation, LNCS 10338, 87-95, Springer International Publishing.

- J. Sorinas, M. D. Grima Murcia, J. Minguillon, F. Sánchez-Ferrer, M. Val-Calvo, J. M. Ferrández, and E. Fernández (June 2017). **Setting the Parameters for an Accurate EEG (Electroencephalography)-Based Emotion Recognition System**. In 7th International Work-Conference on the Interplay Between Natural and Artificial Computation, LNCS 10337, 265-273, Springer International Publishing.

- J. Minguillón, E. Pérez Valero, F. Pelayo and M. A. López-Gordo (July 2018). **K-Attack: Videojuego inclusivo basado en SSVEP**. In 10th Simposio CEA de Bioingeniería, Cognitive Area Networks, 5(1), 77-80.

- E. Pérez Valero, J. Minguillón, and M. A. López Gordo (September 2018). **Neurociencia lúdica e inclusión**. In 33rd Simposium Nacional de la Unión Científica Internacional de Radio, 137.

1.5   Thesis Organization

The rest of this document is organized as follows: Chapter 2 provides an overview of the new trends in BCIs and the main requirements of mobile-BCI-based applications. Chapter 3 provides an overview of the main methods used to develop the biosignal acquisition system and of the main methods used to develop the mobile-BCI-based applications and to conduct the field-research studies of this

thesis. Chapter 4 provides an overview of the main results related to the developed biosignal acquisition system and of the main results related to the developed mobile-BCI-based applications and to the conducted field-research studies of this thesis. Finally, Chapter 5 provides a summary of the main contributions, application fields, limitations and future work of this thesis.

Chapter 2

Trends in Brain-Computer Interfaces

This chapter provides an overview of the new trends in BCIs and the main requirements of mobile-BCI-based applications. This chapter is inspired by the review article published and annexed as part of this thesis (see Appendix C).

2.1 Mobile-BCI-based Applications

As mentioned in Chapter 1, a BCI generates useful information and commands to communicate and control electronic devices after recording and processing the brain activity. For this, the three functional blocks of the BCI interact with each other. The first block is signal acquisition. It is composed of electrodes, amplifiers and analog-digital converters. This block is in charge of the acquisition of EEG signals and the analog-digital conversion. The second block is signal processing. It translates the raw data received from the first block into useful information and control commands. The processing is usually divided into three steps, namely preprocessing, feature extraction and classification. The preprocessing adapts the raw data to further processing (e.g., filtering, artifact removal, normalization, etc.). The feature extraction is the selection of relevant parameters from the preprocessed data. The classification is the decision-making process based on the features. The

decisions are sent to the third functional block (i.e., the control interface). This
block is in charge of interpreting the decisions and producing the necessary control
commands and/or information to control and communicate with a final device
and/or the user (i.e., feedback). The information flow between the functional
blocks by means of communication interfaces [5]. Figure 2.1 shows the basic block
diagram of a BCI.
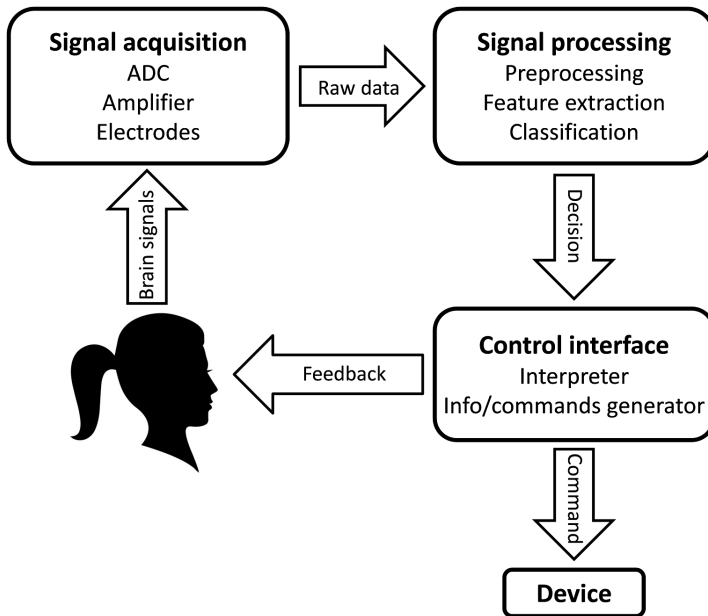
Figure 2.1:   Basic block diagram of a BCI.

Despite classical rehabilitation and assistive applications are still topical issues [6,
7, 8, 9, 10, 11], mobile BCIs have motivated the research community to propose new
applications intended for the general public and daily-life situations. For example,
games [12, 13, 14], sports [15], daily-life communication [16], smart living [17,
18, 19], drowsiness detection [20], workload classification [21] and stress detection
[22, 23, 24].

These mobile-BCI-based applications impose certain requirements in the design of
the BCI. The following sections report an overview of the hardware and software
requirements of mobile-BCI-based applications.

2.2   Hardware

The main hardware requirements are related to the EEG acquisitions systems, the
working environment and the combination of EEG with other physiological signals.

2.2.1   EEG Acquisition Systems

Traditional EEG recording equipment is large, heavy and not portable. However,
portability is a major requirement for mobile BCIs. Nowadays there are a number
of commercial low-cost wireless EEG acquisition systems. For example, the EEG
headband of Cognionics, the EPOC and Insight systems of Emotiv, the MindWave
headset of Neurosky, the g.Nautilus system of g.tec and the Enobio system of
Neuroelectrics. Figure 2.2 shows these systems. Moreover, several researchers have
proposed other wireless systems [25, 24].

Figure 2.2:   Commercial low-cost wireless EEG acquisition systems. From top left
to bottom right: EEG headband (Cognionics), EPOC (Emotiv), Insight(Emotiv),
MindWave (Neurosky), g.Nautilus (g.tec) and Enobio (Neuroelectrics).

Despite the cited commercial systems are cataloged as low-cost, the cost of most of
these systems is more than 4000 euros (only the hardware); and the most affordable
ones are merely gadgets with a number of limitations and useless for multiple
applications.

Other important point is the electrode configuration. Since the publication of the
international 10-20 system for EEG electrode placement [26], most of EEG studies
(including BCI applications) have used a considerable number of electrodes (typ-
ically 64). Nevertheless, a simple electrode configuration (i.e., reduced number of

electrodes) is recommended for mobile-BCI-based applications in order to ensure the usability and the portability. Indeed, the number of channels (i.e., data from electrodes) is typically reduced during the processing step due to the high correlation between nearby electrodes. Only a few of the cited commercial systems implement a simple electrode configuration.

In addition, the electrode technology is crucial in terms of usability. Traditional gel-based electrodes are considered the gold standard. However, the preparation causes fatigue and requires the presence of technical staff. Dry electrodes are a must for mobile-BCI-based applications. Despite some commercial systems implement dry electrodes, there still are a number of important lacks regarding them [27]. Currently, traditional wet electrodes provide much better signal quality.

Last but not least, the configurability of the acquisition system is essential. A mobile-BCI-based application is intended to work in different environmental conditions. Some acquisition parameters such as the amplification gain must be configurable. In this respect, the commercial systems are very limited.

In conclusion, the cited commercial wireless EEG acquisition systems can be improved in terms of portability, cost, usability and configurability.

2.2.2   Working Environment

As mentioned before, a mobile-BCI-based application must work under different environmental conditions, including realistic out-of-lab scenarios. These are distinguished by the presence of a considerable number of artifacts (e.g., signal interferences, motion artifacts, etc.). Robustness and ubiquity are a major requirement. However, most EEG-BCI studies found in literature were performed under very controlled conditions (e.g., in laboratories, with subjects instructed to avoid unnecessary movements, etc.) [28, 29, 30, 31]. Only a few authors have tested their approaches in realistic environments [16, 32, 33, 34].

2.2.3   EEG and Other Physiological Signals

Despite the combined recording and processing of EEG with other physiological signals is not a must, it may be useful and advantageous in certain applications, provided of course that the portability and usability of the system are not compromised. Examples include hybrids NIRS-EEG BCIs [35, 36], BCIs supported by eye-trackers [37, 38], EEG combined with artifact sources such as teeth clench

[38, 39] and EEG combined with multiple biosignals such as electrocardiography (ECG), electromyography (EMG) and galvanic skin response (GSR) [24].

2.3 Software

The main software requirements are related to the processing, the selected EEG features and the artifact removal procedure.

2.3.1 Processing

Although the brain signals were processed offline in a considerable number of BCI studies, a final and functional version of any BCI application (including mobile applications) must work in real-time. Advances in both computation hardware and processing algorithms have made it a reality [31, 40]. In this regard, there are a large number of advanced feature extraction and classification methods which are suitable for real-time operation. Examples include fuzzy-logic [41, 42, 43] and neural networks [44, 45], among others. However, these advanced algorithms usually require to be performed in a personal computer or laptop. In order to minimize the hardware, thus improving portability and usability, cloud-computing solutions with stimulation and real-time feedback presented in mobile devices must be considered.

2.3.2 EEG Features

Several EEG features have been traditionally used in BCI applications. The most relevant are brain rhythms (i.e., frequency bands), evoked potentials (EP) and steady-state responses (SSR).

Rhythm-based BCIs do not require any external stimulation. On the contrary, they usually need a training period that depends on the user [46]. The ERD/ERS of the mu band (typically 8-12 Hz) in motor imagery is one of the most obvious examples [11]. Other examples include theta (4-7 Hz) and alpha bands (8-13 Hz) [47, 20, 19]. See [48] for a review on BCI using brain rhythms.

An evoked potential is the response to a certain stimulus. Therefore, EP-based BCIs require external stimulation. Moreover, precise synchronization between the stimulus player and the acquisition system is needed. This synchronization is improvable in current wireless systems. As an advantage, they do not need as much

training as rhythm-based BCIs. Nevertheless, a considerable number of users are unable to control EP-based BCIs due to the BCI illiteracy phenomenon [49, 50]. The most obvious example of this type of BCI is the P300 (i.e., evoked potential at 300+ ms after the stimulus onset). The P300 has been widely used in applications such as spelling [51, 30, 52], cursor control [53], robot control [54], wheelchair control [9] and classification of auditory events during flight [33].

A train of repetitive stimuli evokes the so-called steady-state responses. SSR-based BCIs generally have the same benefits and limitations than the EP-based BCIs. However, they have a clear advantage in terms of robustness to artifacts. This is because, in the SSR spectrum, most of energy is confined in a narrow frequency band (ideally a single peak) corresponding to the stimulation frequency. Thus, only the energy of the artifacts occupying that band affect the performance of the BCI. The most representative SSR-based BCIs are the ones based on steady-state visual evoked potentials (SSVEP). Examples include spelling [55, 52, 56, 37], wheelchair control [9], attention training [13, 14] and other daily-life applications [57, 16, 38].

To sum up, there are numerous EEG features that can be used in BCI applications. However, in principle no particular requirement can be stated in this regard for mobile-BCI-based applications. The best option depends on the final application.

2.3.3   Artifact Removal

Artifact removal is a must for mobile-BCI-based applications as they are intended to work in realistic scenarios. They affect EEG data in concrete form. For example, ocular artifacts are concentrated at low frequencies (typically below 5 Hz), whilst motion artifacts affect the whole frequency range from 0 to 30 Hz (see Figure 2.3).

Artifact removal procedures must be designed and used according to the requirements described in previous sections. Among the most used approaches, there are filtering-based methods [59], linear regression [60, 58], blind source separation methods such as independent component analysis [61, 62] and canonical correlation analysis [63, 64], source decomposition techniques such as wavelet decomposition [65, 66, 67] and empirical mode decomposition [68, 69, 70, 63, 64], others such as neural networks[71, 72] and neural fuzzy interference systems [72, 73] and mixed approaches [68, 74, 67, 63, 64, 75, 72, 76]. Figure 2.4 shows the main artifact removal approaches proposed since 2006 and their properties regarding the requirements of mobile-BCI-based applications. As an overall conclusion, artifact removal is still lacking in mobile-BCI-based applications and further research in needed [5]. The
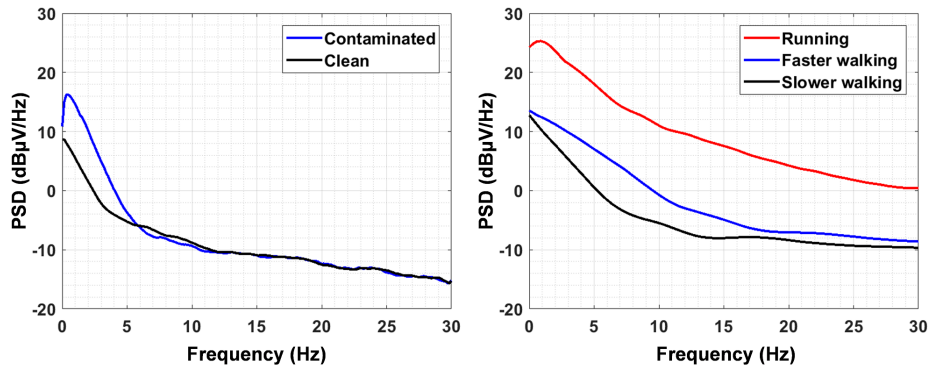
Figure 2.3:   PSD of EEG data contaminated by artifacts. On the left: EEG data contaminated by ocular artifacts. On the right: EEG data contaminated by motion artifacts. Plots on the right have been created from findings in [58].

original figure, its references and further discussion on this topic can be found in the review article that has inspired this chapter (see Appendix C).

	Acharjee et al., 2015	Burger et al., 2015	Castellanos et al., 2006	Chen et al., 2014 (1)	Chen et al., 2014 (2)	Cho et al., 2007	Davies et al., 2007	Geetha et al., 2012	Gu et al., 2014	Guerrero-Mosquera et al., 2009	Gwin et al., 2010	Hsu et al., 2012	Hu et al., 2015	Klados et al., 2011	Kong et al., 2013	Krishnaveni et al., 2006 (1)	Krishnaveni et al., 2006 (2)	Kumar et al., 2008	Ma et al., 2011	Mammone et al., 2012	Mijovic et al., 2010	Mognon et al., 2011	Mourad et al., 2007	Mourad et al., 2013
Performed outdoors																								
Portable-wearable-wireless																								
Real EEG signals	■	■			■	■	■	■		■	■	■	■	■	■			■	■	■		■	■	■
Daily-life tasks			■	■						■														
Simple electrode configuration																								
Dry electrodes																								
Complex artifacts			■	■			■				■			■		■								
Only EEG signals	■	■	■	■	■	■	■	■	■	■	■	■	■	■	■	■	■	■	■	■	■	■	■	■
Online		■														■	■				■			
Single active channel			■	■																	■			■

	Mowla et al., 2015	Nguyen et al., 2012	Nolan et al., 2010	Peng et al., 2013	Porcaro et al., 2015	Puthusserypady et al., 2006	Raduntz et al., 2015	Romo et al., 2012	Sameni et al., 2014	Schlogl et al., 2007	Shao et al., 2009	Sweeney et al., 2013	Sziboo et al., 2012	Teixeira et al., 2006	Teixeira et al., 2007	Teixeira et al., 2008	Tiganj et al., 2010	Wang et al., 2014	Yong et al., 2009 (1)	Yong et al., 2009 (2)	Zeng et al., 2013	Zhang et al., 2015	Zhao et al., 2014	Zikov et al., 2002
Performed outdoors																								
Portable-wearable-wireless				■																			■	
Real EEG signals	■	■	■	■	■	■	■	■	■	■	■	■	■	■	■	■	■	■		■	■	■	■	■
Daily-life tasks		■			■																			
Simple electrode configuration				■																			■	
Dry electrodes																								
Complex artifacts	■	■		■	■	■	■	■	■		■	■		■	■	■	■						■	■
Only EEG signals	■	■	■	■	■	■	■	■	■	■	■	■	■	■	■	■	■	■	■	■	■	■	■	■
Online																		■						
Single active channel	■	■											■	■	■	■	■		■	■	■	■	■	■

Figure 2.4:   Main artifact removal approaches proposed since 2006 and their properties regarding the requirements of mobile-BCI-based applications. Grey color indicates accomplishment and white color indicates no accomplishment or not mentioned. Adapted from preprint of [5] (Appendix C).

Chapter 3

Methods

This chapter provides an overview of the main methods used to develop the biosignal acquisition system (Section 3.1) and of the main methods used to develop the mobile-BCI-based applications and to conduct the field-research studies of this thesis (Section 3.2). Further information can be found in the annexed articles and other cited articles.

3.1 RABio w8: Real-Time Acquisition of Biopotentials

The biosignal acquisition system developed in this thesis is the so-called RABio w8 (Real-Time Acquisition of Biopotentials, wireless, 8 channels).

3.1.1 Design Criteria

In order to use RABio w8 in mobile-BCI-based applications, the design criteria must be in line with the requirements of these applications (see Chapter 2 for an overview of the main requirements of mobile-BCI-based applications). The main design criteria were the following:

Hardware

- Portability: wireless technology, reduced dimensions and reduced number of channels.

- Connectivity: wireless and standardized protocols that provides the required bandwidth and does not need extra dongles (e.g., Bluetooth), and standardized connectors (e.g., USB and standard bio-signal connectors).

- Electrical features: low-noise electronics, common reference, driven right leg (DRL) circuit, proper input range for multiple bio-signal acquisition (e.g., EEG, ECG and EMG) and high input impedance.

- Electrical safety: mechanical isolation between battery charging circuits and acquisition circuits.

- Autonomy: low-power electronics and rechargeable batteries that provide high-autonomy.

- Robustness: robust connectors (preferably through-hole) and solders, and robust casing.

- Cost: market price below 1500 euros.

Software

- Configurability: configuration of acquisition parameters for the compatibility with multiple biosignals such as EEG, ECG and EMG.

- Usability: friendly and easy-to-use graphical user interface (GUI) and application programming interface (API) that makes RABio w8 compatible with other platforms.

- Compatibility with cloud-computing: easy integration of RABio w8 into cloud-computing-based architectures.

- Real-time operation: real-time acquisition, visualization and processing of biosignals.

- Synchronization: precise synchronization with event markers and timers.

3.1.2 Design Tools

Several tools were used in the design and development of different parts of RA-Bio w8. The main developed parts and the corresponding design tools were the following:

Hardware

- Printed circuit board (PCB): it was designed with Altium Designer and manufactured by Millennium Dataware Srl. The electronic components were mounted and soldered by means of reflow soldering.

- Casing: it was designed with SolidWorks and manufactured with a 3D printer.

Software

- Firmware in the microcontroller: it was coded in C using CCS C Compiler and written in the microcontroller using MPLAB X IDE, an in-circuit serial programming tool from Microchip Technology.

- Application programming interface: it was implemented as a Windows dynamic-link library coded in C/C++ using Visual Studio.

- Graphical user interface: it was coded in Matlab.

3.1.3 Validation Tests

Several validation tests were performed after the manufacturing of RABio w8. The main tests were the following:

- Electronic check: checking of test points of the electronics by using an oscilloscope and a multimeter.

- Artificial signal acquisition test: testing of acquisition of an artificial signal generated by a signal generator.

- Real signal acquisition test: testing of acquisition and processing of real biosignals (e.g., EEG, ECG or EMG).

- Clinical test: visual evoked potentials test using an application developed in this thesis (see second paragraph of Section 3.2.4).

3.1.4   Facilities

During the development of RABio w8, several facilities and materials of the Research Center for Information and Communications Technologies of the University of Granada (CITIC-UGR) were utilized:

- BCI laboratory: personal computers and laptops for hardware/software design and implementation, and signal generator, oscilloscope, multimeter and electrophysiological materials (e.g. EEG cap, gel, electrodes, etc.) for validation tests.

- Hardware laboratory: reflow soldering tools for mounting and soldering of electronic components.

- Mechatronics laboratory: 3D printer for printing of plastic casing.

3.2   Applications Based on the RABio w8 System and Field-Research

Several functional and ubiquitous out-of-lab applications based on the RABio w8 system have been developed in this thesis. These applications have been applied to field-research studies in order to validate them and produce scientific results. Apart from that, other field-research studies related to mobile-BCI-based applications have been conducted in this thesis. This section provides an overview of the cited applications and conducted studies.

3.2.1   Attention Detection and Training

According to the American Psychological Association, attention-deficit hyperactivity disorder (ADHD) is a behavioral condition that makes focusing on everyday requests and routines challenging. This disorder is present in a considerable part of the population including children. Utility of EEG in ADHD has been subject of study for many years [77]. Apart from ADHD, attention research is present in other areas such as military defense (e.g. selective attention in multi-talker scenarios). In this thesis, three works have been conducted in relation to attention.

Detection of Attention in Multi-Talker Scenarios: A Fuzzy Approach

In this work [43], a fuzzy approach for the detection of selective attention in multi-talker scenarios was proposed. The proposed detector takes into account the attentional and artifacts effects on the physiological response before performing a fuzzy-based m-PSK classification (see Figure 3.1). A previously utilized database was used to test the approach [78]. This database was formed by the EEG of 13 subjects doing auditory attentional tasks. Detailed information can be found in the preprint (Appendix A) or in the original article [43].
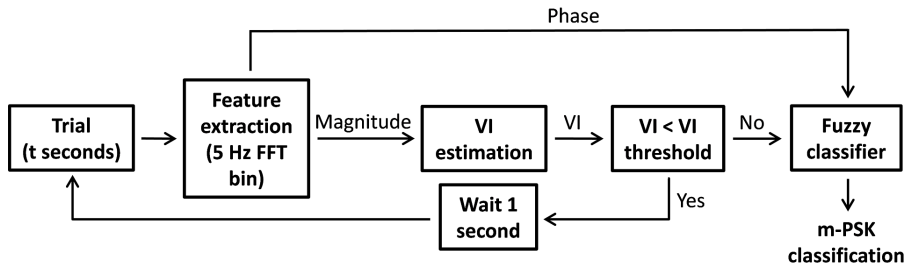
Figure 3.1: Block diagram of the fuzzy-based attention detector. Adapted from preprint of [43] (Appendix A).

K-Attack: Inclusive Videogame Based on SSVEP for Attention Training

In these two works [13, 14], a mobile-BCI-based application for visual attention training was proposed, the so-called K-Attack. K-Attack is an inclusive videogame based on SSVEP. It uses RABio w8 within a cloud-computing-based architecture to provide real-time detection and training of visual attention (see Figure 3.2). Visual attention is detected by using the SNR of both the alpha band and the SSVEP evoked by stimulation based on reversal pattern. This application was tested during the I Telecommunication Meeting of the University of Granada. Figure 3.3 shows the setup of K-Attack. Detailed information can be found in the original articles [13, 14].

3.2.2 Stress Assessment and Detection

Nowadays stress is a major concern in our society [24]. According to the American Psychological Association, most US people regularly experience physical (77 %) and/or psychological (73 %) symptoms related to stress. Stress is usually caused
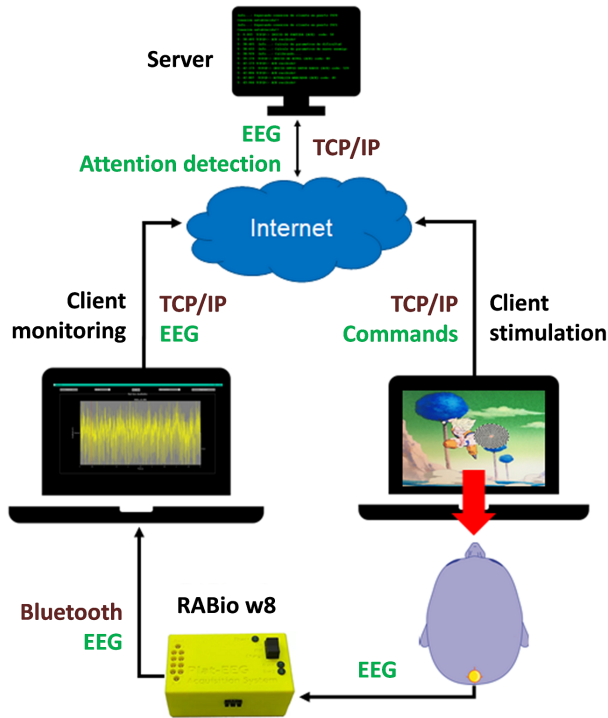
Figure 3.2:   Block diagram of K-Attack. Adapted from [13].

by a variety of cognitive, social or physical factors such as job pressure, economic status, health, and relationships [23]. Detection and prevention of stress is a topical subject of central importance. In this thesis, three works have been carried out regarding stress assessment and detection, in collaboration with the School for Special Education San Rafael of Granada (Orden Hospitalaria de San Juan de Dios).

Stress Assessment by Prefrontal Relative Gamma

In this work [23], the relative gamma (RG) power measured at the prefrontal brain area (electrodes Fp1 and Fp2 of the International System) was proposed as biomarker of stress in mobile-BCI-based applications. The relative gamma is defined as the ratio between the power of gamma band (25-45 Hz) and the power of alpha and theta bands (4-13 Hz). In order to validate it, 6 subjects were stressed and then relaxed while their EEG and ECG signals were recorded. Well-described methodology was used to ensure stress and relax processes. In particular, the
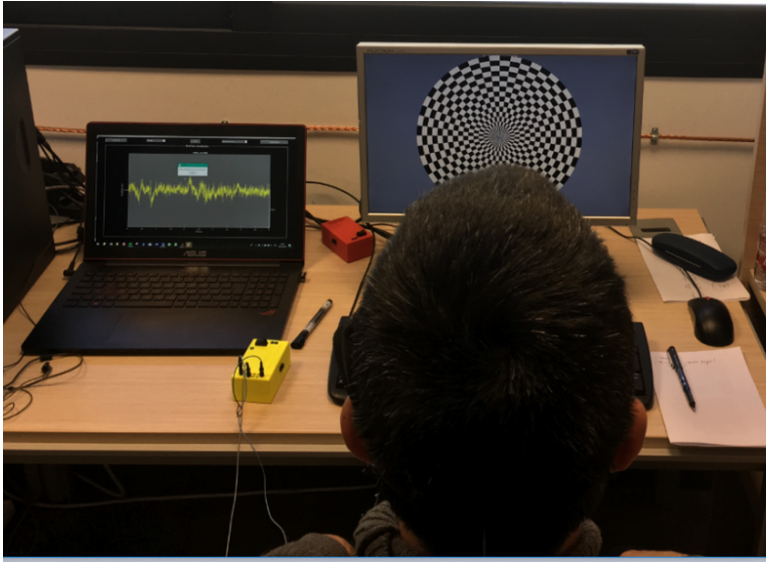
Figure 3.3:   Picture of K-Attack setup. From [13].

Montreal Imaging Stress Task (MIST) was used to induce stress in the subjects [79]. A Matlab-based GUI was implemented for the execution of the MIST. For the relax process, the subjects stayed within a white-lighted relaxation room. Figure 3.4 shows the timeline of the experiment and the expected stress level during the experiment. Apart from the design of the experiment, self-perceived stress level was measured through questionnaires. Detailed information can be found in the original article (Appendix B or [23]).
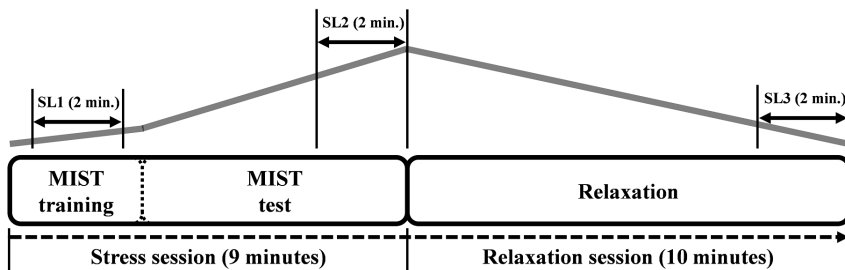
Figure 3.4:   Timeline of the experiment and expected stress level (grey line). From [23].

Blue Lighting Accelerates Post-Stress Relaxation: Results of a Preliminary Study

In this work [80], effects of light during the post-stress relaxation process was studied. In particular, blue lighting was compared with conventional white lighting (see Figure 3.6). For that, other 6 subjects repeated the experiment cited in the previous section, this time using blue lighting in the relaxation room. Figure 3.5 shows the timeline of the experiment. Detailed information can be found in the original article (Appendix D or [80]).
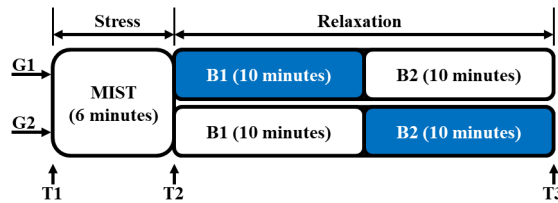
Figure 3.5:   Timeline of the experiment. From [80].

Figure 3.6:   Pictures of the relaxation room. On the left: blue-lighted room. On the right: white-lighted room. From [80].

Portable System for Real-Time Detection of Stress Level

In this work [24], a portable system for real-time detection of stress level was proposed. The detection is based on the processing of multiple biosignals (i.e., EEG, ECG, EMG and GSR). The system uses RABio w8 as acquisition system. The system was validated by a study in which 10 subject were stressed and then relaxed using the same methodology than in the previous stress works (see Figure 3.7). This time, EMG and GSR were also recorded. Although the signal processing was performed offline for this study (see Figure 3.8), the cloud-computing of biosignals

with real-time biofeedback presented in mobile devices was proposed in a final version. Detailed information can be found in the original article (Appendix F or [24]).
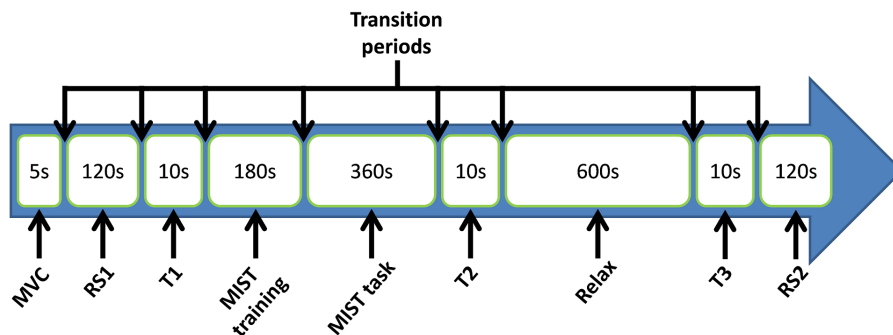
Figure 3.7:   Timeline of the experiment. From [24].
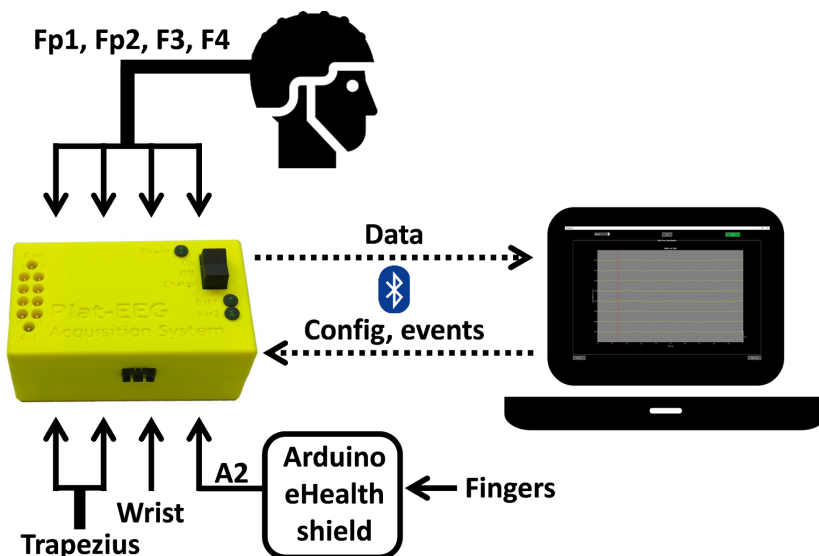
Figure 3.8:   Diagram of the portable system for real-time detection of stress level. The system is composed by the RABio w8, multiple biosignal sensors placed at head, trapezius, wrist and fingers, the Arduino e-Health platform, and a laptop. From [24].

3.2.3   Secure Password Generation Based on EEG

Internet of things (IoT) refers to the digital interconnection of daily-life things through internet. People-centric IoT is a modern concept that refers to heterogeneous and interconnected devices in wireless body area networks (WBAN) [81]. Examples include mobile BCIs and other biosignal-based devices. The communication between these devices is usually based on the automatic renewal of cryptographic passwords. Due to the limited hardware resources, the entropy sources are not good enough to generate secure random passwords for encryption. Because of the randomness of raw EEG, the generation of secure passwords based on EEG signals have been proposed in this thesis. In particular, two works have been conducted in this regard.

Human Neuro-Activity for Securing Body Area Networks: Application of Brain-Computer Interfaces to People-Centric Internet of Things

In this work [81], a method for generating secure passwords through processed EEG data was proposed and assessed. The EEG datasets used (8 subjects, 32 electrodes) were taken from a published study of a P300-based BCI [82]. The statistical tests to assess the security of generated passwords were based on the NIST Statistical Test Suite [83]. Figures and detailed information can be found in the preprint (Appendix E) or in the original article [81].

Securing Passwords Beyond Human Capabilities with a Wearable Neuro-Device

In this work [84], secure password generation through raw EEG data was proposed as a mobile-BCI-based application. Raw EEG data (i.e., not processed) were acquired with RABio w8. Passwords generated with raw EEG data were compared with passwords generated by one person and with passwords generated by a computer. The comparison was given in terms of security using the NIST Statistical Test Suite. Figures and detailed information can be found in the original article [84].

3.2.4   Other Research

Apart from the already described ones, other applications and research have been conducted in this thesis.

A Mobile Brain-Computer Interface for Clinical Applications: From the Lab to the Ubiquity

Visual evoked potentials (VEP) are electrophysiological responses evoked by visual stimuli that can be extracted from EEG data. They are widely used in clinical practice to diagnose and follow the evolution of a considerable number of pathologies. Examples include optic chiasm pathology [85], Parkinson's disease [86], multiple sclerosis [87], cataract [88], retinopathy [89], glaucoma [90], optic neuropathy [91] and stroke [92]. From an electronic point of view, the VEP test requires precise synchronization between the stimulator and the EEG acquisition system. In this work [34], a mobile-BCI-based application for ubiquitous and out-of-lab VEP test was proposed. The proposed application is a cloud-computing solution that uses RABio w8 to acquire EEG data and a mobile device to perform the stimulation. EEG data acquired by RABio w8 are sent to the cloud (i.e., a remote server) in charge of detecting the VEPs in real-time. The remote server sends the results to both the mobile device used for stimulation and the email address specified by the user (see Figure 3.9). The application was tested with 2 subjects under three different conditions (including out-of-lab settings): sitting within a lab, walking through a corridor and traveling in a car. Figures and detailed information can be found in the original article [34]. Apart from the cited work, the application was used in a clinical case of central serous chorioretinopathy. In particular, the patient performed a first test after the diagnosis of the pathology and a second test after the remission of the pathology. These tests consisted of 4 trials of 80 stimuli at 2 stimuli per second and were performed in out-of-lab conditions. The results of both tests are shown in Section 4.2.4.

Setting the Parameters for an Accurate EEG-Based Emotion Recognition System

In this work [93], a processing method (i.e., preprocessing, feature extraction and classification) for emotion recognition from EEG data was proposed. EEG data were obtained from 5 subjects while watching positive-emotion-related and negative-emotion-related video clips. This work is the result of a collaboration with the Biomedical Neuroengineering Research Group of the University Miguel Hernández. Figures and detailed information can be found in the original article [93].
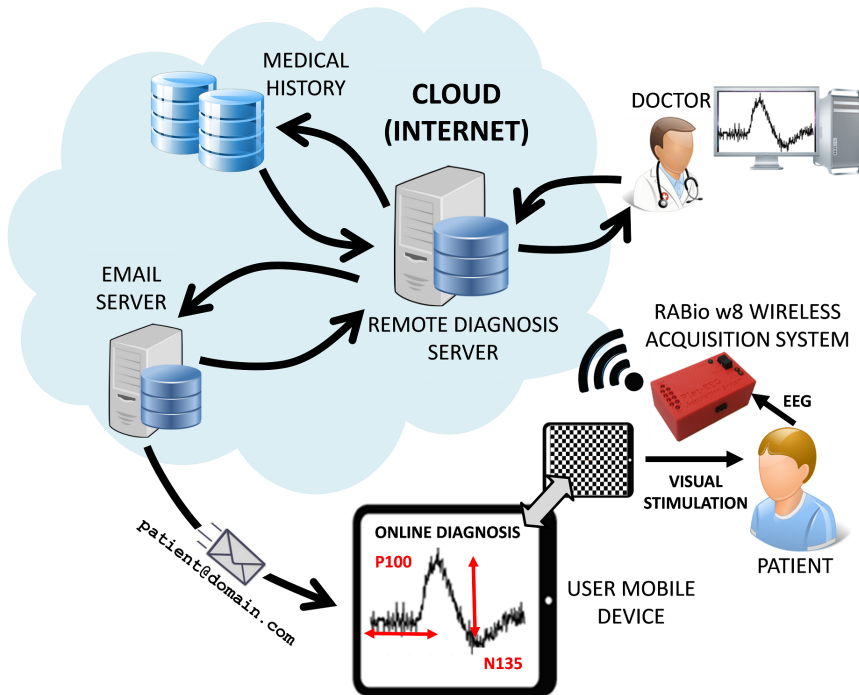
Figure 3.9:   Block diagram of the VEP application. Adapted from preprint of [34].

EEG Topographies Provide Subject-Specific Correlates of Motor Control

In this work [94], the correlation between brain activity and motor control was studied. In particular, EEG microstates and EMG muscle synergies from 8 subjects performing reaching and grasping tasks were analyzed. This work is the result of a collaboration with the Translational Neural Engineering Lab of the École Polytechnique Fédérale de Lausanne (EPFL). Figures and detailed information can be found in the original article [94].

State of the Art of Neurotechnologies for Assistance and Rehabilitation in Spain

In this work [95], the state of the art of neurotechnologies for assistance and rehabilitation in Spain was analyzed and summarized. This work is the result of a collaboration with multiple Spanish research groups belonging to the NeuroTec Cooperative Research Thematic Network on Neurotechnologies for Assistance and

Rehabilitation. Figures and detailed information can be found in the original article [95].

Chapter 4

Results

This chapter provides an overview of the main results related to the developed biosignal acquisition system (Section 4.1) and of the main results related to the developed mobile-BCI-based applications and to the conducted field-research studies of this thesis (Section 4.2). Further information can be found in the annexed articles and other cited articles.

4.1 RABio w8: Real-Time Acquisition of Biopotentials

RABio w8 is a portable, wireless, low-cost hardware/software system for real-time acquisition and processing of biosignals including EEG, ECG and EMG. The RABio w8 system has been used, presented and validated in one JCR journal paper [24] or Appendix F and six conference papers [96, 97, 34, 84, 13, 14]. Detailed information can be found in these works and on the website of RABio w8 [98].

4.1.1 Hardware

The electronic design of RABio w8 is divided into three blocks (see Figure 4.1) [24]. The first block is the acquisition block. It uses advanced integrated circuits from the ADS family of Texas Instruments to amplify and convert analogue signals

into digital data. It provides eight simultaneous channels (i.e., eight channels plus common reference plus DRL), with up to 1000 samples per second and with a resolution of 24 bits per sample. The amplification gain of every single channel and the sampling rate are configurable. The acquisition block interacts with the second block (i.e., the control block) through a serial peripheral interface (SPI). This block is based on a microcontroller from Microchip Technology. It receives, synchronizes, formats and sends the data frames from the acquisition block to the communication block (i.e., the third block) through a universal asynchronous receiver-transmitter (UART) port. The communication block is in charge of the wireless communication (via Bluetooth 2.1) with the software of the RABio w8 system. The electronics are contained in a 3D printed plastic casing (see Figure 4.1) and powered by high-autonomy (more than 24 hours in transmit mode) lithium polymer rechargeable batteries (via USB type-C port). For safety reasons, the battery charging circuit is mechanically isolated. In other words, there is a switch that only allows one operation mode, charge or power on. Hardware dimensions are 93 x 54 x 39 mm (length x width x height).
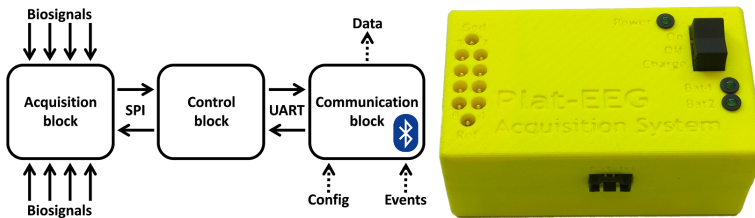
Figure 4.1:   RABio w8 system. On the left: diagram of the electronics. On the right: exterior of the hardware. Adapted from [24].

In addition, a second version of the RABio w8 hardware (i.e., RABio w8 mini) has been developed in this thesis (see Figure 4.2). Hardware dimensions of this version are considerably smaller: 50 x 50 x 18 mm (length x width x height). Figure 4.3 shows pictures of the PCB of the first and the second version of RABio w8. Finally, there are a new version under development which includes an EEG cap with embedded electronics.

4.1.2   Software

The software of RABio w8 consists of a friendly graphical user interface and an application programming interface [24], apart from the firmware in the microcontroller. The GUI of RABio w8 is coded in Matlab and is designed to be easy to use and to overcome the usability-related limitations of commercial GUIs. Figure 4.4

Figure 4.2: Visual comparison between the first and the second version of RABio w8.
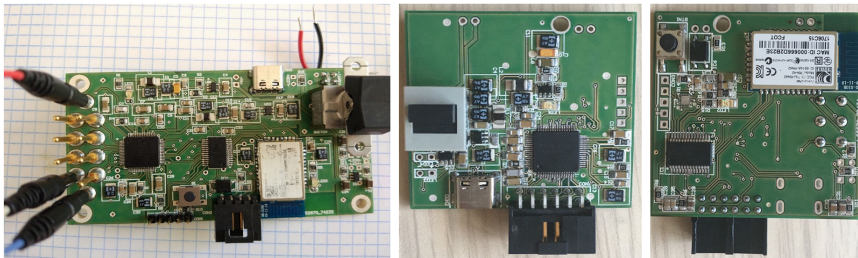
Figure 4.3: Pictures of the PCB of the first (left) and the second version (center and right) of RABio w8.

shows a screenshot of the GUI. It provides real-time data acquisition, visualization and processing, as well as it allows to configure the acquisition parameters (i.e., channels gain and sampling rate) and to send event markers and timers via Bluetooth. Moreover, multiple acquisition devices can operate simultaneously in the same session [97]. The GUI is supported by the API functions. These functions are in charge of managing the Bluetooth connection with the electronics of RABio w8, receiving the data and communicating with it. The API is a Windows dynamic-link library and is coded in C/C++. This makes RABio w8 compatible with other general-purpose software for BCI research such as BCI2000 [99]. In addition, the software of RABio w8 provides easy integration into cloud-computing-based architectures. In the example shown in Figure 4.5, the processing server sends feedback to the multimedia server, which is in charge of generating and sending the stimulation to the mobile device, depending on the processed EEG data (acquired by

RABio w8). All this is performed in real-time.
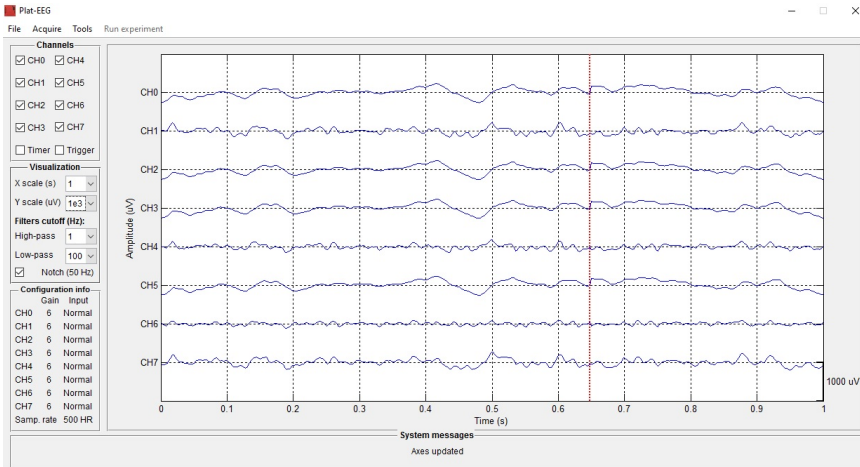
Figure 4.4:   Screenshot of the GUI of RABio w8.
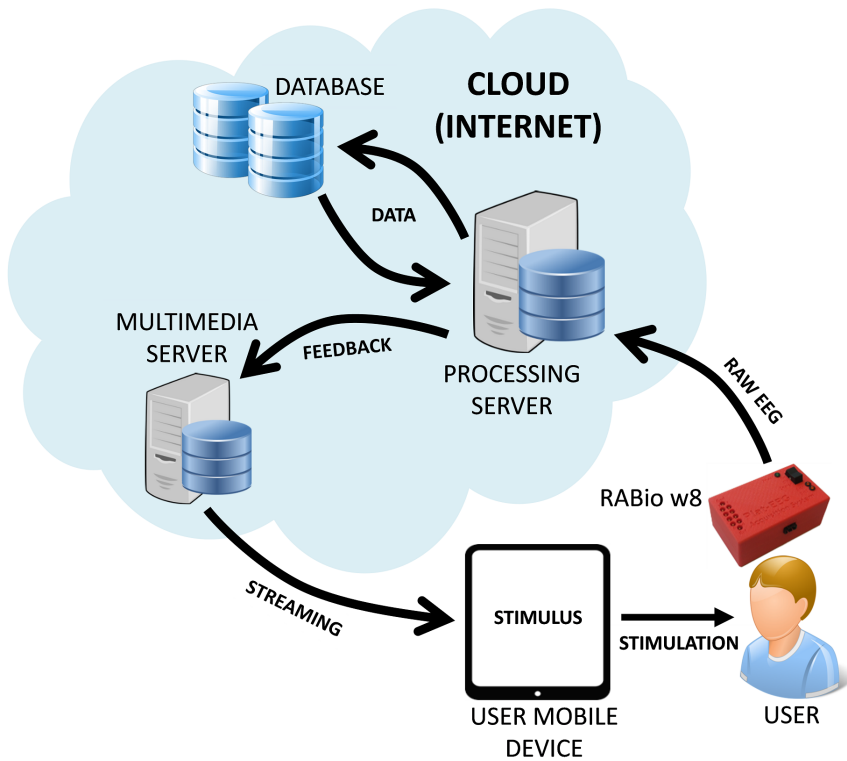
Figure 4.5:   Example of use of RABio w8 in a cloud-computing-based architecture.

4.1.3   Advantages over Commercial Systems

The RABio w8 system presents a set of advantages over current commercial wireless low-cost EEG acquisition systems, in terms of:

- Cost. As mentioned in Section 2.2.1, although the cited commercial systems are cataloged as low-cost, the cost of most of these systems is more than 4000 euros (only the hardware); and the most affordable ones are merely gadgets with a number of limitations and useless for multiple applications. The market price of RABio w8 would be around 1400 euros including software.

- Configurability. Commercial systems are very limited in this regard. The RABio w8 system provides multiple configuration options that can be set by the user such as the channels gain and the sampling rate. This allows the user to acquire multiple bio-signals such as EEG, ECG and EMG.

- Portability. Dimensions and weight of the second version of RABio w8 are considerably smaller than those of current commercial systems.

- Usability. As cited before, the RABio w8 system includes a friendly GUI. This GUI is easier to use than other commercial ones. For example, the user can start a recording session with customized parameters and multiple acquisition devices in three quick and understandable steps. In addition, it is based on Matlab what makes it well suited for research purposes. Finally, it can be easily integrated into cloud-computing-based applications.

- Electrical safety. Commercial systems usually manage the on-off control by means of electronic methods. However, RABio w8 provides a mechanical isolation between the battery charging circuit and the rest of the electronics by means of a switch.

- Autonomy. Most commercial systems provide around 10 hours of continuous recording (e.g., the g.Nautilus of g.tec). RABio w8 provides more than 24 hours of autonomy in transmit mode.

4.2   Applications Based on the RABio w8 System and Field-Research

4.2.1   Attention Detection and Training

Detection of Attention in Multi-Talker Scenarios: A Fuzzy Approach

The main finding of this work (see second paragraph of Section 3.2.1) was to over-
come the performance of the previous published detector [78] in terms of accuracy
(i.e. probability of successful classification) and ITR by using the fuzzy-based de-
tector (see Figure 4.6). Fuzzy logic was proved to be useful in the paradigm of
auditory attention to multiple sources. The results suggest the potential use of the
presented system as a mobile-BCI-based application in many areas such as educa-
tion, public transport, jobs, industry, attention disorders, sports and art. Detailed
information can be found in the preprint (Appendix A) or in the original article
[43].

Part.	Session 1 (4 talkers)							Session 2 (6 talkers)						
	VI thresh	RMI thresh	M_{av}	Chance level	p_a	t_{av} (s)	ITR (bpm)	VI thresh	RMI thresh	M_{av}	Chance level	p_a	t_{av} (s)	ITR (bpm)
P01	1.00	0.80	3.03	0.33	0.68	16.00	1.36	0.55	0.60	4.84	0.21	0.42	1.23	8.16
P02	1.00	0.80	3.10	0.32	0.52	16.00	0.43	0.25	0.60	4.45	0.22	0.39	1.10	5.25
P03	1.00	0.80	3.16	0.32	0.45	16.00	0.22	0.00	0.65	3.00	0.33	0.48	1.00	4.18
P04	0.00	0.85	2.77	0.36	0.45	1.00	1.51	-	-	-	-	-	-	-
P05	0.20	0.55	3.74	0.27	0.42	1.10	4.25	0.00	0.45	6.00	0.17	0.32	1.00	6.29
P06	0.00	0.50	4.00	0.25	0.48	1.00	10.96	1.00	0.60	4.74	0.21	0.42	18.00	0.53
P07	0.85	0.90	2.19	0.46	0.55	1.74	0.85	0.00	0.45	6.00	0.17	0.35	1.00	8.92
P08	0.00	0.95	2.00	0.50	0.65	1.00	3.70	0.90	0.60	4.50	0.22	0.50	2.58	6.20
P09	0.70	0.80	3.16	0.32	0.58	1.48	8.62	0.15	0.55	5.23	0.19	0.45	1.19	12.68
P10	0.70	0.65	3.61	0.28	0.42	1.39	2.92	-	-	-	-	-	-	-
P11	0.75	0.80	2.77	0.36	0.58	1.26	6.87	0.40	0.50	5.71	0.18	0.29	1.16	2.98
P12	0.20	0.75	3.10	0.32	0.65	1.19	15.76	-	-	-	-	-	-	-
P13	0.00	0.85	2.90	0.34	0.61	1.00	12.92	0.15	0.50	5.61	0.18	0.32	1.03	5.08
mean	0.49	0.77	3.04	0.34	0.54	4.63	5.41	0.34	0.55	5.01	0.21	0.39	2.93	6.03
(std)	(0.43)	(0.13)	(0.56)	(0.07)	(0.09)	(6.49)	(5.18)	(0.37)	(0.07)	(0.92)	(0.05)	(0.07)	(5.32)	(3.36)

Figure 4.6:   Results table of the proposed fuzzy-based system. Adapted from
preprint of [43] (Appendix A).

K-Attack: Inclusive Videogame Based on SSVEP for Attention Training

The main contribution of this work (see third paragraph of Section 3.2.1) was to de-
velop a functional mobile-BCI-based and cloud-computing-based application for the

training of visual attention and to successfully use it in out-of-lab conditions such as the I Telecommunication Meeting of the University of Granada (see Figure 4.7 for a example of SSVEP-based attention detection). Despite the real scope of the application is still under study, it might be used as a support tool for the training of attention in people with attentional disorders such as the ADHD. Thanks to the videogame-based environment, it is suitable for children and may contribute to social integration. Specially in children with autism who are more likely to interact in video-based and game-based environments [100]. Detailed information can be found in the original articles [13, 14].
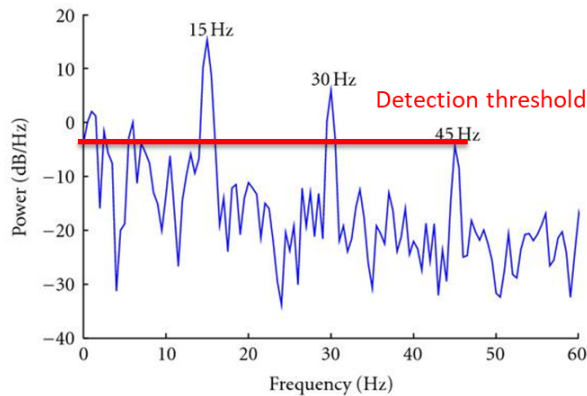
Figure 4.7:   Detection of SSVEP at 15 Hz from PSD.

4.2.2   Stress Assessment and Detection

Stress Assessment by Prefrontal Relative Gamma

The main finding of this work (see second paragraph of Section 3.2.2) was to demonstrate the usefulness of the prefrontal relative gamma (RG) as stress biomarker. It was proved to correlate with the heart rate (HR) (see Figure 4.8), the self-perceived stress level and the expected stress level according to the experiment design. The assessment of stress level by the prefrontal RG has a number of benefits. For example, the temporal resolution. It is higher than in other well-established stress markers such as the HR or the cortisol. Moreover, the measurement of RG only requires a few electrodes located at non-hairy positions (i.e., quick and dry setup). Therefore, it can be used in dry-electrode-based and mobile-BCI-based applications for the real-time and ubiquitous assessment of stress, thus potentially helping to

improve people's quality of life. Detailed information can be found in the original article (Appendix B or [23]).
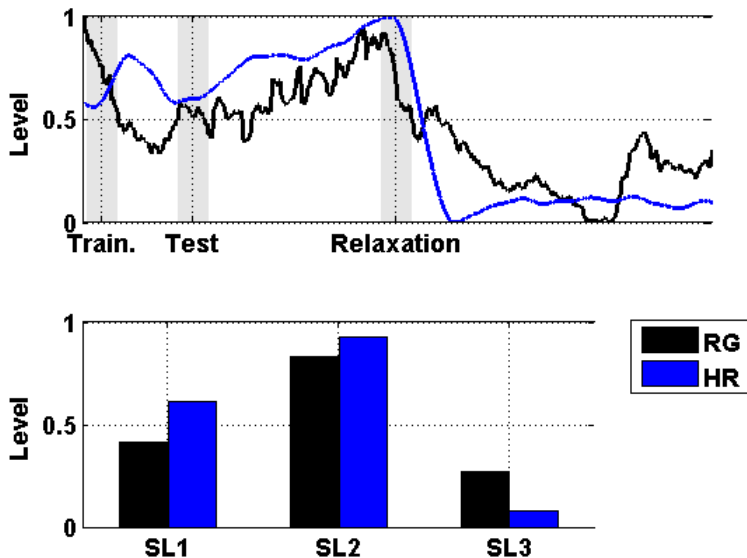
Figure 4.8:   Comparison between the relative gamma and the heart rate. On the top: the evolution of the level of prefrontal RG together with the HR averaged across the six subjects and then normalized. At the bottom: the mean value in SL1, SL2, and SL3. From [23].

Blue Lighting Accelerates Post-Stress Relaxation: Results of a Preliminary Study

The main finding of this work (see third paragraph of Section 3.2.2) was to demonstrate that blue lighting accelerates the relaxation process after acute psychosocial stress (e.g., after having an argument with a friend) in comparison with conventional white lighting. In particular, the relaxation time decreased by approximately three-fold by using blue lighting (1.1 vs. 3.5 minutes). In addition, whatever color was used in the relaxation room, more than circa four minutes did not produce extra benefit (see Figure 4.9). These results were based on electrophysiological measures of stress. More specifically, the relative gamma. Psychologists and other experts that use lighting in their therapies could benefit from them. Furthermore, the findings of this work could have a relevant impact on emerging technologies such as neuromarketing (e.g., use of blue lighting before a negotiation) and in daily-life applications (e.g., use of blue lighting during stressful periods of work). Apart from

the scientific impact, this work has drawn the attention of a considerable number of national and international mass media such as Reuters (see [101] for a journalistic reportage of this media agency), Hindustan Times (see [102]), Sience Daily ([103]), EurekAlert ([104]), Canal UGR ([105]), Investigación y Ciencia ([106]), Europa Press ([107]) and Efe ([108]). Detailed information can be found in the original article (Appendix D or [80]).
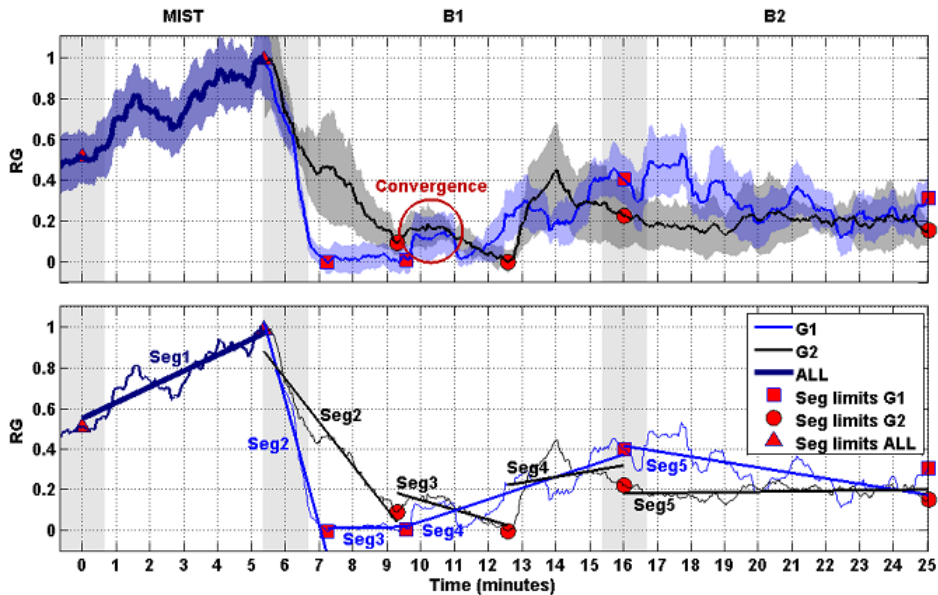
Figure 4.9:   Relative gamma and segments. On the top: Curves represent the normalized RG of G1 (blue) and G2 (black). The SEM of the RG is displayed behind the RG curves. The red circumference indicates the time period in which the curves of both groups converge. At the bottom: The curves of the upper plot are simplified by their respective linear trends (linearized), thus given rise to segments (i.e., Seg1, Seg2, Seg3, Seg4 and Seg5). Red markers indicate limits of the segments. From [80].

Portable System for Real-Time Detection of Stress Level

The main contribution of this work (see fourth paragraph of Section 3.2.2) was to develop and to prove the usefulness of a portable system for real-time detection of stress level usign RABio w8. The system was successfully validated. It was able to classify three levels of stress with up to 86 % of accuracy by combining multiple features from four different biosignals (see Figure 4.10). In particular, the system

combines the relative gamma, the heart rate, the trapezius activity (TA) and the
skin conductance (SC). It could be used as a reliable mobile-BCI-based application
for ubiquitous and real-time stress monitoring, detection, and prevention in daily
life (e.g., prevention of job stress and stress monitoring at school), thus having a
relevant impact on society by improving people's health and quality of life. Detailed
information can be found in the original article (Appendix F or [24]).

Participant	RG, HR, TA	RG, HR, SC	RG, TA, SC	HR, TA, SC	RG, HR, TA, SC
1	91 ± 4	79 ± 6	84 ± 5	92 ± 4	92 ± 4
2	82 ± 6	78 ± 6	83 ± 6	75 ± 6	82 ± 6
3	77 ± 6	93 ± 4	82 ± 6	92 ± 4	93 ± 4
4	68 ± 7	69 ± 7	78 ± 6	82 ± 6	83 ± 6
5	93 ± 4	84 ± 5	73 ± 7	84 ± 5	84 ± 5
6	93 ± 4	97 ± 3	72 ± 7	98 ± 2	98 ± 2
7	86 ± 5	87 ± 5	67 ± 7	89 ± 4	90 ± 4
8	74 ± 6	75 ± 6	64 ± 7	71 ± 7	74 ± 6
9	81 ± 6	80 ± 6	67 ± 7	76 ± 6	81 ± 6
10	72 ± 7	77 ± 6	79 ± 6	79 ± 6	78 ± 6
Mean ± Std	**82 ± 9**	**82 ± 8**	**75 ± 7**	**84 ± 9**	**86 ± 8**

Figure 4.10:   Probability of successful detection of stress level using three or all
the stress markers as features for the leave one-subject-out cross validation. From
[24].

4.2.3   Secure Password Generation Based on EEG

**Human Neuro-Activity for Securing Body Area Networks: Application
of Brain-Computer Interfaces to People-Centric Internet of Things**

The main finding of this work (see second paragraph of Section 3.2.3) was to over-
come previously published findings in terms of password security (based on NIST
test performance) by using the proposed processed-EEG-based method. It gener-
ates much faster sequences with very low latency and inconsiderable computational
cost, in comparison with other ECG-based methods. In addition, it can be used
with a single-channel EEG headset since it only requires one channel located at the
top of the head. The proposed method is a specific implementation of the human-
in-the-loop paradigm, in which humans and devices help one another. Figures and
detailed information can be found in the preprint (Appendix E) or in the original
article [81].

Securing Passwords Beyond Human Capabilities with a Wearable Neuro-Device

The main finding of this work (see third paragraph of Section 3.2.3) was to demonstrate the usefulness of raw EEG data as an efficient option for the generation of secure passwords in mobile scenarios. The security of passwords generated by RABio w8 from EEG signals was higher than the security of manually generated passwords and similar to the security of passwords generated by a computer. As mentioned in Section 3.2.3, the devices of a WBAN cannot generate secure random passwords for encryption due to the limited hardware resources. The results of this work open a door in this regard. Figures and detailed information can be found in the original article [84].

4.2.4 Other Research

A Mobile Brain-Computer Interface for Clinical Applications: From the Lab to the Ubiquity

The main contribution of this work (see second paragraph of Section 3.2.4) was to develop and to demonstrate the robustness of a mobile-BCI-based and cloud-computing-based application for ubiquitous and out-of-lab visual evoked potentials test. The performance of the application under very hostile realistic conditions was proved and compared with the performance in laboratory conditions. The results of this work contribute to the research on mobile-BCI-based applications for clinical practice. Figures and detailed information can be found in the original article [34]. Regarding the clinical case of central serous chorioretinopathy, the results of the VEP tests (performed with the developed application) agreed with the clinical diagnosis, after the diagnosis of the pathology and after the remission of the pathology. Figure 4.11 shows these results. After the diagnosis of the pathology, the affected eye (i.e., right eye) presented an attenuated and delayed P100 (i.e., positive peak around 100 ms after the stimulus onset) in comparison with the healthy eye (i.e., left eye). After the remission of the pathology, both eyes presented similar VEPs. These results suggest that this application may be useful in clinical practice. Nevertheless, a full clinical validation should be conducted.
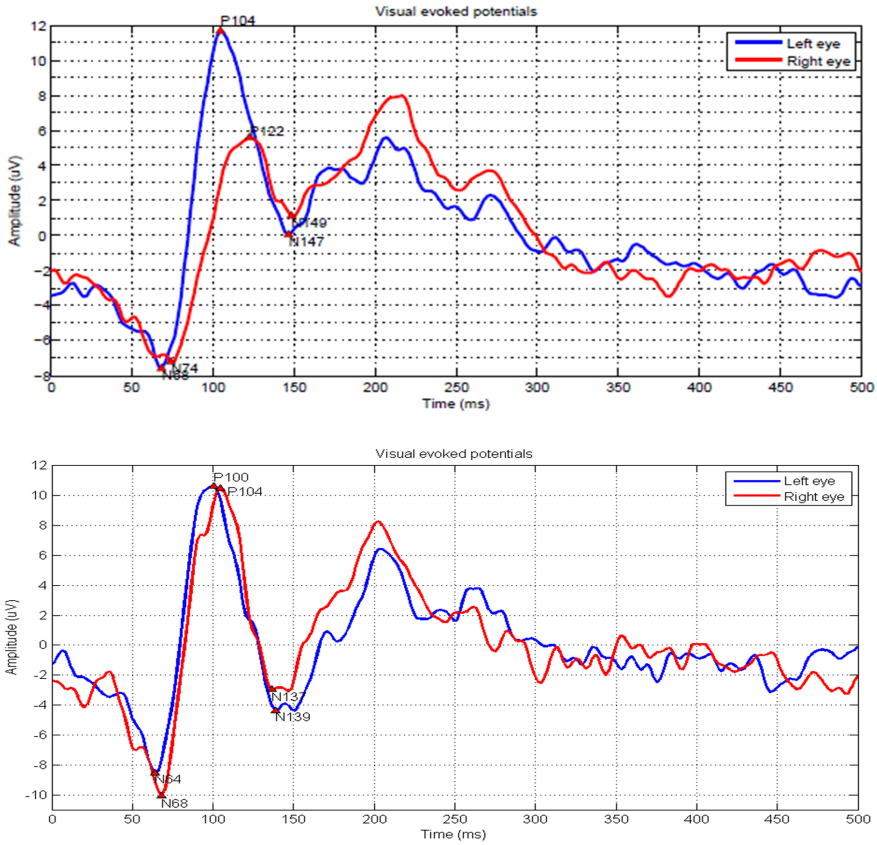
Figure 4.11:   Results of the VEP tests. On the top: test performed during the
pathology. At the bottom: test performed after the remission of the pathology.

Setting the Parameters for an Accurate EEG-Based Emotion Recognition System

The main contribution of this work (see third paragraph of Section 3.2.4) was to
set the parameters for a signal processing methodology (i.e., preprocessing, feature
extraction and classification) for a EEG-based emotion detection system. The
results of this work help to find the most suitable features to obtain an accurate
and reliable classification of positive and negative emotions through EEG data.
Figures and detailed information can be found in the original article [93].

EEG Topographies Provide Subject-Specific Correlates of Motor Control

The main finding of this work (see fourth paragraph of Section 3.2.4) was to demonstrate the correlation of EEG microstates with muscle synergies during reaching and grasping tasks. This suggests that temporal dynamics of microstates encode motor execution. This is supported by the results of microstate-based motor decoding (65 % of accuracy classifying four grasping types). The integration of non-invasive cortico-motor signals (i.e., EEG and EMG) may contribute to the understanding of sensorimotor disorders and to the development of customized neurorehabilitation protocols. Figures and detailed information can be found in the original article [94].

State of the Art of Neurotechnologies for Assistance and Rehabilitation in Spain

The main contribution of this work (see fifth paragraph of Section 3.2.4) was to clarify the state of the art of neurotechnologies for assistance and rehabilitation in Spain. Figures and detailed information can be found in the original article [95].

Chapter 5

Conclusions

This chapter provides a summary of the main contributions, application fields, limitations and future work of this thesis.

5.1 General Conclusions and Contributions

This multidisciplinary thesis have been written by using the format of "group of publications". A bio-signal acquisition system has been developed. Its scalable and adaptable design enables its use in specific applications. Indeed, it has been used in several applications and field-research studies. The specific discussion and conclusions of every single work forming this thesis can be found in the annexed articles, as well as in other publications cited in Section 1.4.

There are three main contributions in this thesis. The first contribution is related to the first particular objective of this thesis and the last two contributions are related to the second particular objective (see Section 1.2):

- After analyzing the hardware and software requirements of mobile-BCI-based applications, limitations of current commercial wireless low-cost EEG acquisition systems have been discussed. This has been used to develop a full (i.e., hardware and software) and functional system, the so-called RABio w8. This approach improves the existing commercial systems in terms of cost, configurability, portability, usability, electrical safety and autonomy. RABio w8

provides simultaneous and configurable acquisition and processing of multiple biosignals (e.g., EEG, ECG, and EMG) in real-time, what is very useful for specific applications. Regarding the existing signal processing algorithms, there are a number of advanced and suitable feature extraction and classification approaches with real-time capability. However, there should be a call for cloud-computing solutions with stimulation and real-time feedback presented in mobile devices. This enables the use of computationally intensive algorithms remotely, thus not compromising the portability and usability of the system (more hardware in the cloud). The RABio w8 system can be easily integrated into cloud-computing-based applications. The developed system may be helpful for the BCI research community and, in the future, for the general public, being a reliable instrument for field studies. In relation to the artifact removal procedures for mobile-BCI-based applications, they are still challenging and further research in needed.

- In addition, several ubiquitous out-of-lab applications based on mobile BCI and on cloud-computing have been developed in this thesis. In particular, for the detection and training of attention, for the assessment and detection of stress level, for the generation of secure passwords through EEG signals and for the diagnosis of visual-system-related pathologies through visual evoked potentials. In most cases the RABio w8 system was used. These applications have demonstrated a considerable potential, with the option of having a relevant impact on society.

- Finally, all the development has been applied to field-research studies related to physiological, cognitive and affective computing. Specifically, in studies related to attention, stress, EEG-based password generation and visual evoked potentials, among others. A relevant amount of valuable scientific results have been obtained and published in international journals with impact factor and congresses (see Section 1.4), thus proving the usefulness of the developed technology. These results could generate a relevant impact on the research community and, potentially, on various areas of society.

5.2   Application Fields

Application fields of this thesis include:

- Work and military defense: cognitive load evaluation, attention detection and stress prevention.

- Education: attention training, videogame-based learning and inclusive learning applications.

- Mental health: emotional state evaluation, stress prevention, colored-lighting-based therapies and mental illness diagnosis.

- Sports and e-sports: attention training and reaction speed training.

- Art: evaluation of emotional and physiological responses to artistic works.

- Communications: bio-based password generation and bio-synchronized transmission.

5.3 Limitations and Future Work

Mobile BCI and wireless EEG acquisition systems are in continuous development and improvement. Although some aspects have been addressed in this thesis, there still is a number of limitations that should be overcome in the future, in order to get fully usable and functional systems and applications.

In relation to the hardware, the biggest challenge is the production of reliable and high-quality dry electrodes. The preparation required by gel-based electrodes causes fatigue and needs the presence of technical staff. Despite some approaches have been proposed and tested under specific conditions, there still are a number of important lacks. Without any doubt, the standardization of dry electrodes would be a milestone in mobile BCI systems. In addition, a more portable (and even wearable) version of the EEG cap embedding the whole electronics is feasible and should be developed.

Regarding the communications part, advanced communication interfaces such as Wifi, 4G and 5G should be incorporated in cloud-computing applications. In the applications developed in this thesis, data are sent from the acquisition system to a portable device (typically smartphone or laptop) that is used as gateway to the cloud. This limits the portability and usability of the system. Last-generation communications (i.e., 5G) will have a relevant role in mobile-BCI-based applications. The extremely low latency of 5G will enable real-time operation of more complex applications (e.g., more channels simultaneously, interactivity with the BCI users video-frame by video-frame, etc.). Other important point in communications is the security. In this thesis, non-secure communication protocols were implemented. In a final version, encrypted communications should be provided. The generation of

secure passwords for encryption could be based on EEG signals as shown in some
articles of this thesis.

As for the signal processing part, artifact removal is the major challenge. Fur-
ther research is needed in order to find a standardized procedure that meets the
requirements of mobile-BCI-based applications.

Finally, new applications applied to field-research should be proposed and con-
ducted, both in clinical and daily-life settings. Examples might include diagnosis
of brain-related disorders such as dementia, Alzheimer's disease and multiple sclero-
sis. Several grants have been requested to develop this future work in collaboration
with the Hospital Virgen de las Nieves of Granada.

Bibliography

[1] H. Berger, "Über das Elektrenkephalogramm des Menschen," *Archiv für Psychiatrie und Nervenkrankheiten*, vol. 87, pp. 527–570, dec 1929.

[2] N. Birbaumer, N. Ghanayim, T. Hinterberger, I. Iversen, B. Kotchoubey, A. Kübler, J. Perelmouter, E. Taub, and H. Flor, "A spelling device for the paralysed.," *Nature*, vol. 398, pp. 297–8, mar 1999.

[3] J. R. Wolpaw, D. J. McFarland, G. W. Neat, and C. a. Forneris, "An EEG-based brain-computer interface for cursor control.," *Electroencephalography and clinical neurophysiology*, vol. 78, no. 3, pp. 252–259, 1991.

[4] G. Pfurtscheller, D. Flotzinger, and J. Kalcher, "Brain-Computer Interface—a new communication device for handicapped persons," *Journal of Microcomputer Applications*, vol. 16, pp. 293–299, jul 1993.

[5] J. Minguillon, M. A. Lopez-Gordo, and F. Pelayo, "Trends in EEG-BCI for daily-life: Requirements for artifact removal," *Biomedical Signal Processing and Control*, vol. 31, pp. 407–418, 2017.

[6] M. Bamdad, H. Zarshenas, and M. A. Auais, "Application of BCI systems in neurorehabilitation: a scoping review.," *Disability and rehabilitation. Assistive technology*, pp. 1–10, jan 2015.

[7] J. J. Daly and J. E. Huggins, "Brain-computer interface: current and emerging rehabilitation applications.," *Archives of physical medicine and rehabilitation*, vol. 96, pp. S1–7, mar 2015.

[8] F. Cincotti, D. Mattia, F. Aloise, S. Bufalari, G. Schalk, G. Oriolo, A. Cherubini, M. G. Marciani, and F. Babiloni, "Non-invasive brain-computer interface system: Towards its application as assistive technology," *Brain Research Bulletin*, vol. 75, no. 6, pp. 796–803, 2008.

[9] Y. Li, J. Pan, F. Wang, and Z. Yu, "A hybrid BCI system combining P300 and SSVEP and its application to wheelchair control.," *IEEE transactions on bio-medical engineering*, vol. 60, pp. 3156–66, nov 2013.

[10] F. Velasco-Álvarez and R. Ron-Angevin, "Audio-Cued SMR Brain-Computer Interface to Drive a Virtual Wheelchair," in *11th International Work-Conference on Artificial Neural Networks*, 2011.

[11] F. Velasco-Álvarez, R. Ron-Angevin, L. da Silva-Sauer, and S. Sancha-Ros, "Audio-cued motor imagery-based brain-computer interface: Navigation through virtual and real environments," *Neurocomputing*, vol. 121, pp. 89–98, 2013.

[12] L. Liao, C. Chen, and I. Wang, "Gaming control using a wearable and wireless EEG-based brain-computer interface device with novel dry foam-based sensors," *Journal of NeuroEngineering and Rehabilitation*, vol. 9, no. 5, pp. 1–11, 2012.

[13] J. Minguillón, E. Pérez-Valero, F. Pelayo, and M. Á. López-Gordo, "K-Attack: Videojuego inclusivo basado en SSVEP," *Cognitive Area Networks*, vol. 5, no. 1, pp. 77–80, 2018.

[14] E. Pérez Valero, J. Minguillón, and M. Á. López Gordo, "Neuroingeniería lúdica e inclusión," in *XXXIII Simposium Nacional de la Unión Científica Internacional de Radio (URSI 2018)*, (Granada), p. 137, 2018.

[15] J. L. Park, M. M. Fairweather, and D. I. Donaldson, "Making the case for mobile cognition: EEG and sports performance.," *Neuroscience and biobehavioral reviews*, vol. 52, pp. 117–130, feb 2015.

[16] Y. Wang, Y. Wang, and T. Jung, "A cell-phone-based brain–computer interface for communication in daily life," *Journal of neural engineering*, vol. 8, no. 2, pp. 1–5, 2011.

[17] C. Guger, C. Holzner, and C. Grönegress, "Control of a smart home with a brain-computer interface," 2008.

[18] C. Lin, F. Lin, and S. Chen, "EEG-based brain-computer interface for smart living environmental auto-adjustment," *Journal of Medical and Biological Engineering*, vol. 30, no. 4, pp. 237–245, 2010.

[19] C. Lin, B. Lin, F. Lin, and C. Chang, "Brain computer interface-based smart living environmental auto-adjustment control system in UPnP home networking," *Systems Journal, IEEE*, vol. 8, no. 2, 2014.

[20] C. Lin, C. Chang, and B. Lin, "A real-time wireless brain–computer interface system for drowsiness detection," *Biomedical Circuits and Systems, IEEE Transactions on*, vol. 4, no. 4, pp. 214 – 222, 2010.

[21] R. Matthews and P. Turner, "Real time workload classification from an ambulatory wireless EEG system using hybrid EEG electrodes," *Engineering in Medicine and Biology Society, 2008. EMBS 2008. 30th Annual International Conference of the IEEE*, pp. 5871 – 5875, 2008.

[22] B. Hu, H. Peng, Q. Zhao, B. Hu, D. Majoe, F. Zheng, and P. Moore, "Signal Quality Assessment Model for Wearable EEG Sensor on Prediction of Mental

Stress.," *IEEE transactions on nanobioscience*, vol. 14, no. 5, pp. 553–61, 2015.

[23] J. Minguillon, M. A. Lopez-Gordo, and F. Pelayo, "Stress Assessment by Prefrontal Relative Gamma," *Frontiers in Computational Neuroscience*, vol. 10, no. September, pp. 1–9, 2016.

[24] J. Minguillon, E. Perez, M. Lopez-Gordo, F. Pelayo, and M. Sanchez-Carrion, "Portable System for Real-Time Detection of Stress Level," *Sensors (Switzerland)*, vol. 18, p. 2504, aug 2018.

[25] S. Lee, Y. Shin, S. Woo, K. Kim, and H.-n. Lee, "Review of Wireless Brain-Computer Interface Systems," *Brain-Computer Interface Systems - Recent Progress and Future Prospects*, 2013.

[26] H. Jasper, "The ten twenty electrode system of the international federation," *Electroencephalography and clinical neurophysiology*, 1958.

[27] M. A. Lopez-Gordo, D. Sanchez Morillo, and F. Pelayo Valle, "Dry EEG electrodes," *Sensors (Switzerland)*, vol. 14, no. 7, pp. 12847–12870, 2014.

[28] G. R. Müller-Putz and G. Pfurtscheller, "Control of an electrical prosthesis with an SSVEP-based BCI," *IEEE Transactions on Biomedical Engineering*, vol. 55, no. 1, pp. 361–364, 2008.

[29] H.-J. Hwang, K. Kwon, and C.-H. Im, "Neurofeedback-based motor imagery training for brain-computer interface (BCI).," *Journal of neuroscience methods*, vol. 179, pp. 150–6, apr 2009.

[30] M. Marchetti and K. Priftis, "Effectiveness of the P3-speller in brain-computer interfaces for amyotrophic lateral sclerosis patients: a systematic review and meta-analysis.," *Frontiers in neuroengineering*, vol. 7, p. 12, jan 2014.

[31] A. N. Belkacem, D. Shin, H. Kambara, N. Yoshimura, and Y. Koike, "Online classification algorithm for eye-movement-based communication systems using two temporal EEG sensors," *Biomedical Signal Processing and Control*, vol. 16, pp. 40–47, feb 2015.

[32] Y. P. Lin, Y. Wang, and T. P. Jung, "A mobile SSVEP-based brain-computer interface for freely moving humans: The robustness of canonical correlation analysis to motion artifacts," *Proceedings of the Annual International Conference of the IEEE Engineering in Medicine and Biology Society, EMBS*, pp. 1350–1353, 2013.

[33] D. E. Callan, G. Durantin, and C. Terzibas, "Classification of single-trial auditory events using dry-wireless EEG during real and motion simulated flight.," *Frontiers in systems neuroscience*, vol. 9, p. 11, jan 2015.

[34] J. Minguillon, M. A. Lopez-Gordo, C. Morillas, and F. Pelayo, "A Mobile Brain-Computer Interface for Clinical Applications: From the Lab to the Ubiquity," in *7th International Work-Conference on the Interplay Between Natural and Artificial Computation* (J. M. Ferrández Vicente, J. R. Álvarez-Sánchez, F. De la Paz López, J. Toledo Moreo, and H. Adeli, eds.), vol. LNCS 10338, (Corunna), pp. 68–76, Springer International Publishing, 2017.

[35] S. Fazli, J. Mehnert, J. Steinbrink, G. Curio, A. Villringer, K.-R. Müller, and B. Blankertz, "Enhanced performance by a hybrid NIRS-EEG brain computer interface.," *NeuroImage*, vol. 59, pp. 519–29, jan 2012.

[36] Y. Tomita, F.-B. Vialatte, G. Dreyfus, Y. Mitsukura, H. Bakardjian, and A. Cichocki, "Bimodal BCI using simultaneously NIRS and EEG.," *IEEE transactions on bio-medical engineering*, vol. 61, pp. 1274–84, apr 2014.

[37] J. H. Lim, J. H. Lee, H. J. Hwang, D. H. Kim, and C. H. Im, "Development of a hybrid mental spelling system combining SSVEP-based brain–computer

interface and webcam-based eye tracking," *Biomedical Signal Processing and Control*, vol. 21, pp. 99–104, aug 2015.

[38] C. Brennan, P. McCullagh, G. Lightbody, L. Galway, D. Feuser, J. L. González, and S. Martin, "Accessing Tele-Services Using a Hybrid BCI Approach," in *Advances in Computational Intelligence. IWANN 2015. Lecture Notes in Computer Science* (I. Rojas, G. Joya, and A. Catala, eds.), vol. 9094, pp. 110–123, Springer, Cham, 2015.

[39] Á. Costa, E. Hortal, E. Iáñez, and J. M. Azorín, "A Supplementary System for a Brain-Machine Interface Based on Jaw Artifacts for the Bidimensional Control of a Robotic Arm," *PloS one*, vol. 9, no. 11, p. e112352, 2014.

[40] S. Kumar and F. Sahin, "A framework for a real time intelligent and interactive Brain Computer Interface," *Computers & Electrical Engineering*, vol. 43, pp. 193–214, apr 2015.

[41] T. Nguyen, A. Khosravi, D. Creighton, and S. Nahavandi, "EEG signal classification for BCI applications by wavelets and interval type-2 fuzzy logic systems," *Expert Systems with Applications*, vol. 42, pp. 4370–4380, jun 2015.

[42] T. Nguyen, A. Khosravi, D. Creighton, and S. Nahavandi, "Fuzzy system with tabu search learning for classification of motor imagery data," *Biomedical Signal Processing and Control*, vol. 20, pp. 61–70, jul 2015.

[43] J. Minguillon, M. A. Lopez-Gordo, and F. Pelayo, "Detection of Attention in Multi-Talker Scenarios: a Fuzzy Approach," *Expert Systems with Applications*, vol. 64, pp. 261–268, 2016.

[44] M. K. Hazrati and A. Erfanian, "An online EEG-based brain-computer interface for controlling hand grasp using an adaptive probabilistic neural network.," *Medical engineering & physics*, vol. 32, pp. 730–9, sep 2010.

[45] M. A. Lopez, H. Pomares, M. Damas, E. Madrid, A. Prieto, F. Pelayo, and E. M. De La Plaza Hernandez, "Use of ANNs as classifiers for selective attention brain-computer interfaces," *Lecture Notes in Computer Science including subseries Lecture Notes in Artificial Intelligence and Lecture Notes in Bioinformatics*, vol. 4507 LNCS, pp. 956–963, 2007.

[46] R. Ron-Angevin, M. A. Lopez, and F. Pelayo, "The training issue in brain-computer interface: A multi-disciplinary field," *Lecture Notes in Computer Science (including subseries Lecture Notes in Artificial Intelligence and Lecture Notes in Bioinformatics)*, vol. 5517 LNCS, no. PART 1, pp. 666–673, 2009.

[47] T. Thompson, T. Steffert, T. Ros, J. Leach, and J. Gruzelier, "EEG applications for sport and performance.," *Methods (San Diego, Calif.)*, vol. 45, pp. 279–88, aug 2008.

[48] H. Yuan and B. He, "Brain-computer interfaces using sensorimotor rhythms: current state and future perspectives.," *IEEE transactions on bio-medical engineering*, vol. 61, pp. 1425–35, may 2014.

[49] C. Guger, S. Daban, E. Sellers, C. Holzner, G. Krausz, R. Carabalona, F. Gramatica, and G. Edlinger, "How many people are able to control a P300-based brain-computer interface (BCI)?," *Neuroscience Letters*, vol. 462, no. 1, pp. 94–98, 2009.

[50] C. Vidaurre and B. Blankertz, "Towards a cure for BCI illiteracy," *Brain topography*, 2010.

[51] Z. Gu, Z. Yu, Z. Shen, and Y. Li, "An online semi-supervised brain-computer interface.," *IEEE transactions on bio-medical engineering*, vol. 60, pp. 2614–23, sep 2013.

[52] E. Yin, Z. Zhou, J. Jiang, F. Chen, Y. Liu, and D. Hu, "A speedy hybrid BCI spelling approach combining P300 and SSVEP.," *IEEE transactions on bio-medical engineering*, vol. 61, pp. 473–83, feb 2014.

[53] J. Long, Y. Li, T. Yu, and Z. Gu, "Target selection with hybrid feature for BCI-based 2-D cursor control," *IEEE Transactions on Biomedical Engineering*, vol. 59, no. 1, pp. 132–140, 2012.

[54] C. J. Bell, P. Shenoy, R. Chalodhorn, and R. P. N. Rao, "Control of a humanoid robot by a noninvasive brain-computer interface in humans.," *Journal of neural engineering*, vol. 5, no. 2, pp. 214–220, 2008.

[55] H. J. Hwang, J. H. Lim, Y. J. Jung, H. Choi, S. W. Lee, and C. H. Im, "Development of an SSVEP-based BCI spelling system adopting a QWERTY-style LED keyboard," *Journal of Neuroscience Methods*, vol. 208, no. 1, pp. 59–65, 2012.

[56] E. Yin, Z. Zhou, J. Jiang, Y. Yu, and D. Hu, "A Dynamically Optimized SSVEP Brain-Computer Interface (BCI) Speller.," *IEEE transactions on bio-medical engineering*, vol. 62, pp. 1447–56, jun 2015.

[57] M. A. Lopez-Gordo, F. Pelayo, and A. Prieto, "A high performance SSVEP-BCI without gazing," in *The 2010 International Joint Conference on Neural Networks (IJCNN)*, pp. 1–5, IEEE, jul 2010.

[58] J. T. Gwin, K. Gramann, S. Makeig, and D. P. Ferris, "Removal of movement artifact from high-density EEG recorded during walking and running.," *Journal of neurophysiology*, vol. 103, no. 6, pp. 3526–3534, 2010.

[59] C. Guerrero-mosquera and A. N. Vazquez, "Automatic Removal of Ocular Artifacts from EEG Data using Adaptive Filtering and Independent Component Analysis," *17th European Signal Processing Conference*, no. Eusipco, pp. 2317–2321, 2009.

[60] a. Schlögl, C. Keinrath, D. Zimmermann, R. Scherer, R. Leeb, and G. Pfurtscheller, "A fully automated correction method of EOG artifacts in EEG recordings," *Clinical Neurophysiology*, vol. 118, no. 1, pp. 98–104, 2007.

[61] P. Comon, "Independent component analysis, a new concept?," *Signal processing*, vol. 36, no. 3, pp. 287–314, 1994.

[62] W. Kong, Z. Zhou, S. Hu, J. Zhang, F. Babiloni, and G. Dai, "Automatic and direct identification of blink components from scalp EEG.," *Sensors (Basel, Switzerland)*, vol. 13, no. 8, pp. 10783–10801, 2013.

[63] K. T. Sweeney, S. F. McLoone, and T. E. Ward, "The use of ensemble empirical mode decomposition with canonical correlation analysis as a novel artifact removal technique.," *IEEE transactions on bio-medical engineering*, vol. 60, no. 1, pp. 97–105, 2013.

[64] X. Chen, A. Liu, H. Peng, and R. Ward, "A Preliminary Study of Muscular Artifact Cancellation in Single-Channel EEG," *Sensors*, vol. 14, no. 10, pp. 18370–18389, 2014.

[65] P. Kumar and R. Arumuganathan, "Removal of Ocular Artifacts in the EEG through Wavelet Transform without using an EOG Reference Channel," *Int. J. Open Problems Compt. Math.*, vol. 1, no. 3, 2008.

[66] W. Y. Hsu, C. H. Lin, H. J. Hsu, P. H. Chen, and I. R. Chen, "Wavelet-based envelope features with automatic EOG artifact removal: Application to single-trial EEG data," *Expert Systems with Applications*, vol. 39, no. 3, pp. 2743–2749, 2012.

[67] H. Peng, B. Hu, Q. Shi, M. Ratcliffe, Q. Zhao, Y. Qi, and G. Gao, "Removal of ocular artifacts in EEG - An improved approach combining DWT and

ANC for portable applications," *IEEE Journal of Biomedical and Health Informatics*, vol. 17, no. 3, pp. 600–607, 2013.

[68] B. Mijović, M. De Vos, I. Gligorijević, J. Taelman, and S. Van Huffel, "Source separation from single-channel recordings by combining empirical-mode decomposition and independent component analysis," *IEEE Transactions on Biomedical Engineering*, vol. 57, no. 9, pp. 2188–2196, 2010.

[69] N. Mourad and R. K. Niazy, "Automatic correction of eye blink artifact in single channel EEG recording using EMD and OMP," *European Signal Processing Conference*, pp. 1–5, 2013.

[70] H. Zeng, A. Song, R. Yan, and H. Qin, "EOG artifact correction from EEG recording using stationary subspace analysis and empirical mode decomposition.," *Sensors (Basel, Switzerland)*, vol. 13, no. 11, pp. 14839–14859, 2013.

[71] H.-A. T. Nguyen, J. Musson, F. Li, W. Wang, G. Zhang, R. Xu, C. Richey, T. Schnell, F. D. McKenzie, and J. Li, "EOG artifact removal using a wavelet neural network," *Neurocomputing*, vol. 97, pp. 374–389, 2012.

[72] J. Hu, C.-s. Wang, M. Wu, Y.-x. Du, Y. He, and J. She, "Removal of EOG and EMG artifacts from EEG using combination of functional link neural network and adaptive neural fuzzy inference system," *Neurocomputing*, vol. 151, pp. 278–287, 2015.

[73] S. Suja Priyadharsini, S. Edward Rajan, and S. Femilin Sheniha, "A novel approach for the elimination of artefacts from EEG signals employing an improved Artificial Immune System algorithm," *Journal of Experimental & Theoretical Artificial Intelligence*, vol. 3079, no. November, pp. 1–21, 2015.

[74] M. a. Klados, C. Papadelis, C. Braun, and P. D. Bamidis, "REG-ICA: A hybrid methodology combining Blind Source Separation and regression tech-

niques for the rejection of ocular artifacts," *Biomedical Signal Processing and Control*, vol. 6, no. 3, pp. 291–300, 2011.

[75] M. Rakibul Mowla, S.-C. Ng, M. S. Zilany, and R. Paramesran, "Artifacts-matched blind source separation and wavelet transform for multichannel EEG denoising," *Biomedical Signal Processing and Control*, vol. 22, pp. 111–118, 2015.

[76] C. Burger and D. J. van den Heever, "Removal of EOG artefacts by combining wavelet neural network and independent component analysis," *Biomedical Signal Processing and Control*, vol. 15, pp. 67–79, 2015.

[77] S. Loo and R. Barkley, "Clinical utility of eeg in attention deficit hyperactivity disorder," *Applied Neuropsychology*, vol. 12, no. 2, pp. 64–76, 2005.

[78] M. Lopez-Gordo, F. Pelayo, E. Fernandez, and P. Padilla, "Phase-shift keying of EEG signals: Application to detect attention in multitalker scenarios," *Signal Processing*, vol. 117, pp. 165–173, 2015.

[79] K. Dedovic, R. Renwick, N. K. Mahani, V. Engert, S. J. Lupien, and J. C. Pruessner, "The Montreal Imaging Stress Task: using functional imaging to investigate the effects of perceiving and processing psychosocial stress in the human brain.," *Journal of psychiatry & neuroscience : JPN*, vol. 30, no. 5, pp. 319–25, 2005.

[80] J. Minguillon, M. A. Lopez-Gordo, D. A. Renedo-Criado, M. J. Sanchez-Carrion, and F. Pelayo, "Blue lighting accelerates post-stress relaxation: Results of a preliminary study," *PLoS ONE*, vol. 12, no. 10, p. e0186399, 2017.

[81] J. F. Valenzuela-valdés, M. A. López, P. Padilla, J. L. Padilla, and J. Minguillon, "Human Neuro-Activity for Securing Body Area Networks: Application of Brain-Computer Interfaces to People-Centric Internet of Things," *IEEE Communications Magazine*, vol. 55, no. 2, pp. 62–67, 2017.

[82] U. Hoffmann, J.-M. Vesin, T. Ebrahimi, and K. Diserens, "An efficient p300-based brain–computer interface for disabled subjects," *Journal of Neuroscience Methods*, vol. 167, no. 1, pp. 115–125, 2008. Brain-Computer Interfaces (BCIs).

[83] "Nist statistical test suite, `https://bit.ly/2NP99cs`."

[84] M. A. Lopez-Gordo, J. Minguillon, J. F. Valenzuela-Valdes, P. Padilla, J. L. Padilla, and F. Pelayo, "Securing Passwords Beyond Human Capabilities with a Wearable Neuro-Device," in *7th International Work-Conference on the Interplay Between Natural and Artificial Computation* (J. M. Ferrández Vicente, J. R. Álvarez-Sánchez, F. De la Paz López, J. Toledo Moreo, and H. Adeli, eds.), vol. LNCS 10338, (Corunna), pp. 87–95, Springer International Publishing, 2017.

[85] J. Brecelj, "A VEP study of the visual pathway function in compressive lesions of the optic chiasm. Full-field versus half-field stimulation," *Electroencephalography and Clinical Neurophysiology/ Evoked Potentials*, vol. 84, no. 3, pp. 209–218, 1992.

[86] S. Nightingale, K. W. Mitchell, and J. W. Howe, "Visual evoked cortical potentials and pattern electroretinograms in Parkinson's disease and control subjects.," *Journal of neurology, neurosurgery, and psychiatry*, vol. 49, pp. 1280–7, nov 1986.

[87] J. L. Frederiksen, H. B. W. Larsson, J. OlesenI, and B. Stigsby, "MRI, VEP, SEP and biothesiometry suggest monosymptomatic acute optic neuritis to be a first manifestation of multiple sclerosis," *Acta Neurologica Scandinavica*, vol. 83, pp. 343–350, may 1991.

[88] D. L. McCulloch and B. Skarf, "Pattern Reversal Visual Evoked Potentials Following Early Treatment of Unilateral, Congenital Cataract," *Archives of Ophthalmology*, vol. 112, p. 510, apr 1994.

[89] J. C. Folk, H. S. Thompson, D. P. Han, and C. K. Brown, "Visual Function Abnormalities in Central Serous Retinopathy," *Archives of Ophthalmology*, vol. 102, pp. 1299–1302, sep 1984.

[90] D. C. Hood and V. C. Greenstein, "Multifocal VEP and ganglion cell damage: applications and limitations for the study of glaucoma," *Progress in Retinal and Eye Research*, vol. 22, no. 2, pp. 201–251, 2003.

[91] W. M. Carroll and F. L. Mastaglia, "Leber's optic neuropathy: a clinical and visual evoked potential study of affected and asymptomatic members of a six generation family.," *Brain : a journal of neurology*, vol. 102, pp. 559–80, sep 1979.

[92] L. Julkunen, O. Tenovuo, V. Vorobyev, J. Hiltunen, M. Teräs, S. K. Jääskeläinen, and H. Hämäläinen, "Functional brain imaging, clinical and neurophysiological outcome of visual rehabilitation in a chronic stroke patient," *Restorative Neurology and Neuroscience*, vol. 24, no. 2, pp. 123–132, 2006.

[93] J. Sorinas, M. D. Grima Murcia, J. Minguillon, F. Sánchez-Ferrer, M. Val-Calvo, J. M. Ferrández, and E. Fernández, "Setting the Parameters for an Accurate EEG (Electroencephalography)-Based Emotion Recognition System," in *7th International Work-Conference on the Interplay Between Natural and Artificial Computation* (J. M. Ferrández Vicente, J. R. Álvarez-Sánchez, F. De la Paz López, J. Toledo Moreo, and H. Adeli, eds.), vol. LNCS 10337, (Corunna), pp. 265–273, Springer International Publishing, 2017.

[94] E. Pirondini, M. Coscia, J. Minguillon, J. d. R. Millán, D. Van De Ville, and S. Micera, "EEG topographies provide subject-specific correlates of motor control," *Scientific Reports*, vol. 7, no. 1, p. 13229, 2017.

[95] L. J. Barrios, J. Minguillón, F. J. Perales, R. Ron-Angevin, J. Solé-Casals, and M. A. Mañanas, "Estado del Arte en Neurotecnologías para la Asis-

tencia y la Rehabilitación en España: Tecnologías Auxiliares, Trasferencia Tecnológica y Aplicación Clínica," *Revista Iberoamericana de Automática e Informática Industrial RIAI*, vol. 14, no. 4, pp. 355–361, 2017.

[96] J. Minguillón, C. Morillas, F. Pelayo, S. Medina, and M. Á. López-Gordo, "Módulos Plat-EEG para medidas laplacianas con electrodo seco," *Cognitive Area Networks*, vol. 3, no. 1, pp. 69–73, 2016.

[97] J. Minguillón, C. Morillas, F. Pelayo, and M. Á. López-Gordo, "Sistema BCI multiusuario," *Cognitive Area Networks*, vol. 4, no. 1, pp. 49–53, 2017.

[98] "Rabio w8, `http://rabiow.wixsite.com/rabio`."

[99] G. Schalk, D. McFarland, T. Hinterberger, N. Birbaumer, and J. Wolpaw, "BCI2000: A General-Purpose Brain-Computer Interface (BCI) System," *IEEE Transactions on Biomedical Engineering*, vol. 51, pp. 1034–1043, jun 2004.

[100] N. Wilkinson, R. P. Ang, and D. H. Goh, "Online video game therapy for mental health concerns: a review.," *The International journal of social psychiatry*, vol. 54, no. 4, pp. 370–382, 2008.

[101] "Thomson reuters: Blue lighting induces relaxation, say spanish researchers, `https://www.reuters.com/video/2018/04/03/blue-lighting-induces-relaxation-say-spa?videoId=414492805`."

[102] "Hindustan times: Blue lighting helps you fight stress and relax. here's how, `https://www.hindustantimes.com/fitness/blue-lighting-helps-you-fight-stress-and-relax-here-s-how/story-BcQcdpazKfgNjsRtvLkENM.html`."

[103] "Science daily: Blue lighting is scientifically proven to help us relax faster than white lighting after an argument, `https://www.sciencedaily.com/releases/2017/11/171110113936.htm`."

[104] "Eurekalert: Blue lighting is scientifically proven to help us relax faster than white lighting after an argument, `https://www.eurekalert.org/pub_releases/2017-11/uog-bli111017.php`."

[105] "Canal ugr: Demuestran científicamente que la luz azul ayuda a relajarnos más rápido que la blanca después de una discusión, `https://canal.ugr.es/noticia/luz-azul-ayuda-relajarnos`."

[106] "Investigación y ciencia: ¿influye el color de la luz en el proceso de relajación?, `https://www.investigacionyciencia.es/noticias/influye-el-color-de-la-luz-en-el-proceso-de-relajacin-15798`."

[107] "Europa press: Demuestran científicamente que la luz azul relaja más rápido que la blanca tras una discusión, `https://bit.ly/2wIq3mH`."

[108] "Efe: Color azul, vitamina para la mente, `http://www.efedata.com/reportaje/color-azul-vitamina-mente/REPORTA/4/3823/53309`."

Appendix A

Article preprint

Detection of Attention in Multi-Talker Scenarios: a Fuzzy Approach

Jesus Minguillon (minguillon@ugr.es) [1, 2*], M. Angel Lopez-Gordo (malg@ugr.es) [3, 4], Francisco Pelayo (fpelayo@ugr.es) [1]

[1] Department of Computer Architecture and Technology, University of Granada, C/ Periodista Daniel Saucedo Aranda, s/n, 18071 Granada, Spain
[2] Research Centre for Information and Communications Technologies (CITIC), University of Granada, C/ Periodista Rafael Gomez Montero, 2, 18014 Granada, Spain
[3] Signal Theory, Telematics and Communications Department, University of Granada, C/ Periodista Daniel Saucedo Aranda, s/n, 18071 Granada, Spain
[4] Nicolo Association, Churriana de la Vega, Spain

[*] Correspondence:
Jesus Minguillon
+34670878422
minguillon@ugr.es

The detection of auditory attention in multi-talker scenarios is a current topic in electroencephalography (EEG)-based Brain-computer Interface (BCIs). Recent works have demonstrated that attention exerted on one auditory source surrounded by many distracting sources can be detected by an approach based on an m-ary Phase Shift Keying (m-PSK) modulation scheme. However, this promising approach does not regard that EEG is a non-stationary signal, subjected to neuro-plasticity and exposed to the non-linear effects of the attention. Hence, we hypothesized that the performance of the m-PSK detector can be improved by modelling these factors and including them in the detection process. In this paper we propose an adaptive m-PSK detector implemented on fuzzy logic as an efficient and simple way to accomplish it. In this experiment we employed a speech corpus used for the assessment of speech intelligibility in military communication to perform detection of attention to one out of

Article preprint

four and six concurrent voices. Speeches were barely perturbed to evoke 4-PSK and 6-PSK constellations of EEG signals and presented to participants in a forced-attention paradigm. Our fuzzy approach outperformed the performance of previous works based on the m-PSK detector in terms of mean information transfer rate (ITR) and accuracy (4-PSK: ITR 5.41 vs. 1.25 bits/m; p_a 0.54 vs. 0.47; 6-PSK: ITR 6.03 vs. 0.74 bits/m; p_a 0.39 vs. 0.32. This outcome could be applied for the online assessment of attention, as assistive technology in attention impairment, in BCIs or to scale the number of speeches in the multi-talker scenario.

Keywords: Brain–computer interfaces, EEG, selective attention, multi-talker detection, fuzzy classification.

1. Introduction

During the last years, Brain-computer Interface technology (BCI) has been used in multitude of applications, for instance in visual spellers (Birbaumer et al., 1999)(Ron-Angevin, Varona-Moya, da Silva-Sauer, & Carrion-Robles, 2014) for wheelchair control (Li et al., 2013), for simple binary volition detectors (e.g., *yes*/*no*) (Hill et al., 2014), for classification and detection of covert visual attention (Lopez-Gordo, Pelayo, & Prieto, 2010) and even in the auditory modality (Höhne & Tangermann, 2014)(Halder et al., 2010).

In this context, new uses and applications for BCIs such as detection of selective attention to auditory sources have emerged. This cognitive ability enables one to attend a target source and ignore the others by means of concomitant cognitive processes (Ikeda et al., 2010). There are examples of it in BCI literature. For instance, in these studies (Kubanek, Brunner, Gunduz, Poeppel, & Schalk, 2013)(Martin et al., 2014) two auditory sources were presented simultaneously to the participants. The authors evidenced that the reconstruction of the envelope

of the attended speech can be obtained by direct analysis of that of the gamma band of electrocorticography (ECoG) signals.

A different approach for the detection of attention in dichotic listening tasks is based on digital modulation of electroencephalography (EEG) signals. In this approach, speeches are barely perturbed to evoke a constellation of Binary Phase-Shift Keying (BPSK) signals (Lopez-Gordo, Fernandez, Romero, Pelayo, & Prieto, 2012)(Lopez-Gordo, Pelayo, Prieto, & Fernandez, 2012)(Lopez-Gordo & Pelayo, 2013). The two counter-phased symbols of the BPSK constellation correspond to the conditions "attend" and "ignore" and the attentional cognitive effort can be robustly detected by means of a BPSK receiver. In these experiments, they obtained an accuracy of 88% with binary detection and an information transfer rate (ITR) of 2 bits/m approximately. In addition to the poor performance of this type of auditory BCI, these three studies were limited to only two simultaneous speeches. Other studies tried to overcome these limitations by developing an attention detector for multi-talker scenarios. The authors in (Lopez-Gordo, Pelayo, Fernandez, & Padilla, 2015) digitally modulated sentences taken form a speech corpus used for the assessment of speech intelligibility in military communication (sentences from the Coordinate Response Measure speech corpus (CRM) (Bolia, Nelson, Ericson, & Simpson, 2000). They used 4-PSK and 6-PSK modulations to detect the attended speech among 4 and 6 concurrent speeches. Although this experiment probed that detection of attention in multi-talker scenarios was possible by means of a m-PSK modulation scheme, the results were poor (an accuracy of 0.47% with four-symbols detection and an ITR of 1.25 bits/m approximately) and they did not significantly improved those of the dichotic modality. As far as we know, the m-PSK is the only BCI approach capable to detect attention in multi-talker scenarios (up to six concurrent speeches).

Article preprint

Improvements to the 4-PSK/6-PSK scheme can be tried in terms of the number of speeches and the performance. Since a SNR of -6 dB could be close to the human limit of what selective attention can filter (Boone, 2008), it seems unreasonable to try to improve the number of concurrent speeches further than 6 (SNR of -7 dB circa). In regard of performance, the use of an m-PSK receiver for the detection of symbols from an m-PSK constellation is optimal in terms of mean square error under some typically-accepted general assumptions. However, EEG signals and attentional paradigms do not meet some of these general assumptions (e.g., i) EEG signals are not stationary; ii) the brain structure that generates them cannot be considered as a linear time-invariant system due to the neuro-plasticity and cognitive factors). Thus, a way to improve the detection of attention is by evolving the m-PSK receiver to one that considers the nature of EEG signals and attentional effects on them.

In this work we aim to improve the performance of detection of attention to one speech in multi-talker scenarios by means of an adaptive m-PSK detector based on fuzzy logic. Our fuzzy approach improves the m-PSK-based detection by modelling both the m-PSK detector and the effects of attention on EEG signals during the execution of the attentional paradigm. In this study we have worked with the same data set used in a pure m-PSK detection (Lopez-Gordo et al., 2015) for a rapid comparison of performances and expecting an improvement in both ITR and accuracy. The benefit of our more efficient fuzzy approach could be used to scale the multi-talker scenario to more speeches, for the online assessment of attention, as assistive technology, for attention impairment, in neuro-marketing or in Brain–computer interfaces.

Article preprint

2. Detection of Auditory Attention in Multi-talker scenarios: The fuzzy approach

In this section we describe 2.1) the fundament of detection of auditory attention in multi-talker scenarios based on the m-PSK approach as described in (Lopez-Gordo et al., 2015), 2.2-2.3) psycho-physiological aspects of the evocation of EEG signals in attentional paradigms and finally 2.4) describe an adaptive m-PSK detector based on fuzzy logic that outperforms the standard m-PSK detector.

2.1 Modulation of the auditory sources

Detection of attention is performed in units called trials. In each trial, each of the m speeches is modulated by a barely-audible distortion. The distortion consisted of the amplitude modulation of the m speeches with m different pure-tones with the same frequency and different phases (phase shifts 0º, 90º, 180º and 360º for m=4 and 0º, 60º, 120º, 180º, 240º and 300º for m=6) as described in (1).

$$s_n(t) = \frac{1}{2}\left[1 + \sin(2\pi f_p 5 + \beta_n)\right]m_n(t) \tag{1}$$

Where $m_n(t)$ corresponds to one of the CRM speeches, with $n \in \{0,1,\ldots,m-1\}$, β_n is the phase assigned to this message and equals $2\pi n/m$, f_p is the frequency of the pure tone and $s_n(t)$ corresponds to one of the modulated messages delivered to participants. Fig. 1 shows 4-PSK and 6-PSK constellations with phase shifts 90º and 60º respectively.
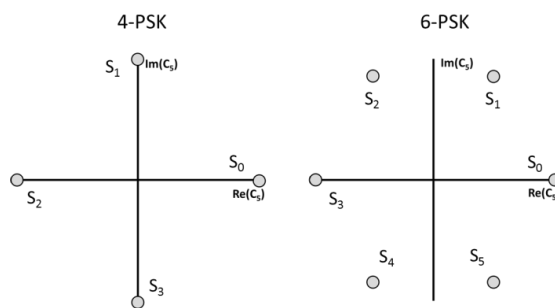
Article preprint

Fig. 1. The m-PSK constellations. The plots of this figure correspond to the representation of the spectral component at 5 Hz of the Fourier transform of the EEG signal. The Cartesian axes are the real and imaginary parts of the symbols of the constellation that are separated 90º or 60 º for 4-PSK or 6-PSK respectively.

2.2 Physiological response: The EEG constellation

The tone pure has a frequency of 5 Hz. This frequency was used because its period is 200 ms. This period fairly matches the time between the stimulus onset and two event-related potentials (ERPs) evoked by the modulated speeches (see Fig. 2). These two ERPS are N1 (negative deflection 100 ms after stimulus onset) and P2 (positive deflection approx. 200 ms after stimulus onset). The repetitive evocation of these two ERPs at a rate of 5 Hz causes a sinusoidal-shaped EEG signal of the same frequency (see Fig. 2). The concurrent presentation of the modulated speeches generates the simultaneous generation of the m symbols of the constellation depicted in Fig. 1. However, since symbols in the constellation are counter-phased, then the physiological response itself would give rise to their mutual cancellation. In other words, this scheme would outcome an m-PSK constellation without EEG signals. At this point is where attention plays a key role.
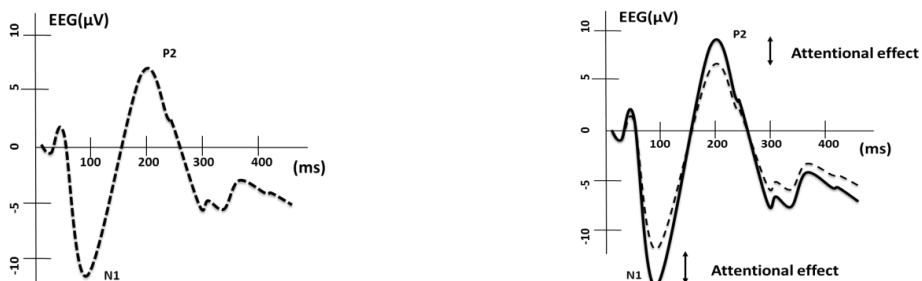
Article preprint
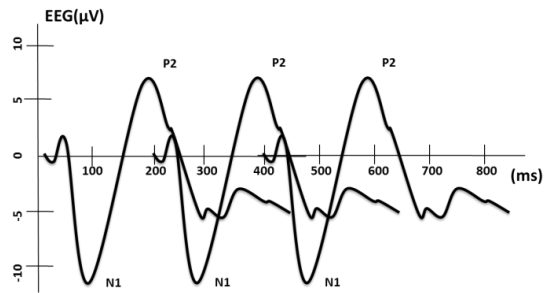
Fig. 2. Evocation of ERPs. Top left: pure physiological response evoked by a single auditory stimulus (e.g. tone pip, click, etc.). It evokes two ERPs, namely N1 and P2). Top right: in an attentional paradigm, the response that corresponds to the selectively attended stimulus is evoked with more amplitude. Therefore, the attentional effort causes an enhancement of N1, and P2 components. Bottom: the attentional effort together with the repetitive presentation of the stimulus at the rate of 5 per second generates a sinusoidal-shaped signal of the constellation.

2.3 Cognitive response: Attentional effects on the physiological response

In the previous paragraph we concluded that a pure physiological response will evoke a zero-constellation of EEG signals. We must state that a well-known effect of selective attention on the attended stimuli is an enhancement of the energy of the corresponding ERP (see Fig. 2). Attentional effort causes modulation of the amplitudes of N1 and P2 and its rationale can be found in multitude of classical studies (Davis, 1964)(Näätanen, 1975)[(Hillyard, Hink, Schwent, & Picton, 1973).

The net effect of selective attention on the constellation of m-PSK signals is that the response of the attended signal is no longer cancelled with its counter-phased symbol. Then, although all EEG physiological responses corresponding to modulated speeches are simultaneously evoked, only the one corresponding to the attended speech will give rise to a symbol in the m-PSK constellation.

Article preprint

We have stated that the standard m-PSK detector cannot cope with the non-linear effects of attention on ERPs, which in turns, is essential to build the constellation of EEG signals. As follows, we briefly present these cases that justify the use of a fuzzy approach as a better solution that just a standard m-PSK detector. They are illustrated in Fig. 3.

2.3.1 Lack of attention without artifacts

The constellation disappears due to mutual cancellation of counter-phased symbols. Then, the signal under detection has low SNR and is located around the (0,0) point in the constellation (black circles within the inner circle in Fig. 3). It is not advisable to perform detection.

2.3.2 Lack of attention with artifacts

In this case, the signal under detection has a very poor SNR that, in turns, gives rise to high probability of error in detection of attention. The signal is located far from the constellation (black circles outside the outer circle in Fig. 3). It is not recommended to perform detection.

2.3.3 Sustained attention without artifacts

In this case, the signal under detection has high SNR and is located very close to the attended symbol in the constellation (black triangles in Fig. 3). Full detection of the attended speech is recommended, that is the detection of one symbol among the *m* of the m-PSK constellation.

2.3.4 Sustained attention with artifacts

In this case, the signal under detection has medium SNR and is likely located in between two symbols (squares and diamonds in Fig. 3). In order to performance deterioration, it is advisable to perform detection of 1 symbol among m/2.

As we have evidenced, the amplitude of the signal under detection is a key factor in our model and corresponds to real aspects of attentional effects (e.g. lack or sustained attention). Furthermore, in attentional paradigms either too much or too little amplitudes are pernicious for

Article preprint

the detection and they must be processed in a different way. However, the standard m-PSK is an angular modulation that does not regard the amplitude of the extracted feature. In this circumstances, the complexity of the cases depicted before suggests the use of a more flexible approach than that of the standard m-PSK detector.
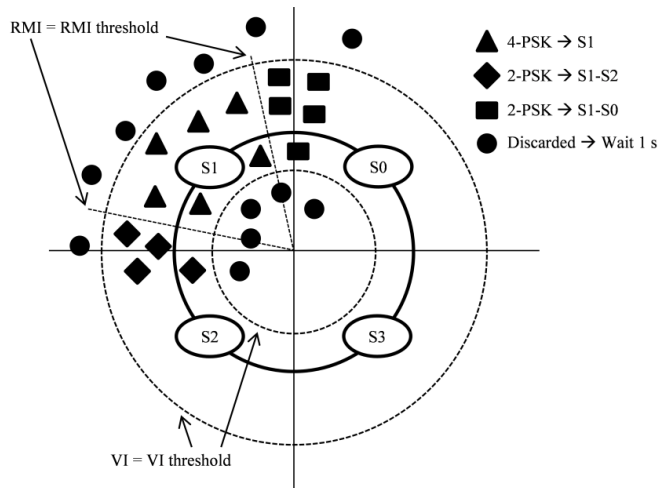
Fig. 3. Example of detections performed by the fuzzy-based adaptive m-PSK detector. Black circles indicate lack of attention with (outside the outer circle) or without (within the inner circle) artifacts. They are discarded. Black triangles indicate sustained attention without artifacts. They are classified on the oMF (i.e., constellation symbol) with highest membership. Black squares and diamonds indicate sustained attention with artifacts. They are classified on the two oMFs with highest membership.

2.4 Fuzzy-based model for adaptive m-PSK detection

In this work, we propose an adaptive m-PSK detector for attentional paradigms based on fuzzy logic. Fuzzy has been thoroughly utilized in many research and engineering fields such as control systems (Wang, Tanaka, & Griffin, 1996)(Feng, 2006)(Zhou, Li, & Shi, 2015)(Cerman, 2013)pattern recognition (Lee, Rahimipour Anaraki, Ahn, & An, 2015)(Melin & Castillo, 2013),

Article preprint

and aerospace (Napolitano, Cnsanova, Windon, Seanor, & Martinelli, 1999)(Barua & Khorasani, 2011). In particular for BCI applications, fuzzy logic has been used for motor imagery classification (Hsu, 2012; Nguyen, Khosravi, Creighton, & Nahavandi, 2015) and mental task recognition (Lledo, Cano, Ubeda, Ianez, & Azorin, 2012)(Palaniappan, Paramesran, Nishida, & Saiwaki, 2002).

According to the problem statement, neurophysiological and EEG features, etc., described in previous sections, we implemented the detector reported in Fig. 4. The detection is given in three main steps.
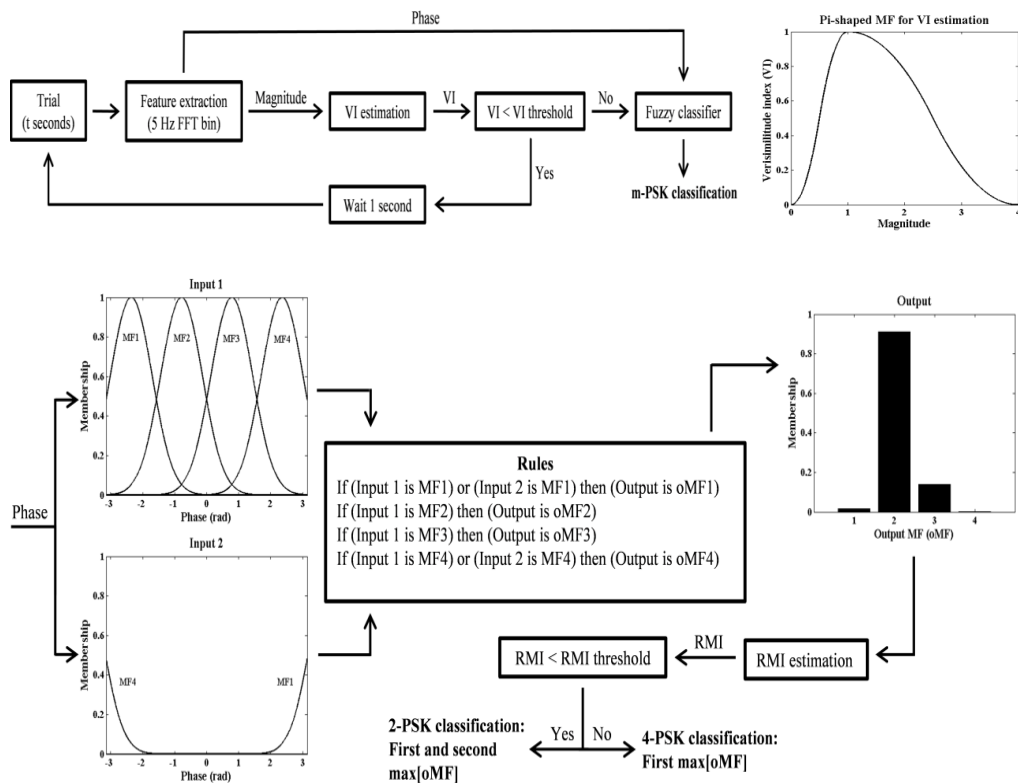
Article preprint

Fig. 4. Fuzzy-based adaptive m-PSK detector. Block diagram of the whole detector on top left. Π-shaped member function for verisimilitude index estimation on top right. Block diagram of the fuzzy classifier at bottom.

2.4.1 Feature extraction

After receiving a trial of t seconds length, the coefficient corresponding to 5 Hz of the Fast Fourier Transform (FFT) of the trial is extracted.

2.4.2 Avoiding lack of attention

As mentioned, features with extreme magnitude values (i.e., amplitude) may be considered lack of attention (without artifacts for low values and with artifacts for high values) and then discarded in order to improve the performance. This step consists in the estimation of an index that provides a measure about the verisimilitude of the feature. The verisimilitude index (VI) is estimated from the normalized magnitude value of the 5 Hz feature by evaluating the π-shaped member function (MF) reported in Fig. 4. This function is modelled on the a priori knowledge about neurophysiology responses and related EEG signals. If the VI is lower than certain threshold, the detector wait 1 second and restart the process (i.e., trial of t + 1 s and feature extraction). Otherwise, the phase of the feature is used as input for the fuzzy classifier (i.e., next step).

2.4.3 Avoiding artifacts in sustained attention

The fuzzy classifier is the last step (4-PSK/2-PSK version is reported in Fig. 4). It consists in a Type-1 Takagi-Sugeno-based fuzzy inference system (FIS). Takagi-Sugeno model (Takagi & Sugeno, 1985) was chosen for simplicity and appropriateness for our problem. Input 1 is composed by 4 Gaussian MFs (α parameter is 0.65) centered at the phase value of each symbol of the 4-PSK constellation. Input 2 is defined in order to take into account the phase periodicity.

Article preprint

Membership level for each MF is evaluated at the output. The relative membership level is estimated as the ratio between the maximum membership level and the sum of all the membership levels. This is the relative membership index (RMI). The RMI provides information about how convincing the classification is, in other words, how artefactual the feature is. If the RMI is lower than certain threshold (i.e., sustained attention with artifacts), the classification is given on the two output MFs (oMFs) with highest membership level (2-PSK). Otherwise (i.e., sustained attention without artifacts), the classification is given on the oMF with highest membership level (4-PSK). In this way, the detector can adapt the number of symbols of the constellation (i.e., 4-PSK or 2-PSK) depending on the level of noise. The 6-PSK/3-PSK/2-PSK version has 6 MFs (input and output) instead of 4.

An example of how the fuzzy-based adaptive 4-PSK/2-PSK detector works is reported in Fig. 3. The proposed detector is intended to work online in order to be useful for BCIs. Although that, the model (i.e., the detector) was tested offline using datasets of a previous published work in order to facilitate performance comparisons.

3. Material and methods

3.1 Experimental data

The database used in (Lopez-Gordo et al., 2015) was utilized in order to validate our model. It consists of EEG data recorded in multi-talker (4 and 6 talkers) scenarios under the paradigm of auditory selective attention. In this section we report a summary of the methodology followed in that work. Please refer to it for further information.

Thirteen healthy subjects participated in the experiment (between 22 and 41 years old and without any auditory or cognitive impairment). EEG data were recorded with one active

electrode placed on the Cz (International 10-20 system) referenced to the mean value of the mastoids. The ground electrode was placed between the Fpz and the Fz. EEG data were recorded at 1000 Hz and band-pass filtered (1-30 Hz).

The stimuli were completely auditory and composed of spoken sentences from the CRM. Randomly selected auditory messages were successively repeated until the trial was completed. Two sessions were recorded. In session 1, trial duration was 16 s with 4 messages being simultaneously played. In session 2, trial duration was 18 s with 6 messages at the same time. Totally, 31 trials per session were performed by the 13 subjects. Subjects were cued to pay selective attention to one message (the rest are considered distraction). Their task was to identify the keywords of the cued message and to report them at the end of the trial. Subjects were fed back with the correct answers between trial and trial.

For the generation of the m-PSK constellation, messages were amplitude-modulated before playing by 5 Hz sinusoidal waves. The phases were shifted and located at equidistant angles depending on the number of symbols of the constellation (4 in session 1 and 6 in session 2), as described in (1).

Every single trial was sectioned into segments of different lengths (minimum length of 1 s and incremental lengths of 1 s each). The FFT of every single segment was computed after applying a tapered cosine window. The FFT coefficient containing the attentional information (i.e., that coefficient corresponding to 5 Hz) was extracted and used as feature for the detector.

The location of symbols of the constellation is unknown a priori. Training is required to setup the phase of the m symbols (S_0, …, S_{m-1}). 30 out of 31 features were used in the Leave-one-out Cross-Validation (LOOCV) training to estimate the optimal constellation (that one that maximizes the classification accuracy). This constellation was utilized to classify the remaining

Article preprint

feature and the process was repeated for each segment length of each trial.

3.2 Detection

The detector proposed in this work (see Fig. 4), unlike the one used in (Lopez-Gordo et al., 2015), is fuzzy-based adaptive m-PSK. The training data is used to configure it. First of all, the median of the magnitude of the 30 training features is used as normalization factor in the VI estimation step. If the VI is higher or equal to the VI threshold, the segment of length t seconds is classified and the classification of the next trial starts. Otherwise, the segment is discarded and the next segment (segment with length t + 1 s) of the same trial is proposed for classification. If the last segment of a trial is achieved (maximum segment length), it is classified ignoring the VI. Afterwards, the phases of symbols of the optimal constellation are used to center the Gaussian functions of the fuzzy classification step (i.e., MF1 is centered at the phase value of symbol S_0, MF2 at the phase value of S_1 and so on). In session 1 (4 talkers): if the RMI is higher or equal to the RMI threshold for 4-PSK classification, the classification is given on one class (i.e., constellation symbol). Otherwise, it is given on two classes (i.e., 2-PSK). In session 2 (6 talkers), classification can adapt from 6-PSK to 3-PSK or 2-PSK depending on the RMI and the RMI threshold.

3.3 Detection accuracy and information transfer rate

The adaptive nature of the proposed classifier leads us to define a jointly detection accuracy (p_a) for session 1 and 2 given by (2) and (3) respectively. It depends on the number of trials (N_t) and the number of successful classifications for each m-PSK ($N_s^{m\text{-PSK}}$).

$$p_a = \frac{N_s^{4\text{-PSK}} + N_s^{2\text{-PSK}}}{N_t} \qquad (2)$$

Article preprint

$$p_a = \frac{N_s^{6\text{-PSK}} + N_s^{3\text{-PSK}} + N_s^{2\text{-PSK}}}{N_t} \tag{3}$$

In order to compare the performance between our detector and the one in (Lopez-Gordo et al., 2015) we define the jointly number of bits per detection (B). It is given by (4) and depends on the p_a and on the average number of constellation symbols (M_{av}) during the 31 trials classification. With the B it is possible to define the jointly information transfer rate (ITR) given by (5). It measures the jointly bit rate in bits/minutes units, with t_{av} the average time to perform the detection during the 31 trials. The original equations are in (Wolpaw et al., 2000).

$$B(\text{bit}) = \log_2 M_{av} + p_a \log_2 p_a + (1 - p_a) \log_2 \frac{1 - p_a}{M_{av} - 1} \tag{4}$$

$$ITR(\text{bpm}) = \frac{60}{t_{av}} B \tag{5}$$

4. Results and discussion

In this section we report the results and discussion. Some participants were excluded from the analysis and discussion in session 2.

4.1 Selection of VI and RMI thresholds

VI and RMI thresholds need to be established in the proposed detector. The subject-averaged ITR and p_a versus the VI and RMI thresholds for both session 1 and session 2 are reported in Fig. 5.

Article preprint
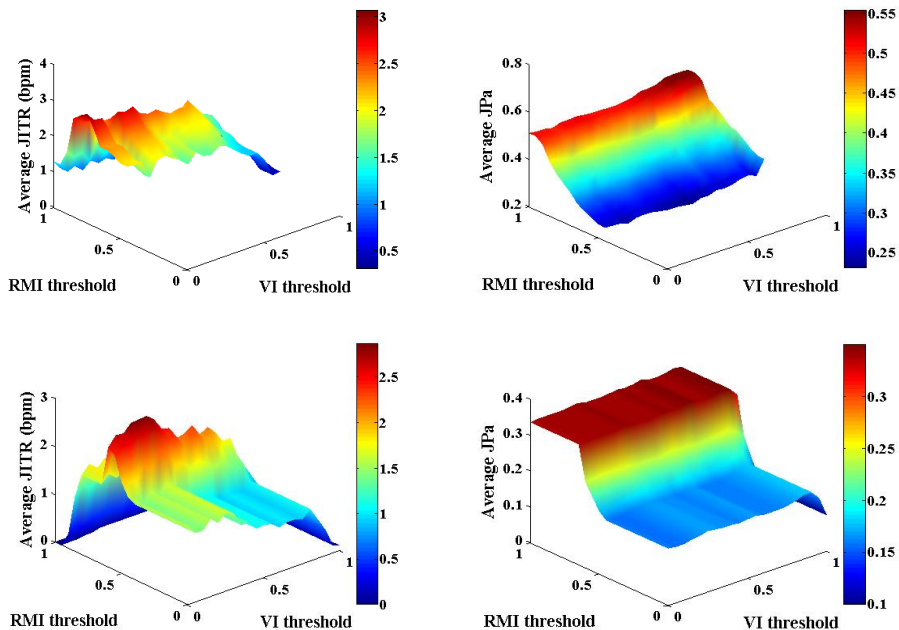
Fig. 5. Subject-average jointly information transfer rate (JITR) and jointly detection accuracy (Jp$_a$) versus VI and RMI thresholds. JITR for session 1 on top left, Jp$_a$ for session 1 on top right, JITR for session 2 at bottom left, and Jp$_a$ for session 2 at bottom right.

In both sessions, the averaged jointly detection accuracy is not affected by the value of the VI threshold whereas it depends on the RMI threshold. The number of successful detections increases as the RMI threshold rises from 0.5 up to 0.95 in session 1 and to 0.7 in session 2, where maximum detection accuracy is achieved. From this value, the adaptive m-PSK detection reduces the average number of constellation symbols to the minimum (i.e., 2-PSK), therefore adaptation is disabled. The same for RMI threshold lower than 0.5, where the number of symbols is always the maximum (i.e., 4-PSK for session 1 and 6-PSK for session 2).

Regarding the averaged jointly information transfer rate, both thresholds influence over that

Article preprint

parameter. The VI threshold optimizes the ITR around 0.3-0.5. For VI threshold near 0, the detector always utilizes trials of 1 s length, thus the ITR is still high. For VI threshold higher than 0.5, the ITR decreases as the threshold rises due to the strictness of the detector, that is, in many cases it utilizes trials with maximum length. The RMI threshold optimizes the ITR around 0.7-0.8 in session 1 and around 0.6 in session 2. In both cases, the ITR increases up to the maximum and then it decreases to the minimum for RMI threshold near 1. It is due to the fact that the average number of constellation symbols is reduced to the minimum (i.e., 2-PSK) whereas the detection accuracy remains stable for RMI threshold approaching 1.

According to the previous analysis, the relative membership index has more influence on both the averaged p_a and the averaged ITR than the verisimilitude index. Despite that, the a priori knowledge about EEG signals under this paradigm (auditory attention detection) stands up for the usefulness of this parameter.

4.2 Adaptive m-PSK vs. m-PSK

It is assumed that everybody cannot control an EEG-based BCI due to the so-called "BCI illiteracy" (Guger et al., 2009)(Volosyak, Valbuena, Luth, Malechka, & Graser, 2011). Subject training is required (Ron-Angevin, Lopez, & Pelayo, 2009). In fact, one of the main goals in EEG-based BCI research is to reduce the training time (Blankertz et al., 2006). Therefore, the inter-subject variability is present in almost all the studies in this field. It may be more proper to estimate optimal VI and RMI thresholds for every single subject. In this section, we report in Table I the results using the VI and RMI thresholds that optimize the ITR for each subject.

Article preprint

Table I
Results table

Part.	Session 1 (4 talkers)							Session 2 (6 talkers)						
	VI thresh	RMI thresh	M_{av}	Chance level	p_a	t_{av} (s)	ITR (bpm)	VI thresh	RMI thresh	M_{av}	Chance level	p_a	t_{av} (s)	ITR (bpm)
P01	1.00	0.80	3.03	0.33	0.68	16.00	1.36	0.55	0.60	4.84	0.21	0.42	1.23	8.16
P02	1.00	0.80	3.10	0.32	0.52	16.00	0.43	0.25	0.60	4.45	0.22	0.39	1.10	5.25
P03	1.00	0.80	3.16	0.32	0.45	16.00	0.22	0.00	0.65	3.00	0.33	0.48	1.00	4.18
P04	0.00	0.85	2.77	0.36	0.45	1.00	1.51	-	-	-	-	-	-	-
P05	0.20	0.55	3.74	0.27	0.42	1.10	4.25	0.00	0.45	6.00	0.17	0.32	1.00	6.29
P06	0.00	0.50	4.00	0.25	0.48	1.00	10.96	1.00	0.60	4.74	0.21	0.42	18.00	0.53
P07	0.85	0.90	2.19	0.46	0.55	1.74	0.85	0.00	0.45	6.00	0.17	0.35	1.00	8.92
P08	0.00	0.95	2.00	0.50	0.65	1.00	3.70	0.90	0.60	4.50	0.22	0.50	2.58	6.20
P09	0.70	0.80	3.16	0.32	0.58	1.48	8.62	0.15	0.55	5.23	0.19	0.45	1.19	12.68
P10	0.70	0.65	3.61	0.28	0.42	1.39	2.92	-	-	-	-	-	-	-
P11	0.75	0.80	2.77	0.36	0.58	1.26	6.87	0.40	0.50	5.71	0.18	0.29	1.16	2.98
P12	0.20	0.75	3.10	0.32	0.65	1.19	15.76	-	-	-	-	-	-	-
P13	0.00	0.85	2.90	0.34	0.61	1.00	12.92	0.15	0.50	5.61	0.18	0.32	1.03	5.08
mean	0.49	0.77	3.04	0.34	0.54	4.63	5.41	0.34	0.55	5.01	0.21	0.39	2.93	6.03
(std)	(0.43)	(0.13)	(0.56)	(0.07)	(0.09)	(6.49)	(5.18)	(0.37)	(0.07)	(0.92)	(0.05)	(0.07)	(5.32)	(3.36)

This table summarizes the results for both sessions using the VI and RMI thresholds that optimize the ITR for each subject. The table is divided in two parts (one per session) and each part is composed by 14 rows (one row per participant and the last one with the mean values) and 8 columns containing values of number of participant, optimal VI, optimal RMI, average number of constellation symbols (M_{av}), corresponding chance level ($1 / M_{av}$), jointly detection accuracy (p_a), average time to perform the detection (t_{av}), and jointly information transfer rate (ITR).

4.2.1 Session 1

For session 1, the mean values of both thresholds are consistent with those estimated in the previous section (0.49 for VI and 0.77 for RMI). The mean value of M_{av} indicates that the detector used 3-PSK detection in average terms. For participant 8 the detector always used 2-PSK whereas it always utilized 4-PSK for participant 6. For the rest, the detector adapted from 4-PSK to 2-PSK when necessary. The p_a values are extensively higher than the chance level for every single participant. Is most cases, they are higher than those values achieved in (Lopez-

Article preprint

Gordo et al., 2015). The mean value is also higher (0.54 vs. 0.47). The mean value of t_{av} indicates that the detector utilized, in average terms, trials of 4.63 seconds. However, t_{av} adopts extreme values subject-by-subject (i.e., near 1 s or 16 s). Apart from participants 2 and 3, the ITR values are higher than the ones achieved in (Lopez-Gordo et al., 2015). The mean value is considerably higher (5.41 vs. 1.25).

4.2.2 Session 2

For session 2, participants 4, 10, and 12 did not achieve ITR with whatever VI and RMI threshold. They were excluded. The mean values of both thresholds are consistent with those estimated in the previous section (0.34 for VI and 0.55 for RMI). The mean value of M_{av} indicates that the detector used 5-PSK detection in average terms. For participant 5 and 8 the detector always used 6-PSK whereas it always utilized 3-PSK for participant 3. For the rest, the detector adapted from 6-PSK to 3-PSK or 2-PSK when necessary. The p_a values are extensively higher than the chance level for every single subject. Is most cases, they are higher than those values achieved in (Lopez-Gordo et al., 2015). The mean value is also higher (0.39 vs. 0.32). The mean value of t_{av} indicates that the detector utilized, in average terms, trials of 2.93 seconds. Apart from subject 8, t_{av} adopts extreme values subject-by-subject (i.e., near 1 s or 18 s). Apart from excluded participants, the ITR values are higher than the ones achieved in (Lopez-Gordo et al., 2015). The mean value is considerably higher (6.03 vs. 0.74). Notice that excluded participants were not taken into account for the calculation of the mean values.

Similar conclusions have been obtained for both sessions in comparison with the results in (Lopez-Gordo et al., 2015). The best results were achieved with the proposed fuzzy-based adaptive m-PSK detector, in terms of detection accuracy and information transfer ratio. In addition to the quantitative results, this novel detector has the advantage of selecting the proper

length of the trial, in an online and automatic manner. However, the fuzzy solution did not work for some participants in session 2 and it presented worse performance than in (Lopez-Gordo et al., 2015) for some few subjects in both sessions. Some aspects of the design should be improved in future works. For upcoming research, it might be interesting to automatically establish VI and RMI thresholds for every single subject during the training of the detector. It might be also interesting to implement an adaptive-network-based fuzzy inference system (ANFIS) (Jang, 1993) instead of the utilized FIS. In this way, the optimal m-PSK constellation would be estimated by ANFIS. On the contrary, more training trials would be required. The number of trials used in this work was the main reason why we did not utilize an ANFIS. Finally, the usage of type-2 fuzzy logic might result useful to handle uncertainties in the detection (Pawel Herman, Prasad, & McGinnity, 2008)(P. Herman, Prasad, & McGinnity, 2005).

5. Conclusion

We have presented a novel adaptive m-PSK detector based on fuzzy logic for auditory attention in multi-talker scenarios. This work has been conducted as improvement of a previous multi-talker study that used 4-PSK and 6-PSK detection. In that study, it was proved that attention to one out of multiple auditory sources can be detected by using digital modulation of EEG signals (e.g., m-PSK). Despite the promising results, some essential aspects such as the non-linear effects of the attentional paradigm, the neuroplasticity of the brain, and the non-stationary nature of EEG signals were not completely taken into account. The use of fuzzy logic could be useful for handling all these uncertainties.

The results show the superiority in performance of the presented detector with respect to other non-adaptive m-PSK detector previously published. Both detection accuracy and information

Article preprint

transfer ratio were increased using the adaptive one. Nevertheless, some aspects of the presented design such as the estimation of the thresholds or the complexity of the fuzzy system could be improved. In conclusion, fuzzy logic has been proved to be useful in the paradigm of auditory attention to multiple sources. Our results stand up for the potential usage of the presented detector in BCI applications, as online tool for the assessment of attention, and as assistive technology in attention impairment.

Acknowledgment

References

Barua, A., & Khorasani, K. (2011). Hierarchical Fault Diagnosis and Fuzzy Rule-Based Reasoning for Satellites Formation Flight. *IEEE Transactions on Aerospace and Electronic Systems*, *47*(4), 2435–2456. http://doi.org/10.1109/TAES.2011.6034643

Birbaumer, N., Ghanayim, N., Hinterberger, T., Iversen, I., Kotchoubey, B., Kübler, A., … Flor, H. (1999). A spelling device for the paralysed. *Nature*, *398*(6725), 297–298. http://doi.org/10.1038/18581

Blankertz, B., Dornhege, G., Krauledat, M., Muller, K.-R., Kunzmann, V., Losch, F., & Curio, G. (2006). The Berlin Brain–Computer Interface: EEG-Based Communication Without

Article preprint

Subject Training. *IEEE Transactions on Neural Systems and Rehabilitation Engineering*, *14*(2), 147–152. http://doi.org/10.1109/TNSRE.2006.875557

Bolia, R. S., Nelson, W. T., Ericson, M. A., & Simpson, B. D. (2000). A speech corpus for multitalker communications research. *The Journal of the Acoustical Society of America*, *107*(2), 1065. http://doi.org/10.1121/1.428288

Boone, M. M. (2008). Hearing glasses, an innovative approach to beat the cocktail party effect. *Europhysics News*, *39*(4), 35–38. http://doi.org/10.1051/epn:2008405

Cerman, O. (2013). Fuzzy model reference control with adaptation mechanism. *Expert Systems with Applications*, *40*(13), 5181–5187. http://doi.org/10.1016/j.eswa.2013.03.014

Davis, H. (1964). Enhancement of Evoked Cortical Potentials in Humans Related to a Task Requiring a Decision. *Science*, *145*(3628), 182–183.

Feng, G. (2006). A Survey on Analysis and Design of Model-Based Fuzzy Control Systems. *IEEE Transactions on Fuzzy Systems*, *14*(5), 676–697. http://doi.org/10.1109/TFUZZ.2006.883415

Guger, C., Daban, S., Sellers, E., Holzner, C., Krausz, G., Carabalona, R., … Edlinger, G. (2009). How many people are able to control a P300-based brain–computer interface (BCI)? *Neuroscience Letters*, *462*(1), 94–98. http://doi.org/10.1016/j.neulet.2009.06.045

Halder, S., Rea, M., Andreoni, R., Nijboer, F., Hammer, E. M., Kleih, S. C., … Kübler, A. (2010). An auditory oddball brain–computer interface for binary choices. *Clinical Neurophysiology*, *121*(4), 516–523. http://doi.org/10.1016/j.clinph.2009.11.087

Herman, P., Prasad, G., & McGinnity, T. M. (2005). Investigation of the Type-2 Fuzzy Logic Approach to Classification in an EEG-based Brain-Computer Interface (pp. 5354–5357). IEEE. http://doi.org/10.1109/IEMBS.2005.1615691

Article preprint

Herman, P., Prasad, G., & McGinnity, T. M. (2008). Design and on-line evaluation of type-2 fuzzy logic system-based framework for handling uncertainties in BCI classification (pp. 4242–4245). IEEE. http://doi.org/10.1109/IEMBS.2008.4650146

Hill, N. J., Ricci, E., Haider, S., McCane, L. M., Heckman, S., Wolpaw, J. R., & Vaughan, T. M. (2014). A practical, intuitive brain–computer interface for communicating "yes" or "no" by listening. *Journal of Neural Engineering*, *11*(3), 035003. http://doi.org/10.1088/1741-2560/11/3/035003

Hillyard, S. A., Hink, R. F., Schwent, V. L., & Picton, T. W. (1973). Electrical Signs of Selective Attention in the Human Brain. *Science*, *182*(4108), 177–180.

Höhne, J., & Tangermann, M. (2014). Towards User-Friendly Spelling with an Auditory Brain-Computer Interface: The CharStreamer Paradigm. *PLoS ONE*, *9*(6), e98322. http://doi.org/10.1371/journal.pone.0098322

Hsu, W.-Y. (2012). Fuzzy Hopfield neural network clustering for single-trial motor imagery EEG classification. *Expert Systems with Applications*, *39*(1), 1055–1061. http://doi.org/10.1016/j.eswa.2011.07.106

Ikeda, Y., Yahata, N., Takahashi, H., Koeda, M., Asai, K., Okubo, Y., & Suzuki, H. (2010). Cerebral activation associated with speech sound discrimination during the diotic listening task: An fMRI study. *Neuroscience Research*, *67*(1), 65–71. http://doi.org/10.1016/j.neures.2010.02.006

Jang, J.-S. R. (1993). ANFIS: adaptive-network-based fuzzy inference system. *IEEE Transactions on Systems, Man, and Cybernetics*, *23*(3), 665–685. http://doi.org/10.1109/21.256541

Article preprint

Kubanek, J., Brunner, P., Gunduz, A., Poeppel, D., & Schalk, G. (2013). The Tracking of Speech Envelope in the Human Cortex. *PLoS ONE*, *8*(1), e53398. http://doi.org/10.1371/journal.pone.0053398

Lee, J.-H., Rahimipour Anaraki, J., Ahn, C. W., & An, J. (2015). Efficient classification system based on Fuzzy–Rough Feature Selection and Multitree Genetic Programming for intension pattern recognition using brain signal. *Expert Systems with Applications*, *42*(3), 1644–1651. http://doi.org/10.1016/j.eswa.2014.09.048

Li, J., Liang, J., Zhao, Q., Li, J., Hong, K., & Zhang, L. (2013). DESIGN OF ASSISTIVE WHEELCHAIR SYSTEM DIRECTLY STEERED BY HUMAN THOUGHTS. *International Journal of Neural Systems*, *23*(03), 1350013. http://doi.org/10.1142/S0129065713500135

Lledo, L. D., Cano, J. M., Ubeda, A., Ianez, E., & Azorin, J. M. (2012). Neuro-fuzzy classifier to recognize mental tasks in a BCI (pp. 207–212). IEEE. http://doi.org/10.1109/BioRob.2012.6290302

Lopez-Gordo, M. A., Fernandez, E., Romero, S., Pelayo, F., & Prieto, A. (2012). An auditory brain–computer interface evoked by natural speech. *Journal of Neural Engineering*, *9*(3), 1–9. http://doi.org/10.1088/1741-2560/9/3/036013

Lopez-Gordo, M. A., & Pelayo, F. (2013). A BINARY PHASE-SHIFT KEYING RECEIVER FOR THE DETECTION OF ATTENTION TO HUMAN SPEECH. *International Journal of Neural Systems*, *23*(04), 1350016. http://doi.org/10.1142/S0129065713500160

Lopez-Gordo, M. A., Pelayo, F., Fernandez, E., & Padilla, P. (2015). Phase-shift keying of EEG signals: Application to detect attention in multitalker scenarios. *Signal Processing*, *117*, 165–173. http://doi.org/10.1016/j.sigpro.2015.05.004

Article preprint

Lopez-Gordo, M. A., Pelayo, F., & Prieto, A. (2010). A high performance SSVEP-BCI without gazing. In *The 2010 International Joint Conference on Neural Networks (IJCNN)* (pp. 193–197). Barcelona, Spain. http://doi.org/10.1109/IJCNN.2010.5596325

Lopez-Gordo, M. A., Pelayo, F., Prieto, A., & Fernandez, E. (2012). An Auditory Brain-Computer Interface with Accuracy Prediction. *International Journal of Neural Systems*, *22*(3), 1–14. http://doi.org/10.1142/S0129065712500098

Martin, S., Brunner, P., Holdgraf, C., Heinze, H.-J., Crone, N. E., Rieger, J., … Pasley, B. N. (2014). Decoding spectrotemporal features of overt and covert speech from the human cortex. *Frontiers in Neuroengineering*, *7*. http://doi.org/10.3389/fneng.2014.00014

Melin, P., & Castillo, O. (2013). A review on the applications of type-2 fuzzy logic in classification and pattern recognition. *Expert Systems with Applications*, *40*(13), 5413–5423. http://doi.org/10.1016/j.eswa.2013.03.020

Näätanen, R. (1975). Seletive Attention and Evoked Potentials in Humans a Critical Review. *Biological Psychology*, *2*, 237–307.

Napolitano, M. R., Cnsanova, J. J., Windon, D. A., Seanor, B., & Martinelli, D. (1999). Neural and fuzzy reconstructors for the virtual flight data recorder. *IEEE Transactions on Aerospace and Electronic Systems*, *35*(1), 61–71. http://doi.org/10.1109/7.745680

Nguyen, T., Khosravi, A., Creighton, D., & Nahavandi, S. (2015). EEG signal classification for BCI applications by wavelets and interval type-2 fuzzy logic systems. *Expert Systems with Applications*, *42*(9), 4370–4380. http://doi.org/10.1016/j.eswa.2015.01.036

Palaniappan, R., Paramesran, R., Nishida, S., & Saiwaki, N. (2002). A new brain-computer interface design using fuzzy ARTMAP. *IEEE Transactions on Neural Systems and Rehabilitation Engineering*, *10*(3), 140–148. http://doi.org/10.1109/TNSRE.2002.802854

Article preprint

Ron-Angevin, R., Lopez, M. A., & Pelayo, F. (2009). The Training Issue in Brain-Computer Interface: A Multi-disciplinary Field. In J. Cabestany, F. Sandoval, A. Prieto, & J. M. Corchado (Eds.), *Bio-Inspired Systems: Computational and Ambient Intelligence* (Vol. 5517, pp. 666–673). Berlin, Heidelberg: Springer Berlin Heidelberg. Retrieved from http://link.springer.com/10.1007/978-3-642-02478-8_83

Ron-Angevin, R., Varona-Moya, S., da Silva-Sauer, L., & Carrion-Robles, T. (2014). A Brain–Computer Interface Speller with a Reduced Matrix: A Case Study in a Patient with Amyotrophic Lateral Sclerosis. Presented at the COGNITIVE 2014 : The Sixth International Conference on Advanced Cognitive Technologies and Applications.

Takagi, T., & Sugeno, M. (1985). Fuzzy identification of systems and its applications to modeling and control. *IEEE Transactions on Systems, Man, and Cybernetics*, *SMC-15*(1), 116–132. http://doi.org/10.1109/TSMC.1985.6313399

Volosyak, I., Valbuena, D., Luth, T., Malechka, T., & Graser, A. (2011). BCI Demographics II: How Many (and What Kinds of) People Can Use a High-Frequency SSVEP BCI? *IEEE Transactions on Neural Systems and Rehabilitation Engineering*, *19*(3), 232–239. http://doi.org/10.1109/TNSRE.2011.2121919

Wang, H. O., Tanaka, K., & Griffin, M. F. (1996). An approach to fuzzy control of nonlinear systems: stability and design issues. *IEEE Transactions on Fuzzy Systems*, *4*(1), 14–23. http://doi.org/10.1109/91.481841

Wolpaw, J. R., Birbaumer, N., Heetderks, W. J., McFarland, D. J., Peckham, P. H., Schalk, G., … Vaughan, T. M. (2000). Brain–Computer Interface Technology: A Review of the First International Meeting. *IEEE Transactions on Rehabilitation Engineering*, *8*(2), 164–173.

Article preprint

Zhou, Q., Li, H., & Shi, P. (2015). Decentralized Adaptive Fuzzy Tracking Control for Robot

Finger Dynamics. *IEEE Transactions on Fuzzy Systems*, *23*(3), 501–510.

http://doi.org/10.1109/TFUZZ.2014.2315661

Article preprint

Detection of Attention in Multi-Talker Scenarios: a Fuzzy Approach

Highlights

- A fuzzy-based m-PSK attention detector for multi-talker scenarios is proposed.
- The approach outperformed the performance of previous works (ITR and accuracy).
- This outcome could have relevant impact on BCI community.

Appendix B

Check for
updates

Stress Assessment by Prefrontal Relative Gamma

Jesus Minguillon [1, 2] *, Miguel A. Lopez-Gordo [3, 4] and Francisco Pelayo [1]

[1] *Department of Computer Architecture and Technology, University of Granada, Granada, Spain,* [2] *Research Centre for Information and Communications Technologies, University of Granada, Granada, Spain,* [3] *Department of Signal Theory, Telematics and Communications, University of Granada, Granada, Spain,* [4] *Nicolo Association, Granada, Spain*

Stress assessment has been under study in the last years. Both biochemical and physiological markers have been used to measure stress level. In neuroscience, several studies have related modification of stress level to brain activity changes in limbic system and frontal regions, by using non-invasive techniques such as functional magnetic resonance imaging (fMRI) and electroencephalography (EEG). In particular, previous studies suggested that the exhibition or inhibition of certain brain rhythms in frontal cortical areas indicates stress. However, there is no established marker to measure stress level by EEG. In this work, we aimed to prove the usefulness of the prefrontal relative gamma power (RG) for stress assessment. We conducted a study based on stress and relaxation periods. Six healthy subjects performed the Montreal Imaging Stress Task (MIST) followed by a stay within a relaxation room while EEG and electrocardiographic signals were recorded. Our results showed that the prefrontal RG correlated with the expected stress level and with the heart rate (HR; 0.8). In addition, the difference in prefrontal RG between time periods of different stress level was statistically significant ($p < 0.01$). Moreover, the RG was more discriminative between stress levels than alpha asymmetry, theta, alpha, beta, and gamma power in prefrontal cortex. We propose the prefrontal RG as a marker for stress assessment. Compared with other established markers such as the HR or the cortisol, it has higher temporal resolution. Additionally, it needs few electrodes located at non-hairy head positions, thus facilitating the use of non-invasive dry wearable real-time devices for ubiquitous assessment of stress.

Keywords: stress, EEG, ECG, prefrontal relative gamma, heart rate

INTRODUCTION

According to the definition provided by the American Institute of Stress (AIS), stress in daily-life context is commonly defined as a physical, mental, or emotional strain (for detailed information, please visit the website of the AIS[1]). However, there is no universally accepted definition of stress. Statistics of 2014 in the United States (US) revealed that 77 and 73% US people regularly experience, respectively, physical (e.g., fatigue, headache, and muscle tension), and psychological (e.g., anger, nervous feeling, and lack of energy) symptoms caused by stress. Stress is usually caused by a variety of cognitive, social or physical factors such as job pressure, economic status, health, and relationships.

---

[1]www.stress.org

Depending on the positive or negative connotations of stress, this can be classified as eustress (i.e., good stress, e.g., concentration on a task, success, and happiness) or distress (i.e., bad stress, e.g., failure and problems). Regarding the stimulus and response, stress can be acute or chronic. Acute stress is characterized by *fight or flight* responses to unexpected stimuli. Psychological and physiological defense mechanisms are activated and take several minutes to return to relax. Furthermore, chronic stress is caused by daily-life circumstances and can affect the health (e.g., metabolism and immune system).

Regarding the research on stress, this has been under study from several years ago (Selye, 1975a,b; Pearlin et al., 1981; Kingston and Hoffman-Goetz, 1996) to nowadays (Caspi et al., 2003; Aschbacher et al., 2013; Friedman et al., 2014; Mahar et al., 2014; Slavish et al., 2015). It is common to make use of methods to induce stress in subjects in stress-related works. Several methods have been proved to successfully achieve this goal such as the Montreal Imaging Stress Task (MIST; Dedovic et al., 2005), the Trier Social Stress Test (TSST; Kirschbaum et al., 1993), and the Mannheim Multicomponent Stress Test (MMST; Kolotylova et al., 2010). In order to assess stress, various biochemical (e.g., cortisol and salivary alpha-amylase) and physiological (e.g., heart rate, blood pressure, galvanic skin response, and pupil size) markers have been proposed (Schleifer and Okogbaa, 1990; Sayette, 1993; Chandiramani et al., 2007; Ranganathan et al., 2012; Reinhardt et al., 2012; Aschbacher et al., 2013; Michels et al., 2013; Regula et al., 2014; Dimitriev and Saperova, 2015; Slavish et al., 2015; Zschucke et al., 2015). See Bali and Jaggi (2015) for a recent review in methods and assessment in stress studies. Unfortunately, most of the established markers such as the cortisol or the heart rate (HR) cannot be easily implemented on wearable real-time devices for ubiquitous assessment of stress. On the contrary, some neurological markers have better temporal resolution, and therefore they can be implemented on those systems.

Brain activity has been studied under stressful circumstances using, for instance, functional magnetic resonance imaging (fMRI; Dagher et al., 2009; Dedovic et al., 2009b), near-infrared spectroscopy (NIRS; Tanida et al., 2007), positron emission tomography (PET; Nagano-Saito et al., 2013), and electroencephalography (EEG; Seo and Lee, 2010; Brouwer et al., 2011; Papousek et al., 2014). These works demonstrated that stress causes changes in regions of prefrontal and frontal areas such as the orbitofrontal regions, frontal lobes, and medium prefrontal cortex. See Dedovic et al. (2009a) for a review in neuroimaging-based stress studies. Regarding the EEG-based studies, they have suggested that the exhibition or inhibition of certain brain rhythms (e.g., alpha, theta, gamma) in frontal cortical areas reflects stress. Markers such as the alpha asymmetry (AA) have been proposed to assess stress (Brouwer et al., 2011; Papousek et al., 2014). This marker is based on the difference in activity between left and right hemispheres. Despite the amount of EEG-based approaches, there is no established marker to assess stress by EEG.

In the present work, we propose an EEG-based marker for stress assessment: the prefrontal relative gamma power (RG). We focus on acute psychosocial stress (i.e., the type of stress induced by the MIST). This marker is based on the complementarity of fast and slow brain rhythms. It has been previously used in meditation-based studies (Lutz et al., 2004; Steinhubl et al., 2015), but not under pure relaxation/stress paradigms. Despite a direct relationship between meditation and relax states has not been demonstrated in the literature, it is usual in meditation studies to utilize relaxation/stress markers such as the HR (Kim et al., 2014; Steinhubl et al., 2015). In addition, results provided by this paper prove the usefulness of the prefrontal RG power for stress assessment. Among its advantages, the temporal resolution is higher than the one of other markers such as the HR or the cortisol. Moreover, it requires the use of few electrodes located at non-hairy head positions. These two features may result in the use of non-invasive dry wearable real-time devices for ubiquitous assessment of stress. These systems might help people to improve their life quality in diverse daily-life activities.

The paper is organized in four sections, including the present introduction (Section Introduction). Methods, subjects, and materials used during the study are reported in Section Methods. Afterwards, results obtained from data analysis are reported in Section Results. Finally, discussion of the results and conclusions are reported in section Discussion.

METHODS

Experimental Design

Subjects and Data Acquisition

Six healthy young volunteers (mean age, 26.3 ± 6.4 years) participated in the study. The subjects declared no previous experience in EEG or stress-related experiments. They were instructed not to take stimulants or relaxants during 24 h prior to the experiment. They wore hospital uniforms during the study. The protocol and informed consent were accepted by the Bioethics Committee of the University of Granada.

Once the informed consent was provided and signed by the subject, EEG, and electrocardiographic (ECG) signals were recorded at 540 Hz with the Miniature Data Acquisition System of Cognionics (Cognionics, Inc., USA). One ECG electrode was placed on the non-dominant wrist. Fifteen EEG electrodes were placed at Fp1, Fp2, Fz, F3, F4, F7, F8, Cz, C3, C4, Pz, T5, T6, O1, and O2 positions of the 10–20 International System. These positions have been included in reports of successful studies on emotions (Jenke et al., 2014). All the electrodes were referenced and grounded to the left ear lobe. The impedance of the electrodes was below 30 KΩ. This value is much lower than the input impedance of the acquisition system, and therefore signal degradation was insignificant.

Stress Session

The subjects were stressed by the MIST (Dedovic et al., 2005). This procedure induces mental arithmetic load together with negative social feedback. It was demonstrated to increase levels of salivary free cortisol in healthy young people and was proposed as tool for functional imaging studies related to psychosocial stress. In fact, the MIST has been already used in various stress-related works (Dagher et al., 2009; Dedovic et al., 2009b; Nagano-Saito et al., 2013; Zschucke et al., 2015). In addition, a recent review

included the MIST in the well-described methods to induce stress in humans (Bali and Jaggi, 2015).

The MIST consists of two stages namely, training and test. During the training stage, the subjects are asked to solve arithmetic operations without any time restriction. The arithmetic operations are organized in five difficulty levels and randomly displayed. During the test stage, the subjects must solve the same type of arithmetic operations with limited time. This limit is visually indicated to the subjects by a progress bar and calculated as the average time of correct answers in the training. The limit is adapted during the test stage depending on the number of consecutive wrong and right answers. In addition, the feedback for the current resolve (i.e., *correct*, *incorrect*, *timeout*) as well as the average performance are displayed after every single operation. The adaptive time limit enforces a range of about 20–45% performance whilst the subjects are asked to reach about 80–90% performance to be useful for the study. The subjects are periodically reminded of the importance of achieving the goal. This fact, together with the impossibility of reaching the asked

FIGURE 1 | The layout of the GUI implemented for the MIST. On the top, the current calculation to be solved is displayed. In the middle, the red bar indicates the remaining time to solve the operation. At the bottom left, instructions and feedback (i.e., *correct*, *incorrect*, *timeout*) are displayed. At the bottom right, the button panel that provides the input. Solutions are ranged in the [0–9] interval.

performance, induces stress in subjects. See Dedovic et al. (2005) for a detailed explanation of the MIST.

In our study, the MIST was implemented using a Matlab (The MathWorks, Inc., USA) graphical user interface (GUI) running on a laptop (see **Figure 1**). The MIST was conducted within a classroom. The subjects were sitting on a comfortable chair. In order to avoid severe artifacts in EEG and ECG signals, they were instructed to exclusively move their hand using the touchpad (i.e., hand without the ECG electrode). The training stage and the test stage lasted, respectively, 3 and 6 min, following the indications in Dedovic et al. (2005). Therefore, the stress session lasted 9 min.

Relaxation Session

A relaxation session was performed immediately after the stress session. The subjects stayed laid on a puff-shaped seat for 10 min, following the indications provided by a psychologist with a wide expertise in lighting-related treatments. The seat was placed inside a white-lighted closed room. The room was specially designed for relaxation. The subjects were instructed not to close their eyes (except for blinking), not to move, nor gaze any part of the room during the relaxation session. In order to check the behavior of the subjects, they were monitored by a video camera.

The timeline of the experiment and the expected stress level are displayed in **Figure 2**. Three stress levels were defined (i.e., SL1, SL2, and SL3). SL1 corresponds to the mean value during the 2 min in the middle of the MIST training. This period was chosen as initial stress level because the subjects generally started the training in a non-relaxed state due to several reasons (e.g., the stress produced by the EEG preparation and the instructions given by the technicians at the beginning of the experiment). SL2 corresponds to the mean value during the 2 last min of the MIST test. It should be the period of maximum stress level. Finally, SL3 corresponds to mean value during the 2 last min of the relaxation session. It should be the period of minimum stress level.

Biosignals Processing
EEG Signals

Recorded EEG data were bandpass filtered using a second order Butterworth IIR filter with cutoff frequencies 1 and 100 Hz.

FIGURE 2 | The timeline of the experiment. The first 3 min corresponds to the training part of the MIST. Afterwards, the MIST test is performed for 6 min. Then the relaxation session starts in the relaxation room and lasts 10 min. The gray line indicates the expected level of stress according to the paradigm. The three stress levels (SL1, SL2, and SL3) and the corresponding time periods are indicated over the gray line.

A notch filter was applied to remove couplings from power-lines. Ocular artifacts were removed using independent component analysis.

After the preprocessing, a spectral analysis was performed. Two-second epochs (no overlap) were extracted, z-scored, and then the power spectral density (PSD) estimated for each EEG channel. The average power at different frequency bands was calculated through the area under the PSD in the intervals corresponding to the bands. These values were averaged across the channels to be jointly analyzed. The RG was computed as the power ratio between gamma (25–45 Hz) and slow rhythms (4–13 Hz). This spectral analysis is based on previous works using the RG (Lutz et al., 2004; Steinhubl et al., 2015). The absolute power at frequency bands theta (4–7 Hz), alpha (8–13 Hz), beta (14–24 Hz), and gamma (25–45 Hz) was also computed. For theta, alpha, and beta, it was the inverse value (i.e., 1/theta, 1/alpha, and 1/beta) for a better comparison with RG and HR. In addition, AA (i.e., relative difference in alpha power between left and right hemispheres) was calculated. This analysis was performed in different cortical areas such as prefrontal (Fp1, Fp2), frontal (Fz, F3, F4, F7, F8), central (Cz, C3, C4), and temporal-parietal (Pz, T5, T6). These frequency bands and cortical areas have been used in emotion-related works (Jenke et al., 2014).

All the results of the spectral analysis were smoothed with a moving average filter (30 samples) in order to better display them. In addition, in the group analysis (i.e., average across the six subjects), results were interpolated to fix inter-subject time warping, smoothed, z-scored, and then averaged. The averaged results were normalized by the maximum and the minimum (i.e., $y_{norm} = [y - \min(y)]/[\max(y) - \min(y)]$).

ECG Signals

Recorded ECG data were bandpass filtered using a second order Butterworth IIR filter with cutoff frequencies 4 and 24 Hz. This filter was 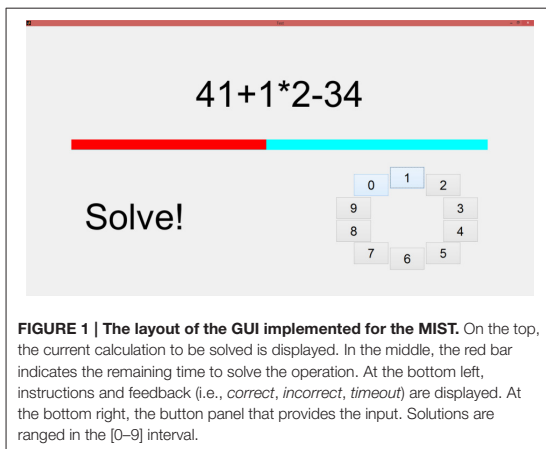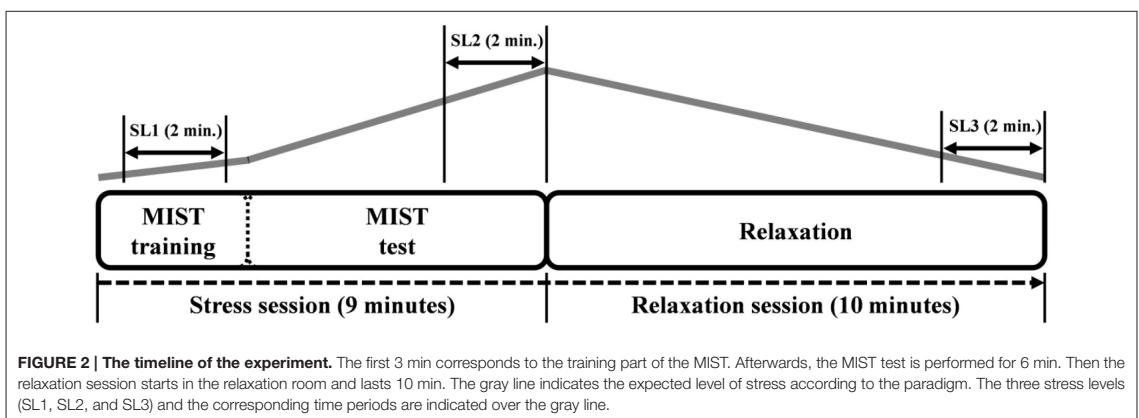applied in order to enhance the R peak of the QRS complex within the ECG signal (Semmlow, 2014). An automatic procedure for R peak detection was performed afterwards. Preprocessed ECG data were used to calculate the HR every 30 s by using a 90 s sliding window with 66% overlap factor.

In addition, in the group analysis (i.e., average across the six subjects), results were interpolated, z-scored and then averaged. The averaged results were normalized in a similar manner to EEG data (see Section EEG Signals).

Statistical Analysis

The mean of EEG power at different frequency bands and locations was computed over the time periods corresponding to SL1, SL2, and SL3. Mean of HR were also calculated over the same periods. The Wilcoxon signed-rank test was applied in order to assess whether mean ranks of repeated measurements (i.e., time periods of SL1, SL2, and SL3) significantly differ ($p < \alpha$) with significance level $\alpha = 0.01$. This test is usually used as an alternative to the paired Student's t-test when the distribution cannot be assumed to be normal (the Kolmogorov-Smirnov test was performed to check for normality). In addition, Pearson's linear correlation coefficient was computed to find correlations of EEG bands power and HR.

RESULTS

EEG Activity

Figure 3A shows the difference in the mean prefrontal RG between SL1, SL2, and SL3. For subjects 2, 3, 4, 5, and 6 the difference between SL2 and SL1 was statistically significant (Wilcoxon; $p < 0.01$). For subject 5, the difference was negative (i.e., the RG was higher in SL1 than in SL2). Similarly, for subjects 1, 2, 3, 4, and 6 the difference between SL2 and SL3 was statistically significant (Wilcoxon; $p < 0.01$). For subject 6, the difference was negative (i.e., the RG was higher in SL3 than in SL2). **Figure 3B** shows the evolution of prefrontal RG averaged across the six subjects and then normalized. In the middle of the MIST training (i.e., SL1), the RG was below 0.5; at the end of the
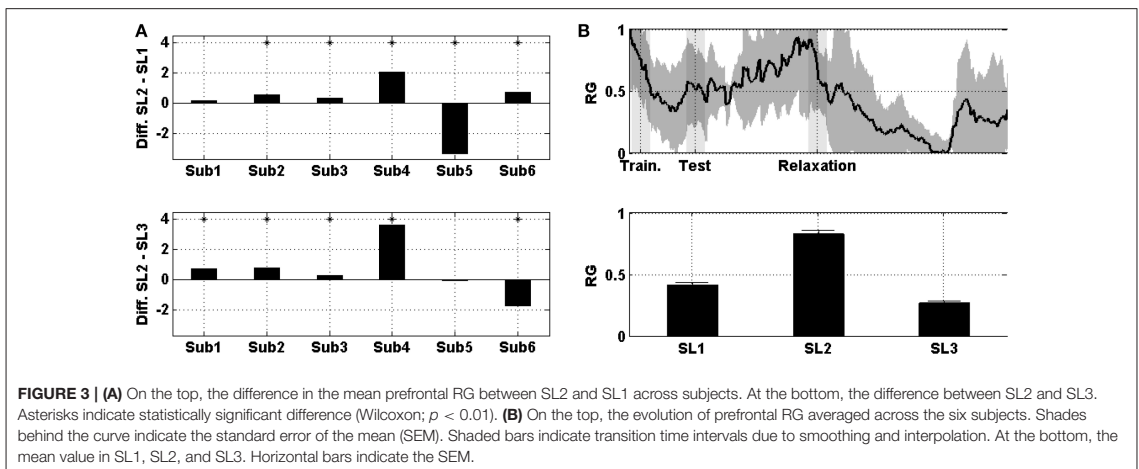
FIGURE 3 | (A) On the top, the difference in the mean prefrontal RG between SL2 and SL1 across subjects. At the bottom, the difference between SL2 and SL3. Asterisks indicate statistically significant difference (Wilcoxon; $p < 0.01$). **(B)** On the top, the evolution of prefrontal RG averaged across the six subjects. Shades behind the curve indicate the standard error of the mean (SEM). Shaded bars indicate transition time intervals due to smoothing and interpolation. At the bottom, the mean value in SL1, SL2, and SL3. Horizontal bars indicate the SEM.

FIGURE 4 | (A) On the top, the evolution of RG, AA, theta, alpha, beta, and gamma in prefrontal area averaged across the six subjects. Shaded bars indicate transition time intervals due to smoothing and interpolation. At the bottom, the mean value in SL1, SL2, and SL3. (B) On the top, the difference in the mean power between SL2 and SL1 for RG, AA, theta, alpha, beta, and gamma in prefrontal area. At the bottom, the difference between SL2 and SL3. Asterisks indicate statistically significant difference (Wilcoxon; $p < 0.01$).
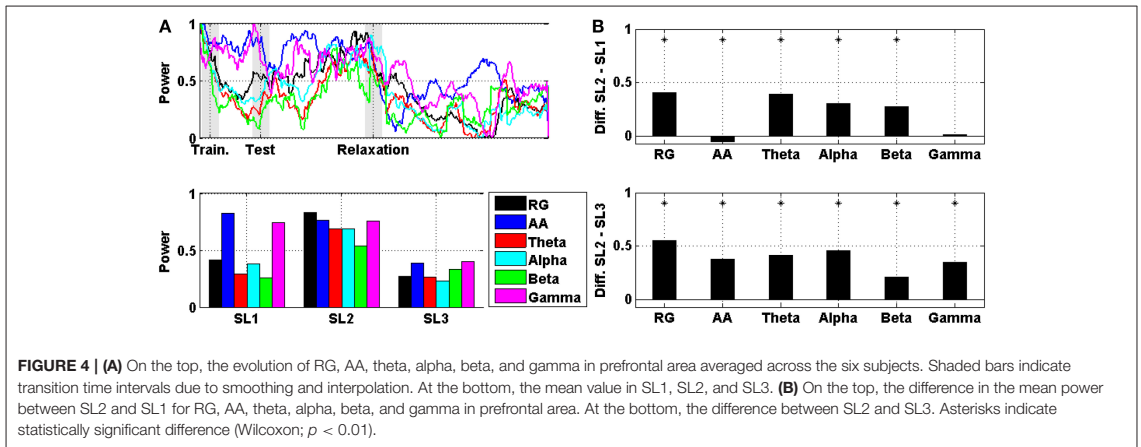
TABLE 1 | Differences in the mean power between SL1, SL2, and SL3 in the group analysis for RG, AA, theta, alpha, beta, and gamma in different cortical areas.

	Prefrontal		Frontal		Central		Temporal-parietal	
	SL2 – SL1	SL2 – SL3	SL2 – SL1	SL2 – SL3	SL2 – SL1	SL2 – SL3	SL2 – SL1	SL2 – SL3
RG	0.41*	0.55*	0.36*	0.57*	0.36*	0.80*	0.33*	0.82*
AA	−0.06*	0.37*	0.05*	0.14*	−0.16*	−0.04*	−0.32*	−0.02
Theta	0.39*	0.42*	0.39*	0.53*	0.51*	0.61*	0.47*	0.66*
Alpha	0.31*	0.45*	0.35*	0.54*	0.30*	0.57*	0.35*	0.66*
Beta	0.28*	0.21*	0.25*	0.49*	0.13*	0.23*	0.26*	0.12*
Gamma	0.01	0.35*	0.12*	0.39*	0.20*	0.55*	0.11*	0.73*

Asterisks indicate statistically significant difference (Wilcoxon; $p < 0.01$). Shadings indicate maximum of each column.

MIST test (i.e., SL2), the RG increased to up to 0.75 and, at the end of the relaxation session (i.e., SL3), the RG was around 0.25.

A comparison between RG, AA, theta, alpha, beta, and gamma averaged across subjects (and then normalized) in prefrontal area is displayed in **Figure 4**. In particular, **Figure 4A** shows the evolution of the power, and **Figure 4B** shows the difference in the mean power between SL1, SL2, and SL3. For RG, AA, theta, alpha, and beta, the difference between SL2 and SL1 was statistically significant (Wilcoxon; $p < 0.01$). For AA, this difference was negative (i.e., the AA was higher in SL1 than in SL2). For RG, AA, theta, alpha, beta, and gamma, the difference between SL2 and SL3 was also statistically significant (Wilcoxon; $p < 0.01$). All these differences, together with those corresponding to other cortical areas (e.g., frontal, central, and temporal-parietal), are reported in **Table 1**. In all areas, the maximum difference between SL2 and SL3 was achieved using the RG (0.55, 0.57, 0.80, and 0.82 in prefrontal, frontal, central, and temporal-parietal areas, respectively). However, the maximum difference between SL2 and SL1 was achieved using the theta power in frontal (0.39), central (0.51) and temporal-parietal (0.47) areas, and using the RG in prefrontal area (0.41).

Additionally, correlations of prefrontal RG with AA, theta, alpha, beta, and gamma in different areas are reported in **Table 2**.

The highest correlations were RG with theta (0.89) and with alpha (0.89), both of them in frontal area. Theta power reached the maximum correlation in prefrontal (0.87) and frontal (0.89) areas. Alpha power was also in frontal area (0.89), and in central (0.87) and temporal-parietal (0.87) areas. Theta, alpha, and beta achieved their maximum correlation in frontal area (0.89, 0.89, and 0.82, respectively). On the other hand, AA and gamma had their maxima, respectively, in prefrontal (0.50) and central (0.82) areas.

ECG Activity

Figure 5A shows the difference in the HR between SL1, SL2, and SL3. For every single subject, the differences between SL2 and SL1, as well as between SL2 and SL3, were statistically significant (Wilcoxon; $p < 0.01$). **Figure 5B** shows the evolution of the HR averaged across the six subjects and then normalized. In the middle of the MIST training (i.e., SL1), the HR was a little above 0.6; at the end of the MIST test (i.e., SL2), the HR increased to up to around 0.9 and, at the end of the relaxation session (i.e., SL3), the HR was around 0.1.

The comparison between levels of prefrontal RG and HR averaged across subjects and then normalized is displayed in **Figure 6**. **Figure 6A** shows the evolution of these levels, and

TABLE 2 | Pearson's linear correlation coefficient and confidence interval (CI) for correlations in the group analysis of prefrontal RG with AA, theta, alpha, beta, and gamma in different cortical areas.

	Prefrontal			Frontal			Central			Temporal-parietal		
	CI low	Corr	CI up	CI low	Corr	CI up	CI low	Corr	CI up	CI low	Corr	CI up
RG	1	1	1	0.96	0.97	0.97	0.88	0.90	0.91	0.82	0.84	0.86
AA	0.44	0.50	0.56	0.29	0.36	0.42	−0.32	−0.24	−0.17	0.03	0.11	0.19
Theta	0.85	0.87	0.89	0.87	0.89	0.91	0.76	0.80	0.82	0.80	0.83	0.85
Alpha	0.84	0.86	0.88	0.87	0.89	0.91	0.85	0.87	0.89	0.85	0.87	0.89
Beta	0.52	0.57	0.62	0.79	0.82	0.85	0.62	0.67	0.71	0.40	0.47	0.53
Gamma	0.78	0.81	0.84	0.76	0.79	0.82	0.80	0.82	0.85	0.74	0.77	0.80

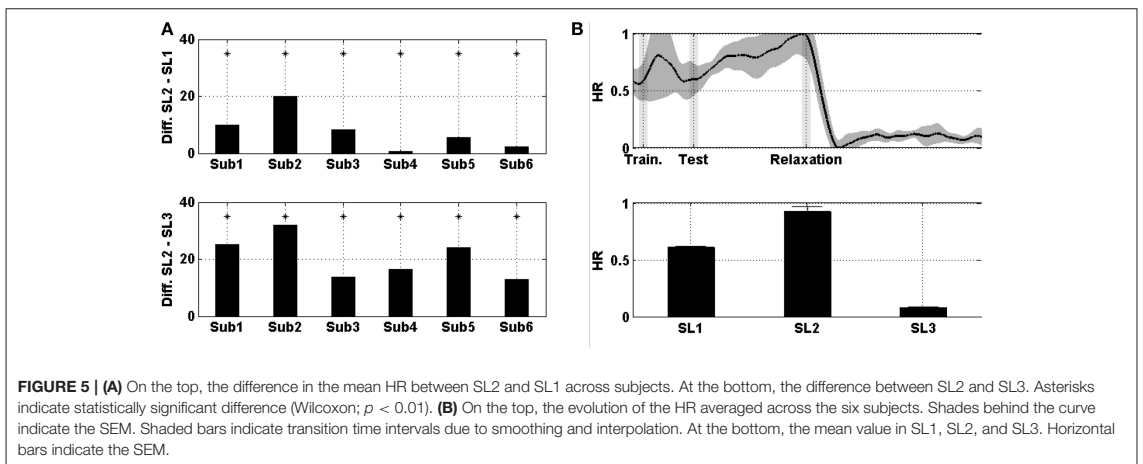*Shadings indicate maximum for each cortical area.*

FIGURE 5 | (A) On the top, the difference in the mean HR between SL2 and SL1 across subjects. At the bottom, the difference between SL2 and SL3. Asterisks indicate statistically significant difference (Wilcoxon; $p < 0.01$). **(B)** On the top, the evolution of the HR averaged across the six subjects. Shades behind the curve indicate the SEM. Shaded bars indicate transition time intervals due to smoothing and interpolation. At the bottom, the mean value in SL1, SL2, and SL3. Horizontal bars indicate the SEM.

FIGURE 6 | (A) On the top, the evolution of the level of prefrontal RG together with the HR averaged across the six subjects and then normalized. Shaded bars indicate transition time intervals due to smoothing and interpolation. At the bottom, the mean value in SL1, SL2, and SL3. **(B)** On the top, the differenc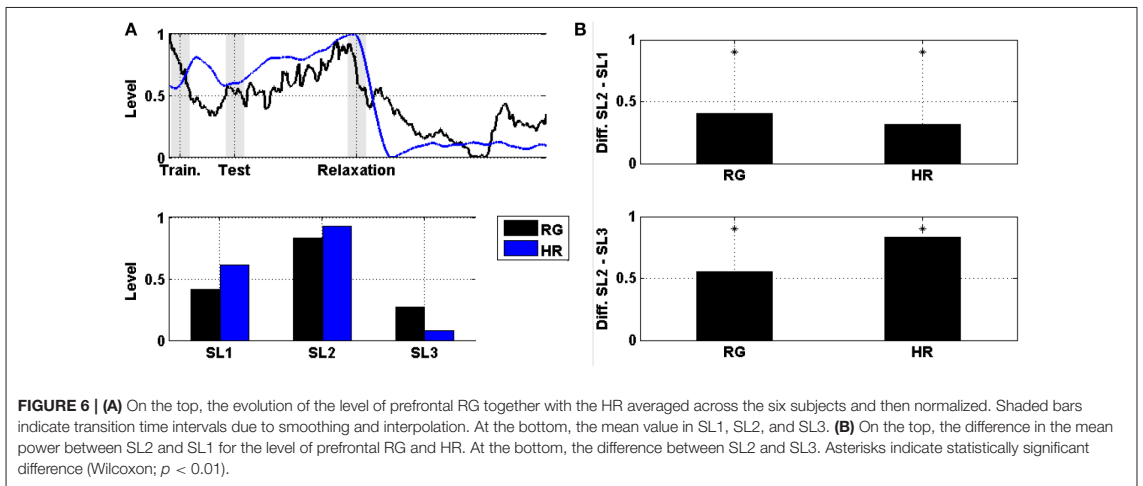e in the mean power between SL2 and SL1 for the level of prefrontal RG and HR. At the bottom, the difference between SL2 and SL3. Asterisks indicate statistically significant difference (Wilcoxon; $p < 0.01$).

Figure 6B shows the difference in the mean power between SL1, SL2, and SL3. For both markers (i.e., prefrontal RG and HR), the difference between SL2 and SL1, as well as between SL2 and SL3, were statistically significant (Wilcoxon; $p < 0.01$). These values are reported in **Table 3**. The maximum difference between SL2 and SL1 was achieved using the prefrontal RG (0.41). On the contrary, the maximum difference between SL2 and SL3 was reached by the HR (0.84).

Finally, correlations of HR with RG, AA, theta, alpha, beta, and gamma in different cortical areas are reported in **Table 4**. The highest correlation was RG in central area (0.95). Alpha power reached the maximum correlation in prefrontal (0.81) and frontal (0.86) areas. However, RG was in central (0.95) and temporal-parietal (0.94) areas. Theta and alpha achieved their maximum correlation in temporal-parietal area (0.88 and 0.92, respectively). Beta had its maximum in frontal area (0.85). Gamma and RG achieved their maxima in central area (0.93 and 0.95, respectively). The AA reached its maximum in prefrontal area (0.75).

DISCUSSION

In this work, the RG was used to assess changes in stress level of healthy subjects. To the best of our knowledge, RG has been previously used to assess meditation states with expert and novice meditators (Lutz et al., 2004; Steinhubl et al., 2015). The RG has never been utilized as a marker to quantify stress level during relaxation/stress sessions. The cited meditation-related works found contrary results regarding the positive or negative correlation between the RG and the meditation level. Our results showed a positive correlation of the RG with the stress level, in particular, with the expected stress level (see **Figure 2**) and with the HR (0.8).

The prefrontal RG was able to significantly differentiate for 5 out of 6 subjects in case of SL1 to SL2, and for the 6 subjects in case of SL2 to SL3. Nevertheless, these differences had negative sign for a couple of subjects, thus indicating a reverse behavior (i.e., not expected) in these cases. The group analysis showed that the RG was the most discriminative marker in prefrontal area for both SL transitions. It is the same for the transition 2–3 in all other areas. However, for the transition 1–2, theta power was the most discriminative marker in frontal, central, and temporal-parietal areas. This fact could have been caused by changes in task attention. Although the AA has been utilized in various recent stress-related works (Brouwer et al., 2011; Papousek et al., 2014), in the present study, the RG was more discriminative than the AA for both SL transitions in all the cortical areas, and therefore better stress marker. This outcome suggests the alternative use of the RG to assess stress level. Results reported in **Table 1** showed that there generally were significant differences in EEG bands power between stress levels in every single area. However, according to related literature, stress is reflected by changes in regions of prefrontal and frontal areas such as the orbitofrontal regions, frontal lobes, and medium prefrontal cortex (Tanida et al., 2007; Dedovic et al., 2009a,b; Nagano-Saito et al., 2013; Papousek et al., 2014). Focusing on those areas, theta and alpha waves were the most weighted components of the RG since gamma waves did not significantly change from SL1 to SL2. It suggests that prefrontal gamma is related to cognitive processes (which remain in both stress levels) rather than psychosocial stress. In fact, this was claimed in previous literature (Başar-Eroglu et al., 1996). It may be important to consider both gamma and slow rhythms (i.e., theta + alpha) in order to assess full stress level, including cognitive and psychosocial relax. Nevertheless, in central area, gamma power did significantly increase for transition 1–2. Indeed, a recent study concluded that high frequency cortical activity measured through Cz electrode was related to affective processing (Sirca et al., 2015), which could be related to stress.

Regarding the HR and its comparative with the EEG, the MIST increased the HR of the subjects and the relaxation

TABLE 3 | Differences in the mean level of prefrontal RG and HR between SL1, SL2, and SL3 in the group analysis.

	SL2 – SL1	SL2 – SL3
Prefrontal RG	0.41*	0.55*
HR	0.31*	0.84*

Asterisks indicate statistically significant difference ($p < 0.01$). Shadings indicate maximum of each column.

TABLE 4 | Pearson's linear correlation coefficient and confidence interval (CI) for correlations in the group analysis of HR with RG, AA, theta, alpha, beta, and gamma in different cortical areas.

	Prefrontal			Frontal			Central			Temporal-parietal		
	CI low	Corr	CI up	CI low	Corr	CI up	CI low	Corr	CI up	CI low	Corr	CI up
RG	0.77	0.80	0.83	0.83	0.85	0.87	0.94	0.95	0.95	0.93	0.94	0.95
AA	0.71	0.75	0.78	0.30	0.37	0.43	−0.17	−0.09	−0.01	0.28	0.35	0.42
Theta	0.59	0.64	0.68	0.72	0.76	0.79	0.72	0.75	0.78	0.86	0.88	0.89
Alpha	0.79	0.81	0.84	0.83	0.86	0.88	0.88	0.90	0.91	0.91	0.92	0.93
Beta	0.42	0.48	0.54	0.82	0.85	0.87	0.54	0.60	0.65	0.33	0.40	0.46
Gamma	0.70	0.74	0.77	0.75	0.79	0.81	0.92	0.93	0.94	0.92	0.93	0.94

Shadings indicate maximum for each cortical area.

session decreased it. This was expected since the HR has been proved to be related with the stress level in previous works (Sayette, 1993; Chandiramani et al., 2007; Ranganathan et al., 2012; Reinhardt et al., 2012; Michels et al., 2013; Regula et al., 2014; Dimitriev and Saperova, 2015). The RG highly correlated with the HR (almost 0.8). However, it was not the maximum correlation in frontal and prefrontal areas. In addition, the maximum correlation of RG with HR was achieved in central cortex. This suggests that prefrontal activity can reflect little changes in stress level that cannot be indicated by neither central EEG nor HR. As mentioned, the maximum difference between SL2 and SL3 was achieved using the HR, but it was the prefrontal RG between SL2 and SL1. It may be due to there was a HR peak during the 2 min of SL1. In general, the HR was more discriminative than the prefrontal RG according to the subject-by-subject and the group analysis. However, the prefrontal RG has better temporal resolution. This advantage might be essential in potential development of real-time devices for online assessment of stress. In addition, the fact of getting reliable measures of stress through few prefrontal electrodes (Fp1, Fp2) facilitates the use of wearable devices for that proposal.

We are aware of the inherent difficulties to follow a sound methodology when EEG is involved in non-controlled experiments (i.e., out-of-the-lab experiments with motor and cognitive artifacts). The conducted experiment was designed to overcome these limitations with a clear and reproducible methodology. Since participants could start the experiment with unknown levels of stress, it was necessary to expose them to a condition in which a homogenous level of stress was caused before applying stimulation. If participants had started the experiment from "zero stress level," no relaxing effects could have observed in any case. A well-established method (i.e., the MIST) was used for that. Stress was undoubtedly caused. In addition, the HR marker also indicated increasing levels of stress during the MIST (see **Figure 5**). We understand that this fact is not under discussion. The way in which the prefrontal RG was successfully measured during the MIST indicates the robustness of our EEG experiment under these adverse circumstances. Right after the stress session, participants got into an isolated room and EEG was recorded under conditions close to the ones of typical EEG experiments. The participants got relaxed after 10 min. laying on a puff-shaped seat in our specific room designed to cause relax (broadly used in Education Centers after an outbreak of violence to cause relax), isolated of disturbances and with no stimulation apart of the white lighting. As expected, the HR marker indicated decreasing levels of stress during the relaxation session (see **Figure 5**). For the authors, it is unquestionable that the participants got relaxed at the end of the relaxation session. Under both circumstances, stress and relaxation, we found the main claim of this paper: a correlation of the prefrontal RG with the stress level.

In conclusion, we found that the prefrontal RG can be used as a marker for stress assessment. It has been previously used in meditation studies, but not under relaxation/stress paradigms. We analyzed and compared it with several EEG frequency bands and with the HR during relaxation/stress sessions. The prefrontal RG significantly discriminated stress levels, and highly correlated with the expected stress level and the HR. The paper reports the methodology and results of a preliminary study that can motivate further research in the field. Only six subjects participated in the study. In addition, it is difficult to determine a "healthy volunteer" about stress since there are many constraints (e.g., social, family, personal, and work) that may influence stress as to restrict the study to only six people. Therefore, more case studies are needed to draw more accurate and reliable conclusions. Despite that, our findings could have relevant impact on stress assessment research. The assessment of stress level by the prefrontal RG has two main advantages. On one hand, the prefrontal RG has higher temporal resolution than other established stress markers such as the HR or the cortisol. On the other hand, it implies the use of few electrodes located at non-hairy head positions. Therefore, it facilitates the use of non-invasive dry wearable real-time devices for ubiquitous assessment of stress, thus potentially helping to improve the life quality of people in daily-life activities.

AUTHOR CONTRIBUTIONS

FUNDING

ACKNOWLEDGMENTS

REFERENCES

Aschbacher, K., O'Donovan, A., Wolkowitz, O. M., Dhabhar, F. S., Su, Y., and Epel, E. (2013). Good stress, bad stress and oxidative stress: insights from anticipatory cortisol reactivity. *Psychoneuroendocrinology* 38, 1698–1708. doi: 10.1016/j.psyneuen.2013.02.004

Bali, A., and Jaggi, A. S. (2015). Clinical experimental stress studies: methods and assessment. *Rev. Neurosci.* 26, 555–579. doi: 10.1515/revneuro-2015-0004

Başar-Eroglu, C., Strüber, D., Schürmann, M., Stadler, M., and Başar, E. (1996). Gamma-band responses in the brain: a short review of psychophysiological correlates and functional significance. *Int. J. Psychophysiol.* 24, 101–112. doi: 10.1016/S0167-8760(96)00051-7

Brouwer, A.-M., Neerincx, M. A., Kallen, V., van der Leer, L., and ten Brinke, M. (2011). EEG alpha asymmetry, heart rate variability and cortisol in response to Virtual Reality induced stress. *J. CyberTher. Rehabil.* 4, 27–40.

Caspi, A., Sugden, K., Moffitt, T. E., Taylor, A., Craig, I. W., Harrington, H., et al. (2003). Influence of life stress on depression: moderation by a polymorphism in the 5-HTT gene. *Science* 301, 386–389. doi: 10.1126/science.1083968

Chandiramani, S., Cohorn, L. C., and Chandiramani, S. (2007). Heart rate changes during acute mental stress with closed loop stimulation: report on two single-blinded, pacemaker studies. *Pacing Clin. Electrophysiol.* 30, 976–984. doi: 10.1111/j.1540-8159.2007.00795.x

Dagher, A., Tannenbaum, B., Hayashi, T., Pruessner, J. C., and McBride, D. (2009). An acute psychosocial stress enhances the neural response to smoking cues. *Brain Res.* 1293, 40–48. doi: 10.1016/j.brainres.2009.07.048

Dedovic, K., D'Aguiar, C., and Pruessner, J. C. (2009a). What stress does to your brain: a review of neuroimaging studies. *Can. J. Psychiatry* 54, 6–15. doi: 10.1177/070674370905400104

Dedovic, K., Renwick, R., Mahani, N. K., Engert, V., Lupien, S. J., and Pruessner, J. C. (2005). The montreal imaging stress task: using functional imaging to investigate the effects of perceiving and processing psychosocial stress in the human brain. *J. Psychiatry Neurosci.* 30, 319–325.

Dedovic, K., Rexroth, M., Wolff, E., Duchesne, A., Scherling, C., Beaudry, T., et al. (2009b). Neural correlates of processing stressful information: an event-related fMRI study. *Brain Res.* 1293, 49–60. doi: 10.1016/j.brainres.2009.06.044

Dimitriev, D. A., and Saperova, E. V. (2015). Heart rate variability and blood pressure during mental stress. *Ross. Fiziol. Zh. Im. I.M. Sechenova* 101, 98–107.

Friedman, A. K., Walsh, J. J., Juarez, B., Ku, S. M., Chaudhury, D., Wang, J., et al. (2014). Enhancing depression mechanisms in midbrain dopamine neurons achieves homeostatic resilience. *Science* 344, 313–319. doi: 10.1126/science.1249240

Jenke, R., Peer, A., and Buss, M. (2014). Feature extraction and selection for emotion recognition from EEG. *IEEE Trans. Affect. Comput.* 5, 327–339. doi: 10.1109/TAFFC.2014.2339834

Kim, D.-K., Rhee, J.-H., and Kang, S. W. (2014). Reorganization of the brain and heart rhythm during autogenic meditation. *Front. Integr. Neurosci.* 7:109. doi: 10.3389/fnint.2013.00109

Kingston, S. G., and Hoffman-Goetz, L. (1996). Effect of environmental enrichment and housing density on immune system reactivity to acute exercise stress. *Physiol. Behav.* 60, 145–150. doi: 10.1016/0031-9384(95)02241-4

Kirschbaum, C., Pirke, K. M., and Hellhammer, D. H. (1993). The "Trier social stress test"–A tool for investigating psychobiological stress responses in a laboratory setting. *Neuropsychobiology* 28, 76–81.

Kolotylova, T., Koschke, M., Bär, K.-J., Ebner-Priemer, U., Kleindienst, N., Bohus, M., et al. (2010). [Development of the "Mannheim Multicomponent Stress Test" (MMST)]. *Psychother. Psychosom. Med. Psychol.* 60, 64–72. doi: 10.1055/s-0028-1103297

Lutz, A., Greischar, L. L., Rawlings, N. B., Ricard, M., and Davidson, R. J. (2004). Long-term meditators self-induce high-amplitude gamma synchrony during mental practice. *Proc. Natl. Acad. Sci. U.S.A.* 101, 16369–16373. doi: 10.1073/pnas.0407401101

Mahar, I., Bambico, F. R., Mechawar, N., and Nobrega, J. N. (2014). Stress, serotonin, and hippocampal neurogenesis in relation to depression and antidepressant effects. *Neurosci. Biobehav. Rev.* 38, 173–192. doi: 10.1016/j.neubiorev.2013.11.009

Michels, N., Sioen, I., Clays, E., De Buyzere, M., Ahrens, W., Huybrechts, I., et al. (2013). Children's heart rate variability as stress indicator: association with reported stress and cortisol. *Biol. Psychol.* 94, 433–440. doi: 10.1016/j.biopsycho.2013.08.005

Nagano-Saito, A., Dagher, A., Booij, L., Gravel, P., Welfeld, K., Casey, K. F., et al. (2013). Stress-induced dopamine release in human medial prefrontal cortex–18F-fallypride/PET study in healthy volunteers. *Synapse* 67, 821–830. doi: 10.1002/syn.21700

Papousek, I., Weiss, E. M., Schulter, G., Fink, A., Reiser, E. M., and Lackner, H. K. (2014). Prefrontal EEG alpha asymmetry changes while observing disaster happening to other people: cardiac correlates and prediction of emotional impact. *Biol. Psychol.* 103, 184–194. doi: 10.1016/j.biopsycho.2014.09.001

Pearlin, L. I., Lieberman, M. A., Menaghan, E. G., and Mullan, J. T. (1981). The stress process. *J. Health Soc. Behav.* 22, 337–356. doi: 10.2307/2136676

Ranganathan, G., Rangarajan, R., and Bindhu, V. (2012). Estimation of heart rate signals for mental stress assessment using neuro fuzzy technique. *Appl. Soft Comput.* 12, 1978–1984. doi: 10.1016/j.asoc.2012.03.019

Regula, M., Socha, V., Kutilek, P., Socha, L., Hana, K., Hanakova, L., et al. (2014). "Study of heart rate as the main stress indicator in aircraft pilots," in *Proceedings of the 16th International Conference on Mechatronics - Mechatronika 2014* (Brno: IEEE), 639–643.

Reinhardt, T., Schmahl, C., Wüst, S., and Bohus, M. (2012). Salivary cortisol, heart rate, electrodermal activity and subjective stress responses to the Mannheim Multicomponent Stress Test (MMST). *Psychiatry Res.* 198, 106–111. doi: 10.1016/j.psychres.2011.12.009

Sayette, M. A. (1993). Heart rate as an index of stress response in alcohol administration research: a critical review. *Alcohol. Clin. Exp. Res.* 17, 802–809. doi: 10.1111/j.1530-0277.1993.tb00845.x

Schleifer, L. M., and Okogbaa, O. G. (1990). System response time and method of pay: cardiovascular stress effects in computer-based tasks. *Ergonomics* 33, 1495–1509. doi: 10.1080/00140139008925349

Selye, H. (1975a). Confusion and controversy in the stress field. *J. Hum. Stress* 1, 37–44. doi: 10.1080/0097840X.1975.9940406

Selye, H. (1975b). Stress and distress. *Compr. Ther.* 1, 9–13.

Semmlow, J. L. (2014). *Biosignal and Medical Image Processing, 3rd Edn.* CRC Press Book. Available online at: https://www.crcpress.com/Biosignal-and-Medical-Image-Processing-Third-Edition/Semmlow-Griffel/9781466567368

Seo, S.-H., and Lee, J. T. (2010). "Stress and EEG," in *Convergence and Hybrid Information Technologies*, ed M. Crisan (InTech), 413–426.

Sirca, F., Onorati, F., Mainardi, L., and Russo, V. (2015). Time-varying spectral analysis of single-channel EEG: application in affective protocol. *J. Med. Biol. Eng.* 35, 367–374. doi: 10.1007/s40846-015-0044-5

Slavish, D. C., Graham-Engeland, J. E., Smyth, J. M., and Engeland, C. G. (2015). Salivary markers of inflammation in response to acute stress. *Brain Behav. Immun.* 44, 253–269. doi: 10.1016/j.bbi.2014.08.008

Steinhubl, S. R., Wineinger, N. E., Patel, S., Boeldt, D. L., Mackellar, G., Porter, V., et al. (2015). Cardiovascular and nervous system changes during meditation. *Front. Hum. Neurosci.* 9, 1–10. doi: 10.3389/fnhum.2015.00145

Tanida, M., Katsuyama, M., and Sakatani, K. (2007). Relation between mental stress-induced prefrontal cortex activity and skin conditions: a near-infrared spectroscopy study. *Brain Res.* 1184, 210–216. doi: 10.1016/j.brainres.2007.09.058

Zschucke, E., Renneberg, B., Dimeo, F., Wüstenberg, T., and Ströhle, A. (2015). The stress-buffering effect of acute exercise: evidence for HPA axis negative feedback. *Psychoneuroendocrinology* 51, 414–425. doi: 10.1016/j.psyneuen.2014.10.019

Appendix C

Article preprint

Trends in EEG-BCI for Daily-Life: Requirements for Artifact Removal

Jesus Minguillon[*], Miguel Angel Lopez-Gordo, Francisco Pelayo

Abstract

Since the discovery of the EEG principles by Berger in the 20's, procedures for artifact removal have been essential in its pre-processing. In literature, diverse approaches based on signal processing, data mining, statistic models, and others compile information from multiple electrodes to build filters for artifact removal in the time, frequency or space domains. For almost one century, EEG acquisitions have required strict experimental conditions that included an isolated room, clinical acquisition systems, rigorous experimental protocols and very precise stimulation control. Under these steady experimental conditions, artifact removal techniques have not significantly evolved since then. However, in the last decade technological advances in brain-computer interfaces permit EEG acquisition by means of wireless, mobile, dry, wearable, and low-cost EEG headsets, with new potential daily-life applications, such as in entertainment or industry. New aspects not considered before, such as massive muscular and electrical artifacts, reduced number of electrodes, uncontrolled concomitant stimulus or the need for online processing are now essential. In this paper, we present a critical review of EEG artifact removal approaches, discuss their applicability to daily-life EEG-BCI applications, and give some directions and guidelines for upcoming research in this topic. Based on the results of the review, existing artifact removal techniques need further evolution to be applied in daily-life EEG-BCI. The use of multiple-step procedures is recommended, combining source decomposition with blind source separation and adaptive filtering. It is also recommendable to define and characterize most of artifacts evoked in daily-life EEG-BCI for a more effective removal.

Keywords: Electroencephalogram, EEG, artifact removal, brain-computer interface, BCI, daily-life application.

1. Introduction

A brain-computer interface (BCI) provides a communication channel that interconnects the brain with an external device. In particular for BCI based on electroencephalogram (EEG), electric potentials recorded from electrodes placed on the scalp provide direct measure of brain activity. However, EEG recordings are usually contaminated by undesired signals called artifacts. Artifacts are a source of noise in EEG acquisitions and they are caused by endogenous (e.g., physiological sources such as eye, muscle and cardiac activity) and exogenous (e.g., non-physiological sources such as impedance mismatch, power-line coupling, etc.) reasons. Since Hans Berger reported the first acquisition of human EEG in 1929 [1], different methods have been used to handle EEG artifacts. These include three different groups of

techniques, namely i) artifact avoidance (e.g., telling subjects to avoid moving or blinking during the experiment and gaze at a central fixation point), ii) artifact rejection (e.g., discarding contaminated trials by visual inspection or by automatic procedures), and iii) artifact removal based on pre-processing of the EEG data [2]. In this review we focus on the third group. It comprises a huge variety of algorithms that combine EEG recordings with information about the experimental conditions to obtain the most efficient filter for artifact removal.

Classical EEG-BCI experiments require strict laboratory conditions far from those of daily-life. Almost all the studies found in literature for this review were carried out following rigorous experimental protocols, including very precise stimulation control. Most of them were performed within isolated environments and used clinical acquisition systems [3]–[8]. Under these strict conditions there are methods that efficiently remove artifacts such as those caused by eye blinks, eye movements or teeth clenching (see reviews [2], [9]–[12]).

Thanks to technological advances, EEG headsets have dramatically evolved in the last years. Current portable-wearable-wireless EEG acquisition systems permit ubiquitous acquisition outside a laboratory. In addition, the development of dry electrodes [13]–[18] may facilitate the use of EEG-BCIs in daily-life environments. Apart from hardware, progress in signal processing is also essential for the deployment of these modern systems. In particular, artifact removal in daily-life applications is one of the decisive areas for that goal [19]. Nevertheless, artifact removal techniques have not evolved accordingly. For instance, most studies found in the literature only focused on removal of in-lab artifacts (e.g., the removal of ocular artifacts [20]–[22]). However, EEG in daily-life environments is affected by both in-lab well-known artifacts (e.g., ocular, cardiac, power-line noise, etc.), and outdoor not well-known artifacts caused by massive movement (e.g., muscular and mechanical artifacts) and a variety of electromagnetic causes.

In summary, existing approaches for artifact removal have become impractical in daily-life scenarios. Thus, new techniques need to be investigated and developed. Despite some incipient contributions, there is no commonly accepted methodology for artifact removal in daily-life EEG-BCI applications. In this paper we present a review of existing EEG artifact removal approaches and discuss them in this new context. After analyzing the main aspects of daily-life EEG-BCI applications in section 2, we establish the main requirements for artifact removal in daily-life in section 3. In section 4, we summarize most of artifact removal approaches in the last decade and discuss about their applicability to the daily-life requirements. In section 5, we suggest some directions and guidelines for future solutions.

2. Daily-Life EEG-BCI Applications

Since the first papers using the term 'brain-computer interface' appeared in the early 90's [23], [24] the study of BCIs has grown dramatically [25]. EEG-BCIs decode electrical potentials recorded on the scalp and convert them into valuable pieces of physiological and cognitive information. The translation of neurophysiological signals into information enables the user to control electronic devices and establish bidirectional communication with them. This translation is performed throughout different blocks within the BCI (see Fig. 1).

The design of a BCI requires every single element (e.g., electrodes, communication channel, processing methods, etc.) to be chosen from all the available technological options according to the final application. Thus, the evolution of EEG-BCI applications is bound to the changes and advances in technology, together with other important factors such as people activities and necessities. Since their origin, researchers have mainly used EEG-BCIs as a communication tool for disabled people such as patients in a complete locked-in state [26]–[28] or patients with severe motor impairment [29], [30]. EEG-BCIs have been also used as rehabilitation tools [31], [32], as assistive technology [33]–[36], and others [37]. For instance, a P300 speller EEG-BCI was proposed in [38]. Another example of classical use is the control of neuroprostheses
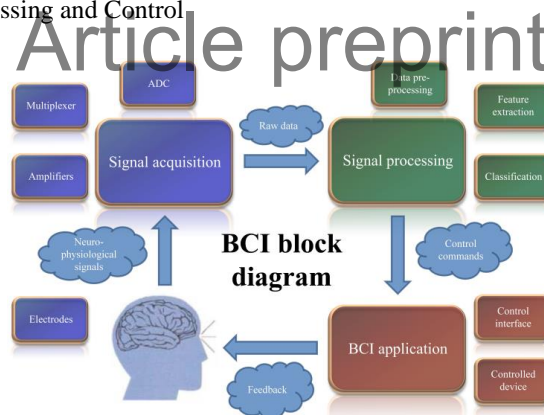
Article preprint

Fig. 1. Basic block diagram of a BCI. The first block is signal acquisition (blue color in Fig. 1). It is composed of electrodes, amplifiers, multiplexer and analog to digital converter and it is responsible for the acquisition of neurophysiological signals and their conversion to digital values. The second block is signal processing (green color in Fig. 1). It translates the raw data received from the first block into construable control commands. The translation usually requires three steps, namely data preprocessing, feature extraction and classification. The data preprocessing adapts the raw data to further processing (e.g., filtering, artifact removal, normalization, etc.). The feature extraction obtains the relevant parameters from the preprocessed information. Finally these features are classified to generate suitable control commands. These are sent to the third functional block, the BCI application (red color in Fig. 1). This block includes a control interface in charge of interpreting the control commands and producing the necessary signals to control and communicate with the final device. The information transfer between the functional blocks is performed by communication interfaces. They usually include a transmitter and/or receiver which places/takes the information into/from the communication channel following certain protocol, and a synchronization system (e.g., a microcontroller). Information flows from the BCI application to the subject resulting in a closed-loop (i.e., feedback). In some cases the feedback consists in a representation of the brain activity, the so-called neurofeedback.

[8] with potential application for restoring movement. However, current EEG-BCIs are not intended to work exclusively in health applications but also in daily-life environments.

Although the interest in health applications remains, the development of portable-wearable-wireless hardware and the appearance of improved techniques for EEG processing have motivated the emergence of novel EEG-BCI applications. These applications challenge the classical definition and functional structure of a BCI (e.g., open-loop operation in some applications). For example, the interest in neuromarketing has grown in the last years [39] and some studies related to the attention to human speech [40]–[43] have suggested EEG-BCIs as a useful tool for that. In arts, EEG-BCIs have been applied as translators from brain activity into music (Neural Music program [44], or the 'Concert: Music and Brain', as part of the IWINAC2015 Congress). In defense, an example is the DARPA Augmented Cognition technology [45], [46]. In entertainment, gaming control has been proposed as a EEG-BCI application [47] (see Fig. 2a). In addition, some applications in smart living environments have been reported [48]–[51]. In cognitive neuroscience, various EEG-BCIs have been proposed for brain workload [52] and conscious awareness [53] measurement, and for drowsiness detection [54]. Finally, sport professionals have become more and more interested in the potential advantages of neuroimaging [55] (see Fig. 2b).

Despite the number of studies reporting advances in EEG-BCI research, some aspects are still lacking. In the next subsections, some of the more relevant aspects of EEG-BCIs (e.g., EEG acquisition systems and headsets, processing, physiological signals, working environment, and EEG features) are analyzed under the framework of daily-life applications.

Article preprint

(a)   (b)

Fig. 2. Example of daily-life EEG-BCI applications. The graphical user interface proposed in [47] for EEG-BCI gaming control is displayed in (a). The mobile EEG system proposed in [55] for outdoor activity is displayed in (b).

2.1. EEG Acquisition Systems and Headsets

Both EEG acquisition systems and headsets have undergone some changes in recent years. In particular, portable-wearable-wireless acquisition systems and headsets with a few dry electrodes have been commercialized. They are analyzed in the next subsections.

2.1.1. EEG Acquisition Systems

Traditional EEG acquisition systems consist of several electrodes attached to the scalp and connected to a front-end amplifier by leads [56]. Those systems do not facilitate the execution of motion tasks due to the cables, size, weight, and portability of the devices. Hence traditional acquisition systems may be appropriate for daily-life applications during the prototype phase, but they may be less appropriate in final implementation (products).

Fortunately some companies and research groups have created modern systems that use wireless communication such as Bluetooth (see Fig. 3a-3c). Moreover, they are small in size and efficient in power consumption, thus providing portability and wearability. These features allow modern EEG headsets to be assembled in user friendly styles such as headbands or baseball caps (see [25] for a thorough review). Various commercial products and research prototypes are presented in Fig. 3. It must be taken into account that these wireless systems may be inconvenient for applications that need synchronization between the

(a)   (b)   (c)   (d)   (e)   (f)

(g)   (h)   (i)   (j)   (k)   (l)
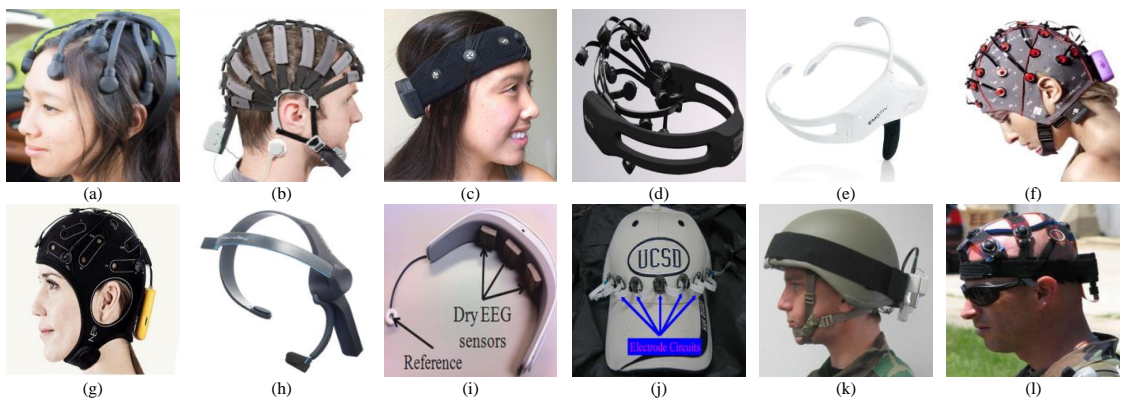
Fig. 3. Various portable wireless headsets and acquisition systems for EEG recording. (a) (b) (c) Miniature Wireless Acquisition Systems by Cognionics with Quick-20 Dry EEG Headset, 72-Channel Dry EEG Headset and Multiposition Dry EEG Headband respectively, (d) (e) EPOC and Insight wireless EEG acquisition systems by Emotiv, (f) g.Nautilus wireless EEG acquisition system by g.tec, (g) ENOBIO 8 wireless EEG system by Neuroelectrics, (h) MindWave Mobile EEG acquisition headset by NeuroSky, (i) wearable EEG acquisition headset [47], (j) baseball cap-based EEG acquisition system [14], (k) soldier's Kevlar helmet-based ambulatory wireless EEG system [52], and (l) wireless EEG sensor headset by Advanced Brain Monitoring used in [46].

stimulus and the recording. Some commercial products include a supplementary module that provides synchronization by using proprietary software, but not between the stimulus player and the headset. Therefore wireless headsets are still not intended for paradigms in which synchronism is essential (e.g., evoked potentials). In addition, the usage of an extra module implies extra hardware that limits portability. These could justify why most daily-life applications work with brain rhythms or steady-state responses (see subsection 2.5 for further information).

2.1.2. EEG Headsets

Since the extended international 10-20 system for EEG electrode location [57] was published in 1958, the number of channels recorded during EEG experiments typically did not exceed 64. New standards such as 10-10 (ten percent) [58] and 10-5 (five percent) [59] allowed for high density EEG studies with 128-256 channels [5], [60]. That is useful for spatial filtering such common average reference (CAR) which subtracts the mean of all channels in order to reduce noise. Many channels are needed to obtain a proper common reference. Laplacian montages have been proved to be highly effective in, for example, artifact identification and elimination [12], saccadic spike potentials reduction [61], and one-dimension cursor control [62]. Nevertheless, the cost in terms of preparation time and usability rule out the use of high density EEG headsets to execute daily-life activities. The necessity of a simple and rapid electrical montage for daily-life applications is evident. Simple electrode montages have been implemented in modern EEG headsets such as the EEG headband of Cognionics (see Fig. 3c), the EPOC and Insight wireless acquisition systems of Emotiv (see Fig. 3d and 3e respectively) or the MindWave mobile acquisition headset of NeuroSky (see Fig. 3h).

Another evolved aspect is the electrode type. Traditional wet EEG electrodes are considered the gold standard [13]. They require the use of skin prep and conductive gel to improve impedance of the electrode-scalp interface. This preparation takes time, contributes to user fatigue, and requires support from technical staff. It seems to be unsuitable for daily-life applications. In the literature, different approaches of dry EEG electrodes have been proposed as a solution for that problem [14]–[18]. Ideally, dry EEG electrodes are able to record potentials from the scalp without preparation. They have been tested under alpha-beta rhythms [63], steady-state visual evoked potentials (SSVEPs) [64], [65], and auditory event-related potentials (ERPs) paradigms [66]. Nevertheless, there still are some lacks regarding dry EEG electrodes. For example, evaluation procedures are questionable [13]. Only some studies presented a comparison of dry versus wet electrodes [15], [16], [67], [68]. Some headsets carrying dry EEG electrodes are reported in Fig. 3a-c.

2.2. Processing

The online capability of an EEG-BCI application depends on, between others, the computing efficiency of the processing block. In this context, the term 'online' refers to real-time operation of the application (i.e., processing and output are performed during the experiment with acceptable delay for the specific application); the term 'offline' implies that processing and output are performed after the experiment, or during it but with an unacceptable delay for the specific application. Offline processing has been generally utilized in EEG studies. Its main advantage is that it does not need high performance in terms of processing time. Nevertheless, automatic real-time operation is fundamental for daily-life applications such as gaming [47] or cell-phone control [48]. Fortunately, advances in both hardware and processing methods have made online operation a reality [3], [69]. For instance, novel feature extractors and classifiers which have improved EEG processing (e.g., fuzzy-logic [70], [71], neural-networks [72], [73], etc.).

Article preprint

2.3. Physiological Signals

Among the different types of BCIs, hybrid systems have been proposed in recent studies. They are based on the simultaneously acquisition of EEG and other physiological signals. For example, near-infrared spectroscopy (NIRS) provides information about local neural activity by measuring the level of oxygen saturation in blood. NIRS BCIs [74] and hybrid NIRS-EEG BCIs [75]–[77] have been used in motor imagery applications. In addition, electromyography (EMG) signals were used for error correction during spelling tasks in a P300-based BCI [78]. Other BCIs have been used in combination with eye trackers [79], [80]. Also typical artifact sources such as teeth clench [80], [81] and ocular movements [20], [22], [82]–[86] have been combined with EEG activity for BCI control and artifact removal respectively.

2.4. Working Environment

The vast majority of EEG-BCI studies found in the literature were performed within isolated environments (e.g., laboratories), and participants were instructed to limit their movements [3], [6]–[8]. Thanks to this, the presence of external interferences and massive movements that penalize the quality of the EEG (i.e., artifacts) is reduced. On the contrary, daily-life applications are supposed to work while performing everyday-life tasks outdoors, for instance, walking on the street among other people. However, limited success has been obtained with EEG-BCIs working in these conditions. Even some applications intended for daily-life environments such as smart living environmental auto-adjustment [49] or drowsiness detection [54] were exclusively tested using in-lab virtual reality.

Although the evolution from laboratory to daily-life environment is still challenging for researchers, some authors reported promising results. A recent study proposed a classifier of single-trial auditory ERPs with EEG during real and simulated flight [66]. A cell phone-based EEG-BCI for communication in daily-life was tested with ten volunteers located in an office room without electromagnetic isolation [48]. In addition, an EEG-BCI for freely moving humans was successfully examined with ten subjects walking a treadmill in a naturalistic environment [64]. Nevertheless, both cell phone and freely moving human EEG-BCIs utilized SSVEPs probably due to their artifact-robustness (see section 3.1 for detailed information).

2.5. EEG Features

EEG-BCIs can be classified into three main groups regarding the EEG features that they utilize: brain rhythms, evoked potentials (EPs) and steady-state responses.

2.5.1. Rhythms-Based EEG-BCIs

When an EEG is analyzed, low amplitude periodic signals (microvolts) at different frequencies (i.e., rhythms) are observed as a result of neuron interactions (see Table I). Rhythms-based EEG-BCIs (e.g., alpha-based, mu-based, etc.) do not require external stimulation for their elicitation. The so-called thought translation device (TTD) is an example [87]. Regarding the mu rhythm, one of the first works consisted in the vertical shifting of an object displayed on a screen [23]. A mu rhythm was also employed in the control of a hand orthosis by a tetraplegic patient [88] as well as in binary motor imagery EEG-BCI applications [36]. Beta and theta rhythms have been utilized in neurofeedback for assessment and effective intervention of attention deficit hyperactivity disorder (ADHD) [89].

Regarding daily-life applications, theta rhythm have been employed together with alpha in sporting performance [90], drowsiness detection [54], smart living environment [49], [50] or gaming control [47] (see [91] for a review). However, user training [92], [93] is needed in this type of EEG-BCI [94], [95]. The calibration time (i.e., user training) leads us to think that they may be not appropriate for daily-life applications. Furthermore, some of the cited daily-life rhythms-based EEG-BCIs were only tested under unrealistic conditions, for example, using virtual reality and/or within a laboratory. Their applicability in daily-life environments was not verified.

TABLE I
EEG RHYTHMS

Rhythm	Frequency (Hz)
Slow cortical potentials (SCPs)	< 3
Delta	< 4
Theta	4-7
Alpha	8-13
Beta	13-30
Gamma	> 30
Mu	8-12

2.5.2. EP-Based EEG-BCIs

Evoked potentials are electrical signals in the EEG produced as response to stimuli (e.g., auditory and visual). One of the most utilized EPs in EEG-BCI is the P300 (positive deflection at least 300 ms after the stimulus onset). In the EEG-BCI context, P300 is usually produced by a physical sensory stimulus followed by a cognitive task (e.g., count of stimuli). Spelling [7], [38], [96], 2-D cursor control [97] and humanoid robot control [98] are examples of classical P300-based EEG-BCI.

Few EP-based daily-life applications have been found in the literature [66]. One of the main advantages of EP-based EEG-BCIs is that they do not require user training. However, there can be some users unable to control EP-based EEG-BCIs due to the 'BCI illiteracy' [99]–[103]. In addition, precise synchronization between the stimulus player and the acquisition system is required in EP paradigms since evoked potentials appear a short time (milliseconds) after the stimulus presentation. Moreover, EPs are usually denoised by trial averaging, thus the significance of the synchronism. As mentioned in previous sections, the synchronization between the stimulus player and the acquisition system is still lacking in wireless EEG-BCIs.

2.5.3. Steady-State-Based BCIs

A train of repetitive stimuli can cause periodic responses; the so-called steady-state evoked potentials. Depending on the stimulation, they can be either SSVEPs for visual stimuli or auditory steady-state responses (ASSRs) for auditory stimuli. SSVEPs have been utilized in classical EEG-BCI applications such as spelling [79], [104]–[106], prosthesis [8], and wheelchair control [34]. Characterization of SSVEPs and stimulation enhancement have been object of research in the last years [107]–[109].

Some daily-life applications are based on SSVEPs, for instance, EEG-BCI for freely moving humans [64], tele-services accessing [80] and cell phone-based EEG-BCI [48]. ASSRs were employed in studies for selective attention [43], [73], [110]. The extended use of steady-state-based EEG-BCIs might be because they combine the 'plug and play' feature (i.e., no user training is needed) of EP-based EEG-BCIs with the robustness of rhythms-based BCIs in presence of artifacts (see section 3.1 for detailed information).

3. EEG Artifact Removal in Daily-Life

As mentioned, artifact removal is one of the decisive areas for the deployment of daily-life EEG-BCIs. Once the main aspects of daily-life EEG-BCIs applications have been analyzed, it may be interesting to set up the main requirements for artifact removal methods in this context. In the next subsections we report those requirements together with a brief survey of EEG artifact removal.

3.1. Requirements for Daily-Life

Each aspect of daily-life EEG-BCIs analyzed in section 2 results in certain requirements and limitations for artifact removal methods. These are related to both the algorithm to remove artifacts and the experiment to record the EEG.

- *EEG Acquisition Systems and Headsets*: the use of portable-wearable-wireless EEG acquisition systems in daily-life suggests testing artifact removal approaches with EEG recorded by that type of system. In addition, the necessity of a simple and rapid electrical montage suggests that algorithms should be able to work with a single active channel (channel + reference + ground) on the one hand, and that EEG for testing has to be recorded by using simple montage (e.g., three or less electrodes, apart from reference and ground). It would also be desirable to use dry electrodes.
- *Processing*: online processing is mandatory for daily-life applications. As part of the processing block of an EEG-BCI, artifact removal algorithms must be able to work under real-time requirements.
- *Physiological signals*: despite the combined use of EEG with other physiological signals may result advantageous in some cases, it requires the use of multiple electrodes, thus it is contrary to a simple montage. Therefore, artifact removal algorithms for daily-life applications must be able to work with EEG signals exclusively, and the EEG used to test them must have been real (i.e., not simulated EEG).
- *Working environment*: the daily-life environment suggests testing approaches with EEG recorded outdoors while performing everyday-life tasks (e.g., walking, running, etc.). Under these circumstances, complex artifacts (i.e., those resulting from massive movement and a variety of electromagnetic causes) are present together with well-known artifacts (e.g., ocular, cardiac and 50/60 Hz power-line artifacts). Therefore, artifact removal algorithms are required to eliminate complex artifacts.
- *EEG Features*: rhythms-based and steady-state-based EEG-BCIs have an advantage regarding the artifacts. Whilst ocular artifacts are usually located at low frequencies (see Fig. 4a), muscle artifacts are normally related to higher frequencies [111]. Indeed, all the artifacts resulting from daily-life tasks such as walking or running (e.g., ocular, muscular, electrical, mechanical, etc.) are present at a wide frequency band, and their spectral power directly depends on the quantity of movement (see Fig. 4b). Rhythms-based and steady-state-based EEG-BCIs are less sensitive to artifacts than others due to the gathering of power at narrow frequency bands; hence they have high signal to noise ratio (SNR) at those frequencies. Only high power (compared with the signal power) artifacts occupying the same narrow band might be problematic. A simple band-pass filtering might be enough to remove the rest. Despite that, artifact removal might be useful in this type of EEG-BCI in daily-life context. Feature extraction and classification duration might be reduced, and then the information transfer rate (ITR) increased. For daily-life EP-based EEG-BCIs, artifact removal methods might turn out to be useful in terms of improving the accuracy and reducing the number of needed stimuli; hence increasing the ITR. However, we cannot set up any special requirement for daily-life EEG-BCIs regarding the EEG features utilized.
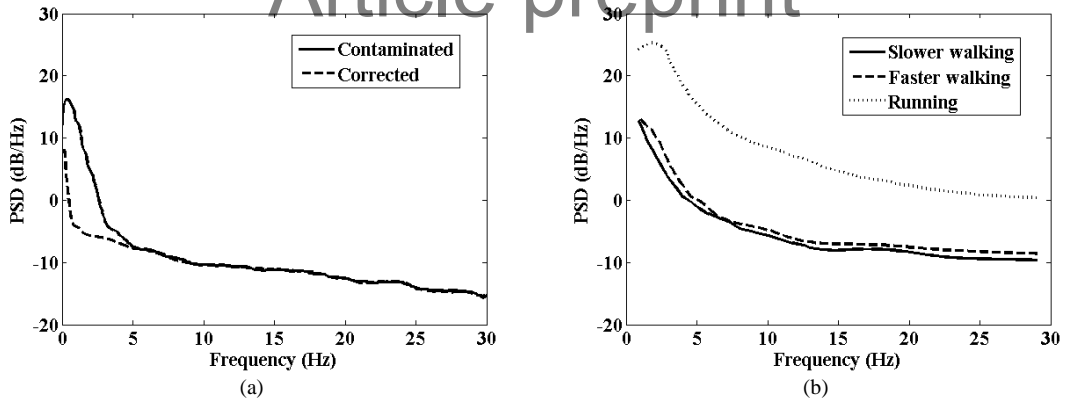
Article preprint

Fig. 4. Artifact localization in the frequency spectrum. The power spectral density (PSD) of EEG containing ocular artifacts (continuous line) and the PSD of corrected EEG (dashed line) is displayed in (a). Significant difference at low frequencies can be observed. The figure has been created from findings in [131]. The PSD of EEG containing artifacts resulting from real-life tasks (running, faster walking and slower walking) is displayed in (b). A direct dependence of the PSD on the quantity of movement can be observed. The figure has been created from findings in [5].

Table II summarizes the above requirements.

TABLE II
REQUIREMENTS OF EEG ARTIFACT REMOVAL APPROACHES IN DAILY-LIFE APPLICATIONS

Related to experiment	Related to algorithm
Performed outdoors	Removes complex artifacts
Use of portable-wearable-wireless device	Works with EEG signals exclusively
Use of real EEG signals	Works online
Performance of daily-life tasks	Works with single active channel
Use of simple electrical montage	
Use of dry electrodes	

3.2. Survey of EEG Artifact Removal

In this subsection a brief summary of the main EEG artifact removal approaches is reported. The aim of this work is not to review the state of the art of EEG artifact removal (see [9] for a recent and thorough review) but to compile and discuss the principal methods in the last years in the context of daily-life EEG-BCIs. However, it may be proper to provide some comments on artifact removal approaches in order to facilitate the subsequent discussion.

They are usually classified in different categories:

- *Filtering*: it is frequently used in EEG preprocessing. Filter coefficients are estimated and applied to a signal according to the desired order (i.e., filter aggressiveness), frequency response (e.g., low-pass, high-pass, band-pass, etc.), impulse response (e.g., FIR, IIR, and TIIR), etc. Filtering is non-adaptive if its coefficients are static; filtering is adaptive if they iteratively change according to an optimization criteria. Among the non-adaptive filters, Wiener FIR filter is one of the most utilized. It minimizes the mean square error between the desired signal and the estimated signal. Wiener filtering is more appropriate for linear time-invariant signals; it cannot work with EEG in real-time. Adaptive filters continuously adjust their coefficients in order to minimize the error between the desired and the estimated signal by using algorithms such as the least mean squares (LMS) or the recursive least squares (RLS). These are more appropriate for linear time-variant signals (e.g., EEG) than non-adaptive filters. They are efficient in real-time artifact removal but *a priori* knowledge of artifacts is

required [20], [84]. Sometimes a reference signal is used; e.g., electro-oculogram (EOG) for ocular artifacts. Alternatively, the *a priori* can iteratively be estimated (without a reference signal) by probabilistic filters after initial calibration. Kalman filters are the linear approximation of probabilistic Bayesian filters. They have been utilized in removal of transcranial magnetic stimulation (TMS)-induced artifacts [112], [113].

- *Linear regression*: it is based on the superposition principle. It is assumed that the signal of every single EEG channel is the sum of clean EEG signal (i.e., from non-noisy sources) and a portion of one or several artifact signals (i.e., from artefactual sources). These artifact signals are available by means of reference channels (e.g., EOG, EMG, ECG, etc.) or artifact templates. Thus regression aims to estimate the optimal value for the factor that determines the portion of the artifact signal within each EEG channel. Linear regression has been widely used in ocular [85] and movement [5] artifact removal.

- *Blind source separation*: blind source separation (BSS) provides a matrix of estimated sources (each column corresponds to the time-signal of a source) from a matrix of observations (each row corresponds to the time-signal of a recorded EEG channel) without using any artefactual reference. Once the sources have been estimated, those corresponding to artifacts can be identified and extracted, thus recomposing the EEG with the non-artefactual sources. Several assumptions need to be met for success in separation. Principal component analysis (PCA) is a representative BSS method. It provides a set of linearly uncorrelated variables (i.e., principal components) by using the orthogonality of the observed variables. The most used BSS method in artifact removal is the so-called independent component analysis (ICA) [86], [114]–[116]. It is based on the assumption that the recorded EEG signals are a lineal combination of several unknown and statistically independent sources. ICA has been proved to be more efficient than PCA in artifact removal. It is probably due to the better adaptation of its assumptions for the nature of the sources (i.e., artifacts and brain activity are usually independent enough). However, PCA is often applied during the ICA preprocessing. There are some derivative ICA methods such as temporally [117] and spatially [82] constrained ICA. Apart from PCA and ICA, there are other BSS-based methods that have been used for artifact removal: canonical correlation analysis (CCA) [111], [118], [119], sparse component analysis (SCA) [120], singular spectrum analysis (SSA) [121], etc.

- *Source decomposition*: it aims to decompose every single EEG channel into basic waveforms. As for BSS, these components (i.e., waveforms) can represent either brain activity or artefactual activity. Hence signals can be recomposed without artifacts components. Unlike BSS methods, source decomposition can independently be performed in every single channel. Wavelet decomposition has been widely utilized for artifact removal [21], [83], [122], [123]. The discrete wavelet transform (DWT) provides time-frequency signal breakdown (i.e., time coefficients at different frequency bands) by using a mother wavelet. The empirical mode decomposition (EMD) is also located in this category. It provides several zero-mean amplitude-frequency-modulated components, the so-called intrinsic mode functions (IMFs). EMD has been used for artifact removal in recent years [124]–[126]. Other derivative methods such as stationary wavelet transform (SWT) [127], [128] and ensemble empirical mode decomposition (EEMD) [118], [119], [129] have also been used for artifact removal with success.

- *Others*: some authors have used neural networks (NN) [130], [131] and adaptive neural fuzzy inference systems (ANFIS) [132], [133] in their methods to remove artifacts.

According to the above references, we notice that combining methods is very frequent. Indeed, some authors have compared the efficiency of different methods [134]. This fact might indicate that there is no universal method for artifact removal. The election of the artifact removal procedure deeply depends on the individual problem or application. We discuss about that in the next section.

Article preprint

4. Summary and Discussion

In this section we report a summary table (see Table III) containing the most relevant methods on artifact removal found in literature in the last decade. In particular, forty eight proposals were collected. We focus on proposals in which the artifact removal method is the main task during the EEG preprocessing. Other interesting works focused on feature extraction/classification were not considered.

Some features of the collected methods are also reported in the table. In total, ten features were analyzed for the gathered methods according to the main requirements for daily-life EEG-BCIs described in the previous section; the first six are related to the experiment employed for the evaluation of the approach and the last four concern important capabilities of the utilized algorithm. In particular, 'Performed outdoors' means the experiment was performed in a non-isolated environment (no laboratory); 'Portable-wearable-wireless device' means the employed EEG headset and acquisition system were wireless, user friendly style, and small size, 'Real EEG signals' means the processed data were real EEG acquired signals (not simulated), 'Daily-life tasks' means the EEG was recorded while performing any daily-life task (e.g., walking), 'Simple electrical montage' means the EEG was recorded from three or less electrodes (apart from reference and ground), 'Dry electrodes' means the EEG was recorded using dry EEG electrodes, 'Complex artifacts' means the algorithm can remove some artifacts related to daily-life tasks such as those resulting from massive movement (e.g., muscular and mechanical artifacts) and a variety of electromagnetic causes, 'Only EEG signals' means the algorithm can work using EEG data exclusively (without using other physiological signals such as EMG or EOG), 'Online' means the algorithm can be used under real-time requirements, and 'Single active channel' means the algorithm can work with single-channel EEG data.

It is remarkable that no method was tested in a daily-life environment; all of them were only tested to work within a laboratory. In addition, the EEG was recorded by wet electrodes in all cases. Just 2 out of 48 cases used portable-wearable-wireless devices. Real EEG data were utilized in 46 cases; simulated EEG data were employed in 2 experiments. In only 8 studies EEG was recorded while executing daily-life tasks. Simple electrical montage was employed in 3 experiments, 2 of them match with the portable-wearable-wireless device-based studies. Regarding the capabilities of the algorithms, all the collected methods can eliminate well-known artifacts (i.e., ocular, cardiac and 50/60 Hz power-line artifact) at least. However, only 19 procedures are able to remove complex artifacts, but nonetheless just 6 of them were tested using daily-life task-based EEG. Most algorithms (39) can work merely using EEG sources. Less than half (20) can work online. Finally, 23 algorithms can eliminate artifacts using single-channel EEG data.

The fact that no author has tested his method outdoors [5], [20]–[22], [82]–[86], [111], [114], [115], [118], [119], [121], [122], [124]–[132], [135]–[157] (despite some of them handled complex artifacts) indicates the difficulty when handling artifacts in a real situation (i.e., daily-life environment). For example, movement artifacts considerably vary across subject, speed and electrode location while walking [158]. Even so, it would be desirable that researchers test their methods outdoors, what would add important value to their works.

Regarding the low quantity of studies that used portable-wearable-wireless devices [122], [137], it might be caused by the recent commercialization of these systems. Indeed, both studies are from 2013 and 2014. Another fact to take into account is the synchronization problem of wireless EEG headsets. The lack of precise synchronization might have a negative effect on some artifact removal studies. For example, those that utilize evoked potentials to demonstrate the efficiency of the method. More artifact removal works using portable-wearable-wireless devices may be expected next years.

To the best of our knowledge, all the studies on artifact removal used wet electrodes. In some cases, they were active wet electrodes [5], [86] which include a pre-amplifier, with or without gain, which reduces the noise induced in the cables [159]. It is understandable taking into account the current limitations of dry electrodes. Worse results might be expected by using dry electrodes.

Article preprint

The requirement of simple electrical montage (used in [122], [127], [137]) limits the use of procedures that require information from multiple channels. It is indispensable to employ methods capable of operating with a few channels or even with a single active channel. However, most of the algorithms found in literature are based on multichannel BSS techniques (e.g., ICA). These cease to be suitable under this new scenario. In order to overcome this limitation, several authors proposed procedures for single-channel artifact removal. They are based on single-channel ICA [149], EMD [124], [126] or wavelet decomposition [122], [130], [137]. The latter has low computing cost and takes advantage of the fact that ocular artifacts are localized at low frequency bands [137]. However, in these wavelet-based approaches, EEG electrodes were placed on frontal areas, typically Fz, Fpz, F1, and F3 in the 10-20 system. At these locations ocular activity is powerful, thus the ocular component in the recorded EEG is evident. Testing those methods with central EEG activity might be recommendable in order to corroborate their robustness. The deployment of portable-wearable-wireless devices with simple electrical montages and dry electrodes will probably increase the number of artifact removal studies on daily-life tasks.

Although all the compiled proposals obtained promising results, most of them handled a very limited set of target artifacts (e.g., eye blinks and eye movement). They were not proved to be efficient with all the massive electrical, mechanical and muscular artifacts resulting from daily-life environments. However, there are some methods that were proved to eliminate more complex artifacts. For example, artifacts resulting from daily-life tasks such as walking/running [5], [158] or cycling [118], [129]. In addition, CCA was proved to be robust in SSVEP-based EEG-BCIs working under daily-life conditions in two studies [48], [64].

As mentioned before, all the algorithms running in the processing block of a daily-life EEG-BCI must have online capability. Numerous algorithms for artifact removal can be considered offline methods [86], [138], [145] due to their high computing cost which causes unacceptable delays for these applications. Fortunately, alternative solutions have been proposed. Among these proposals, adaptive filtering and wavelet decomposition are suitable procedures for real-time artifact removal.

Table IV is included in order to elucidate which methods might be more appropriate for daily-life EEG-BCI applications and to give some guidelines for future research. Within the group of very appropriate methods, there are three of them based on a combination of BSS and source decomposition, in particular, ICA or CCA joined with EEMD. The other four approaches are wavelet-based combined with adaptive filters or neural networks.

As mentioned in [9], most researchers prefer to use ICA because they believe that the assumption of independence models the brain activity better than others. Unfortunately, to the best of our knowledge and according to recent publications [9], [12], [160], there is no standardized and universally efficient artifact removal method. This has motivated the pursuit of alternative solutions such as research paradigms intending to extract narrow-band EEG features [41], [42], [161], or precautionary protocols to avoid artifacts during the experiments. For example, EEG-BCI studies usually require many trials in order to rule out artefactual activities. Long experiments may increase subject fatigue, hence provoking undesirable results. Improvement of existing methods might help to reduce the number of trials needed as well as their duration by improving feature extraction and classification. This is a particularly delicate matter when dealing with artifacts in daily-life context. The continuous appearance of noise coming from multiple artifact sources is not a trivial problem, especially when artifact sources have different natures and features (e.g., movement artifacts [158]). It is understandable that artifact removal is still lacking in daily-life EEG-BCI but it is important to progress in this area for the deployment of these modern systems [19]. In addition, advances in hardware are still essential. For example, improvement of current dry electrodes might help to reduce the number of artifacts in daily-life applications.

Article preprint

5. Conclusion

A critical review of existing artifact removal approaches and their applicability to daily-life EEG-BCIs is presented in this paper. The main requirements for EEG-BCIs in daily-life context were established. After compiling the principal artifact removal methods in the last decade, several reasons indicate that there is no definitive artifact removal technique for these applications. First of all, none of the collected approaches accomplished all the requirements; some of them reached 6 out of 10 required features but, in general, low accomplishment was achieved. Secondly, most of the procedures were only tested using well-known artifacts such as ocular and cardiac. In addition, some of the complex artifact-capable methods were never proved to work using EEGs resulting from daily-life tasks and outside a laboratory. Dealing with artifacts in daily-life context is a complex problem due to the continuous appearance of noise coming from multiple artifact sources (with different natures and features) during recordings. Although it is understandable that artifact removal is still lacking in daily-life EEG-BCI, it is important to progress in this area for the deployment of these modern systems. Advances in hardware (e.g., dry EEG electrodes) are still essential. It would be desirable that researchers continue to work on daily-life artifact removal, with special attention to the requirements analyzed in this paper. As guideline and according to results reported in tables III and IV, we would recommend the use of multiple-step procedures, combining source decomposition (in particular, wavelet or EMD) with blind source separation (in particular, CCA) and adaptive filtering. It may also be interesting to define and characterize most of artifacts evoked in daily-life EEG-BCI in order to use them as reference or template in the cited methods.

Article preprint

TABLE III
SUMMARY TABLE

Feature	Acharjee et al., 2015	Burger et al., 2015	Castellanos et al., 2006	Chen et al., 2014 (1)	Chen et al., 2014 (2)	Cho et al., 2007	Davies et al., 2007	Geetha et al., 2012	Gu et al., 2014	Guerrero-Mosquera et al., 2009	Gwin et al., 2010	Hsu et al., 2012	Hu et al., 2015	Klados et al., 2011	Kong et al., 2013	Krishnaveni et al., 2006 (1)	Krishnaveni et al., 2006 (2)	Kumar et al., 2008	Ma et al., 2011	Mammone et al., 2012	Mijovic et al., 2010	Mognon et al., 2011	Mourad et al., 2007	Mourad et al., 2013
Performed outdoors																								
Portable-wearable-wireless device																								
Real EEG signals	■	■	■	■	■		■	■	■		■	■	■	■	■	■	■	■		■	■	■	■	■
Daily-life tasks				■	■				■												■			
Simple electrical montage																								
Dry electrodes																								
Complex artifacts	■	■	■				■		■	■	■		■		■				■	■	■	■	■	■
Only EEG signals	■	■	■	■	■	■		■	■	■		■	■	■	■	■	■	■	■	■		■	■	■
Online			■		■	■			■		■					■	■	■						■
Single active channel				■	■									■				■						■

Feature	Mowla et al., 2015	Nguyen et al., 2012	Nolan et al., 2010	Peng et al., 2013	Porcaro et al., 2015	Puthusserypady et al., 2006	Raduntz et al., 2015	Romo et al., 2012	Sameni et al., 2014	Schlogl et al., 2007	Shao et al., 2009	Sweeney et al., 2013	Sziboo et al., 2012	Teixeira et al., 2006	Teixeira et al., 2007	Teixeira et al., 2008	Tiganj et al., 2010	Wang et al., 2014	Yong et al., 2009 (1)	Yong et al., 2009 (2)	Zeng et al., 2013	Zhang et al., 2015	Zhao et al., 2014	Zikov et al., 2002*
Performed outdoors																								
Portable-wearable-wireless device				■																			■	■
Real EEG signals	■	■	■	■	■		■	■		■		■	■	■	■	■	■	■	■	■	■	■	■	■
Daily-life tasks		■		■															■	■			■	
Simple electrical montage																							■	■
Dry electrodes																								
Complex artifacts	■	■				■	■	■	■		■		■				■	■			■	■		
Only EEG signals	■		■	■	■	■	■	■	■	■	■		■	■	■	■	■	■	■	■	■	■		■
Online		■		■						■			■	■	■			■	■	■			■	■
Single active channel		■											■	■					■	■			■	■

This table summarizes the main EEG artifact removal methods proposed in the last decade (since 2006) and their principal features according to the requirements of daily-life EEG-BCI applications. Each column represents one artifact removal procedure, named as first author and year of publication. Each row represents one of the main desirable features for artifact removal techniques in daily-life EEG-BCI applications. Grey color indicates accomplishment and white color indicates no accomplishment or not mentioned. *This reference has been included despite being 2002 because of its high degree of adaption to the requirements. Indeed, several methods in this table have been inspired by it.

TABLE IV
ADAPTION LEVEL TO DAILY-LIFE EEG-BCI REQUIREMENTS OF ARTIFACT REMOVAL APPROACHES

Very appropriate	Chen et al., 2014 (1,2)	Mijovic et al., 2010	Nguyen et al., 2012	Peng et al., 2013	Zhao et al., 2014
	Zikov et al., 2002				
Appropriate	Burger et al., 2015	Cho et al., 2007	Davies et al., 2007	Gu et al., 2014	Gwin et al., 2010
	Hu et al., 2015	Krishnav. et al., 2006 (1,2)	Kumar et al., 2008	Mognon et al., 2011	Mourad et al., 2007
	Mourad et al., 2013	Mowla et al., 2015	Porcaro et al., 2015	Raduntz et al., 2015	Romo et al., 2012
	Shao et al., 2009	Sweeney et al., 2013	Sziboo et al., 2012	Teixeira et al., 2006	Teixeira et al., 2007
	Teixeira et al., 2008	Tiganj et al., 2010	Wang et al., 2014	Yong et al., 2009 (1,2)	Zeng et al., 2013
Less appropriate	Acharjee et al., 2015	Castellanos et al., 2006	Geetha et al., 2012	Gue.-Mos. et al., 2009	Hsu et al., 2012
	Klados et al., 2011	Kong et al., 2013	Ma et al., 2011	Mamm. et al., 2012	Nolan et al., 2010
	Puthusser. et al., 2006	Sameni et al., 2014	Schlogl et al., 2007	Zhang et al., 2015	

Each method in Table III is classified in Table IV depending on its adaption to the daily-life EEG-BCI requirements considered in this paper: less appropriate, appropriate, very appropriate. Under no circumstance are we questioning the validity of the methods for their original purpose.

References

[1] H. Berger, "Über das Elektrenkephalogramm des Menschen," *Arch. Psychiatr. Nervenkr.*, vol. 87, no. 1, pp. 527–570, Dec. 1929.

[2] M. Fatourechi, A. Bashashati, R. K. Ward, and G. E. Birch, "EMG and EOG artifacts in brain computer interface systems: A survey," *Clin. Neurophysiol.*, vol. 118, no. 3, pp. 480–494, 2007.

[3] A. N. Belkacem, D. Shin, H. Kambara, N. Yoshimura, and Y. Koike, "Online classification algorithm for eye-movement-based communication systems using two temporal EEG sensors," *Biomed. Signal Process. Control*, vol. 16, pp. 40–47, Feb. 2015.

[4] T. Fujioka, N. Mourad, C. He, and L. J. Trainor, "Comparison of artifact correction methods for infant EEG applied to extraction of event-related potential signals," *Clin. Neurophysiol.*, vol. 122, no. 1, pp. 43–51, 2011.

[5] J. T. Gwin, K. Gramann, S. Makeig, and D. P. Ferris, "Removal of movement artifact from high-density EEG recorded during walking and running.," *J. Neurophysiol.*, vol. 103, no. 6, pp. 3526–3534, 2010.

[6] H.-J. Hwang, K. Kwon, and C.-H. Im, "Neurofeedback-based motor imagery training for brain-computer interface (BCI).," *J. Neurosci. Methods*, vol. 179, no. 1, pp. 150–6, Apr. 2009.

[7] M. Marchetti and K. Priftis, "Effectiveness of the P3-speller in brain-computer interfaces for amyotrophic lateral sclerosis patients: a systematic review and meta-analysis.," *Front. Neuroeng.*, vol. 7, no. MAY, p. 12, Jan. 2014.

[8] G. R. Müller-Putz and G. Pfurtscheller, "Control of an electrical prosthesis with an SSVEP-based BCI," *IEEE Trans. Biomed. Eng.*, vol. 55, no. 1, pp. 361–364, 2008.

[9] J. A. Urigüen and B. Garcia-Zapirain, "EEG artifact removal-state-of-the-art and guidelines.," *J. Neural Eng.*, vol. 12, no. 3, p. 31001, 2015.

[10] R. J. Croft and R. J. Barry, "Removal of ocular artifact from the EEG: A review," *Neurophysiol. Clin.*, vol. 30, no. 1, pp. 5–19, 2000.

[11] M. Sood, V. Kumar, and S. V Bhooshan, "Review of State of Art in Electrooculogram Artifact Removal from Electroencephalogram Signals," vol. 2, no. 5, pp. 71–80, 2013.

[12] S. D. Muthukumaraswamy, "High-frequency brain activity and muscle artifacts in MEG/EEG: a review and recommendations.," *Front. Hum. Neurosci.*, vol. 7, no. April, p. 138, 2013.

[13] M. A. Lopez-Gordo, D. Sanchez Morillo, and F. Pelayo Valle, "Dry EEG electrodes," *Sensors (Switzerland)*, vol. 14, no. 7, pp. 12847–12870, 2014.

[14] T. J. Sullivan, S. R. Deiss, T. P. Jung, and G. Cauwenberghs, "A brain-machine interface using dry-contact, low-noise EEG sensors," *Proc. - IEEE Int. Symp. Circuits Syst.*, pp. 1986–1989, 2008.

[15] C. T. Lin, L. De Liao, Y. H. Liu, I. J. Wang, B. S. Lin, and J. Y. Chang, "Novel dry polymer foam electrodes for long-term EEG measurement," *IEEE Trans. Biomed. Eng.*, vol. 58, no. 5, pp. 1200–1207, 2011.

[16] L. De Liao, I. J. Wang, S. F. Chen, J. Y. Chang, and C. T. Lin, "Design, fabrication and experimental validation of a novel dry-contact sensor for measuring electroencephalography signals without skin preparation," *Sensors*, vol. 11, no. 6, pp. 5819–5834, 2011.

[17] G. Gargiulo, R. a. Calvo, P. Bifulco, M. Cesarelli, C. Jin, A. Mohamed, and A. van Schaik, "A new EEG recording system for passive dry electrodes," *Clin. Neurophysiol.*, vol. 121, no. 5, pp. 686–693, 2010.

[18] J. R. Estepp, J. C. Christensen, J. W. Monnin, I. M. Davis, and G. F. Wilson, "Validation of a Dry Electrode System for EEG," *Hum. Factors Ergon. Soc. Annu. Meet. Proc.*, vol. 53, no. 18, pp. 1171–1175, 2009.

[19] V. Mihajlovi, B. Grundlehner, R. Vullers, and J. Penders, "Wearable, Wireless EEG Solutions in Daily Life Applications: What are we Missing?," *Ieee J. Biomed. Heal. Informatics*, vol. 19, no. 1, pp. 6–21, 2015.

[20] C. Guerrero-mosquera and A. N. Vazquez, "Automatic Removal of Ocular Artifacts from EEG Data using Adaptive Filtering and Independent Component Analysis," *17th Eur. Signal Process. Conf.*, no. Eusipco, pp. 2317–2321, 2009.

[21] P. Kumar and R. Arumuganathan, "Removal of Ocular Artifacts in the EEG through Wavelet Transform without using an EOG Reference Channel," *Int. J. Open Probl. Compt. Math.*, vol. 1, no. 3, 2008.

[22] R. Sameni and C. Gouy-Pailler, "An iterative subspace denoising algorithm for removing electroencephalogram ocular artifacts," *J. Neurosci. Methods*, vol. 225, pp. 97–105, 2014.

[23] J. R. Wolpaw, D. J. McFarland, G. W. Neat, and C. a Forneris, "An EEG-based brain-computer interface for cursor control.," *Electroencephalogr. Clin. Neurophysiol.*, vol. 78, no. 3, pp. 252–259, 1991.

[24] G. Pfurtscheller, D. Flotzinger, and J. Kalcher, "Brain-Computer Interface—a new communication device for handicapped persons," *J. Microcomput. Appl.*, vol. 16, no. 3, pp. 293–299, Jul. 1993.

[25] S. Lee, Y. Shin, S. Woo, K. Kim, and H. Lee, "Review of Wireless Brain-Computer Interface Systems," *Brain-Computer Interface Syst. - Recent Prog. Futur. Prospect.*, 2013.

[26] M. A. Lopez-Gordo, E. Fernandez, S. Romero, F. Pelayo, and A. Prieto, "An auditory brain–computer interface evoked by natural speech," *J. Neural Eng.*, vol. 9, no. 3, p. 036013, 2012.

[27] M. A. Lopez-Gordo, R. Ron-Angevin, and F. Pelayo Valle, "Auditory brain-computer interfaces for complete locked-in patients," *Lect. Notes Comput. Sci. (including Subser. Lect. Notes Artif. Intell. Lect. Notes Bioinformatics)*, vol. 6691 LNCS, no. PART 1, pp. 378–385, 2011.

[28] A. Kübler and N. Birbaumer, "Brain-computer interfaces and communication in paralysis: extinction of goal directed thinking in completely paralysed patients?," *Clin. Neurophysiol.*, vol. 119, no. 11, pp. 2658–66, Nov. 2008.

[29] N. Birbaumer, N. Ghanayim, T. Hinterberger, I. Iversen, B. Kotchoubey, A. Kübler, J. Perelmouter, E. Taub, and H. Flor, "A spelling device for the paralysed.," *Nature*, vol. 398, no. 6725, pp. 297–8, Mar. 1999.

[30] I. Volosyak, "SSVEP-based Bremen–BCI interface—boosting information transfer rates," *J. Neural Eng.*, vol. 8, no. 3, p. 036020, 2011.

[31] M. Bamdad, H. Zarshenas, and M. A. Auais, "Application of BCI systems in neurorehabilitation: a scoping review.," *Disabil. Rehabil. Assist. Technol.*, pp. 1–10, Jan. 2015.

[32] J. J. Daly and J. E. Huggins, "Brain-computer interface: current and emerging rehabilitation applications.," *Arch. Phys. Med. Rehabil.*, vol. 96, no. 3 Suppl, pp. S1–7, Mar. 2015.

[33] F. Cincotti, D. Mattia, F. Aloise, S. Bufalari, G. Schalk, G. Oriolo, A. Cherubini, M. G. Marciani, and F. Babiloni, "Non-invasive brain-computer interface system: Towards its application as assistive technology," *Brain Res. Bull.*, vol. 75, no. 6, pp. 796–803, 2008.

[34] Y. Li, J. Pan, F. Wang, and Z. Yu, "A hybrid BCI system combining P300 and SSVEP and its application to wheelchair control.," *IEEE Trans. Biomed. Eng.*, vol. 60, no. 11, pp. 3156–66, Nov. 2013.

[35] F. Velasco-Álvarez and R. Ron-Angevin, "Audio-Cued SMR Brain-Computer Interface to Drive a Virtual Wheelchair," in *11th International Work-Conference on Artificial Neural Networks*, 2011.

[36] F. Velasco-Álvarez, R. Ron-Angevin, L. da Silva-Sauer, and S. Sancha-Ros, "Audio-cued motor imagery-based brain-computer interface: Navigation through virtual and real environments," *Neurocomputing*, vol. 121, pp. 89–98, 2013.

[37] M. A. Lopez-Gordo, F. Pelayo, and A. Prieto, "A high performance SSVEP-BCI without gazing," in *The 2010 International Joint Conference on Neural Networks (IJCNN)*, 2010, pp. 1–5.

[38] E. Donchin, K. M. Spencer, and R. Wijesinghe, "The mental prosthesis: Assessing the speed of a P300-based brain- computer interface," *IEEE Trans. Rehabil. Eng.*, vol. 8, no. 2, pp. 174–179, 2000.

[39] A. Pradeep, "The buying brain: Secrets for selling to the subconscious mind," 2010.

[40] R. K. Maddox, W. Cheung, and A. K. C. Lee, "Selective attention in an overcrowded auditory scene: implications for auditory-based brain-computer interface design.," *J. Acoust. Soc. Am.*, vol. 132, no. 5, pp. EL385–90, Nov. 2012.

[41] M. A. Lopez-Gordo, F. Pelayo, E. Fernandez, and P. Padilla, "Phase-shift keying of EEG signals: Application to detect attention in multitalker scenarios," *Signal Processing*, vol. 117, pp. 165–173, 2015.

[42] M. A. Lopez-Gordo and F. Pelayo, "a Binary Phase-Shift Keying Receiver for the Detection of Attention To Human Speech," *Int. J. Neural Syst.*, vol. 23, no. 4, p. 12, 2013.

[43] M. A. Lopez, H. Pomares, M. Damas, A. Prieto, and E. M. D. L. P. Hernandez, "Use of Kohonen maps as feature selector for selective attention brain-computer interfaces," *Bio-Inspired Model. Cogn. Tasks, Pt 1, Proc.*, vol. 4527, pp. 407–415, 2007.

[44] M. M. Moore, "Real-World Applications for Brain – Computer Interface Technology," *Rehabilitation*, vol. 11, no. 2, pp. 162–165, 2003.

[45] M. St. John and D. Kobus, "Overview of the DARPA augmented cognition technical integration experiment," *Int. J. Hum. Comput. Interact.*, vol. 17, no. 2, pp. 131–179, 2004.

[46] M. Dorneich, S. Whitlow, and S. Mathan, "Augmented cognition transition," 2009.

[47] L. Liao, C. Chen, and I. Wang, "Gaming control using a wearable and wireless EEG-based brain-computer interface device with novel dry foam-based sensors," *J. Neuroeng. Rehabil.*, vol. 9, no. 5, 2012.

[48] Y. Wang, Y. Wang, and T. Jung, "A cell-phone-based brain–computer interface for communication in daily life," *J. Neural Eng.*, 2011.

Article preprint

[49]   C. Lin, F. Lin, and S. Chen, "EEG-based brain-computer interface for smart living environmental auto-adjustment," *J. Med. Biol. Eng.*, vol. 30, no. 4, pp. 237–245, 2010.

[50]   C. Lin, B. Lin, F. Lin, and C. Chang, "Brain computer interface-based smart living environmental auto-adjustment control system in UPnP home networking," *Syst. Journal, IEEE*, vol. 8, no. 2, 2014.

[51]   C. Guger, C. Holzner, and C. Grönegress, "Control of a smart home with a brain-computer interface," 2008.

[52]   R. Matthews and P. Turner, "Real time workload classification from an ambulatory wireless EEG system using hybrid EEG electrodes," *Eng. Med. Biol. Soc. 2008. EMBS 2008. 30th Annu. Int. Conf. IEEE*, pp. 5871 – 5875, 2008.

[53]   R. D'Arcy and S. Hajra, "Towards brain first-aid: a diagnostic device for conscious awareness," *Biomed. Eng. IEEE Trans.*, vol. 58, no. 3, pp. 750 – 754, 2011.

[54]   C. Lin, C. Chang, and B. Lin, "A real-time wireless brain–computer interface system for drowsiness detection," *Biomed. Circuits Syst. IEEE Trans.*, vol. 4, no. 4, pp. 214 – 222, 2010.

[55]   J. L. Park, M. M. Fairweather, and D. I. Donaldson, "Making the case for mobile cognition: EEG and sports performance.," *Neurosci. Biobehav. Rev.*, vol. 52, pp. 117–130, Feb. 2015.

[56]   C. Guger, A. Schlögl, C. Neuper, D. Walterspacher, T. Strein, and G. Pfurtscheller, "Rapid prototyping of an EEG-based brain-computer interface (BCI).," *IEEE Trans. Neural Syst. Rehabil. Eng.*, vol. 9, no. 1, pp. 49–58, 2001.

[57]   H. Jasper, "The ten twenty electrode system of the international federation," *Electroencephalogr. Clin. Neurophysiol.*, 1958.

[58]   G. E. Chatrian, E. Lettich, and P. L. Nelson, "Ten Percent Electrode System for Topographic Studies of Spontaneous and Evoked EEG Activities," *Am. J. EEG Technol.*, Feb. 1985.

[59]   R. Oostenveld and P. Praamstra, "The five percent electrode system for high-resolution EEG and ERP measurements," *Clin. Neurophysiol.*, vol. 112, no. 4, pp. 713–719, 2001.

[60]   I. Pisarenco, M. Caporro, C. Prosperetti, and M. Manconi, "High-density electroencephalography as an innovative tool to explore sleep physiology and sleep related disorders.," *Int. J. Psychophysiol.*, vol. 92, no. 1, pp. 8–15, Jan. 2014.

[61] A. S. Keren, S. Yuval-Greenberg, and L. Y. Deouell, "Saccadic spike potentials in gamma-band EEG: Characterization, detection and suppression," *Neuroimage*, vol. 49, no. 3, pp. 2248–2263, 2010.

[62] Y. Boudria, A. Feltane, and W. Besio, "Significant improvement in one-dimensional cursor control using Laplacian electroencephalography over electroencephalography.," *J. Neural Eng.*, vol. 11, no. 3, p. 035014, 2014.

[63] C. J. Harland, T. D. Clark, and R. J. Prance, "Remote detection of human electroencephalograms using ultrahigh input impedance electric potential sensors," *Appl. Phys. Lett.*, vol. 81, no. 17, pp. 3284–3286, 2002.

[64] Y. P. Lin, Y. Wang, and T. P. Jung, "A mobile SSVEP-based brain-computer interface for freely moving humans: The robustness of canonical correlation analysis to motion artifacts," *Proc. Annu. Int. Conf. IEEE Eng. Med. Biol. Soc. EMBS*, pp. 1350–1353, 2013.

[65] M. Oehler, P. Neumann, M. Becker, G. Curio, and M. Schilling, "Extraction of SSVEP signals of a capacitive EEG helmet for human machine interface.," *Conf. Proc. IEEE Eng. Med. Biol. Soc.*, vol. 2008, no. factor 2, pp. 4495–4498, 2008.

[66] D. E. Callan, G. Durantin, and C. Terzibas, "Classification of single-trial auditory events using dry-wireless EEG during real and motion simulated flight.," *Front. Syst. Neurosci.*, vol. 9, p. 11, Jan. 2015.

[67] N. S. Dias, J. P. Carmo, a. F. Da Silva, P. M. Mendes, and J. H. Correia, "New dry electrodes based on iridium oxide (IrO) for non-invasive biopotential recordings and stimulation," *Sensors Actuators, A Phys.*, vol. 164, no. 1–2, pp. 28–34, 2010.

[68] E. Forvi, M. Bedoni, R. Carabalona, M. Soncini, P. Mazzoleni, F. Rizzo, C. O'Mahony, C. Morasso, D. G. Cassarà, and F. Gramatica, "Preliminary technological assessment of microneedles-based dry electrodes for biopotential monitoring in clinical examinations," *Sensors Actuators, A Phys.*, vol. 180, pp. 177–186, 2012.

[69] S. Kumar and F. Sahin, "A framework for a real time intelligent and interactive Brain Computer Interface," *Comput. Electr. Eng.*, vol. 43, pp. 193–214, Apr. 2015.

[70] T. Nguyen, A. Khosravi, D. Creighton, and S. Nahavandi, "Fuzzy system with tabu search learning for classification of motor imagery data," *Biomed. Signal Process. Control*, vol. 20, pp. 61–70, Jul. 2015.

[71] T. Nguyen, A. Khosravi, D. Creighton, and S. Nahavandi, "EEG signal classification for BCI applications by wavelets and interval type-2 fuzzy logic systems," *Expert Syst. Appl.*, vol. 42, no. 9, pp. 4370–4380, Jun. 2015.

Article preprint

[72] M. K. Hazrati and A. Erfanian, "An online EEG-based brain-computer interface for controlling hand grasp using an adaptive probabilistic neural network.," *Med. Eng. Phys.*, vol. 32, no. 7, pp. 730–9, Sep. 2010.

[73] M. A. Lopez, H. Pomares, M. Damas, E. Madrid, A. Prieto, F. Pelayo, and E. M. De La Plaza Hernandez, "Use of ANNs as classifiers for selective attention brain-computer interfaces," *Lect. Notes Comput. Sci. Incl. Subser. Lect. Notes Artif. Intell. Lect. Notes Bioinforma.*, vol. 4507 LNCS, pp. 956–963, 2007.

[74] S. Kanoh, Y. M. Murayama, K. I. Miyamoto, T. Yoshinobu, and R. Kawashima, "A NIRS-based brain-computer interface system during motor imagery: System development and online feedback training," *Proc. 31st Annu. Int. Conf. IEEE Eng. Med. Biol. Soc. Eng. Futur. Biomed. EMBC 2009*, pp. 594–597, 2009.

[75] S. Fazli, J. Mehnert, J. Steinbrink, G. Curio, A. Villringer, K.-R. Müller, and B. Blankertz, "Enhanced performance by a hybrid NIRS-EEG brain computer interface.," *Neuroimage*, vol. 59, no. 1, pp. 519–29, Jan. 2012.

[76] B. Koo, H.-G. Lee, Y. Nam, H. Kang, C. S. Koh, H.-C. Shin, and S. Choi, "A hybrid NIRS-EEG system for self-paced brain computer interface with online motor imagery.," *J. Neurosci. Methods*, vol. 244, pp. 26–32, Apr. 2015.

[77] Y. Tomita, F.-B. Vialatte, G. Dreyfus, Y. Mitsukura, H. Bakardjian, and A. Cichocki, "Bimodal BCI using simultaneously NIRS and EEG.," *IEEE Trans. Biomed. Eng.*, vol. 61, no. 4, pp. 1274–84, Apr. 2014.

[78] A. Riccio, E. M. Holz, P. Aricò, F. Leotta, F. Aloise, L. Desideri, M. Rimondini, A. Kübler, D. Mattia, and F. Cincotti, "Hybrid P300-based brain-computer interface to improve usability for people with severe motor disability: electromyographic signals for error correction during a spelling task.," *Arch. Phys. Med. Rehabil.*, vol. 96, no. 3 Suppl, pp. S54–61, Mar. 2015.

[79] J. H. Lim, J. H. Lee, H. J. Hwang, D. H. Kim, and C. H. Im, "Development of a hybrid mental spelling system combining SSVEP-based brain–computer interface and webcam-based eye tracking," *Biomed. Signal Process. Control*, vol. 21, pp. 99–104, Aug. 2015.

[80] C. Brennan, P. McCullagh, G. Lightbody, L. Galway, D. Feuser, J. L. González, and S. Martin, "Accessing Tele-Services Using a Hybrid BCI Approach," vol. 6691, pp. 386–392, 2011.

[81] Á. Costa, E. Hortal, E. Iáñez, and J. M. Azorín, "A Supplementary System for a Brain-Machine Interface Based on Jaw Artifacts for the Bidimensional Control of a Robotic Arm," *PLoS One*, vol. 9, no. 11, p. e112352, 2014.

[82] G. Geetha and S. N. Geethalakshmi, "Artifact removal from EEG using spatially constrained independent component analysis and wavelet denoising with Otsu's thresholding technique," *Procedia Eng.*, vol. 30, no. 2011, pp. 1064–1071, 2012.

[83] W. Y. Hsu, C. H. Lin, H. J. Hsu, P. H. Chen, and I. R. Chen, "Wavelet-based envelope features with automatic EOG artifact removal: Application to single-trial EEG data," *Expert Syst. Appl.*, vol. 39, no. 3, pp. 2743–2749, 2012.

[84] M. a. Klados, C. Papadelis, C. Braun, and P. D. Bamidis, "REG-ICA: A hybrid methodology combining Blind Source Separation and regression techniques for the rejection of ocular artifacts," *Biomed. Signal Process. Control*, vol. 6, no. 3, pp. 291–300, 2011.

[85]   a. Schlögl, C. Keinrath, D. Zimmermann, R. Scherer, R. Leeb, and G. Pfurtscheller, "A fully automated correction method of EOG artifacts in EEG recordings," *Clin. Neurophysiol.*, vol. 118, no. 1, pp. 98–104, 2007.

[86] H. Nolan, R. Whelan, and R. B. Reilly, "FASTER: Fully Automated Statistical Thresholding for EEG artifact Rejection," *J. Neurosci. Methods*, vol. 192, no. 1, pp. 152–162, 2010.

[87] N. Birbaumer, "slow Cortical Potentials: Plasticity, Operant Control, and Behavioral Effects," *Neurosci.*, vol. 5, no. 2, pp. 74–78, 1999.

[88] G. Pfurtscheller, C. Guger, G. Müller, G. Krausz, and C. Neuper, "Brain oscillations control hand orthosis in a tetraplegic," *Neurosci. Lett.*, vol. 292, no. 3, pp. 211–214, 2000.

[89] T. H. Budzynski, H. K. Budzynski, J. R. Evans, and A. Abarbanel, *Introduction to Quantitative EEG and Neurofeedback: Advanced Theory and Applications*, Second Edi. Elsevier Inc., 2009.

[90] T. Thompson, T. Steffert, T. Ros, J. Leach, and J. Gruzelier, "EEG applications for sport and performance.," *Methods*, vol. 45, no. 4, pp. 279–88, Aug. 2008.

[91] H. Yuan and B. He, "Brain-computer interfaces using sensorimotor rhythms: current state and future perspectives.," *IEEE Trans. Biomed. Eng.*, vol. 61, no. 5, pp. 1425–35, May 2014.

[92] R. J. Huster, Z. N. Mokom, S. Enriquez-Geppert, and C. S. Herrmann, "Brain-computer interfaces for EEG neurofeedback: Peculiarities and solutions," *Int. J. Psychophysiol.*, vol. 91, no. 1, pp. 36–45, 2014.

[93] R. Ron-Angevin, M. A. Lopez, and F. Pelayo, "The training issue in brain-computer interface: A multi-disciplinary field," *Lect. Notes Comput. Sci. (including Subser. Lect. Notes Artif. Intell. Lect. Notes Bioinformatics)*, vol. 5517 LNCS, no. PART 1, pp. 666–673, 2009.

Article preprint

[94] J. Kamiya, "Operant control of the EEG alpha rhythm and some of its reported effects on consciousness," *Altered states consciousness. New York Wiley*, pp. 489 – 501, 1969.

[95] D. H. Walsh, "Interactive Effects of Alpha Feedback and Instructional Set on Subjective State," *Psychophysiology*, vol. 11, no. 4, pp. 428–435, Jul. 1974.

[96] Z. Gu, Z. Yu, Z. Shen, and Y. Li, "An online semi-supervised brain-computer interface.," *IEEE Trans. Biomed. Eng.*, vol. 60, no. 9, pp. 2614–23, Sep. 2013.

[97] J. Long, Y. Li, T. Yu, and Z. Gu, "Target selection with hybrid feature for BCI-based 2-D cursor control," *IEEE Trans. Biomed. Eng.*, vol. 59, no. 1, pp. 132–140, 2012.

[98] C. J. Bell, P. Shenoy, R. Chalodhorn, and R. P. N. Rao, "Control of a humanoid robot by a noninvasive brain-computer interface in humans.," *J. Neural Eng.*, vol. 5, no. 2, pp. 214–220, 2008.

[99] B. Blankertz and F. Losch, "The Berlin Brain--Computer Interface: accurate performance from first-session in BCI-naive subjects," *Biomed. Eng. IEEE Trans.*, vol. 55, no. 10, pp. 2452 – 2462, 2008.

[100] F. Popescu, B. Blankertz, and K. R. Müller, "Computational Challenges for Noninvasive Brain Computer Interfaces," *IEE Intell. Syst.*, 2008.

[101] C. Vidaurre and B. Blankertz, "Towards a cure for BCI illiteracy," *Brain Topogr.*, 2010.

[102] C. Guger, S. Daban, E. Sellers, C. Holzner, G. Krausz, R. Carabalona, F. Gramatica, and G. Edlinger, "How many people are able to control a P300-based brain-computer interface (BCI)?," *Neurosci. Lett.*, vol. 462, no. 1, pp. 94–98, 2009.

[103] B. Allison, I. Volosyak, D. Valbuena, T. Lüth, T. Malechka, and A. Gräser, "BCI demographics II: How many (and What Kinds of) people can use a high-frequency SSVEP BCI?," *IEEE Trans. Neural Syst. Rehabil. Eng.*, vol. 19, no. 3, pp. 232–239, 2011.

[104] H. J. Hwang, J. H. Lim, Y. J. Jung, H. Choi, S. W. Lee, and C. H. Im, "Development of an SSVEP-based BCI spelling system adopting a QWERTY-style LED keyboard," *J. Neurosci. Methods*, vol. 208, no. 1, pp. 59–65, 2012.

[105] E. Yin, Z. Zhou, J. Jiang, F. Chen, Y. Liu, and D. Hu, "A speedy hybrid BCI spelling approach combining P300 and SSVEP.," *IEEE Trans. Biomed. Eng.*, vol. 61, no. 2, pp. 473–83, Feb. 2014.

[106] E. Yin, Z. Zhou, J. Jiang, Y. Yu, and D. Hu, "A Dynamically Optimized SSVEP Brain-Computer Interface (BCI) Speller.," *IEEE Trans. Biomed. Eng.*, vol. 62, no. 6, pp. 1447–56, Jun. 2015.

[107] M. A. Lopez-Gordo, A. Prieto, F. Pelayo, and C. Morillas, "Customized stimulation enhances performance of independent binary SSVEP-BCIs," *Clin. Neurophysiol.*, vol. 122, no. 1, pp. 128–133, 2011.

[108] M. A. Lopez-Gordo, A. Prieto, F. Pelayo, and C. Morillas, "Use of Phase in Brain–Computer Interfaces based on Steady-State Visual Evoked Potentials," *Neural Process. Lett.*, vol. 32, no. 1, pp. 1–9, May 2010.

[109] M. A. Lopez, F. Pelayo, E. Madrid, and A. Prieto, "Statistical characterization of steady-state visual evoked potentials and their use in brain-computer interfaces," *Neural Process. Lett.*, vol. 29, no. 3, pp. 179–187, 2009.

[110] M. A. Lopez, H. Pomares, F. Pelayo, J. Urquiza, and J. Perez, "Evidences of cognitive effects over auditory steady-state responses by means of artificial neural networks and its use in brain-computer interfaces," *Neurocomputing*, vol. 72, no. 16–18, pp. 3617–3623, 2009.

[111] M. Rakibul Mowla, S.-C. Ng, M. S. a. Zilany, and R. Paramesran, "Artifacts-matched blind source separation and wavelet transform for multichannel EEG denoising," *Biomed. Signal Process. Control*, vol. 22, pp. 111–118, 2015.

[112] F. Morbidi, A. Garulli, D. Prattichizzo, C. Rizzo, P. Manganotti, and S. Rossi, "Off-line removal of TMS-induced artifacts on human electroencephalography by Kalman filter," *J. Neurosci. Methods*, vol. 162, no. 1–2, pp. 293–302, 2007.

[113] F. Morbidi, A. Garulli, D. Prattichizzo, C. Rizzo, and S. Rossi, "Application of Kalman filter to remove TMS-induced artifacts from EEG recordings," *IEEE Trans. Control Syst. Technol.*, vol. 16, no. 6, pp. 1360–1366, 2008.

[114] W. Kong, Z. Zhou, S. Hu, J. Zhang, F. Babiloni, and G. Dai, "Automatic and direct identification of blink components from scalp EEG.," *Sensors (Basel).*, vol. 13, no. 8, pp. 10783–10801, 2013.

[115] A. Mognon, J. Jovicich, L. Bruzzone, and M. Buiatti, "ADJUST: An automatic EEG artifact detector based on the joint use of spatial and temporal features," *Psychophysiology*, vol. 48, no. 2, pp. 229–240, 2011.

[116] P. Comon, "Independent component analysis, a new concept?," *Signal Processing*, vol. 36, no. 3, pp. 287–314, 1994.

[117] C. J. James and O. J. Gibson, "Temporally constrained ICA: An application to artifact rejection in electromagnetic brain signal analysis," *IEEE Trans. Biomed. Eng.*, vol. 50, no. 9, pp. 1108–1116, 2003.

[118] X. Chen, C. He, and H. Peng, "Removal of Muscle Artifacts from Single-Channel EEG Based on Ensemble Empirical Mode Decomposition and Multiset Canonical Correlation Analysis," *J. Appl. Math.*, vol. 2014, pp. 1–10, 2014.

[119] K. T. Sweeney, S. F. McLoone, and T. E. Ward, "The use of ensemble empirical mode decomposition with canonical correlation analysis as a novel artifact removal technique.," *IEEE Trans. Biomed. Eng.*, vol. 60, no. 1, pp. 97–105, 2013.

[120] S. Gribonval, Rémi;Lesage, "A survey of Sparse Component Analysis for Blind Source Separation: principles, perspectives, and new challenges," *Eur. Symp. Artif. Neural Networks*, no. April, pp. 323–330, 2006.

[121] A. R. Teixeira, A. M. Tomé, E. W. Lang, P. Gruber, and A. Martins da Silva, "Automatic removal of high-amplitude artefacts from single-channel electroencephalograms," *Comput. Methods Programs Biomed.*, vol. 83, no. 2, pp. 125–138, 2006.

[122] H. Peng, B. Hu, Q. Shi, M. Ratcliffe, Q. Zhao, Y. Qi, and G. Gao, "Removal of ocular artifacts in EEG - An improved approach combining DWT and ANC for portable applications," *IEEE J. Biomed. Heal. Informatics*, vol. 17, no. 3, pp. 600–607, 2013.

[123] S. V. Ramanan, N. V. Kalpakam, and J. S. Sahambi, "A novel wavelet based technique for detection and de-noising of ocular artifact in normal and epileptic electroencephalogram," *2004 Int. Conf. Commun. Circuits Syst. (IEEE Cat. No.04EX914)*, vol. 2, pp. 180–183, 2004.

[124] N. Mourad and R. K. Niazy, "Automatic correction of eye blink artifact in single channel EEG recording using EMD and OMP," *Eur. Signal Process. Conf.*, pp. 1–5, 2013.

[125] H. Zeng, A. Song, R. Yan, and H. Qin, "EOG artifact correction from EEG recording using stationary subspace analysis and empirical mode decomposition.," *Sensors (Basel).*, vol. 13, no. 11, pp. 14839–14859, 2013.

[126] B. Mijović, M. De Vos, I. Gligorijević, J. Taelman, and S. Van Huffel, "Source separation from single-channel recordings by combining empirical-mode decomposition and independent component analysis," *IEEE Trans. Biomed. Eng.*, vol. 57, no. 9, pp. 2188–2196, 2010.

[127] T. Zikov, S. Bibian, G. A. Dumont, M. Huzmezan, and C. R. Ries, "A wavelet based de-noising technique for ocular artifact correction of the electroencephalogram," *Proceedings. 8th Russ. Int. Symp. Sci. Technol. 2004. KORUS 2004.*, vol. 3, pp. 98–105, 2002.

[128] V. Krishnaveni, S. Jayaraman, L. Anitha, and K. Ramadoss, "Removal of ocular artifacts from EEG using adaptive thresholding of wavelet coefficients.," *J. Neural Eng.*, vol. 3, no. 4, pp. 338–346, 2006.

Article preprint

[129] X. Chen, A. Liu, H. Peng, and R. Ward, "A Preliminary Study of Muscular Artifact Cancellation in Single-Channel EEG," *Sensors*, vol. 14, no. 10, pp. 18370–18389, 2014.

[130] H.-A. T. Nguyen, J. Musson, F. Li, W. Wang, G. Zhang, R. Xu, C. Richey, T. Schnell, F. D. McKenzie, and J. Li, "EOG artifact removal using a wavelet neural network," *Neurocomputing*, vol. 97, pp. 374–389, 2012.

[131] C. Burger and D. J. van den Heever, "Removal of EOG artefacts by combining wavelet neural network and independent component analysis," *Biomed. Signal Process. Control*, vol. 15, pp. 67–79, 2015.

[132] J. Hu, C. Wang, M. Wu, Y. Du, Y. He, and J. She, "Removal of EOG and EMG artifacts from EEG using combination of functional link neural network and adaptive neural fuzzy inference system," *Neurocomputing*, vol. 151, pp. 278–287, 2015.

[133] S. Suja Priyadharsini, S. Edward Rajan, and S. Femilin Sheniha, "A novel approach for the elimination of artefacts from EEG signals employing an improved Artificial Immune System algorithm," *J. Exp. Theor. Artif. Intell.*, vol. 3079, no. November, pp. 1–21, 2015.

[134] D. Safieddine, a Kachenoura, L. Albera, G. Birot, a Karfoul, a Pasnicu, a Biraben, F. Wendling, L. Senhadji, and I. Merlet, "Removal of muscle artifact from EEG data: Comparison between stochastic (ICA and CCA) and deterministic (EMD and wavelet-based) approaches," *EURASIP J. Adv. Signal Process.*, vol. 2012, p. 127: 1–15, 2012.

[135] R. Romo Vázquez, H. Vélez-Pérez, R. Ranta, V. Louis Dorr, D. Maquin, and L. Maillard, "Blind source separation, wavelet denoising and discriminant analysis for EEG artefacts and noise cancelling," *Biomed. Signal Process. Control*, vol. 7, no. 4, pp. 389–400, 2012.

[136] N. Mammone, F. La Foresta, and F. C. Morabito, "Automatic artifact rejection from multichannel scalp EEG by wavelet ICA," *IEEE Sens. J.*, vol. 12, no. 3, pp. 533–542, 2012.

[137] Q. Zhao, B. Hu, Y. Shi, Y. Li, P. Moore, M. Sun, and H. Peng, "Automatic identification and removal of ocular artifacts in EEG - Improved adaptive predictor filtering for portable applications," *IEEE Trans. Nanobioscience*, vol. 13, no. 2, pp. 109–117, 2014.

[138] N. P. Castellanos and V. a. Makarov, "Recovering EEG brain signals: Artifact suppression with wavelet enhanced independent component analysis," *J. Neurosci. Methods*, vol. 158, no. 2, pp. 300–312, 2006.

[139] V. Krishnaveni, S. Jayaraman, S. Aravind, V. Hariharasudhan, and K. Ramadoss, "Automatic identification and Removal of ocular artifacts from EEG using Wavelet transform," *Meas. Sci. Rev.*, vol. 6, no. 4, pp. 45–57, 2006.

[140] D. Szibbo, A. Luo, and T. J. Sullivan, "Removal of blink artifacts in single channel EEG," *Proc. Annu. Int. Conf. IEEE Eng. Med. Biol. Soc. EMBS*, pp. 3511–3514, 2012.

[141] S. Puthusserypady and T. Ratnarajah, "Robust adaptive techniques for minimization of EOG artefacts from EEG signals," *Signal Processing*, vol. 86, no. 9, pp. 2351–2363, 2006.

[142] S. P. Cho, M. H. Song, Y. C. Park, H. S. Choi, and K. J. Lee, "Adaptive noise canceling of electrocardiogram artifacts in single channel electroencephalogram," *Annu. Int. Conf. IEEE Eng. Med. Biol. - Proc.*, pp. 3278–3281, 2007.

[143] T. Radüntz, J. Scouten, O. Hochmuth, and B. Meffert, "EEG artifact elimination by extraction of ICA-component features using image processing algorithms," *J. Neurosci. Methods*, vol. 243, pp. 84–93, 2015.

[144] Y. K. Wang, S. A. Chen, and C. T. Lin, "An EEG-based brain-computer interface for dual task driving detection," *Neurocomputing*, vol. 129, pp. 85–93, 2014.

[145] J. Ma, S. Bayram, P. Tao, and V. Svetnik, "High-throughput ocular artifact reduction in multichannel electroencephalography (EEG) using component subspace projection," *J. Neurosci. Methods*, vol. 196, no. 1, pp. 131–140, 2011.

[146] A. R. Teixeira, A. M. Tome, E. W. Lang, and A. Martins da Silva, "Subspace techniques to remove artifacts from EEG: a quantitative analysis.," *Conf. Proc. IEEE Eng. Med. Biol. Soc.*, vol. 2008, pp. 4395–4398, 2008.

[147] X. Yong, R. K. Ward, and G. E. Birch, "Generalized Morphological Component Analysis for EEG source separation and artifact removal," *2009 4th Int. IEEE/EMBS Conf. Neural Eng.*, pp. 343–346, 2009.

[148] A. R. Teixeira, N. Alves, A. M. Tomé, M. Böhm, E. W. Lang, and C. G. Puntonet, "Single-channel electroencephalogram analysis using non-linear subspace techniques," *2007 IEEE Int. Symp. Intell. Signal Process. WISP*, pp. 7–12, 2007.

[149] M. E. Davies and C. J. James, "Source separation using single channel ICA," *Signal Processing*, vol. 87, no. 8, pp. 1819–1832, 2007.

[150] Z. Tiganj, M. Mboup, C. Pouzat, and L. Belkoura, "An algebraic method for eye blink artifacts detection in single channel EEG recordings," *IFMBE Proc.*, vol. 28, pp. 175–178, 2010.

[151] N. Mourad, J. P. Reilly, H. De Bruin, G. Hasey, and D. MacCrimmon, "A simple and fast algorithm for automatic suppression of high-amplitude artifacts in EEG data," *ICASSP, IEEE Int. Conf. Acoust. Speech Signal Process. - Proc.*, vol. 1, pp. 393–396, 2007.

[152] S. Y. Shao, K. Q. Shen, C. J. Ong, E. P. V Wilder-Smith, and X. P. Li, "Automatic EEG artifact removal: A weighted support vector machine approach with error correction," *IEEE Trans. Biomed. Eng.*, vol. 56, no. 2, pp. 336–344, 2009.

[153] J. N. Gu, H. J. Liu, H. T. Lu, and B. L. Lu, "An integrated hierarchical Gaussian mixture model to estimate vigilance level based on EEG recordings," *Lect. Notes Comput. Sci. (including Subser. Lect. Notes Artif. Intell. Lect. Notes Bioinformatics)*, vol. 7062 LNCS, no. PART 1, pp. 380–387, 2014.

[154] X. Yong, R. Ward, and G. Birch, "Artifact Removal in Eeg Using Morphological Component Analysis," *Acoust. Speech Signal Process. 2009. ICASSP 2009. IEEE Int. Conf.*, pp. 345–348, 2009.

[155] P. P. Acharjee, R. Phlypo, L. Wu, V. D. Calhoun, and T. Adali, "Independent vector analysis for gradient artifact removal in concurrent EEG-fMRI data," *IEEE Trans. Biomed. Eng.*, vol. 62, no. 7, pp. 1750–8, 2015.

[156] C. Zhang, H.-B. Bu, Y. Zeng, J.-F. Jiang, B. Yan, and J.-X. Li, "Prior Artifact Information based Automatic Artifact Removal from," in *7th Annual International IEEE EMBS Conference on Neural Engineering*, 2015.

[157] C. Porcaro, M. T. Medaglia, and A. Krott, "Removing speech artifacts from electroencephalographic recordings during overt picture naming," *Neuroimage*, vol. 105, pp. 171–180, 2015.

[158] J. E. Kline, H. J. Huang, K. L. Snyder, and D. P. Ferris, "Isolating gait-related movement artifacts in electroencephalography during human walking," *J. Neural Eng.*, vol. 12, no. 4, p. 046022, 2015.

[159] J. Xu, R. F. Yazicioglu, B. Grundlehner, P. Harpe, K. a a Makinwa, and C. Van Hoof, "A 160 µw 8-channel active electrode system for EEG monitoring," *IEEE Trans. Biomed. Circuits Syst.*, vol. 5, no. 6, pp. 555–567, 2011.

[160] S. Motamedi-Fakr, M. Moshrefi-Torbati, M. Hill, C. M. Hill, and P. R. White, "Signal processing techniques applied to human sleep EEG signals—A review," *Biomed. Signal Process. Control*, vol. 10, pp. 21–33, 2014.

[161] M. A. Lopez-Gordo, F. Pelayo, A. Prieto, and E. Fernandez, "an Auditory Brain-Computer Interface With Accuracy Prediction," *Int. J. Neural Syst.*, vol. 22, no. 03, p. 1250009, 2012.

Appendix D

RESEARCH ARTICLE

Blue lighting accelerates post-stress relaxation: Results of a preliminary study

Jesus Minguillon[1,2]*, Miguel Angel Lopez-Gordo[3,4], Diego A. Renedo-Criado[3], Maria Jose Sanchez-Carrion[5], Francisco Pelayo[1,2]

1 Department of Computer Architecture and Technology, University of Granada, Granada, Spain,
2 Research Centre for Information and Communications Technologies (CITIC), University of Granada, Granada, Spain, **3** Department of Signal Theory, Telematics and Communications, University of Granada, Granada, Spain, **4** Nicolo Association, Churriana de la Vega, Spain, **5** School for Special Education San Rafael, San Juan de Dios, Granada, Spain

* minguillon@ugr.es

Abstract

Several authors have studied the influence of light on both human physiology and emotions. Blue light has been proved to reduce sleepiness by suppression of melatonin secretion and it is also present in many emotion-related studies. Most of these have a common lack of objective methodology since results and conclusions are based on subjective perception of emotions. The aim of this work was the objective assessment of the effect of blue lighting in post-stress relaxation, in comparison with white lighting, by means of bio-signals and standardized procedures. We conducted a study in which twelve healthy volunteers were stressed and then performed a relaxation session within a chromotherapy room with blue (test group) or white (control group) lighting. We conclude that the blue lighting accelerates the relaxation process after stress in comparison with conventional white lighting. The relaxation time decreased by approximately three-fold (1.1 vs. 3.5 minutes). We also observed a convergence time (3.5–5 minutes) after which the advantage of blue lighting disappeared. This supports the relationship between color of light and stress, and the observations reported in previous works. These findings could be useful in clinical and educational environments, as well as in daily-life context and emerging technologies such as neuromarketing. However, our study must be extended to draw reliable conclusions and solid scientific evidence.

Introduction

Light has an essential role in our ecosystem. For example, plants use the energy of sunlight to live through the photosynthesis process. Light is also vital for many other living beings including humans. Chromotherapy, also named cromatherapy, colorology or therapy of colors, is an old alternative medicine method that uses the energy of electromagnetic radiations in the visible spectrum (i.e., colored light) to produce changes in the human body [1]. Although therapy of colors is not well-described and frequently considered pseudoscience, a number of studies have tried to explain the effects of colors on the human body. Some of them have focused on

physiological and others on emotional changes. Next two paragraphs elaborate on these two aspects.

On the one hand, several studies have investigated the influence of color of light on human physiology throught biochemical markers such as cortisol [2,3] or melatonin [2–4] level, and bio-signals such as electrocardiographic (ECG) [3,4] or electroencephalographic (EEG) [3,5–11] signals. In this sense, only a few colors have been investigated and blue is in most of the studies. It has been proved that turquoise (a variant of blue) light is an effective way to treat jaundice in newborns [12]. Long exposures (several hours) to blue light provoke melatonin suppression and phase shifting in the circadian system with sleepiness reduction and alertness augmentation [4,5,13,14]. Light can modulate alertness-related subcortical activity, thus stimulating cortical activity not involved in visual cognitive processes [15]. A recent study suggested that early EEG responses (e.g., event-related potentials during the first milliseconds) depend on their adaptation to different colors of light [11]. Another recent and preliminary work showed that a short stay (20 minutes) inside a blue room caused cortisol level reduction in a woman [3].

On the other hand, some colors have been related to emotions. For example, different hues were linked to different pleasure and arousal levels [16]. Lighting was demonstrated to affect the mood of elderly people [17]. A study about the influence of color of walls in learning environments proved that pale colors caused more relaxation than vivid colors, and that heart rate decreased with short-wavelength colors (e.g., violet, blue and green) in comparison with longer-wavelength (e.g., yellow and red) [18]. In addition, a few authors have successfully treated people with behavior disorders by influencing their emotional states (e.g., causing mental calm) by color lighting. For instance, pink light was successfully utilized to reduce aggressiveness of delinquents in prison [19]. Furthermore, another color-lighting-based method with blue light have been used for disruptive behavior disorders in the School for Special Education San Rafael, Granada (Spain) with substantial improvements [20]. However, these emotion-related studies, with a few exceptions [21], have a common lack. Methodology, results and conclusions were based on empirical and, in some cases, subjective observations [22,23]. This lack of methodology reduces the ability to reproduce the results. Objective information obtained by a methodological procedure is much more powerful than reported subjective feelings [24]. The way to assess emotions through a methodological procedure is still an open question to address.

In the literature, there are recent examples of rigorous procedures to recognize emotions based on bio-signals such as EEG or ECG [25] [26]. Specifically, several authors have demonstrated that stress is reflected by changes in brain rhythms measured at frontal cortical areas [27–29]. The Relative Gamma (RG) power, which is a power ratio between brain rhythms (see section EEG signals for further details), is suitable for that purpose. In fact, it has been previously utilized in meditation-relaxation [30,31] and stress [32] studies. In addition, the heart rate (HR) is, under certain conditions, commonly accepted as stress marker [33–37]. Also, brain imaging techniques such as functional magnetic resonance imaging (fMRI) [38,39], near-infrared spectroscopy (NIRS) [40] and positron emission tomography (PET) [41] have been applied with the same or similar purpose.

For a better control of the conditions under which stress is measured, various techniques have been developed. For instance the Montreal Imaging Stress Task (MIST) [42]. The MIST is a well-described method to cause stress in humans with a methodological procedure [36]. It induces mental arithmetic load together with psychosocial stress. It has been used in various stress-related works [38,39,41,43]. Finally the use of a time-out room or a specific chromotherapy room provides the enough level of isolation to perform stress-related experiments with environmental condition under control.

The aim of this pioneering study was the objective assessment of the effect of blue lighting (test group) in post-stress relaxation, in comparison with white lighting (control group), by means of biosignals and standardized procedures. In particular, we used technics and features detailed in the previous paragraph, namely the stress markers RG, HR, a stressing procedure (i.e., the MIST) to elicit a similar initial level of stress in the participants, and the same time-out room used in [20] to guarantee a successful relaxation with stimulus and environmental factors under control. We have designed a reproducible experiment that avoids conclusions based on subjective observations. The results were compared with those of conventional-white lighting and practical implications were inferred.

Methods

Experimental design

Participants. Twelve healthy volunteers (age range of 18–37 years, mean age of 25.3 ± 4.8 years) participated in the study. Apart from age, no other baseline demographic characteristics were recorded. The participants were recruited during the month prior to the beginning of the study. They voluntarily contacted the research team to participate and were not paid for that. No participant was excluded from the study. The participants declared no experience in EEG or stress-related experiments. They were instructed not to take stimulants or relaxants during 24 hours prior to the experiment. The protocol and informed consent were approved by the Bioethics Committee of the University of Granada (see S1 File). The participants provided their written informed consent to participate in the study.

Experimental procedure. Once the informed consent was understood and signed by the participants, they dressed in white hospital uniforms and were equipped for EEG and ECG recordings (datasets available in S2–S13 Files). They were randomly assigned to two experimental groups G1 (test group) and G2 (control group), therefore groups of six participants. Thereupon a stress session was conducted. During that session, all participants performed an adapted version of the MIST. As mentioned, the MIST is a well-described method to cause stress in humans. The goal of this session was to elicit a uniform level of stress in all participants of this experiment. After a training period of 3 minutes, the MIST lasted 6 minutes.

Afterwards, a relaxation session was conducted by using either blue or white lighting within the chromotherapy room. This session was divided into two consecutive blocks of 10 minutes each (i.e., B1 and B2), with the only difference of the color of the light projected in the room. The color sequence was blue-white for G1 and white-blue for G2. During their stay, the participants were monitored by a video camera for safety and artifacts removal purposes.

In order to assess the self-perception of stress, oral tests were taken by the participants three times during the experiment. In particular, the same test was repeated before the MIST (T1), after the MIST (T2) and after the relaxation session (T3). The timeline of the experiment is displayed in Fig 1.

Experimental setup

One ECG electrode was placed on the non-dominant wrist of the participants. Seven EEG electrodes were placed at Fp1, Fp2, Fz, F3, F4, F7, F8 positions of the 10–20 International System. These positions have been used in reports of successful studies on stress [27–29]. All the electrodes were referenced and grounded to the left ear lobe. The impedance of the electrodes was below 30 KΩ. This value is much lower than the input impedance of the acquisition system and it is enough to guarantee an insignificant degradation of the recorded signals. EEG and ECG signals were recorded at 540 Hz with the Miniature Data Acquisition System of Cognionics (Cognionics, Inc., USA).
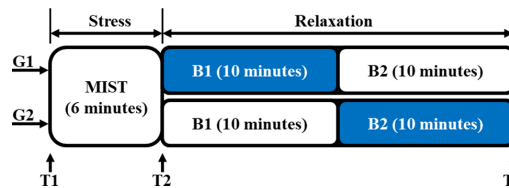
Fig 1. Timeline of the experiment. Both groups G1 and G2 performed the MIST, which lasted 6 minutes. Afterwards, the relaxation session was conducted within the chromotherapy room. This session was divided into two consecutive 10-minute blocks B1 and B2. The color sequence of B1-B2 was blue-white for G1 and white-blue for G2. Three oral tests were taken by the participants before the MIST (T1), after the MIST (T2) and at the end of the experiment (T3).

The MIST was conducted within a classroom. A graphical user interface (GUI) of the MIST was implemented in Matlab R2014a (The MathWorks, Inc., USA). During the task, the participants were sat on a chair while they played the Matlab-based GUI using the touchpad of a laptop. In order to avoid severe artifacts in EEG and ECG signals, they were instructed to exclusively move their dominant hand using the touchpad.

During the relaxation session, the participants stayed laid on a comfortable puff-shaped seat placed inside a 6 m2 chromotherapy room. This room was specially designed for relaxation and has been used in the school as time-out room for children with behavior disorders. The walls were compounded by a white padded material. The illumination system consisted of three sets of light-emitting diodes (LEDs): red (616 nm wavelength and 2.19 cd/m^2 luminance), green (550 nm wavelength and 4.02 cd/m^2 luminance) and blue (471 nm wavelength and 1.37 cd/m^2 luminance) LEDs. White light (similar to typical office room light) was generated by powering up all the LEDs. Blue light was generated by powering up the blue LEDs with red and green LEDs powered down. Wavelength and luminance were measured by the i1 Display Pro calibration device (X-Rite, Inc., USA). The chromotherapy room is displayed in Fig 2. The participants were instructed not to close their eyes (except for blinking) and to avoid moving or gazing any part of the room (i.e., the thousand-yard stare) during the relaxation session.

The oral test for assessment of the subjective self-perception of stress was based on the Spanish version of the Perceived Stress Scale (PSS) [44]. Only one question was analyzed in this paper: *If 0 is the minimum level and 4 is the maximum level, what is your stress level?* The third test T3 included the following extra question: *Which color, blue or white, have you felt more relaxed with?*

Signal processing

EEG signals. Recorded EEG signals were bandpass filtered (1–100 Hz) using a second order Butterworth IIR filter. A notch filter was applied to remove power-line couplings. Ocular

Fig 2. Chromotherapy room. (A) Chromotherapy room with blue lighting. (B) Chromotherapy room with white lighting.

artifacts were removed using independent component analysis. It was performed by using the EEGLAB Matlab toolbox (Swartz Center for Computational Neuroscience, USA).

A spectral analysis was applied to the preprocessed data of each subject. Two-second epochs (no overlap) were extracted, z-scored and then the power spectral density (PSD) estimated for each EEG channel. The mean power at different frequency bands was calculated through the PSD and then averaged across all channels. The RG was computed as described in (1). It corresponds to the power ratio between Gamma rhythm (25–45 Hz) and the slow rhythms Theta (4–7 Hz) and Alpha (8–13 Hz). These spectral features were used in previous emotion-related works [25,30–32].

$$RG = Power_{25-45\ Hz}/Power_{4-13\ Hz} \qquad (1)$$

Then the RG were interpolated (inter-participant time warping), smoothed with a moving average filter (40 samples), z-scored and then averaged across the participants of each group, G1 and G2. In the MIST, the results were averaged across all the participants (i.e., G1 plus G2) since the task and the experimental conditions were the same for groups.

ECG signals.   The recorded ECG signal was bandpass filtered (4–24 Hz). A second order Butterworth IIR filter was used to enhance the R-peak of the QRS complex [45]. The HR was computed every 30 seconds with 90-second epochs (66% overlap) by estimating R-peak intervals with an automatic procedure. The HR was interpolated (inter-participant time warping), smoothed with a moving average filter (2 samples), z-scored and then averaged across the participants of each group, G1 and G2. As it was done for the RG, the HR was averaged across all the participants in the MIST.

Statistical analysis

The mean and the standard error of the mean (SEM) of the subjective self-perceived stress level were estimated from the answers to tests in T1, T2 and T3. The one-way ANOVA test was applied to compare answers of groups G1 and G2. The Kolmogorov-Smirnov (KS) test was used to assess normality.

The SEM was also computed for the RG and the HR. In order to simplify the analysis, RG and HR plots were divided into adjacent segments corresponding to linear trends (i.e., linearized RG and linearized HR, respectively). The first segment (i.e., Seg1) corresponds to the MIST (from minute 0 up to the point of maximum RG or HR within the transition time interval between the MIST and B1). This segment is shared by all groups since all the participants were averaged together in the MIST. The second segment (i.e., Seg2) ends at the point matching with the first minimum of RG or HR. The third segment (i.e., Seg3) ends at the second minimum of RG. The fourth segment (i.e., Seg4) ends at minute 16 (transition from B1 to B2). In case of the HR, Seg3 and Seg4 were merged into one segment (i.e., Seg3). The last segment (i.e., Seg5 of RG and Seg4 of HR) ends at minute 25, that is, one minute before the end of B2 (the last minute of B2 contained residual data from processing, thus it was omitted). These segments were fitted to a line by simple linear regression. The goodness of the fit was evaluated by means of R^2. For each segment, the slopes of G1 and G2 were estimated. The slopes are numerical indicator of the rate of decreasing of stress level that we use to compare the effects of blue and white lighting during the relaxation session. The null hypothesis that both slopes were the same was checked by estimating the Student's t statistic on N-4 (N is sample size) degrees of freedom. Student's t statistic was computed using (2), where b_1 is the slope 1, b_2 is the slope 2 and SE_{b1-b2} is the standard error of the difference.

$$t = (b_1 - b_2)/SE_{b_1-b_2} \qquad (2)$$

In order to estimate the time instants of zero RG from the linear regressions, zero-crossings of some segments were computed. For that, the equation of the regression (i.e., $y = bx + a$ where b is the slope and a is the intercept) was evaluated at y = 0.

Finally, the RG was averaged minute-by-minute (from the beginning of the relaxation session). Then an inter-group comparison was performed by the Kruskal-Wallis (KW) test. Relative gamma is the ratio of the power of frequency bands of EEG signals. None of these terms follow a normal distribution and nor the ratio. Thus, the RG was not expected to follow a normal distribution. In fact, data did not pass the normality test Kolmogorov-Smirnov (KS) (p-value > 0.05). Similar results were obtained for the HR (p-value > 0.05). In this situation ANOVA could not be applied since it requires normally distributed data. For this reason the Kruskal-Wallis test was chosen. This non-parametric test is utilized to check if two datasets come from the same distribution. It can be used as an alternative to the ANOVA test when the distribution cannot be assumed to be normal. For all the statistical tests of this paper, the significance level was set at α = 0.05.

Results

Subjective self-perception of stress

The mean and SEM of the answers to the question asked to G1 and G2 in T1, T2 and T3 are displayed in Fig 3. In T1, T2 and T3, G2 reported more self-perceived stress. The ANOVA test did not disclose statistically significant inter-group differences in T1 (p-value = 0.40), T2 (p-value = 0.28) and T3 (p-value = 0.66). However, the same test found significant intra-groups differences. For G1: T1-T2 (p-value = 0.02) and T2-T3 (p-value = 0.00); for G2: T1-T2 (p-value = 0.01) and T2-T3 (p-value = 0.00). Regarding the extra question asked in T3 about the light which causes more relaxation, 10 out of 12 participants (83% with confidence interval [55, 95] %) answered that they felt more relaxed with the blue light.

Frontal relative gamma and heart rate

This section shows the results obtained from the processing of EEG and ECG signals.
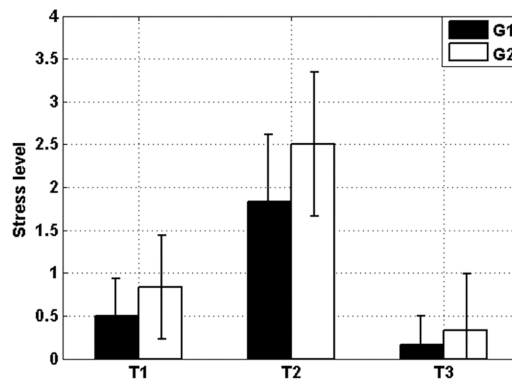

Fig 3. Mean (bars) and SEM (errorbars) of the subjective self-perceived stress level. G1 (black) and G2 (white). At each time (T1, T2 and T3) there was no significant inter-group difference. The intra-group analysis reveals significant differences of subjective stress level T1-T2 and T2-T3 for both groups. The latter proves that both the stress and relaxation sessions were satisfactory completed.
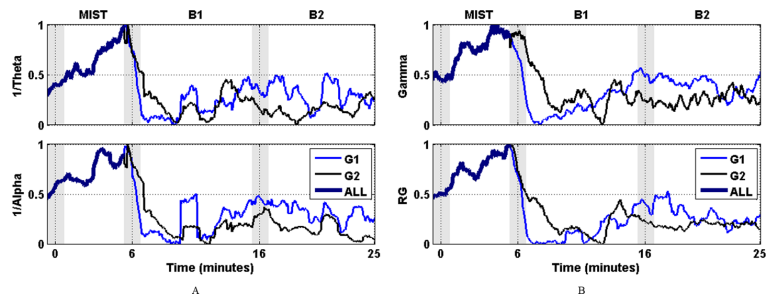
Fig 4. Normalized mean spectral power of G1 (blue) and G2 (black). Shaded bars indicate transition time intervals due to smoothing and interpolation. (A) Gamma power on the top and the RG at the bottom. (B) 1/Theta power on the top and 1/Alpha power at the bottom. The four plots show that despite they exhibit a high level of correlation and similar envelope, the RG computes a smoother version that emphasizes the differences of curves of G1 and G2 during the transition to B1.

The mean inverse power at frequency bands Theta and Alpha, and Gamma and RG power for both groups G1 and G2 are displayed in Fig 4. Shaded bars at T1, T2 and T3 indicate the fuzzy boundary between the stress session (MIST) and blocks of the relaxation session (B1 and B2) due to smoothing and interpolation of epochs during signal processing.

The mean and the SEM of the RG of both groups G1 and G2 are shown in Fig 5 (upper plot). For sake of clarity, five segments were regressed on the RG curves and presented in Fig 5 (bottom plot, see section Statistical analysis for a detailed explanation). Table 1 shows the
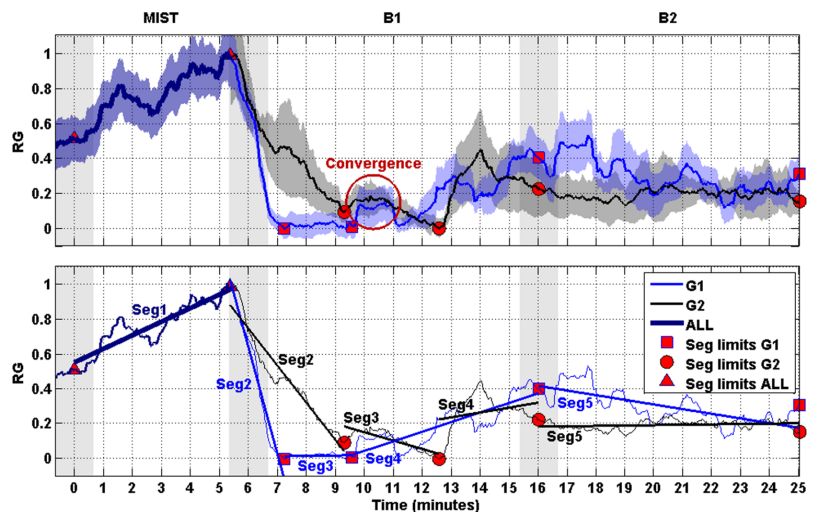

Fig 5. RG and segments. Upper: Curves represent the normalized RG of G1 (blue) and G2 (black). The SEM of the RG is displayed behind the RG curves. Shaded bars indicate transition time intervals due to smoothing and interpolation. The red circumference indicates the time period in which the curves of both groups converge. Bottom: The curves of the upper plot are simplified by their respective linear trends (linearized), thus given rise to segments (i.e., Seg1, Seg2, Seg3, Seg4 and Seg5). Red markers indicate limits of the segments.

Table 1. Information about the linear regression of segments of the RG.

Segment	Initial time (min.)	End time (min.)	Slope (min⁻¹)	R^2	t statistic	p-value
Seg1 ALL	0.0	5.4	0.08	0.82		
Seg2 G1	5.4	7.2	-0.61	0.97	25.96	0.00*
Seg2 G2	5.4	9.3	-0.21	0.93		
Seg3 G1	7.2	9.6	0.00	0.02	13.97	0.00*
Seg3 G2	9.3	12.6	-0.05	0.70		
Seg4 G1	9.6	16.0	0.05	0.72	2.76	0.01*
Seg4 G2	12.6	16.0	0.03	0.07		
Seg5 G1	16.0	25.0	-0.03	0.53	17.59	0.00*
Seg5 G2	16.0	25.0	0.00	0.04		

* indicates statistically significant difference (p-value<0.05).

initial and end time and slopes of the segments. The table also shows the goodness of the fit (R2) and the comparison of slopes. Asterisks indicate statistically significant difference (p-value<0.05).

Table 2 shows the time instants of zero RG. They were estimated from the linear regressions of Fig 5 bottom (see section Statistical analysis for a detailed explanation). The first zero for G1 and G2 corresponds to the zero-crossing of the fitted line of Seg2. The second zero for G1 corresponds to the zero-crossing of the fitted line of Seg4. The second zero of G2 corresponds to the zero-crossing of the fitted line of Seg3.

Fig 6 shows the values of the RG of both groups G1 and G2 minute-by-minute during the relaxation session. Differences were analyzed by means of the KW test. Asterisks indicate statistically significant difference (p-value<0.05).

The mean and the SEM of the HR of both groups G1 and G2 are shown in Fig 7 (upper plot). As it was done before for the RG in Fig 5, segments were regressed on the HR curves and presented in Fig 7 (bottom plot).

Discussion and conclusions

The results reported in the previous section suggest that color of light influence the relaxation process after the stress session. Specifically, the presence of blue lighting accelerates the reduction of stress level in comparison with conventional white lighting. In our experiment a reduction of more than three minutes (1.1 vs. 3.5 minutes) was achieved with the blue lighting till level of stress converged in both groups. Furthermore, the minimum level of stress remained stable longer with the blue than with the white (3 minutes vs. less than one minute respectively). Although it could seem a small fraction of time, these findings could mean a significant change in the way that time-out rooms are used in episodes of behavior disorders. See section Practical implications and future works for a short discussion of their practical implications.

Table 2. Time instants of zero RG.

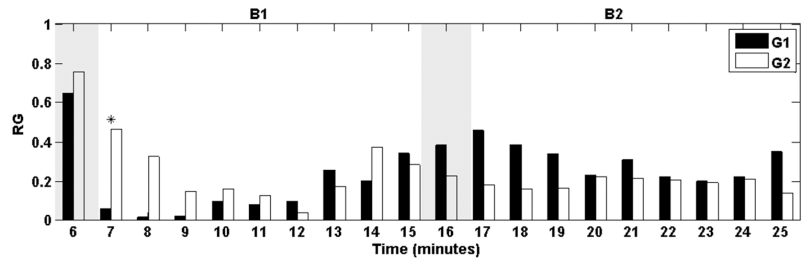| Zero-crossing	Time (min.)	Time from B1 (min.)
Seg2 G1	7.1	1.1
Seg2 G2	9.5	3.5
Seg4 G1	9.2	3.2
Seg3 G2	13.2	7.2

Fig 6. Normalized RG averaged minute-by-minute (from the beginning of the relaxation session). G1 (black) and G2 (white). Shaded bars indicate transition time intervals due to smoothing and interpolation. Asterisks indicate statistically significant difference (KW; p-value<0.05).

https://doi.org/10.1371/journal.pone.0186399.g006

Subjective self-perception of stress

Fig 3 shows no significant differences in the level of self-perceived stress between groups at the beginning (T1), after the stress session (T2) and at the end of the experiment (T3). This is an expected result since participants were randomly assigned to the groups. Each group significantly increased the self-perceived stress during the stress session (T1-T2), thus assuring that both groups achieved approximately the same level of self-perceived stress before the beginning of stimulation at T2. The latter also means that the MIST session attained its goal. Likewise, each group decreased their self-perceived level of stress during the relaxation session with significant differences between T2 and T3. It is a fact that reduction of the stress level happens after a certain time in a time-out room with standard white light. Fig 3 shows differences
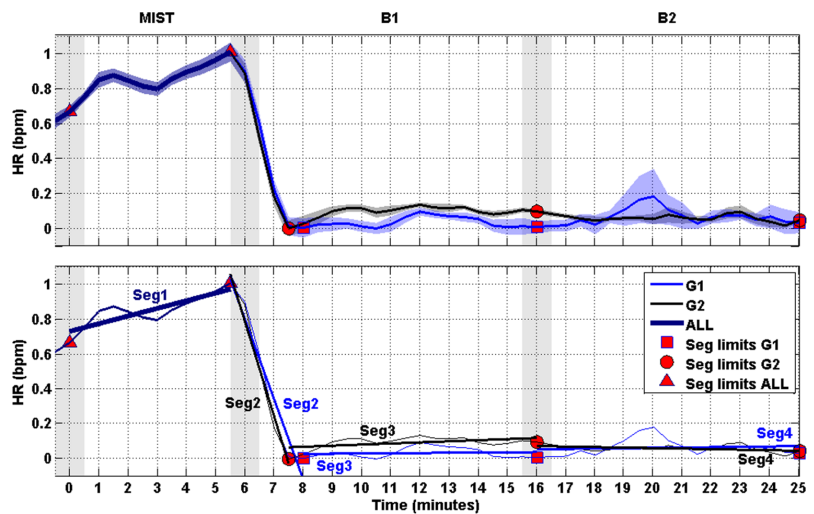

Fig 7. HR and segments. Upper: Curves represent the normalized HR of G1 (blue) and G2 (black). The SEM of the HR is displayed behind the HR curves. Shaded bars indicate transition time intervals due to smoothing and interpolation. The red circumference indicates the time period in which the curves of both groups converge. Bottom: The curves of the upper plot are simplified by their respective linear trends (linearized), thus given rise to four segments (i.e., Seg1, Seg2, Seg3 and Seg4). Red markers indicate limits of the segments.

https://doi.org/10.1371/journal.pone.0186399.g007

between T1, T2 and T3 not as a result of our experiment, but as a proof that the stress session (MIST) and the relaxation session (the time-out room) played their roles correctly. In summary, the significant differences of self-perceived stress T1-T2 and T2-T3 corroborate that both the stress and relaxation sessions satisfactory fulfilled their respective goals. The analysis of the subjective self-perception of stress was useful to quantify the level of stress at the beginning, during and at the end of the relaxation session and validate our methodology used in the stress (MIST) and relaxation (chromoterapy room) sessions.

Finally, the fact that most of the participants (83%) reported that the blue lighting made them get significantly more relaxed that the conventional white is a clear indication of the advantage of the use of blue lighting.

Frontal relative gamma and heart rate

Fig 4 shows the normalized mean spectral power of Gamma, 1/Theta, 1/Alpha and the RG. These spectral bands have been used in literature to assess the level of stress [27–29]. The four plots present similar curves and they all show the drastic decrement of stress level during B1. The RG (left-bottom plot of Fig 4) is a combination of the others (see section EEG signals) that has recently used in studies relatives to meditation-relaxation [30,31] and stress [32]. The four plots exhibit a high level of correlation and a similar envelope; however the RG computes a smoother version that emphasizes the differences of curves of G1 and G2 during the transition to B1. This, together with the fact that the RG generally correlates with the HR, which is a commonly accepted stress marker [33–37], supports the use of the RG to measure the level of stress.

According to results of the linearized RG (shown in Fig 5 bottom) and the zero-crossing analysis reported in Table 2, all participants were stressed by the MIST (Seg1). Then the participants of G1 (test group), who experienced the blue lighting in B1, got the minimum level of stress approximately 1.1 minutes after the beginning of the block. However, for G2 (control group), who experienced white lighting in B1, got relaxed after approximately 3.5 minutes from the beginning of B1. The levels of stress G1-G2 measured at 1 minute after the beginning of relaxation session are significantly different (see Fig 6, minute 7). Therefore, the participants who were exposed to blue light achieved their minimum level of stress in the third part of time compared with the ones who stayed with white light. Indeed, the slope of Seg2 of G1 was significantly different of that of G2. It was approximately three-fold the slope of Seg2 of G2 (see Fig 5 bottom and Table 1, third row), thus indicating a faster acceleration of the relaxation process with blue lighting. In addition, the participants exposed to blue lighting during B1 kept the minimum level of stress for much longer time (total length of Seg3 of G1) than participants exposed to conventional white (only the initial time of Seg3).

The upper plot of Fig 5 also shows a convergence of the RG curve of both groups after 3.5–5 minutes in B1. Afterwards, the values of RG of both groups increased without significant difference (Seg4 and Seg5 in Fig 5 bottom). This fact is interpreted as follows: i) after a period of time (4 minutes approximately), there is no advantage in the use of blue lighting in comparison with the conventional white. Although the discussion about the physiological mechanism that justifies this finding is out of the scope of this work, we suggest that the sensory adaptation [46] and the tedious nature of the task could increase the level of stress; ii) then, after the convergence time (3.5–5 minutes), extended exposition to either blue or white lighting causes no additional benefit.

Fig 7 shows the HR (upper plot) and, in a similar way to the analysis performed with the RG, the linearized version (bottom plot). The linearized HR suggests that the participants experienced four phases during the experiment, one per segment. The first one (Seg1) was due

to the stressful effect of the MIST. The second one (Seg2) was a consequence of the beginning of the relaxation session. These two phases corresponded to the two first phases described by the RG. The third phase (Seg3) indicated a stabilization of the stress level, that is, once the minimum was achieved, it remained low for the rest of B1. The last phase (Seg4) was similar to the previous one.

In view of Fig 7 we can state that some of the light-color-related differences indicated by the RG curves during the relaxation process cannot be observed with the HR curves. Despite the HR is generally accepted as stress marker, it has some limitations in terms of temporal resolution. In order to minimize error, the HR is usually computed through long epochs (from one to several minutes) of signal in comparison with the RG (a few seconds). In fact, we used 90-second epochs with 66% overlap and 2-second epochs without overlap for the HR and the RG, respectively. This prevents the HR from providing significant short-term differences. However, in this work, differences indicated by the RG were brief and presented at the very beginning of the relaxation session. Therefore the RG provided short-term differences in stress level that the HR was not able to highlight. In addition, we suggest that not all the neuro processes cause changes in the cardiovascular physiology. Sometimes they do affect the cardiovascular system but the changes are camouflaged with other factors that cause more powerful changes. For example, when someone is running the HR is high compared with the resting HR, but nonetheless this person may be less mentally stressed than in resting state. In the context of this paper, changes in mental stress at the beginning of the relaxation session were reflected by the RG, but they could not be indicated by the HR probably due to the full relaxed position of the participants.

Blue vs. white lighting

In this paper we have shown that blue lighting accelerates the post-stress relaxation in comparison with conventional white. We have performed objective measures with well-known standardized procedures. In the chromoterapy room, white lighting was produced as the combination of the three sets of LEDs (red, green and blue). However, the blue one was obtained as the suppression of red and green LEDs ceteris paribus. The set of blue LEDs was the only light source in common during the whole relaxation session and paradoxically, whatever differences found in the comparison blue-white cannot be due to this wavelength, but the absence of green and red. In this sense our main claim is stated in the title of this paper and our main contribution must be understood in practical terms. The research of the influence of red or green in the level or stress is out of the scope of this study. An alternative experimental design would be to present the white light with the same luminance as the blue light. This would allow testing whether the wavelength makes a difference. However, this alternative implies different intensities of blue in each condition, together with the fact of having different color components. In this case, the analysis might be more confusing.

The fact that blue lighting accelerates the post-stress relaxation seems to be heading in the opposite direction from previous works related to melatonin suppression, sleepiness reduction and alertness augmentation [4,5,13,14,47]. Nevertheless, there are several fundamental differences between these works and our study that can explain the controversy. First of all, we analyzed post-stress relaxation instead of sleep disturbances. Secondly, the stimulus used in sleep-related works is different. Finally, the exposure time is rather short in our study. Despite that, physiological and psicological mechanisms underlying the influence of color on human beings are out of the scope of this study.

Practical implications and future works

The findings of this work could be useful in clinical and educational environments. Psychologists and other experts that use lighting in their therapies could benefit from them. For instance, the time spent in the time-out room used in schools in episodes of violence outbreaks, can be reduced drastically to just one minute and extended for three more minutes if blue lighting is used instead of the conventional white. This would report a direct benefit to the student, who could quickly reintegrate with the rest of classmates without sense of guilt or shame and minimum impact in the training.

Furthermore, whatever color is used in the time-out room, we have shown that more than circa four minutes causes no extra benefit (potentials causes have been suggested in section Frontal relative gamma and heart rate). Previous color-lighting-related studies [19,20] spent much longer sessions of 10–15 and 30 minutes respectively. We have reported a reproducible methodology that, perhaps, will optimize results of new experiments with much shorter sessions. Obviously the results obtained in this study with healthy participants cannot be directly extrapolated to patients or students with behavioral or emotional disorders, but we have provided an easy methodology that can be applied individually to each subject and context.

Only twelve volunteers participated in the study. This sample is not large enough to obtain solid scientific evidence but, as a first approach, it may establish the pillars for future studies. The paper reports the methodology and results of a preliminary study that can motivate further research in the field. Our results must be extended to draw reliable conclusions. Despite that, the statistics revealed promising results that are relevant for the scientific community.

Apart from that, the information reported here could influence in emerging technologies such as neuromarketing (e.g., the use of a blue lighting for a short while just before starting a negotiation) and in daily-life context (e.g., during stressful periods of work or at home). Stress has an important role in people life and this preliminary work might be used as a source to investigate stress-color relationship through an accurate methodology based on bio-signals.

Supporting information

S1 File. Study protocol and bioethics committee endorsement.
(ZIP)

S2 File. Datasets of subject 1.
(ZIP)

S3 File. Datasets of subject 2.
(ZIP)

S4 File. Datasets of subject 3.
(ZIP)

S5 File. Datasets of subject 4.
(ZIP)

S6 File. Datasets of subject 5.
(ZIP)

S7 File. Datasets of subject 6.
(ZIP)

S8 File. Datasets of subject 7.
(ZIP)

S9 File. Datasets of subject 8.
(ZIP)

S10 File. Datasets of subject 9.
(ZIP)

S11 File. Datasets of subject 10.
(ZIP)

S12 File. Datasets of subject 11.
(ZIP)

S13 File. Datasets of subject 12.
(ZIP)

Acknowledgments

Author Contributions

Conceptualization: Jesus Minguillon, Miguel Angel Lopez-Gordo, Maria Jose Sanchez-Carrion, Francisco Pelayo.

Data curation: Jesus Minguillon.

Formal analysis: Jesus Minguillon, Miguel Angel Lopez-Gordo, Maria Jose Sanchez-Carrion, Francisco Pelayo.

Funding acquisition: Francisco Pelayo.

Investigation: Jesus Minguillon, Miguel Angel Lopez-Gordo, Diego A. Renedo-Criado, Maria Jose Sanchez-Carrion, Francisco Pelayo.

Methodology: Jesus Minguillon, Miguel Angel Lopez-Gordo, Diego A. Renedo-Criado.

Project administration: Miguel Angel Lopez-Gordo, Francisco Pelayo.

Resources: Francisco Pelayo.

Software: Jesus Minguillon.

Supervision: Miguel Angel Lopez-Gordo, Francisco Pelayo.

Validation: Jesus Minguillon, Francisco Pelayo.

Visualization: Jesus Minguillon.

Writing – original draft: Jesus Minguillon.

Writing – review & editing: Jesus Minguillon, Miguel Angel Lopez-Gordo, Diego A. Renedo-Criado, Maria Jose Sanchez-Carrion, Francisco Pelayo.

References

1. Yousuf Azeemi ST, Raza SM. A critical analysis of chromotherapy and its scientific evolution. Evidence-based Complement Altern Med. 2005; 2: 481–488. https://doi.org/10.1093/ecam/neh137 PMID: 16322805

2. Küller R, Wetterberg L. Melatonin, cortisol, EEG, ECG and subjective comfort in healthy humans: Impact of two fluorescent lamp types at two light intensities. Light Res Technol. 1993; 25: 71–80.

3. Sroykham W, Promraksa T, Wongsathikun J, Wongsawat Y. The red and blue rooms affect to brain activity, cardiovascular activity, emotion and saliva hormone in women. BMEiCON 2014–7th Biomed Eng Int Conf. 2015; https://doi.org/10.1109/BMEiCON.2014.7017432

4. Cajochen C, Münch M, Kobialka S, Kräuchi K, Steiner R, Oelhafen P, et al. High sensitivity of human melatonin, alertness, thermoregulation, and heart rate to short wavelength light. J Clin Endocrinol Metab. 2005; 90: 1311–1316. https://doi.org/10.1210/jc.2004-0957 PMID: 15585546

5. Münch M, Kobialka S, Steiner R, Oelhafen P, Wirz-Justice A, Cajochen C. Wavelength-dependent effects of evening light exposure on sleep architecture and sleep EEG power density in men. Am J Physiol Regul Integr Comp Physiol. 2006; 290: R1421–R1428. https://doi.org/10.1152/ajpregu.00478.2005 PMID: 16439671

6. Ali MR. Pattern of EEG recovery under photic stimulation by light of different colors. Electroencephalogr Clin Neurophysiol. 1972; 33: 332–335. https://doi.org/10.1016/0013-4694(72)90162-9 PMID: 4114919

7. Hi LS, Atsuura TK, Himomura YS, Wanaga KI. Effects of Different Light Source Color Temperatures during Physical Exercise on Human EEG and Subjective Evaluation. J Human-Environmental Syst. 2009; 12: 27–34.

8. Yoto A, Katsuura T, Iwanaga K, Shimomura Y. Effects of object color stimuli on human brain activities in perception and attention referred to EEG alpha band response. J Physiol Anthropol. 2007; 26: 373–379. https://doi.org/10.2114/jpa2.26.373 PMID: 17641457

9. Moridis CN, Klados MA, Kokkinakis IA, Terzis V, Economides AA, Karlovasitou A, et al. The impact of audio-visual stimulation on alpha brain oscillations: An EEG study. Proc IEEE/EMBS Reg 8 Int Conf Inf Technol Appl Biomed ITAB. 2010; 3–6. https://doi.org/10.1109/ITAB.2010.5687651

10. Deguchi T, Sato M. The Effect of Color Temperature of Lighting Sources on Mental Activity Level. Biol Pharm Bull. 1992; 11: 37–43.

11. Münch M, Plomp G, Thunell E, Kawasaki A, Scartezzini JL, Herzog MH. Different colors of light lead to different adaptation and activation as determined by high-density EEG. Neuroimage. Elsevier Inc.; 2014; 101: 547–554. https://doi.org/10.1016/j.neuroimage.2014.06.071 PMID: 25016138

12. Ebbesen F, Agati G, Pratesi R. Phototherapy with turquoise versus blue light. Arch Dis Child Fetal Neonatal Ed. 2003; 88: F430–1. https://doi.org/10.1136/fn.88.5.F430 PMID: 12937051

13. Rahman SA, Flynn-Evans EE, Aeschbach D, Brainard GC, Czeisler CA, Lockley SW. Diurnal spectral sensitivity of the acute alerting effects of light. Sleep. 2014; 37: 271–81. https://doi.org/10.5665/sleep.3396 PMID: 24501435

14. Wright HR, Lack LC. Effect of Light Wavelength on Suppression and Phase Delay of the Melatonin Rhythm. Chronobiol Int. 2001; 18: 801–808. https://doi.org/10.1081/CBI-100107515 PMID: 11763987

15. Vandewalle G, Balteau E, Phillips C, Degueldre C, Moreau V, Sterpenich V, et al. Daytime Light Exposure Dynamically Enhances Brain Responses. Curr Biol. 2006; 16: 1616–1621. https://doi.org/10.1016/j.cub.2006.06.031 PMID: 16920622

16. Valdez P, Mehrabian A. Effects of Color on Emotions. J Exp Psychol Gen. 1994; 123: 394–409. Available: http://www.scopus.com/inward/record.url?eid=2-s2.0-0028713240&partnerID=tZOtx3y1 PMID: 7996122

17. Kuijsters A, Redi J, De Ruyter B, Heynderickx I. Lighting to make you feel better: Improving the mood of elderly people with affective ambiences. PLoS One. 2015; 10: 1–22. https://doi.org/10.1371/journal.pone.0132732 PMID: 26192281

18. Al-Ayash A, Kane RT, Smith D, Green-Armytage P. The influence of color on student emotion, heart rate, and performance in learning environments. Color Res Appl. 2015; https://doi.org/10.1002/col.21949

19. Schauss AG. Tranquilizing effect of color reduces aggressive behavior and potential violence. J Orthomol Psychiatry. 1979; 8: 218–221.

20. Sánchez-Carrión MJ. Combined cromotherapy's method for disruptive behavior disorders. Particip Educ Rev del Cons Esc del estado. 2013; 2: 105–109. https://doi.org/10.1017/CBO9781107415324.004

21. Besenecker U, Krueger T, Bullough J, Zachary P, Gerlach R. The experience of equivalent luminous colors at architectural scale. In: Gadia D, editor. Colour and Colorimetry Multidisciplinary Contributions Proceedings of the 12th Conferenza del Colore. XII B. 2016. pp. 109–117.

22. Casciani D, Musante F, Rossi M. Warm white, neutral white, cold white: the design of new lighting fixtures for different working scenarios. In: Gadia D, editor. Colour and Colorimetry Multidisciplinary Contributions Proceedings of the 12th Conferenza del Colore. XII B. 2016. pp. 81–92.

23. Bellia L, Fragliasso F, Stefanizzi E. LED light scenes for artworks colour perception. In: Gadia D, editor. Colour and Colorimetry Multidisciplinary Contributions Proceedings of the 12th Conferenza del Colore. XII B. 2016. pp. 129–140.

24. Picard RW. Affective Computing: From laughter to IEEE. IEEE Trans Affect Comput. 2010; 1: 11–17. https://doi.org/10.1109/T-AFFC.2010.10

25. Jenke R, Peer A, Buss M. Feature extraction and selection for emotion recognition from EEG. IEEE Trans Affect Comput. 2014; 5: 327–339. https://doi.org/10.1109/TAFFC.2014.2339834

26. Nardelli M, Valenza G, Greco A, Lanata A, Scilingo EP. Recognizing emotions induced by affective sounds through heart rate variability. IEEE Trans Affect Comput. 2015; 6: 385–394. https://doi.org/10.1109/TAFFC.2015.2432810

27. Seo S, Lee J. Stress and EEG. Convergence and Hybrid Information Technologies. 2010. pp. 413–426. https://doi.org/10.5772/235

28. Papousek I, Weiss EM, Schulter G, Fink A, Reiser EM, Lackner HK. Prefrontal EEG alpha asymmetry changes while observing disaster happening to other people: cardiac correlates and prediction of emotional impact. Biol Psychol. Elsevier B.V.; 2014; 103: 184–94. https://doi.org/10.1016/j.biopsycho.2014.09.001 PMID: 25224180

29. Brouwer A-M, Neerincx MA, Kallen V, van der Leer L, ten Brinke M. EEG alpha asymmetry, heart rate variability and cortisol in response to Virtual Reality induced stress. J CyberTherapy Rehabil. 2011; 4: 27–40.

30. Lutz A, Greischar LL, Rawlings NB, Ricard M, Davidson RJ. Long-term meditators self-induce high-amplitude gamma synchrony during mental practice. Proc Natl Acad Sci U S A. 2004; 101: 16369–16373. https://doi.org/10.1073/pnas.0407401101 PMID: 15534199

31. Steinhubl SR, Wineinger NE, Patel S, Boeldt DL, Mackellar G, Porter V, et al. Cardiovascular and nervous system changes during meditation. Front Hum Neurosci. 2015; 9: 1–10. https://doi.org/10.3389/fnhum.2015.00145

32. Minguillon J, Lopez-Gordo MA, Pelayo F. Stress Assessment by Prefrontal Relative Gamma. Front Comput Neurosci. 2016; 10: 1–9. https://doi.org/10.3389/fncom.2016.00101

33. Reinhardt T, Schmahl C, Wüst S, Bohus M. Salivary cortisol, heart rate, electrodermal activity and subjective stress responses to the Mannheim Multicomponent Stress Test (MMST). Psychiatry Res. 2012; 198: 106–11. https://doi.org/10.1016/j.psychres.2011.12.009 PMID: 22397919

34. Dimitriev DA, Saperova E V. Heart rate variability and blood pressure during mental stress. Ross Fiziol Zh Im I M Sechenova. 2015; 101: 98–107. Available: http://www.scopus.com/inward/record.url?eid=2-s2.0-84938513897&partnerID=tZOtx3y1 PMID: 25868330

35. Chandiramani S, Cohorn LC, Chandiramani S. Heart rate changes during acute mental stress with closed loop stimulation: report on two single-blinded, pacemaker studies. Pacing Clin Electrophysiol. 2007; 30: 976–84. https://doi.org/10.1111/j.1540-8159.2007.00795.x PMID: 17669080

36. Bali A, Jaggi AS. Clinical experimental stress studies: methods and assessment. Rev Neurosci. 2015; 26: 555–79. https://doi.org/10.1515/revneuro-2015-0004 PMID: 26020552

37. Regula M, Socha V, Kutilek P, Socha L, Hana K, Hanakova L, et al. Study of heart rate as the main stress indicator in aircraft pilots. Proceedings of the 16th International Conference on Mechatronics—Mechatronika 2014. Brno, Czech Republic: IEEE; 2014. pp. 639–643. https://doi.org/10.1109/MECHATRONIKA.2014.7018334

38. Dedovic K, Rexroth M, Wolff E, Duchesne A, Scherling C, Beaudry T, et al. Neural correlates of processing stressful information: An event-related fMRI study. Brain Res. Elsevier B.V.; 2009; 1293: 49–60. https://doi.org/10.1016/j.brainres.2009.06.044 PMID: 19555674

39. Dagher A, Tannenbaum B, Hayashi T, Pruessner JC, McBride D. An acute psychosocial stress enhances the neural response to smoking cues. Brain Res. Elsevier B.V.; 2009; 1293: 40–48. https://doi.org/10.1016/j.brainres.2009.07.048 PMID: 19632211

40. Tanida M, Katsuyama M, Sakatani K. Relation between mental stress-induced prefrontal cortex activity and skin conditions: A near-infrared spectroscopy study. Brain Res. 2007; 1184: 210–216. https://doi.org/10.1016/j.brainres.2007.09.058 PMID: 17950258

41. Nagano-Saito A, Dagher A, Booij L, Gravel P, Welfeld K, Casey KF, et al. Stress-induced dopamine release in human medial prefrontal cortex—18F-fallypride/PET study in healthy volunteers. Synapse. 2013; 67: 821–30. https://doi.org/10.1002/syn.21700 PMID: 23939822

42. Dedovic K, Renwick R, Mahani NK, Engert V, Lupien SJ, Pruessner JC. The Montreal Imaging Stress Task: using functional imaging to investigate the effects of perceiving and processing psychosocial stress in the human brain. J Psychiatry Neurosci. 2005; 30: 319–25. Available: http://www.pubmedcentral.nih.gov/articlerender.fcgi?artid=1197276&tool=pmcentrez&rendertype=abstract PMID: 16151536

43. Zschucke E, Renneberg B, Dimeo F, Wüstenberg T, Ströhle A. The stress-buffering effect of acute exercise: Evidence for HPA axis negative feedback. Psychoneuroendocrinology. Elsevier Ltd; 2015; 51: 414–25. https://doi.org/10.1016/j.psyneuen.2014.10.019 PMID: 25462913

44. Remor E. Psychometric Properties of a European Spanish Version of the Perceived Stress Scale (PSS). Span J Psychol. Cambridge University Press; 2014; 9: 86–93. https://doi.org/10.1017/S1138741600006004

45. Semmlow JL. Biosignal and Medical Image Processing [Internet]. Third Edit. CRC Press Book; 2014. Available: https://www.crcpress.com/Biosignal-and-Medical-Image-Processing-Third-Edition/Semmlow-Griffel/9781466567368

46. Wark B, Lundstrom BN, Fairhall A. Sensory adaptation. Curr Opin Neurobiol. 2007; 17: 423–429. https://doi.org/10.1016/j.conb.2007.07.001 PMID: 17714934

47. Figueiro MG, Bullough JD, Bierman A, Fay CR, Rea MS. On light as an alerting stimulus at night. Acta Neurobiol Exp (Wars). 2007; 67: 171–178.

Appendix E

Article preprint

Human neuro-activity for securing Body Area Networks: application of Brain-Computer interfaces to People-centric Internet of Things

J.F. Valenzuela-Valdés, M.A. López-Gordo, P. Padilla, J.L Padilla and J. Minguillón

Abstract— A former definition states that a Brain-computer Interface (BCI) provides a direct communication channel to the brain without the need of muscles and nerves. With the emergence of wearable and wireless BCIs, they evolved to become part of wireless Body Area Networks (WBAN) offering people-centric applications such as cognitive workload assessment or detection of selective attention. Currently, WBAN are mostly integrated by low-cost devices that, because of their limited hardware resources, cannot generate secure random numbers for encryption. This is a critical issue in the context of new IoT device communication and its security. Such devices require securing their communication, mostly by means of the automatic renewing of the cryptographic keys. In the domain of the People-centric Internet of Things, we propose to use wireless BCIs as a secure source of entropy, based on neuro-activity, capable to generate secure keys that outperforms other generation methods. In our approach, current wireless BCI technology is an attractive option to offer novel services emerged from novel necessities in the context of People-centric Internet of Things. Our proposal is an implementation of the Human-in-the-loop paradigm, in which devices and humans indistinctly request and offer services each other for mutual benefit.

Index Terms— Secure communication, neuro-activity, Brain-Computer interfaces, IoT, wireless body area networks, encryption.

I. INTRODUCTION

The people-centric Internet of Things (IoT), the wearable Internet of Things (WIoT) or the health Internet of Things are the different names that are emerging to represent the paradigm for a smart world in which ubiquitous communication occurs among heterogeneous and interconnected devices in wireless Body Area Networks (WBAN). These networks involve a variety of low-cost devices, sensors or gadgets with wireless communication capabilities that are placed surrounding the human body for physiological monitoring. Such WBAN devices are required to be compact, wearable and energy efficient, in order to achieve a practical system with sufficient lifetime. These requirements impose non negligible limitations regarding data acquisition, computation, or transmission capabilities. However, those are not the unique limitations to be considered: due to the shared wireless medium between the WBAN devices, the communication security may be compromised. In this way, it is possible to have malicious attacks on body-centric systems. To avoid this, the transmitted data must be secured as it is generated, transmitted, received, stored or analyzed within the complete system. As a consequence, WBAN security is a challenge that arises, with novel and ongoing solutions.

The WBAN nature makes necessary to combine security with energy-efficiency to provide a practical solution for wearable devices and sensors. In particular, the resources for security are very scarce and, as a consequence, the solution is not trivial. There are traditional upper layer security solutions, such as the Advanced Encryption Standard (AES), the Diffie–Hellman key algorithm, elliptic curve cryptography or hash chains, among others, which have high computational costs. However, if lower latency or computational costs are required, it could be convenient to explore the lower layers to provide security, such as the physical one [1]. In this way of providing low complexity and latency, an additional approach that may provide an efficient solution is to encrypt the data prior to communication by generating random binary sequences from the communication device signals. This approach can be especially useful in the case of wireless sensors, wearable devices and bio-signals, for which the body and its acquired signals are the essential part of the communication system. Up to now, different bio-signals from wearable devices and bio-inspired solutions have been used for securing WBANs [2]. In the last years, studies have used bio-signals such as photoplethysmogram [3], interpulse interval [4] or electrocardiogram [5], among others, to generate secure keys in the context of WBANs. In this way, other interesting signals such as EEG ones may be used for securing WBANs, which is the purpose in this work.

In comparison with ECG, EEG signals present better characteristics for the generation of random binary sequences.

For instance, unlike ECG, EEG is a non-stationary signal that, after very simple whitening processing, presents the nearly flat spectrum corresponding to a Normal distribution. These two aspects kindly facilitates the generation of truly random and independent sequences with a minimum processing and memory usage. Another aspect to consider is the bit rate. Considering the most advanced techniques in ECG, the generation of 128 random bits would take 6-10 seconds [5]. However, EEG signals are typically acquired at a rate of 1KSamples/second with 24 bits of resolution. This computes a binary stream of 24Kbps. This estimation is the case of just one single EEG channel. Then, EEG acquisitions constituted by independent electrodes located at relatively separated positions could easily multiply this rate. In summary and taking into account that a fraction of the total bit rate will be discarded due to existing redundancies of EEG signals, EEG has the extraordinary potential to provide very large sets of random numbers per second. This could enable the delivery of secure transmission among the devices of a particular WBAN or to feed a repository with cryptographic passwords for a complete People-centric Internet of Things environment (see Fig. 1).

In this article, a novel approach to provide security to wireless body area network communications is proposed, based on secure key generation by means of EEG signals acquisition. This approach is oriented to People-centric Internet of Things (IoT) paradigm. The paper is organized as follows: Section II is referred to Brain-Computer interfaces in the People-centric Internet of Things environment. Section III presents the experimental frame of the work. Section IV is devoted to the experimental results and their discussion. Finally, conclusions are drawn in Section V.

II. WIRELESS BRAIN-COMPUTER INTERFACES IN THE PEOPLE-CENTRIC INTERNET OF THINGS ECOSYSTEM

The most relevant function of a Wireless Brain-computer interface (WBCI) is to establish a communication channel between the brain and other entities of the people-centric Internet of Things or the so called Internet of People (IoP) [6-7]. Typically, WBCIs extract endogenous cognitive information from EEG neuro-correlates, codify this info into a binary sequence of data and stream them out [8]. The data stream is normally used either to feedback the user, thus constituting a closed-loop communication system or as commands to computers and actuators. In the last years, WBCIs have been used for different purposes related to the Human-in-the-Loop paradigm, such as for the assessment of level of attention in multi-talker scenarios [9] or the cognitive workload as well as in neuro-marketing or in Ambient Assisted Living.

The new people-centric IoT paradigm enables WBCI to be part an environment in which other nodes can benefit of the generation of cognitive and electro-physiological information. Figure 1 reproduces the IoP architecture proposed in [7]. In this architecture, WBCIs are nodes of the Physical Space that upload cognitive information by means of an aggregation node towards the IoP Runtime Space. The IoP Runtime Space provides uniform access of services and applications to nodes of the Physical Space by an Open API that abstracts their

technical details. Then, applications and services of different IoP scenarios could access a pool of shared resources and their data.
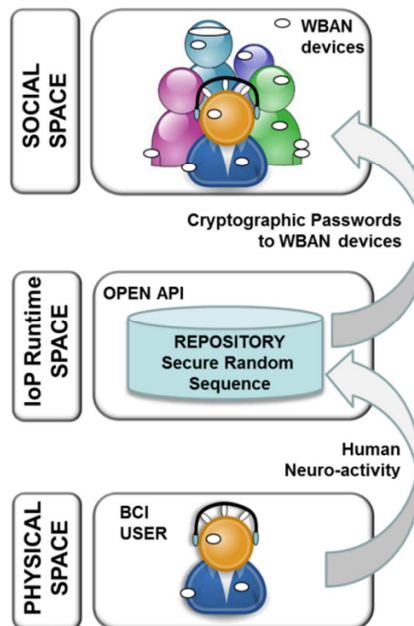

Figure 1. IoP infrastructure components.

In this context, humans are both data sources and sinks in the same way that WBAN devices of the physical space are so. In our approach, WBCIs can offer to the IoP infrastructure truly random binary sequences that can be used as passwords to establish secure transactions between applications and WBAN devices that, as mentioned before, lack this capability. In this paradoxical approach, humans have the capability to offer services to applications and devices that, in turns, serve to humans.

III. EXPERIMENTAL FRAME

In this section, the experimental background is provided, in terms of description of: EEG signal acquisition, processing techniques for the experimental validation and the statistical tests that have to be passed in order to assess the suitability of EEG signals as a source for secure communication key generation.

A. EEG signals for the experimentation

The EEG datasets used to produce the results in this work have been provided by the Multimedia Signal Processing group (MMSPG) of the EPFL (Ecole Polytechnique Fédérale de Lausanne) [10]. The acquisition system is an efficient P300-based brain-computer interface for disabled subjects. The datasets contain raw EEG data from eight subjects. Each one is formed by 32 electrode signals. The electrode positions are Fp1, AF3, F7, F3, FC1, FC5, T7, C3, CP1, CP5, P7, P3, Pz, PO3, O1, Oz, O2, PO4, P4, P8, CP6, CP2, C4, T8, FC6,

FC2, F4, F8, AF4, Fp2, Fz, and Cz of the 10-20 International System (see Fig. 2). The sampling rate is 2048 Hz.
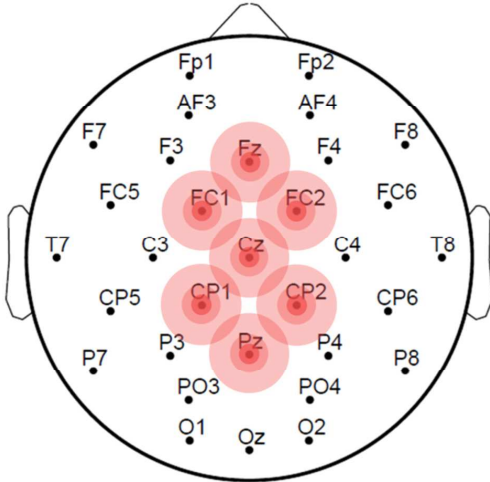

Fig. 2. Electrode head map used in the experiments [10]. Red circles correspond to the electrodes on central-top positions, which provide the best results in the supervised analysis (see section IV).

It must be highlighted that all experiments were performed under real-world conditions. This means that the data processed in this study contain artifacts caused by eye-blinks, eye-movements, muscle-activity, among others, and the subjects were not always perfectly concentrated in particular tasks for the experiments.

B. Techniques for EEG signal processing

Due to their nature, the EEG data contain the information mixed with artifacts and noise, typically from neuro-motor activity and electrical couplings. As a consequence, the experimentation (section III) may be affected. To overcome possible limitations, it may be recommendable to define procedures for proper EEG data processing and further analysis based on the extraction of the data relevant information from the noisy captured data. Some procedures have been proposed in the literature, such as Principal Component Analysis (PCA) or Independent Component Analysis (ICA) [11-12]. These approaches can extract the main components of a dataset by means of standard projection models so that noise and artifacts can be neglected or conveniently reduced.

The first one, PCA, is applied to find the space of maximum variance in the M-dimensional feature space of a dataset, formed by N samples of M variables each one. In the case of EEG data, the M samples correspond to the different EEG acquisition channels and the N variables are the registered signal values during the signal registration period. PCA performs a linear transformation of the original set of samples into a lower number K of uncorrelated features, called principal components (PCs), according to the computed K-subspace projection vectors. Those projection vectors are the basis for the EEG analysis in this work.

The second one, ICA is a method for separating a signal into additive subcomponents (blind source separation). It is based on the computation of the independent vectors that compound the analyzed set of signals. ICA finds the independent components (latent sources) by maximizing the statistical independence of the estimated components. The ICA separation of mixed signals gives very good results if two assumptions are satisfied: the source signals are independent of each other and the values in each source signal have non-Gaussian distributions, which are premises that are valid in the case of EEG.

The result in both cases, PCA and ICA, is a set of independent vectors that represent the subspace in which the signal can be represented, maximizing the independence of such vectors.

C. The NIST test

The NIST Test Suite [13] is a tool for security test developed by the National Institute of Standards and Technology (USA) that is widely used for validating the performance of secure keys [14-15]. This tool is used in this work for testing the randomness of the generated sequences in our experimentation. For processing the generated data, it is partitioned the data into 100 sequences, each sequence with 20000 bits. The NIST Test Suite provides 15 different tests. For the sake of simplicity, only the most significate six tests are reported in this paper, as it is done in [14].

IV. RESULTS AND DISCUSSION

In this section, both the supervised and the unsupervised approaches are considered. In both cases, it is tried to determine if the EEG signals can be used as the source signals for secure key generation, analysing the robustness of the secured sequence by means of the NIST test.

A. Supervised analysis

The first approach is the one in which the EEG signal acquisition points (EEG channels) for key generation have to be properly studied. In this case, it is necessary to identify which are the adequate EEG acquisition positions to obtain the best performance in terms of key generation and its robustness. Figure 2 provides the electrode head map used in the experimentation.

All the 32 channels have been analysed to determine which ones provide a good performance and pass the NIST tests (score above 95%). The next Table provides the main NIST test results for the code generated by the EEG signals, according to their electrode position.

Table 1. NIST test results for the 32 EEG channel signals.

	Channel NIST performance [%]										
	Fp1	AF3	F7	F3	**FC1**	FC5	T7	C3	**CP1**	CP5	P7
Frequency	98	89	92	96	**99**	87	55	87	**100**	69	38
Block	67	77	16	27	**97**	22	0	35	**99**	18	26
FFT	100	100	91	100	**100**	100	100	98	**100**	98	100
Rank	98	100	99	100	**99**	98	92	99	**100**	99	98
Entropy	20	24	15	24	**100**	16	2	35	**99**	99	38
Linear	99	99	97	98	**99**	100	97	98	**100**	98	99

Article preprint

Complexity											
	P3	Pz	PO3	O1	Oz	O2	PO4	P4	P8	CP6	**CP2**
Frequency	45	99	97	99	100	100	97	93	15	39	**99**
Block	38	37	92	98	35	42	83	89	7	80	**97**
FFT	100	99	98	100	100	97	99	99	100	100	**98**
Rank	99	100	100	100	99	99	100	99	99	98	**99**
Entropy	40	93	37	97	94	94	87	88	14	79	**95**
Linear Complexity	100	98	99	40	99	99	99	99	100	99	**98**

	C4	T8	FC6	FC2	F4	F8	AF4	Fp2	**Fz**	**Cz**
Frequency	32	88	27	98	78	25	87	98	**96**	**100**
Block	82	30	9	92	13	4	15	28	**98**	**100**
FFT	99	99	100	100	98	100	56	98	**100**	**100**
Rank	99	99	94	98	96	93	96	93	**99**	**97**
Entropy	85	26	36	42	13	3	62	21	**92**	**94**
Linear Complexity	100	100	88	99	100	98	100	100	**97**	**100**

As it can be noticed, the best electrode positions are: CP1, FC1, Fz, CP2 and Cz, sorted in terms of performance. If their positions in Fig. 2 map are analysed, it clearly appears that the acquisition points on the Vertex (central-top of the head) are the best ones for the acquisition: the Cz and surrounding electrodes (see Fig. 2). Figure 3 provides the detailed results of the electrodes in this area. This result is of importance considering the usability point of view: the best acquisition area is easily accessible and disguisable under a cap. It can be monitored with a quite simple EEG acquisition system with only one central electrode or more, situated on Cz position and surroundings respectively.

If the different NIST tests are compared, it is noticed that the most demanding tests are the Frequency, Block and Entropy ones. Figure 4 provides the mean success rate of the electrodes for these three demanding tests, which ratifies the suitability of the Cz zone for the acquisition.

In comparison with other advanced proposals based on ECG [5], our EEG approach can generate binary sequences at a much faster rate. If the best five EEG channels are used (see Table 1), then the binary rate will be improved five times, thus enabling the delivery of secure passwords per data flow or even transaction. In addition, the NIST test results of our approach from all the best five channels clearly exceed those of the ECG approach in [5].

B. Unsupervised analysis

This second approach is the one in which the EEG-electrode positions for key generation are not a priori known. In this situation, if there is not previous knowledge of the proper EEG acquisition positions to obtain the best performance, techniques such as PCA (principal component analysis) or ICA (independent component analysis) may be employed. According to the noisy nature of the EEG signals, ICA is suitable to extract different independent signals that underlying in the 32-channel EEG set of signals. With these independent signals, it can be constructed one unique signal as a compendium of the constituting ICA signals. The next Table provides the main NIST test results for the code generated by this compendium signal.

Table 2. NIST test results for the processed compendium signal.

NIST performance [%]					
Frequency	Block	FFT	Rank	Linear. Compl.	Entropy
PCA	99	38	99	100	99	99
ICA	**99**	**96**	**99**	**100**	**96**	**100**

As it can be seen, both approaches have a significant impact in terms of NIST test performance results. In fact, ICA is the one that provides the best results, fulfilling successfully all the different tests. This case is useful in cases where the user is not familiarized with EEG signal acquisition and the suitability of the different acquisition channels is not known in advance (e.g., BCI users with cognitive impairment or brain damage of simply due to subject inter-variability). This would avoid the need of a calibration session, thus improving the usability and plug-and-play character of our approach.
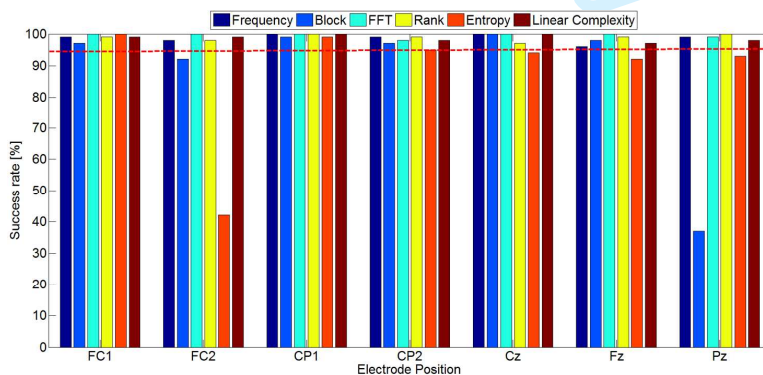

Fig. 3. Detailed results of the NIST tests for the electrodes in the Cz/Fz zone and surrounding area.
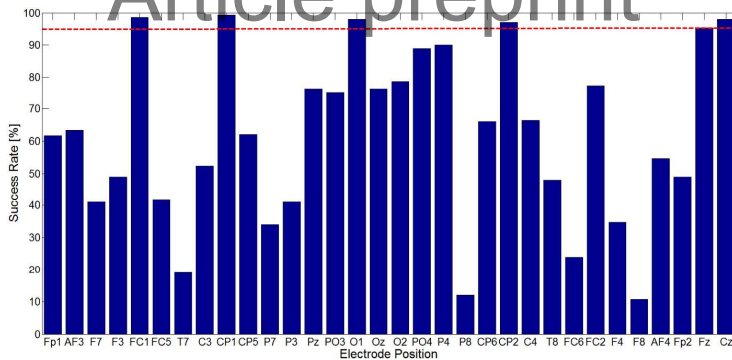
Fig. 4. Mean success rate of the electrodes for the most three demanding NIST tests (Frequency, Block and Entropy). The red line is the NIST threshold of success.

Whatever the approach considered (either supervised or not), the experiments reveal that EEG is a suitable source for secure communication key generation in WBAN. Additionally, people with very limited communication skills such as former BCI users and the severe motor impaired, may also benefit of the generation of secure passwords for their BCI communication systems with no cognitive effort and further complexity.

V. CONCLUSION

This paper presents a novel approach to provide security to wireless body area network communications (WBAN), based on secure key generation by means of EEG data. This proposed approach is oriented to cope with People-centric Internet of Things (IoT) paradigm.

WBAN are mostly integrated by low-cost devices that, because of their limited hardware resources, cannot generate secure random numbers for encryption. In the context of new IoT device communication and its security, such devices require securing their communication, mostly by means of the automatic renewing of the cryptographic keys. Thus, in the way of providing people-centric applications, security is a critical issue.

Our approach is based on Brain-computer Interface (BCI) signal acquisition for key generation. The raw EEG signals act as the source data, based on neuro-activity, capable to generate secure keys that outperform other key generation methods. Considering the different head acquisition points available, it must be stated which positions provide the best results for secure key generation. As a consequence, two cases are considered: supervised and unsupervised analysis. The first one let determine which positions are the best for signal acquisition, whereas the second one is used when no previous knowledge about location suitability is available in advance. In the case of the supervised analysis, it is identified that the best acquisition points are the ones on top of the head (Cz/Fz zone and surrounding area: CP1, FC1 and CP2). In the case of the unsupervised analysis, the ICA signal decomposition into independent components and a compendium generation is the optimal solution for the secure communication key generation.

Compared with other proposed methods in literature such as ECG, our EEG approach generates much faster sequences with very low latency and a negligible computational cost. In addition, the usability is assured as only one channel located at the top of the head is required, thus permitting the use of a low-cost and small BCI Headset with a very reduced number of channels hidden under a cap.

In an open view, our proposal can be cataloged as a particular implementation of the Human-in-the-loop paradigm, in which devices and humans indistinctly request and offer services each other for mutual benefit.

REFERENCES

[1] X. Wang, P. Hao and L. Hanzo, "Physical-layer authentication for wireless security enhancement: current challenges and future developments," in IEEE Communications Magazine, vol. 54, no. 6, pp. 152-158, June 2016.

[2] S. Bitam, S. Zeadally and A. Mellouk, "Bio-inspired cybersecurity for wireless sensor networks," in IEEE Communications Magazine, vol. 54, no. 6, pp. 68-74, June 2016.

[3] K. K. Venkatasubramanian, A. Banerjee, and S. K. S. Gupta, "Plethysmogram-based secure inter-sensor communication in Body Area Networks," 2008, pp. 1–7.

[4] C. C. Y. Poon, Yuan-Ting Zhang, and Shu-Di Bao, "A novel biometrics method to secure wireless body area sensor networks for telemedicine and m-health," IEEE Communications Magazine, vol. 44, no. 4, pp. 73–81, Apr. 2006.

[5] G. Zheng, G. Fang, R. Shankaran, M. Orgun, J. Zhou, L. Qiao, and K. Saleem, "Multiple ECG Fiducial Points based Random Binary Sequence Generation for Securing Wireless Body Area Networks," IEEE Journal of Biomedical and Health Informatics, pp. 1–9, 2016.

[6] Boavida, F., Silva, J.S.: IoP—Internet of People. Future Internet Networking Session. ICT 2013, Vilnius, Lithuania. http://ec.europa.eu/digital-agenda/events/cf/ict2013/item-display.cfm?id=10400 (2013). Accessed 1 June 2015

[7] F. Boavida, A. Kliem, T. Renner, J. Riekki, C. Jouvray, M. Jacovi, S. Ivanov, F. Guadagni, P. Gil, and A. Triviño, "People-Centric Internet of Things—Challenges, Approach, and Enabling Technologies," in Intelligent Distributed Computing IX, vol. 616, P. Novais, D. Camacho,

C. Analide, A. El Fallah Seghrouchni, and C. Badica, Eds. Cham: Springer International Publishing, 2016, pp. 463–474.

[8] M. A. Lopez-Gordo and F. Pelayo Valle, "Brain-Computer Interface as Networking Entity in Body Area Networks," in Wired/Wireless Internet Communications, vol. 9071, M. C. Aguayo-Torres, G. Gómez, and J. Poncela, Eds. Cham: Springer International Publishing, 2015, pp. 274–285.

[9] M. A. Lopez-Gordo, F. Pelayo, E. Fernandez, and P. Padilla, "Phase-shift keying of EEG signals: Application to detect attention in multitalker scenarios," Signal Processing, vol. 117, pp. 165–173, Dec. 2015.

[10] U. Hoffmann, J.M. Vesin, T. Ebrahimi, and K. Diserens, "An efficient P300-based brain-computer interface for disabled subjects," Journal of Neuroscience Methods, vol. 167, no. 1, pp. 115–125, 2008.

[11] J. Jackson, "A User's Guide to Principal Components", Wiley-Interscience, England, 2003.

[12] J.V. Stone, "Independent component analysis : a tutorial introduction". Cambridge, Mass. [u.a.]: MIT Press. ISBN 0-262-69315-1, 2004.

[13] A. Rukhin, Barker E, Leigh S, Levenson M, Vangel M, Banks D, Heckert A, Dray J, Vo S. A statistical test suite for random and pseudorandom number generators for cryptographic applications, NIST-National Institute of Standards and Technology: Gaithersburg, MD, USA, 2010.

[14] S. L. Hong and C. Liu, "Sensor-Based Random Number Generator Seeding," in IEEE Access, vol. 3, no. , pp. 562-568, 2015.

[15] Giuseppe Lo Re, Fabrizio Milazzo and Marco Ortolani "Secure random number generation in wireless sensor networks" Proceedings of the 4th international conference on Security of information and networks Pages 175-182 ACM New York, NY, USA ©2011

Appendix F

Portable System for Real-Time Detection of Stress Level

Jesus Minguillon [1,2,3,*] , Eduardo Perez [2,3], Miguel Angel Lopez-Gordo [2,3,4],
Francisco Pelayo [1,2] and Maria Jose Sanchez-Carrion [5]

1   Department of Computer Architecture and Technology, University of Granada, 18014 Granada, Spain;
     fpelayo@ugr.es
2   Research Centre for Information and Communications Technologies (CITIC), University of Granada,
     18014 Granada, Spain; edu@ugr.es (E.P.); malg@ugr.es (M.A.L.-G.)
3   Department of Signal Theory, Telematics and Communications, University of Granada,
     18014 Granada, Spain
4   Nicolo Association, 18194 Churriana de la Vega, Spain
5   School for Special Education San Rafael, 18001 Granada, Spain; MariaJose.SanchezC@sjd.es
*   Correspondence: minguillon@ugr.es; Tel.: +34-958-241-778

Abstract: Currently, mental stress is a major problem in our society. It is related to a wide variety of diseases and is mainly caused by daily-life factors. The use of mobile technology for healthcare purposes has dramatically increased during the last few years. In particular, for out-of-lab stress detection, a considerable number of biosignal-based methods and systems have been proposed. However, these approaches have not matured yet into applications that are reliable and useful enough to significantly improve people's quality of life. Further research is needed. In this paper, we propose a portable system for real-time detection of stress based on multiple biosignals such as electroencephalography, electrocardiography, electromyography, and galvanic skin response. In order to validate our system, we conducted a study using a previously published and well-established methodology. In our study, ten subjects were stressed and then relaxed while their biosignals were simultaneously recorded with the portable system. The results show that our system can classify three levels of stress (stress, relax, and neutral) with a resolution of a few seconds and 86% accuracy. This suggests that the proposed system could have a relevant impact on people's lives. It can be used to prevent stress episodes in many situations of everyday life such as work, school, and home.

Keywords: stress; biosignal; EEG; ECG; EMG; GSR; real-time; healthcare; e-Health; m-Health

1. Introduction

Stress is a major concern in our modern society. According to the 2014 report of the American Psychological Association, most of U.S. population regularly experience physical (77%) or psychological (73%) symptoms caused by stress, the main ones being fatigue (51%), headache (44%), and upset stomach (34%). In addition, chronic stress has been proved to facilitate the development of diseases due to weakening of the immune system [1]. All this adds up to important costs in terms of people's quality of life and loss of money (USD 300 billion of annual cost to employers in stress related health care and missed work). According to the same report, the top causes of stress in the US are job pressure, money, health, and relationships. Therefore, stress is mainly caused by everyday-life factors. Thus, it is crucial to develop reliable and usable systems for real-time detection of stress level in people's daily life.

New technologies have attempted to improve people's quality of life in the last few years [2]. The development of pervasive and ubiquitous systems and applications has led us into modern terms such as e-Health and m-Health. These two concepts encompass information, communication, and mobile technologies for healthcare purposes. e-Health has shown a relevant impact on the quality and safety of healthcare [3]. For example, facilitating the communications between institutions [4], incrementing patient engagement to treatment [5], promoting physical activity in older adults [6], and improving mental health services for trauma survivors [7]. m-Health, for its part, has shown its effectiveness in multiple scopes, such as monitoring health in elderly people [8], promoting early diagnosis of cardiovascular diseases [9], differentiating between Parkinson's disease and essential tremor diagnosis [10], improving hypertension control in stroke survivors [11], and supporting recovery from drug addiction [12].

Regarding the stress detection, methods and systems based on biosignal analysis are under study. These objective approaches are usually more powerful than self-perception of stress level [13]. For example, some patterns extracted from electrocardiography (ECG) such as heart rate or heart rate variability have been related to mental stress [14–19]. The activity of some muscles such as the trapezius has been proved to be connected with stress [20–23]. The muscle activity can be measured by electromyography (EMG). Other studies have demonstrated the relationship between stress and certain brain rhythms measured by electroencephalography (EEG) [24–31]. The skin conductance has also been correlated with stress [32–34]. This parameter can be measured using galvanic skin response (GSR) sensors. All this knowledge has been used by many researchers to propose portable systems for assessment and detection of mental stress. These systems usually combine multiple biosignals. Examples include wearable assessment of mental stress of combatants [35], wristband sensor to measure stress level for people with dementia [36], and stress detection in drivers [37–39]. In short, much useful work has been done. Nevertheless, beyond the commercial gadgets, ambulatory stress-monitoring has not matured yet in applications that are reliable and valid enough to convincingly improve people's health and quality of life. Further research is needed in this field aimed at tackling such an important and serious problem.

In this work, we present and validate a portable system for real-time detection of stress level, based on the RABio w8 (real-time acquisition of biosignals, wireless, eight channels) system. We have designed and implemented both hardware and software in our laboratory. The hardware is made of portable, wireless, and low-cost electronics. The software is composed by an application programming interface (API) and a graphical user interface (GUI). We conducted a study to validate our system using proven and well-established methodology to induce different levels of stress. Our results demonstrate the potential application of our system as a useful tool for ubiquitous stress monitoring, detection, and prevention.

2. Materials and Methods

2.1. Description of the System

As mentioned before, the portable system for real-time detection of stress level presented in this work is based on the RABio w8 system. RABio w8 is a portable, wireless, low-cost hardware–software system for the acquisition and processing of multiple biosignals such as EEG, ECG, and EMG. It has been used in previous works [40].

The electronics of RABio w8 is composed of three blocks (see Figure 1a): acquisition block, control block, and communication block. The acquisition block uses advanced integrated circuits for biosignal acquisition from the ADS family of Texas Instruments (Dallas, TX, USA). This block is in charge of the amplification and the analogue-digital conversion of eight simultaneous channels, up to 1000 samples per second with 24-bit sample resolution. The gain factor of every single channel and the sampling rate are configurable. This block interacts with the control block through a serial peripheral interface (SPI). The control block uses a microcontroller from Microchip Technology

(Chandler, AZ, USA) to receive, synchronize, format, and send the data frames from the first block to the communication block through a universal asynchronous receiver–transmitter (UART) port. Finally, the communication block is responsible for the wireless communication with the software of RABio w8 via Bluetooth. All the electronics are powered by high-autonomy lithium polymer rechargeable batteries and contained in a 3D printed plastic casing (see Figure 1b).
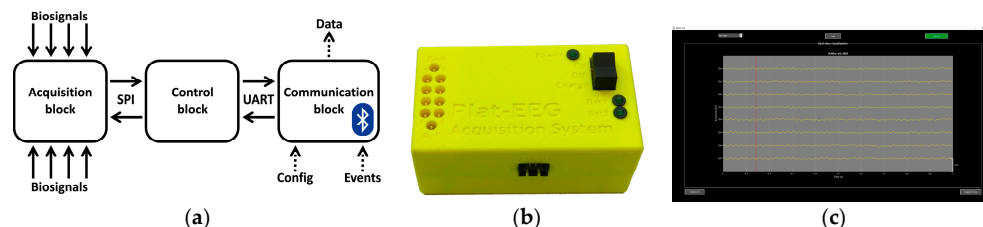

Figure 1. RABio w8 system: (**a**) Diagram of the electronics; (**b**) Picture of the hardware; (**c**) Screenshot of the graphical user interface (GUI).

The software of RABio w8 is composed by an application programming interface and a graphical user interface. The API is a dynamic-link library of Windows OS coded in C/C++. It allows one to receive data frames from the electronics of RABio w8, as well as to configure the acquisition parameters (i.e., channels gain and sampling rate) and to send event markers via Bluetooth. The GUI of RABio w8 (see Figure 1c) is coded in Matlab from The Mathworks (Natick, MA, USA). The GUI uses the functions provided by the API to allow the user to visualize process and record the signals acquired by the electronics in real-time. Configuration of acquisition parameters and event marking is also available for the user.

The full portable system for real-time detection of stress level (see Figure 2) consists of multiple biosignal sensors (EEG, ECG, EMG, and GSR electrodes), the RABio w8 system, a laptop, and the e-Health sensor platform of Arduino. The EEG, ECG, and EMG electrodes are directly attached to input channels of the RABio w8 hardware. The GSR electrodes are attached to the e-Health shield. This shield is powered by an Arduino board and provides skin conductance measurements. The measured values are sent to the RABio w8 hardware by connecting the analogue output of the shield (A2) to an input channel of RABio w8. The laptop is in charge of visualizing, processing, and recording the acquired biosignals using the API and the GUI of RABio w8.
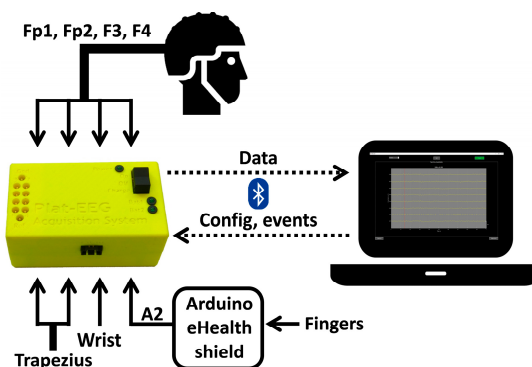

Figure 2. Diagram of the full portable system for real-time detection of stress level. The system is composed by the RABio w8, multiple biosignal sensors placed at head, trapezius, wrist and fingers, the Arduino e-Health platform, and a laptop.

For the purpose of this work (i.e., presentation and validation of our system), a laptop was used. However, in a final version, we propose the cloud-computing of biosignals with real-time biofeedback presented in mobile devices such as tablets or smartphones. Also, a more wearable version of the EEG cap embedding the whole electronics is feasible and under development.

2.2. Experimental Procedure

We conducted a study in order to validate our system, following the well-established methodology of previous published stress studies [28,31]. Ten healthy volunteers were involved in the study (five male, five female, age range of 18–23 years, mean age of 20 ± 2 years, all of them novice in stress-related experiments). The recruitment process started one month prior to the beginning of the study by means of informative emails. The participants were instructed to avoid stimulants or relaxant substances in the 3 h prior to the experiment. They were not paid for their participation. They were provided with the experiment's information sheet and the informed consent, both of which were approved by the Bioethics Committee of the University of Granada.

The participants were prepared by the research staff after they read, understood, and signed the informed consent (see Figure 3a). They wore white hospital clothes during the experiment. Four EEG electrodes were placed at Fp1, Fp2, F3, and F4 positions of the 10–20 International System using an EEG cap. These positions have been successfully used in stress studies [24,25,27,28,31]. One ECG electrode was placed on the wrist of the non-dominant hand. Two EMG electrodes were placed on the trapezius muscle of the non-dominant-hand side, with an inter-electrode distance of 25 mm. The activity of the trapezius has been related to stress in several published studies [20–23]. Two GSR electrodes were placed on the index and the middle fingers of the non-dominant hand [32,33]. All the electrodes were referenced and grounded to the ear lobe of the dominant-hand side. All the electrode impedances were below 30 KΩ. The EEG, ECG, and EMG electrodes were directly attached to the input channels 0–6 of RABio w8. The GSR electrodes were attached to the Arduino e-Health shield and the analogue output A2 was connected to the input channel 7 of RABio w8, as described in Section 2.1.
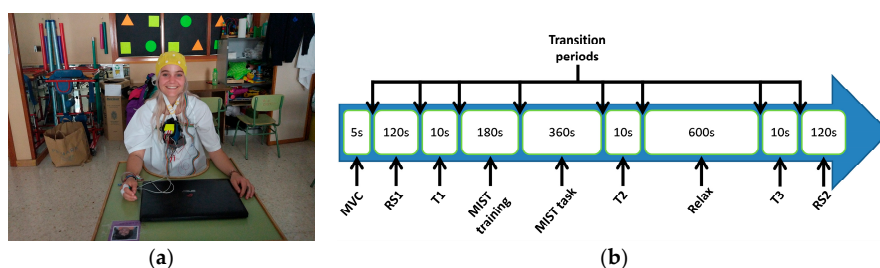

(a)   (b)

Figure 3. (**a**) Picture of one participant ready for the experiment after preparation; (**b**) timeline of the experiment. Duration of each part is in seconds (s). The total duration was around 30 min, including the transition periods (see text for details). MVC—maximum voluntary contraction; RS—resting state block; MIST—Montreal imaging stress task.

Once the participants were prepared, they were instructed to avoid unnecessary movements during the experiment in order to prevent severe artifacts in recordings. They performed a maximum voluntary contraction (MVC) of the trapezius during 5 s and a resting state block (RS1) with closed eyes during 2 min. Afterwards, they were asked about their self-perceived level of stress (T1). The question was posed in Spanish. The English translation is: *If 0 is the minimum level and 4 is the maximum level, what is your level of stress?* The participants then started a stress session. In that session, they performed the Montreal imaging stress task (MIST), a proven methodology that induces psychosocial stress in people [41]. Despite that there are other well-described stress methods such as the variants of the Trier social stress task [42], the MIST has been used in a considerable number of stress-related

works [28,31,41,43–45]. It was classified as well-described stress method by a recent review [46]. The MIST consists of two parts: training and task. In the training part, the participant is asked to solve arithmetic operations without time limit per operation. The difficulty level of the operations randomly varies (five levels). In the task part, the participant has to solve arithmetic operations with time limit. The time limit adapts according to the number of consecutive wrong and right answers. This enforces a range of 20–45% success ratio, while the participant is asked to achieve about 80–90%. The participant is periodically reminded of the relevance of achieving the goal. Detailed information of this protocol can be found in the literature [41]. In our study, after a training of 3 min, the task lasted 6 min. During that session, the participants were seated on a comfortable chair within a classroom while they were using the touchpad of a laptop to play a Matlab-based GUI of the MIST. This GUI was developed by us and further details including screenshots can be found in the literature [28]. After the stress session, the question about the self-perceived level of stress was asked again (T2).

Immediately after the stress session, the participants started a relaxing session. During that session, they stayed laid (resting state with opened eyes) down in a blue-lighted room for 10 min. Blue light was recently proven to accelerate the relaxation process after the MIST in comparison with conventional white light [31]. In this work, the same room and light were used. Once again, the question about the self-perceived stress level was asked at the end of the relaxing session (T3). Finally, a new resting state block (RS2) with closed eyes was performed for 2 min. The timeline of the experiment is shown in Figure 3b.

All the biosignals (raw data) were recorded during the whole experiment at 1000 samples per second with amplification gain of 3 for EEG channels and 1 for the others. All the events (e.g., start of stress session, end of stress session, etc.) were marked in the data. For the aim of this work (i.e., presentation and validation of our system), the biosignals were processed and analyzed offline. The real-time capability of our system is discussed in Section 4.2.

2.3. Signal Processing

2.3.1. EEG

EEG data were zero-phase bandpass filtered (1–48 Hz) with a fourth-order Butterworth infinite impulse response (IIR) filter. Data corresponding to regions of interest (i.e., central minute of each resting-state block, stress session, and relaxing session) were segmented into two-second epochs (no overlap of consecutive epochs). Detrending and z-score normalization was applied to each epoch. The power in theta–alpha (4–13 Hz) and gamma (25–45 Hz) bands was estimated for each channel and then averaged across channels. The average relative gamma (RG) was computed for every single epoch as the power ratio between the average gamma power and the average theta–alpha power. The RG is a stress marker used in emotion and stress studies [28–31]. The following equation defines the RG:

$$RG = AvPower\ (25–45\ Hz)/AvPower\ (4–13\ Hz) \tag{1}$$

2.3.2. ECG

ECG data were zero-phase bandpass filtered (16–24 Hz) with a second-order Butterworth IIR filter in order to enhance the R-peak of the QRS complex. Data corresponding to parts of interest were segmented into 10-s epochs (no overlap of consecutive epochs). The average heart rate (HR) in beats per minute was computed for each epoch by means of the average R–R-interval length. It was not possible to compute the HR using two-second epochs. The set of HR values corresponding to 10-s epochs was interpolated using a spline to obtain values corresponding to two-second epochs. The HR is also a stress marker widely used in stress studies [14–19]. The following equation defines the HR:

$$HR\ (bpm) = 60/AvRR \tag{2}$$

2.3.3. EMG

EMG data were zero-phase bandpass filtered (1–350 Hz) with a second-order Butterworth IIR filter. In order to obtain differential EMG data, data corresponding to the electrode further from the backbone was subtracted from data corresponding to the electrode closer to the backbone. Differential data corresponding to parts of interest were segmented into two-second epochs (no overlap of consecutive epochs). The average trapezius activity (TA) was computed for each epoch as the ratio between the root mean square (RMS) value in the epoch and the RMS value in the MVC test. As in the case of RG and HR, the TA is also a stress marker used in several stress studies [20–23]. The following equation defines the TA:

$$TA = RMS \text{ (epoch)}/RMS \text{ (MCV test)} \tag{3}$$

2.3.4. GSR

GSR data corresponding to parts of interest were directly segmented into two-second epochs (no overlap of consecutive epochs). The average skin conductance (SC) in Siemens was computed for each epoch by using the equation provided by the Arduino e-Health platform tutorial. The SC is one of the most used stress markers in literature [32–34]. The following equation defines the SC:

$$SC = 2 \times (AvVoltage - 0.5)/100,000 \tag{4}$$

2.4. Statistical Analysis

The grand-average across subjects of the time evolution of processed stress markers in the regions of interests (i.e., set of values of RG, HR, TA, and SC corresponding to two-second epochs) was computed. For a better visualization, individual data were z-scored and smoothed using a moving average filter (10 samples) before the computation of the grand-average. The grand-average of the self-perceived stress level (SPSL) at the three test points (i.e., T1, T2, and T3) was also computed. A paired-sample t-test was applied in order to assess if the stress markers and the SPSL significantly differ (p-value $< \alpha$ with $\alpha = 0.05$) at different time periods. In particular, T1, T2, and T3 were compared for the SPSL. The last 30 s of the first resting state block, the last 30 s of the stress session, and the second-to-last 30 s of the relaxing session were compared for the stress markers. Finally, the Pearson's correlation coefficient (PCC) between grand-averaged stress markers and the corresponding 95% confidence interval (CI) was calculated.

2.5. Three-Level Stress Classification

A linear discriminant analysis (LDA) was performed to detect the level of stress using the processed stress markers (i.e., RG, HR, TA, and SC) as features. Three classes (i.e., levels of stress) were defined: stress, relax, and neutral. The values corresponding to the two-second epochs of the minutes 7–8 of the stress session were labeled as stress. These epochs corresponds to the period of maximum stress. The values corresponding to the two-second epochs of the minutes 2–3 of the relaxing session were labeled as relax. These epochs corresponds to the period of minimum stress. The values corresponding to the two-second epochs of the central minute of each resting-state block were labeled as neutral. These epochs corresponds to the periods of baseline stress level. Therefore, 60 observations (120 s with two-second-epoch values) per class were used. A leave-one-out cross validation (LOOCV) was performed for the three-class LDA. That is, for all the observations, 179 out of 180 observations were used in training to classify the remaining observation. In addition to the leave-one-epoch-out cross validation, a leave-one-subject-out cross validation was conducted. That is, for all the subjects, the epochs of one subject were classified using the epochs of the remaining subjects as training data. The classification accuracy or probability of success (p_a) in stress level detection was computed as the

ratio between the number of successfully classified observations and the total number of observations (i.e., n = 180). The 95% CI was also estimated as follows:

$$CI = p_a \pm 1.96 \times sqrt(p_a \times (1 - p_a)/n)$$ (5)

3. Results

3.1. Time Evolution of Biosignal-Based Markers

Figure 4a–d show the grand-average across subjects of the time evolution of processed stress markers in the regions of interests. Figure 4e also shows the grand-average of the SPSL at the three test points (i.e., T1, T2 and T3).
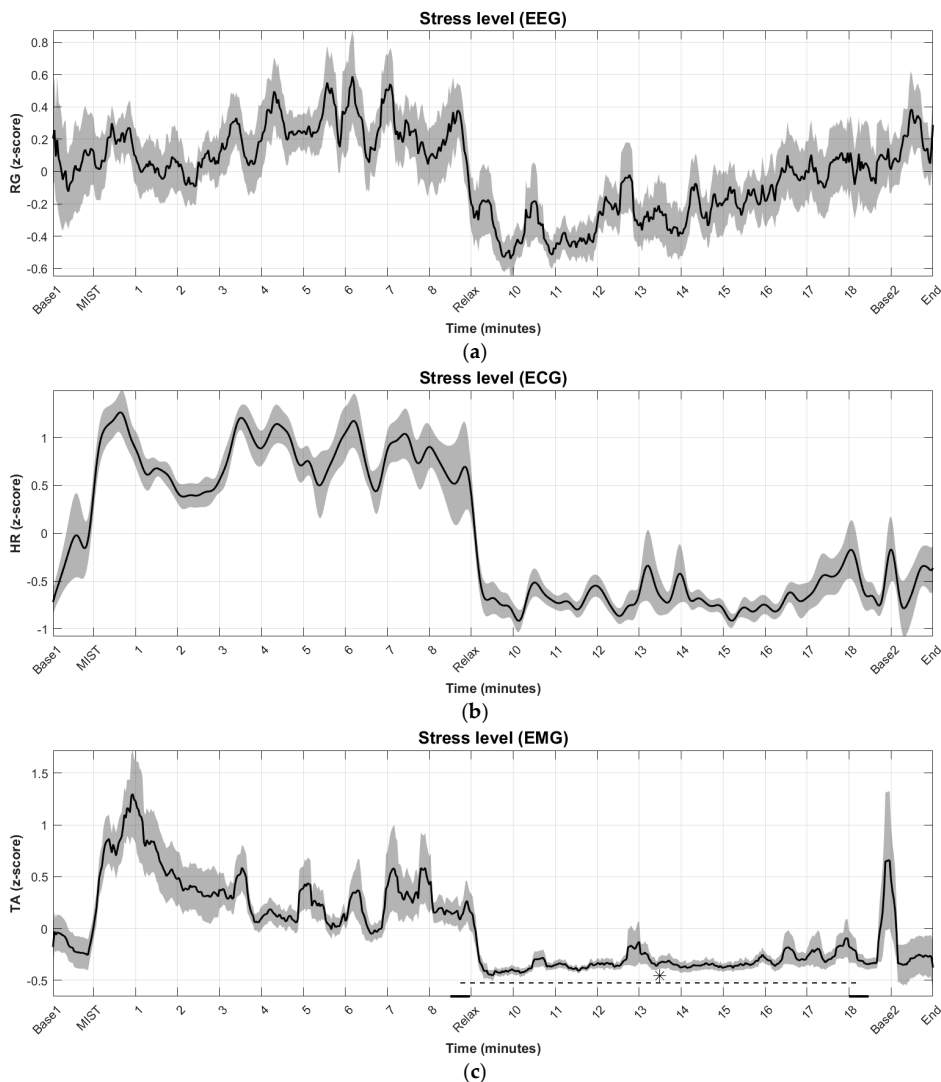

(a)

(b)

(c)

Figure 4. *Cont.*
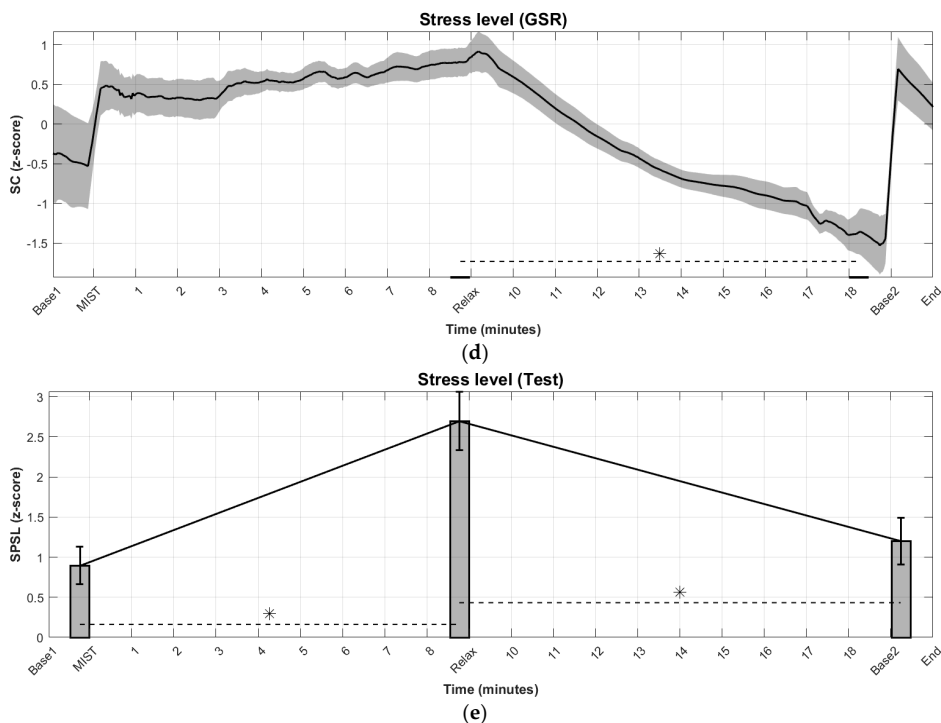
(**d**)

(**e**)

Figure 4. Grand-average across subjects of the time evolution of processed stress markers in the regions of interests. Base1 and Base2 correspond to the central minutes of resting state blocks RS1 and RS2, respectively. MIST indicates the beginning of the stress session (3 min of training and 6 min of task). Relax indicates the beginning of the relaxing session. Shades behind the plots and error bars indicate the standard error of the mean (SEM): (**a**) relative gamma (RG) estimated from electroencephalography (EEG) data; (**b**) average heart rate (HR) estimated from electrocardiography (ECG) data; (**c**) trapezius activity (TA) estimated from electromyography (EMG) data. Asterisk indicates statistically significant difference (p-value < 0.05) in average TA between the last 30 s of the stress session and the second-to-last 30 s of the relaxing session; (**d**) skin conductance (SC) estimated from galvanic skin response (GSR) data. Asterisk indicates statistically significant difference (p-value < 0.05) in average SC between the last 30 s of the stress session and the second-to-last 30 s of the relaxing session; (**e**) self-perceived stress level (SPSL) obtained from questions at T1, T2, and T3 points. X-axis only comprises regions of interests and T1, T2, and T2 would actually be located before the stress session (i.e., just before MIST), after the stress session (i.e., just after minute 9), and after the relaxing session (i.e., just after minute 19), respectively. Asterisks indicate statistically significant difference (p-value < 0.05) in SPSL between the T1–T2 and between T2–T3.

In addition, the Pearson's correlation coefficient (PCC) between stress markers and the corresponding 95% confidence interval is reported in Table 1.

Table 1. Pearson's correlation coefficient (PCC) between processed stress markers and the corresponding lower (CI low) and upper (CI up) bounds for a 95% confidence interval (CI). RG—relative gamma; HR—average heart rate; TA—trapezius activity; SC—skin conductance.

Pair	PCC	CI Low	CI Up
RG, HR	0.7296	0.6909	0.7642
RG, TA	0.5753	0.5206	0.6253
RG, SC	0.3293	0.2579	0.3972
HR, TA	0.8338	0.8083	0.8561
HR, SC	0.6327	0.5834	0.6773
TA, SC	0.4632	0.3995	0.5224

3.2. Stress Level Detection

The classification accuracy or probability of success (p_a) in detection of stress level (stress, relax, and neutral) and the 95% confidence interval are reported in this section. In particular, Table 2 shows these values when using one stress marker as feature for the LDA classifier. Table 3 shows the same statistics when using two stress markers as features. Table 4 shows the same when using three or all the stress markers. Finally, Table 5 shows the same as Table 4, but using a leave-one-subject-out cross validation instead of leave-one-epoch-out. In these four tables, main values indicate the pa and error values indicate the 95% CI. Last row indicates the mean and the standard deviation of the mean. All the values are expressed in percentage.

Table 2. Probability of successful detection of stress level using ones stress marker as feature.

Participant	RG	HR	TA	SC
1	72 ± 7	74 ± 6	31 ± 7	49 ± 7
2	61 ± 7	57 ± 7	28 ± 7	69 ± 7
3	61 ± 7	45 ± 7	29 ± 7	84 ± 5
4	51 ± 7	60 ± 7	61 ± 7	51 ± 7
5	28 ± 7	93 ± 4	22 ± 6	69 ± 7
6	44 ± 7	94 ± 3	45 ± 7	61 ± 7
7	47 ± 7	82 ± 6	66 ± 7	60 ± 7
8	33 ± 7	77 ± 6	21 ± 6	61 ± 7
9	67 ± 7	77 ± 6	52 ± 7	18 ± 6
10	33 ± 7	62 ± 7	62 ± 7	76 ± 6
Mean ± Std	50 ± 15	72 ± 16	42 ± 18	60 ± 18

Table 3. Probability of successful detection of stress level using two stress markers as features.

Participant	RG, HR	RG, TA	RG, SC	HR, TA	HR, SC	TA, SC
1	76 ± 6	83 ± 6	69 ± 7	86 ± 5	71 ± 7	64 ± 7
2	73 ± 6	82 ± 6	73 ± 6	61 ± 7	70 ± 7	78 ± 6
3	77 ± 6	60 ± 7	81 ± 6	52 ± 7	92 ± 4	90 ± 4
4	59 ± 7	64 ± 7	72 ± 7	70 ± 7	68 ± 7	87 ± 5
5	92 ± 4	46 ± 7	54 ± 7	93 ± 4	84 ± 5	76 ± 6
6	94 ± 3	69 ± 7	64 ± 7	93 ± 4	96 ± 3	71 ± 7
7	84 ± 5	66 ± 7	64 ± 7	86 ± 5	86 ± 5	66 ± 7
8	74 ± 6	48 ± 7	61 ± 7	76 ± 6	71 ± 7	64 ± 7
9	82 ± 6	72 ± 7	64 ± 7	78 ± 6	73 ± 6	49 ± 7
10	67 ± 7	54 ± 7	67 ± 7	73 ± 6	77 ± 6	81 ± 6
Mean ± Std	78 ± 11	64 ± 13	67 ± 7	77 ± 14	79 ± 10	73 ± 12

Table 4. Probability of successful detection of stress level using three or all the stress markers as features.

Participant	RG, HR, TA	RG, HR, SC	RG, TA, SC	HR, TA, SC	RG, HR, TA, SC
1	91 ± 4	79 ± 6	84 ± 5	92 ± 4	92 ± 4
2	82 ± 6	78 ± 6	83 ± 6	75 ± 6	82 ± 6
3	77 ± 6	93 ± 4	82 ± 6	92 ± 4	93 ± 4
4	68 ± 7	69 ± 7	78 ± 6	82 ± 6	83 ± 6
5	93 ± 4	84 ± 5	73 ± 7	84 ± 5	84 ± 5
6	93 ± 4	97 ± 3	72 ± 7	98 ± 2	98 ± 2
7	86 ± 5	87 ± 5	67 ± 7	89 ± 4	90 ± 4
8	74 ± 6	75 ± 6	64 ± 7	71 ± 7	74 ± 6
9	81 ± 6	80 ± 6	67 ± 7	76 ± 6	81 ± 6
10	72 ± 7	77 ± 6	79 ± 6	79 ± 6	78 ± 6
Mean $\pm$ Std	82 ± 9	82 ± 8	75 ± 7	84 ± 9	86 ± 8

Table 5. Probability of successful detection of stress level using three or all the stress markers as features for the leave one-subject-out cross validation.

Participant	RG, HR, TA	RG, HR, SC	RG, TA, SC	HR, TA, SC	RG, HR, TA, SC
1	33 ± 7	33 ± 7	36 ± 7	33 ± 7	33 ± 7
2	67 ± 7	37 ± 7	58 ± 7	64 ± 7	65 ± 7
3	33 ± 7	41 ± 7	36 ± 7	33 ± 7	36 ± 7
4	47 ± 7	36 ± 7	33 ± 7	49 ± 7	34 ± 7
5	66 ± 7	41 ± 7	37 ± 7	64 ± 7	38 ± 7
6	36 ± 7	34 ± 7	33 ± 7	34 ± 7	34 ± 7
7	33 ± 7	33 ± 7	39 ± 7	33 ± 7	33 ± 7
8	34 ± 7	53 ± 7	51 ± 7	54 ± 7	54 ± 7
9	41 ± 7	60 ± 7	56 ± 7	51 ± 7	66 ± 7
10	48 ± 7	48 ± 7	48 ± 7	36 ± 7	42 ± 7
Mean $\pm$ Std	44 ± 13	42 ± 9	43 ± 10	45 ± 13	44 ± 13

4. Discussion

4.1. Stress and Biosignals

At first sight, the time evolution of all the stress markers indicates agreement with the self-perception of stress level. This is partially supported by the statistical tests (see Figure 4). The MIST causes a significant increase in self-perceived stress level and the relaxing session causes a significant decrease. However, only two stress markers presented significant differences in stress level at different time periods. These are the TA and the SC. The significant differences were only between the end of the stress session (maximum level of stress) and the end of the relax session (minimum or very low level of stress). The other two markers (i.e., RG and HR) did not present significant differences despite the noticeable changes. All the markers reflect that the increase in stress level is gradual. This behavior has been reported in previous literature [28,31]. However, there are some visible differences between markers. In particular, the RG, the HR, and the TA indicates that the minimum level of stress is quickly achieved once the relaxing session starts (less than 1 min from the beginning of this session), while the SC denotes a gradual decrease. This is due to the fact that the sweating process is fast, while the reabsorption process is slow in comparison with other physiological responses. Accordingly, the SC has a drawback in terms of time of response. In addition, the RG is the only marker that reflects a gradual increase in stress level during the relaxing session. This fits with results reported in previous literature and may be caused by boredom of the participants during this part of the experiment [28,31]. The other markers indicate a more rapid increase at the end of the relaxing session. In this regard, the RG has an advantage in terms of response time. In other words, the boredom may have an immediate effect on EEG, while it may have a delayed effect on the other biosignals.

Regarding the PCC between stress markers, all of them are generally correlated (see Table 1). The one that correlates the most with the others is the HR (72.96% with RG, 83.38% with TA, and 63.27% with SC). The SC is the least correlated marker (32.93% with RG, 63.27% and 46.32% with TA). This is due to the response time discussed in the previous paragraph and to the fact that the GSR is the least noisy biosignal (see Figure 4). The ECG is the second least noisy biosignal. This suggests that ECG and GSR are the more appropriate biosignals in the presence of artifacts. Nevertheless, the stress markers extracted from these two biosignals and from the EMG can be misrepresented by physical activity (e.g., physical activity may increase the HR even without being stressed). In this respect, the RG is advantageous.

4.2. Real-Time Detection of Stress Level

The results of the three-class LDA with leave-out-epoch-out cross validation (see Tables 1–4) indicate that the more biosignals (thus more stress markers) that are combined, the higher probability of successful detection of stress level (i.e., accuracy). With single markers, the probabilities are 50%, 72%, 42%, and 60% for RG, HR, TA, and SC, respectively. With two markers, probabilities are 78% (RG–HR), 64% (RG–TA), 67% (RG–SC), 77% (HR–TA), 79% (HR–SC), and 73% (TA–SC). However, the probabilities increase up to 82% (RG–HR–TA), 82% (RG–HR–SC), 75% (RG–TA–SC) and 84% (HR–TA–SC). There is no relevant improvement by adding the RG to the trio HR–TA–SC (86%). By using three or all the markers, the results overcome accuracies reported in previous studies of biosignal-based systems for stress detection and measurement [32,33,35,39,47]. Nevertheless, this is not meaningful because the cited studies were neither carried out in the same experimental conditions, with comparable number of subjects, nor were they conducted with a similar methodology. In reference to the results of the leave-one-subject-out cross validation (see Table 5), the probabilities of success are generally close to the chance level (i.e., 33%), taking into account the confidence intervals. This indicates that the system needs to be calibrated for every single subject. This was expected as stress markers and thresholds may vary across subjects. Regarding the optimal combination of markers, it depends on the particular conditions in which the stress has to be detected (e.g., response time and external factors). For example, in this work, the use of EEG signals does not optimize the results in terms of accuracy. The EEG has a distinct set of advantages and limitations. Among the advantages, as cited in Section 4.1, the markers based on brain activity (e.g., the RG) present a shorter response time and are less susceptible to physical activity. Additionally, the EEG provides powerful endogenous and cognitive information such as attention [48–50] that can be useful in certain scenarios. Regarding the limitations, the use of EEG provides a number of technical challenges such as additional sensors (thus less portability) or higher computational complexity. In order to overcome some of these limitations, we are developing a more wearable version of the EEG cap embedding the whole electronics and based on dry electrodes [51]. Our results demonstrate the reliability of our system in the detection of three levels of stress with a resolution of a few seconds. Still, the results could improve by extracting more features (i.e., stress markers) from biosignals [38] and by using more powerful classifiers such as artificial neural networks [52,53]. For the aim of this work, biosignals were processed offline. We used two-second epochs of data with a low-cost preprocessing, feature extraction, and classification in terms of computation time. This provides our system with real-time capability. In addition, for the sake of simplicity, the participants of the study were instructed to avoid unnecessary movements during the experiment in order to prevent severe artifacts in recordings. This is an unrealistic scenario. For the use of the proposed system in daily-life scenarios, advanced processing for artifact removal should be included [2]. Based on the accuracies obtained in this work, we expect that our system can still work in hostile environments by adding the artifact removal part.

5. Conclusions

In this work, we have proposed a portable system for real-time detection of stress level. We have presented the methodology and the results of a study aimed at validating the system. In the study,

ten volunteers were stressed and then relaxed using well-established methods, while their biosignals were recorded. Our portable system can simultaneously record and process four types of biosignals (i.e., EEG, ECG, EMG, and GSR) in real-time, thereby enabling the detection of three levels of stress very accurately (86%). The system has some limitations that have been discussed (e.g., portability and performance under artifacts). In order to overcome them, we are working on a final version in which the biosignals are cloud-computed, including the needed processing for artifact removal. The real-time biofeedback (i.e., 2 s plus the computation time) will be presented in mobile devices such as tablets or smartphones. Moreover, a more wearable version of the EEG cap embedding the whole electronics is feasible and under development. Having overcome the cited limitations, our system could be used as a reliable tool for real-time stress monitoring, detection, and prevention in daily life. For example, prevention of job stress in periods of high level of work intensity, stress monitoring in children at school, or discovery of new stressors through stress detection in the domestic environment. All of this has a relevant impact on society as stress is a major problem nowadays and this system could substantially improve people's health and quality of life.

References

1. Cohen, S.; Janicki-Deverts, D.; Doyle, W.J.; Miller, G.E.; Frank, E.; Rabin, B.S.; Turner, R.B. Chronic stress, glucocorticoid receptor resistance, inflammation, and disease risk. *Proc. Natl. Acad. Sci. USA* **2012**, *109*, 5995–5999. [CrossRef] [PubMed]

2. Minguillon, J.; Lopez-Gordo, M.A.; Pelayo, F. Trends in EEG-BCI for daily-life: Requirements for artifact removal. *Biomed. Signal Process. Control* **2017**, *31*, 407–418. [CrossRef]

3. Black, A.D.; Car, J.; Pagliari, C.; Anandan, C.; Cresswell, K.; Bokun, T.; McKinstry, B.; Procter, R.; Majeed, A.; Sheikh, A. The impact of ehealth on the quality and safety of health care: A systematic overview. *PLoS Med.* **2011**, *8*, e1000387. [CrossRef] [PubMed]

4. Blaya, J.A.; Fraser, H.S.F.; Holt, B. E-health technologies show promise in developing countries. *Health Aff.* **2010**, *29*, 244–251. [CrossRef] [PubMed]

5. Barello, S.; Triberti, S.; Graffigna, G.; Libreri, C.; Serino, S.; Hibbard, J.; Riva, G. eHealth for patient engagement: A Systematic Review. *Front. Psychol.* **2016**, *6*. [CrossRef] [PubMed]

6. Muellmann, S.; Forberger, S.; Möllers, T.; Bröring, E.; Zeeb, H.; Pischke, C.R. Effectiveness of eHealth interventions for the promotion of physical activity in older adults: A systematic review. *Prev. Med.* **2018**, *108*, 93–110. [CrossRef] [PubMed]

7. Morland, L.A.; Greene, C.J.; Rosen, C.S.; Kuhn, E.; Hoffman, J.; Sloan, D.M. Telehealth and eHealth interventions for posttraumatic stress disorder. *Curr. Opin. Psychol.* **2017**, *14*, 102–108. [CrossRef] [PubMed]

8. Lorenz, A.; Oppermann, R. Mobile health monitoring for the elderly: Designing for diversity. *Pervasive Mob. Comput.* **2009**, *5*, 478–495. [CrossRef]

9. Nguyen, H.H.; Silva, J.N.A. Use of smartphone technology in cardiology. *Trends Cardiovasc. Med.* **2016**, *26*, 376–386. [CrossRef] [PubMed]

10. Woods, A.M.; Nowostawski, M.; Franz, E.A.; Purvis, M. Parkinson's disease and essential tremor classification on mobile device. *Pervasive Mob. Comput.* **2014**, *13*, 1–12. [CrossRef]

11. Lakshminarayan, K.; Westberg, S.; Northuis, C.; Fuller, C.C.; Ikramuddin, F.; Ezzeddine, M.; Scherber, J.; Speedie, S. A mHealth-based care model for improving hypertension control in stroke survivors: Pilot RCT. *Contemp. Clin. Trials* **2018**, *70*, 24–34. [CrossRef] [PubMed]

12. Liang, D.; Han, H.; Du, J.; Zhao, M.; Hser, Y.I. A pilot study of a smartphone application supporting recovery from drug addiction. *J. Subst. Abuse Treat.* **2018**, *88*, 51–58. [CrossRef] [PubMed]

13. Picard, R.W. Affective Computing: From laughter to IEEE. *IEEE Trans. Affect. Comput.* **2010**, *1*, 11–17. [CrossRef]

14. Dimitriev, D.A.; Saperova, E.V. Heart rate variability and blood pressure during mental stress. *Ross Fiziol Zh Im I M Sechenova* **2015**, *101*, 98–107. [PubMed]

15. Ranganathan, G.; Rangarajan, R.; Bindhu, V. Estimation of heart rate signals for mental stress assessment using neuro fuzzy technique. *Appl. Soft Comput.* **2012**, *12*, 1978–1984. [CrossRef]

16. Chandiramani, S.; Cohorn, L.C.; Chandiramani, S. Heart rate changes during acute mental stress with closed loop stimulation: Report on two single-blinded, pacemaker studies. *Pacing Clin. Electrophysiol.* **2007**, *30*, 976–984. [CrossRef] [PubMed]

17. Regula, M.; Socha, V.; Kutilek, P.; Socha, L.; Hana, K.; Hanakova, L.; Szabo, S. Study of heart rate as the main stress indicator in aircraft pilots. In Proceedings of the 16th IEEE International Conference on Mechatronics—Mechatronika, Brno, Czech Republic, 3–5 December 2014; pp. 639–643.

18. Sayette, M.A. Heart rate as an index of stress response in alcohol administration research: A critical review. *Alcohol Clin. Exp. Res.* **1993**, *17*, 802–809. [CrossRef] [PubMed]

19. Michels, N.; Sioen, I.; Clays, E.; De Buyzere, M.; Ahrens, W.; Huybrechts, I.; Vanaelst, B.; De Henauw, S. Children's heart rate variability as stress indicator: Association with reported stress and cortisol. *Biol. Psychol.* **2013**, *94*, 433–440. [CrossRef] [PubMed]

20. Lundberg, U.; Kadefors, R.; Melin, B.; Palmerud, G.; Hassmén, P.; Engström, M.; Dohns, I.E. Psychophysiological stress and EMG activity of the trapezius muscle. *Int. J. Behav. Med.* **1994**, *1*, 354–370. [CrossRef] [PubMed]

21. Wijsman, J.; Grundlehner, B.; Penders, J.; Hermens, H. Trapezius muscle EMG as predictor of mental stress. *ACM Trans. Embed. Comput. Syst.* **2013**, *12*. [CrossRef]

22. Larsson, S.E.; Larsson, R.; Zhang, Q.; Cai, H.; Åke Öberg, P. Effects of psychophysiological stress on trapezius muscles blood flow and electromyography during static load. *Eur. J. Appl. Physiol. Occup. Physiol.* **1995**, *71*, 493–498. [CrossRef] [PubMed]

23. Schleifer, L.M.; Spalding, T.W.; Kerick, S.E.; Cram, J.R.; Ley, R.; Hatfield, B.D. Mental stress and trapezius muscle activation under psychomotor challenge: A focus on EMG gaps during computer work. *Psychophysiology* **2008**, *45*, 356–365. [CrossRef] [PubMed]

24. Papousek, I.; Weiss, E.M.; Schulter, G.; Fink, A.; Reiser, E.M.; Lackner, H.K. Prefrontal EEG alpha asymmetry changes while observing disaster happening to other people: Cardiac correlates and prediction of emotional impact. *Biol. Psychol.* **2014**, *103*, 184–194. [CrossRef] [PubMed]

25. Seo, S.; Lee, J. Stress and EEG. In *Convergence and Hybrid Information Technologies*; Crisan, M., Ed.; IntechOpen: London, UK, 2010; pp. 413–426.

26. Hu, B.; Peng, H.; Zhao, Q.; Hu, B.; Majoe, D.; Zheng, F.; Moore, P. Signal Quality Assessment Model for Wearable EEG Sensor on Prediction of Mental Stress. *IEEE Trans. Nanobiosci.* **2015**, *14*, 553–561. [CrossRef]

27. Brouwer, A.-M.; Neerincx, M.A.; Kallen, V.; van der Leer, L.; ten Brinke, M. EEG alpha asymmetry, heart rate variability and cortisol in response to Virtual Reality induced stress. *J. Cyberther. Rehabil.* **2011**, *4*, 27–40.

28. Minguillon, J.; Lopez-Gordo, M.A.; Pelayo, F. Stress Assessment by Prefrontal Relative Gamma. *Front. Comput. Neurosci.* **2016**, *10*, 1–9. [CrossRef] [PubMed]

29. Steinhubl, S.R.; Wineinger, N.E.; Patel, S.; Boeldt, D.L.; Mackellar, G.; Porter, V.; Redmond, J.T.; Muse, E.D.; Nicholson, L.; Chopra, D.; et al. Cardiovascular and nervous system changes during meditation. *Front. Hum. Neurosci.* **2015**, *9*, 1–10. [CrossRef] [PubMed]

30. Lutz, A.; Greischar, L.L.; Rawlings, N.B.; Ricard, M.; Davidson, R.J. Long-term meditators self-induce high-amplitude gamma synchrony during mental practice. *Proc. Natl. Acad. Sci. USA* **2004**, *101*, 16369–16373. [CrossRef] [PubMed]

31. Minguillon, J.; Lopez-Gordo, M.A.; Renedo-Criado, D.A.; Sanchez-Carrion, M.J.; Pelayo, F. Blue lighting accelerates post-stress relaxation: Results of a preliminary study. *PLoS ONE* **2017**, *12*, e0186399. [CrossRef] [PubMed]

32. Sriramprakash, S.; Prasanna, V.D.; Murthy, O.V.R. Stress Detection in Working People. *Procedia Comput. Sci.* **2017**, *115*, 359–366. [CrossRef]

33. Villarejo, M.V.; Zapirain, B.G.; Zorrilla, A.M. A stress sensor based on galvanic skin response (GSR) controlled by ZigBee. *Sensors* **2012**, *12*, 6075–6101. [CrossRef] [PubMed]

34. Sessa, F.; Messina, G.; Valenzano, A.; Messina, A.; Salerno, M.; Marsala, G.; Bertozzi, G.; Daniele, A.; Monda, V.; Russo, R. Sports training and adaptive changes. *Sport Sci. Health* **2018**, 1–4. [CrossRef]

35. Seoane, F.; Mohino-Herranz, I.; Ferreira, J.; Alvarez, L.; Buendia, R.; Ayllón, D.; Llerena, C.; Gil-Pita, R. Wearable biomedical measurement systems for assessment of mental stress of combatants in real time. *Sensors* **2014**, *14*, 7120–7141. [CrossRef] [PubMed]

36. Kikhia, B.; Stavropoulos, T.G.; Andreadis, S.; Karvonen, N.; Kompatsiaris, I.; Sävenstedt, S.; Pijl, M.; Melander, C. Utilizing a wristband sensor to measure the stress level for people with dementia. *Sensors* **2016**, *16*, 1989. [CrossRef] [PubMed]

37. Zheng, R.; Yamabe, S.; Nakano, K.; Suda, Y. Biosignal analysis to assess mental stress in automatic driving of trucks: Palmar perspiration and masseter electromyography. *Sensors* **2015**, *15*, 5136–5150. [CrossRef] [PubMed]

38. Ollander, S.; Godin, C.; Charbonnier, S. Feature and Sensor Selection for Detection of Driver Stress. In Proceedings of the 3rd International Conference on Physiological Computing Systems, Lisbon, Portugal, 27–28 July 2016; pp. 115–122.

39. Keshan, N.; Parimi, P.V.; Bichindaritz, I. Machine learning for stress detection from ECG signals in automobile drivers. In Proceedings of the 2015 IEEE International Conference on Big Data, Santa Clara, CA, USA, 29 October–1 November 2015; pp. 2661–2669. [CrossRef]

40. Minguillon, J.; Lopez-Gordo, M.A.; Morillas, C.; Pelayo, F. A Mobile Brain-Computer Interface for Clinical Applications: From the Lab to the Ubiquity. In *Proceedings of the 7th International Work-Conference on the Interplay between Natural and Artificial Computation*; Ferrández Vicente, J.M., Álvarez-Sánchez, J.R., De la Paz López, F., Toledo Moreo, J., Adeli, H., Eds.; Springer International Publishing: Corunna, Spain, 2017; pp. 68–76. [CrossRef]

41. Dedovic, K.; Renwick, R.; Mahani, N.K.; Engert, V.; Lupien, S.J.; Pruessner, J.C. The Montreal Imaging Stress Task: Using functional imaging to investigate the effects of perceiving and processing psychosocial stress in the human brain. *J. Psychiatry Neurosci.* **2005**, *30*, 319–325. [PubMed]

42. Kirschbaum, C.; Pirke, K.-M.; Hellhammer, D.H. The "Trier Social Stress Test"—A Tool for Investigating Psychobiological Stress Responses in a Laboratory Setting. *Neuropsychobiology* **1993**, *28*, 76–81. [CrossRef] [PubMed]

43. Dedovic, K.; D'Aguiar, C.; Pruessner, J.C. What stress does to your brain: A review of neuroimaging studies. *Can. J. Psychiatry* **2009**, *54*, 6–15. [CrossRef] [PubMed]

44. Zschucke, E.; Renneberg, B.; Dimeo, F.; Wüstenberg, T.; Ströhle, A. The stress-buffering effect of acute exercise: Evidence for HPA axis negative feedback. *Psychoneuroendocrinology* **2015**, *51*, 414–425. [CrossRef] [PubMed]

45. Nagano-Saito, A.; Dagher, A.; Booij, L.; Gravel, P.; Welfeld, K.; Casey, K.F.; Leyton, M.; Benkelfat, C. Stress-induced dopamine release in human medial prefrontal cortex—18F-fallypride/PET study in healthy volunteers. *Synapse* **2013**, *67*, 821–830. [CrossRef] [PubMed]

46. Bali, A.; Jaggi, A.S. Clinical experimental stress studies: Methods and assessment. *Rev. Neurosci.* **2015**, *26*, 555–579. [CrossRef] [PubMed]

47. Bichindaritz, I.; Breen, C.; Cole, E.; Keshan, N.; Parimi, P. Feature Selection and Machine Learning Based Multilevel Stress Detection from ECG Signals. In *Innovation in Medicine and Healthcare 2017*; Chen, Y.-W., Tanaka, S., Howlett, R.J., Jain, L.C., Eds.; Springer International Publishing: Cham, Switzerland, 2018; pp. 202–213.

48. Lopez-Gordo, M.A.; Pelayo, F. A Binary Phase-Shift Keying Receiver for the Detection of Attention to Human Speech. *Int. J. Neural Syst.* **2013**, *23*, 12. [CrossRef] [PubMed]

49. Minguillon, J.; Lopez-Gordo, M.A.; Pelayo, F. Detection of Attention in Multi-Talker Scenarios: A Fuzzy Approach. *Expert Syst. Appl.* **2016**, *64*, 261–268. [CrossRef]
50. Lopez-Gordo, M.A.; Pelayo, F.; Fernandez, E.; Padilla, P. Phase-shift keying of EEG signals: Application to detect attention in multitalker scenarios. *Signal Process.* **2015**, *117*, 165–173. [CrossRef]
51. Lopez-Gordo, M.A.; Sanchez Morillo, D.; Pelayo Valle, F. Dry EEG electrodes. *Sensors* **2014**, *14*, 12847–12870. [CrossRef] [PubMed]
52. Singh, M.; Bin Queyam, A. A Novel Method of Stress Detection Using Physiological Measurements of Automobile Drivers. *Int. J. Electron. Eng.* **2013**, *5*, 13–20.
53. Alić, B.; Sejdinović, D.; Gurbeta, L.; Badnjevic, A. Classification of stress recognition using Artificial Neural Network. In Proceedings of the 2016 5th Mediterranean Conference on Embedded Computing (MECO), Bar, Montenegro, 12–16 June 2016; pp. 297–300.